SITE CHARACTERIZATION
40 CFR 146.82(a)(2), (3), (5), (6) and 40 CFR 146.83

RUSSELL CO_2 CAPTURE AND SEQUESTRATION

Facility Information

Facility name: Russell CO_2 Storage Complex
CSS #1

Facility contact: Aaron Buettner, Chief Executive Officer
13632 W 95th St
Lenexa, KS 66215
Phone: (785) 261-0355
Email: Aaron.Buettner@PureField.com

Well location: Un-incorporated, Russell County, Kansas
Lat: 38.8855219472 Long: -98.7504253861 NAD 83 (2011)
Sec 27 T 13 S R 13 W 0' FSL – 2005' FEL

List of Tables

List of Figures

List of Appendices

List of Acronyms and Abbreviations

3D = three-dimensional ANSS = Advanced National Seismic System AoR = Area of Review bbl = barrels bbl/yr per km^2 = barrel per year per squared kilometer bpd = barrels per day CKU = Central Kansas Uplift CO_2 = carbon dioxide ComCat = Comprehensive Earthquake Catalog EOR = enhanced oil recovery FMI = Formation Micro-Imager ft = feet ft bgs = feet below ground surface ft MSL = feet, referenced to mean sea level g/cc = grams per cubic centimeter gpm = gallons per minute GS = geologic sequestration GSDT = Geologic Sequestration Data Tool KGS = Kansas Geological Survey km = kilometers mb_lg = mg_lg scale, short-period surface wave magnitude scale	mD = millidarcy mg/L = milligrams per liter M_L = local magnitude MMA = maximum monitoring area MMI = Modified Mercalli Intensity mmol/L = millimoles per liter mmol $m^{-2}s^{-1}$ = micromoles per square meter per second mS/cm = micro-Siemens per centimeter OPAS = Ozark Plateaus aquifer system PCC = PureField Carbon Capture, LLC ppm = parts per million psi/ft = pound-force per square inch per foot Sv = vertical stress SHmax = maximum horizontal stress Shmin = minimum horizontal stress TDS = total dissolved solids UIC = Underground Injection Control US = United States USDW = Underground Source of Drinking Water US EPA = United States Environmental Protection Agency USGS = United States Geological Survey WIPAS = Western Interior Plains aquifer system

A.I.1. Summary

PureField Carbon Capture, LLC (PCC) provides this Site Characterization attachment to the Application Narrative that meets the requirements of 40 CFR 146.82(a)(2), (3), (5), (6) and 40 CFR 146.83. The types of site characterization information provided include:

An overview of regional geology, hydrogeology, and local structural geology [40 CFR 146.82(a)(3)(vi)]

A thorough evaluation of regional geology, hydrogeology, and local geology is presented using geologic maps, topographic maps, and cross sections. The full stratigraphic sequence from ground surface to Precambrian basement is provided, along with hydrogeologic units and their associated structures. In the vicinity of the geologic sequestration (GS) site, the shallow geologic units include a series of interbedded shales, limestone, and sandstone formations. The corresponding aquifer systems generally include a shallow (water-table) aquifer, and the Dakota Aquifer (aka Great Plains aquifer) that is the lowermost Underground Source of Drinking Water (USDW) in the region.

Particular attention is given to the Arbuckle Group (gross injection interval within the Arbuckle of 3,448 to 3,606 feet below ground surface [ft bgs]) since it contains the target injection zone, and also provides the primary upper confining layer and a lower confining unit. The majority of the Arbuckle Group is composed of porous carbonates. Additionally, the Arbuckle injection zone is vertically separated from the lowermost USDW by a thickness of approximately 2,900 feet (ft) that includes multiple confining units comprised of multiple shale sequences plus thick anhydrite and salt zones. Detailed information is provided on the Arbuckle Group depositional setting, geologic structure, and the regional aquifer system associated the group (extent, salinity, hydraulic head, groundwater velocity, and groundwater temperatures). The Lansing (2,993 to 3,053 ft bgs) and Kansas City Groups (3,053 to 3,133 ft bgs) provide a potential second injection zone for permitting at a later date.

Maps and cross sections of the area of review (AoR) [40 CFR 146.82(a)(3)(i) and 146.82(a)(2)]

Data from a combination of CSS #1 well logs, adjacent well logs, and information from the baseline three-dimensional (3D) seismic survey were used to create structural cross sections, seismic cross lines, and isopach maps to aid in the evaluation of the AoR and its vicinity. The assessment indicates that both the sequestration interval and the confining units are present and continuous across the AoR, and the site and its vicinity are characterized by uninterrupted flat-lying stratigraphy.

The location, orientation, and properties of known or suspected faults and fractures that may transect the confining zone(s) in the AoR, along with a determination that they will not interfere with containment [40 CFR 146.82(a)(3)(ii)]

PCC has found no evidence to date of any faults or fractures large enough to offset strata or located in a manner that would interfere with containment. Sources examined within the AoR

include open literature sources, analysis of the baseline 3D surface seismic survey conducted for the project, and observations and analysis of data obtained during the drilling of CSS #1.

Injection and confining zone details [40 CFR 146.82(a)(3)(iii)]

Data on the depth, areal extent, thickness, mineralogy, porosity, permeability, and capillary pressure of the injection and confining zone and on lithology and facies changes are provided. This information was assembled and evaluated by PCC as part of site characterization from literature and the site-specific pre-operational testing program. There are numerous confining layers separating the Arbuckle Group from the lowermost USDW: over 20 shale layers, the Stone Corral Anhydrite, and the Hutchinson Salt.

Geomechanical information within confining zone(s) [40 CFR 146.82(a)(3)(iv)]

Geomechanical information on fractures, stress, ductility, rock strength, and in situ fluid pressures was assembled from literature and site-specific data obtained from pre-operational testing of CSS #1. A fracture gradient of 0.78 pounds per square inch per foot (psi/ft) for the top of the Arbuckle Group injection zone is utilized, consistent with the results from the geomechanics model based on dynamic elastic properties (Young's modulus, Poisson's ratio) estimated from the density log and compressional and shear interval transit time logs from CSS #1 with confirmation of elastic properties from triaxial compressive strength testing of CSS #1 core samples.

Information on the seismic history of the area, including the presence and depths of seismic sources, and a determination that the seismicity will not interfere with containment [40 CFR 146.82(a)(3)(v)]

PCC searched two seismic event databases and found three recorded events with a local magnitude (M_L) of 2.7 M_L or greater in Russell County. These occurred between 2018 and 2022 – two 2.8 M_L events located more than 16 miles from CSS #1, and one 2.7 M_L event located approximately 11.4 miles away from CSS #1. PCC found over forty additional records for seismic events less than 2.7 M_L in Russell County.

PCC believes the risk of a seismic event occurring with sufficient intensity to interfere with containment for the GS project is low, mitigated by the following factors:

- Favorable Seismic History – Records show little evidence of past events in the area with sufficient intensity to damage infrastructure.
- Favorable Site Stratigraphy – The stratigraphic column at CSS #1 provides confining layers both above and below the injection zone, plus the Reagan Sandstone layer beneath the lower confining layer serves as a dissipation interval to further mitigate the impact of seismic events on containment. The Arbuckle Group has been the focus of multiple regional studies since it has been identified as a primary target for carbon sequestration.
- Modest Injection Rate – The GS project injection rate is up to 150,000 metric ton per year = 3,200 barrels per day (bpd), which is modest when compared to total injection rates for existing Class II wells within Russell County.

- Integrated Testing and Monitoring Plan – The plan contains integrated mechanical integrity testing and monitoring elements to assure the GS project wells are in suitable mechanical condition to withstand expected seismic intensities over their service life. The plan also integrates elements for continuous monitoring of two regional earthquake monitoring networks and a dedicated passive seismic system to track micro-seismic events across the GS site, which together provide timely information to properly manage GS project operations.
- Aligned Emergency and Remedial Response Plan – The Emergency and Remedial Response Plan defines suitable actions to be followed in case of a seismic event and is aligned with the response plan delineated in the Kansas Seismic Action Plan that state-level agencies follow for regulation of Class I through V wells in Kansas.

Maps and stratigraphic cross sections indicating the general vertical and lateral limits of all USDWs, water wells, and springs within the AoR, their positions relative to the injection zone(s), and the direction of water movement (where known) [40 CFR 146.82(a)(5)]

The Dakota Formation outcrops in eastern Russell County in the low-lying valleys associated with the Smoky Hill River, Saline River, and Cedar Creek systems. Springs and seepages are known to occur where these valley systems erode into the top of the Dakota. The general horizontal groundwater flow direction is toward the east to northeast on a regional and local basis. The vertical groundwater flow direction is typical downward from the shallow aquifers into the underlying Dakota formation, except where these overlying units are absent, and the Dakota formation outcrops. Due to the high total dissolved solids (TDS) content in the Dakota, this formation is used mainly for agricultural purposes and limited potable consumption. Few water wells occur within the areal extent of the AoR, and fewer still penetrate the Dakota - the bottom of the deepest water well within the areal extent of the AoR is over 3,000 ft above the Arbuckle.

Baseline geochemical data on subsurface formations, including all USDWs in the AoR [40 CFR 146.82(a)(6)]

Site-specific baseline geochemistry data have been collected for the Dakota Formation groundwater (lowermost USDW), the Water Table aquifer groundwater, the vadose zone, and at ground surface since the Fall of 2022. Collectively, these are referred to as the "Shallow Zones". Groundwater in the Dakota is relatively hard, has a high TDS, and exhibits variable salinity content. "Deep Zones" are those below the Dakota Formation (lowermost USDW), for which data collection started with pre-operational testing of CSS #1. These data will be used as a baseline for comparison of groundwater samples taken during the Injection and PISC periods to monitor for changes in groundwater quality that could warn of unanticipated movement of formation fluids or non-containment of carbon dioxide (CO_2).

Data to support a demonstration to the Project Director of site suitability for the GS project with respect to injection zone and confining zone(s) properties [40 CFR 146.83]

PCC believes the site is suitable for the GS project. The injection zone is of sufficient areal extent, thickness, porosity, and permeability to receive the total anticipated volume of the carbon dioxide stream. The computational model, which is based upon site-specific reservoir properties,

predicts the AoR is an inverted irregular circular cone with an areal extent of 3.1 mi^2 for a total injection of 1.8 million metric ton CO_2, resulting in a storage capacity of 580,000 metric ton CO_2/mi^2. There is confinement with sufficient areal extent and integrity to contain the injected carbon dioxide stream and displaced formation fluids and allow injection at proposed maximum pressures and volumes without initiating or propagating fractures in the confining zones.

A.I.2. Regional Geology, Hydrogeology, and Local Structural Geology [40 CFR 146.82(a)(3)(vi)]

A thorough evaluation of regional geology, hydrogeology, and local geology is presented using geologic maps, topographic maps, and cross sections. The full stratigraphic sequence from ground surface to Precambrian basement is provided, along with hydrogeologic units and their associated structures. In the vicinity of the geologic sequestration (GS) site, the shallow geologic units include a series of interbedded shales, limestone, and sandstone formations. The corresponding aquifer systems generally include a shallow (water-table) aquifer, and the Dakota Aquifer (aka Great Plains aquifer) that is the lowermost USDW in the region.

Particular attention is given to the Arbuckle Group (gross injection interval within the Arbuckle of 3,448 to 3,606 ft bgs) since it contains the target injection zone, and also provides the primary upper confining layer and a lower confining unit. The majority of the Arbuckle Group is composed of porous carbonates. Additionally, the Arbuckle injection zone is vertically separated from the lowermost USDW by a thickness of approximately 2,900 feet (ft) that includes multiple confining units comprised of multiple shale sequences plus thick anhydrite and salt zones. Detailed information is provided on the Arbuckle Group depositional setting, geologic structure, and the regional aquifer system associated the group (extent, salinity, hydraulic head, groundwater velocity, and groundwater temperatures). The Lansing (2,993 to 3,503 ft bgs) and Kansas City Groups (3,053 to 3,133 ft bgs) provide a potential second injection zone for permitting at a later date.

The planned CO_2 injection and monitoring area is east of Russell, Kansas (Figure A.I.2-1) within the Smoky Hills physiographic province. The landscape has a mantle of Quaternary loess, sometimes missing due to erosion (Figure A.I.2-2). Rock outcrops in the area generally include chalks and shales. Across the Central Kansas Uplift are sequences of sedimentary rocks containing fresh to saline fluids and two discrete hydrocarbon systems.

Figure A.I.2-1. Topographic Map
Modified From: 2013 National Geographic Society

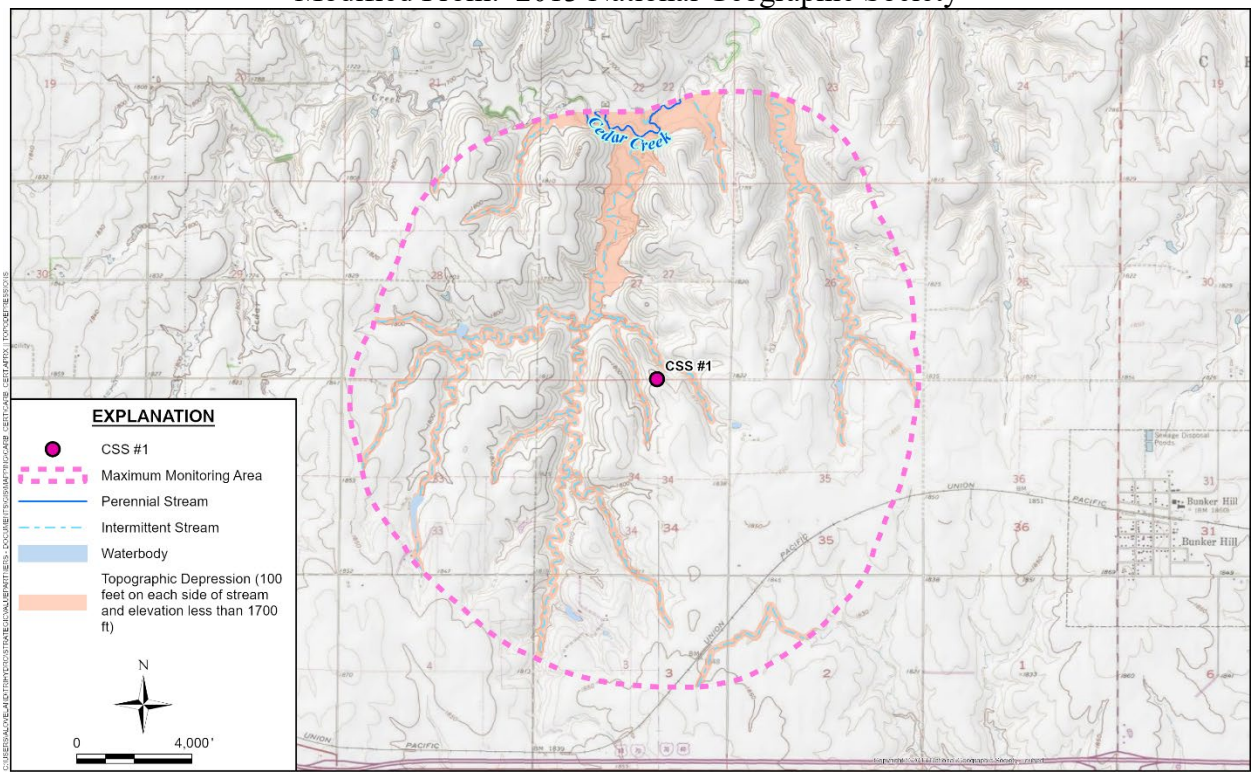

Figure A.I.2-2. Surface Geology Map
Modified From: Johnson and Arbogast 1996

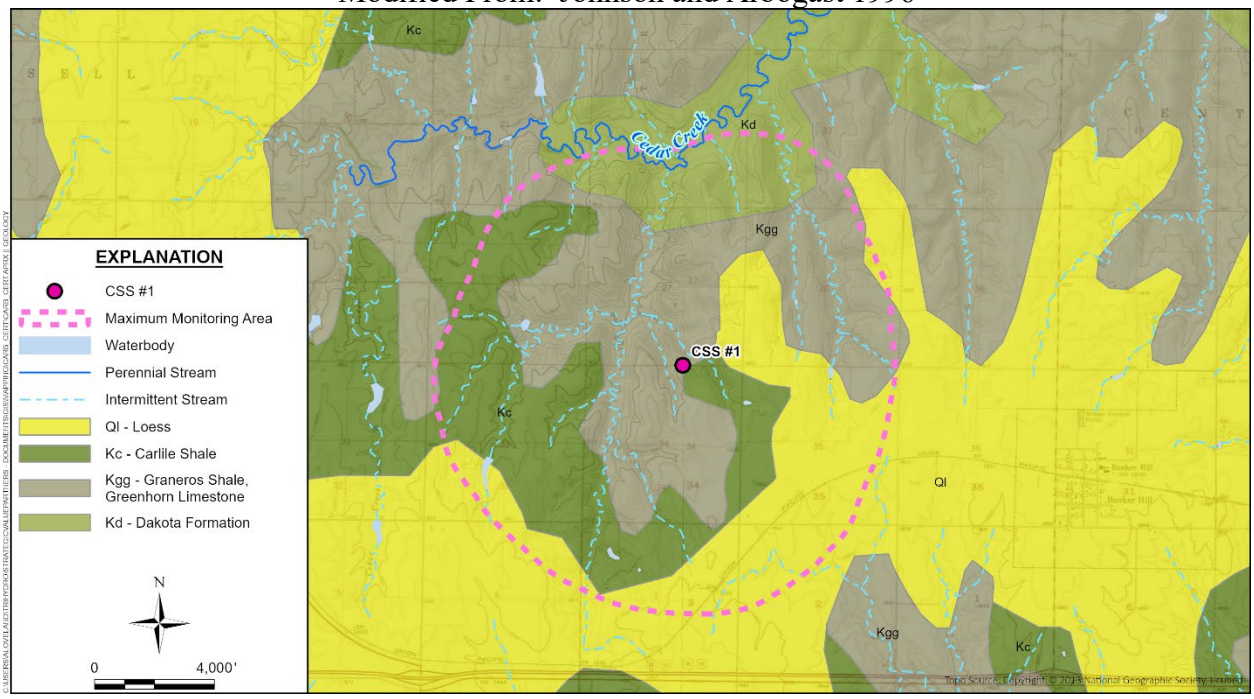

A.I.2.1. Overview of Full Stratigraphic Sequence from Ground Surface to Precambrian Basement

The sedimentary section in Kansas ranges from 560 to 10,800 ft thick. Most of these sedimentary layers were deposited on a shallow-shelf marine environment during the Paleozoic (Franseen et al., 2004; Watney, 1980; Watney et al., 2008), with additional deposition occurring as part of the Western Interior Seaway during the Cretaceous. Much of the stratigraphic sequence in central Kansas was affected by the structural development of the ancestral Central Kansas Uplift (CKU) which started in the early Paleozoic. Russell County, Kansas is intersected from the northwest to the southeast by the CKU as illustrated on Figures A.I.2-3 and A.I.2-4. The uplift resulted in removal of Mississippian strata at the GS site, such that the Arbuckle Group is overlain by Pennsylvanian age strata. The Kansas Geological Survey's type log for Russell County indicates the Arbuckle Group is immediately overlain by the Marmaton Group.

Sedimentation on and nearby the CKU was interrupted several times by several major unconformities that significantly altered the stratigraphic sequence (Merriam, 1963) and led to relatively thicker sediments in the Salina Basin than thicknesses typically observed along the CKU. These unconformities were seen in the stratigraphic column at CSS #1 with the absence of the Mississippian-aged strata.

Figure A.I.2-3. Generalized Structural Features of the Mid-Continent
Modified From: Merriam 1963, and Jorgensen et al. 1993

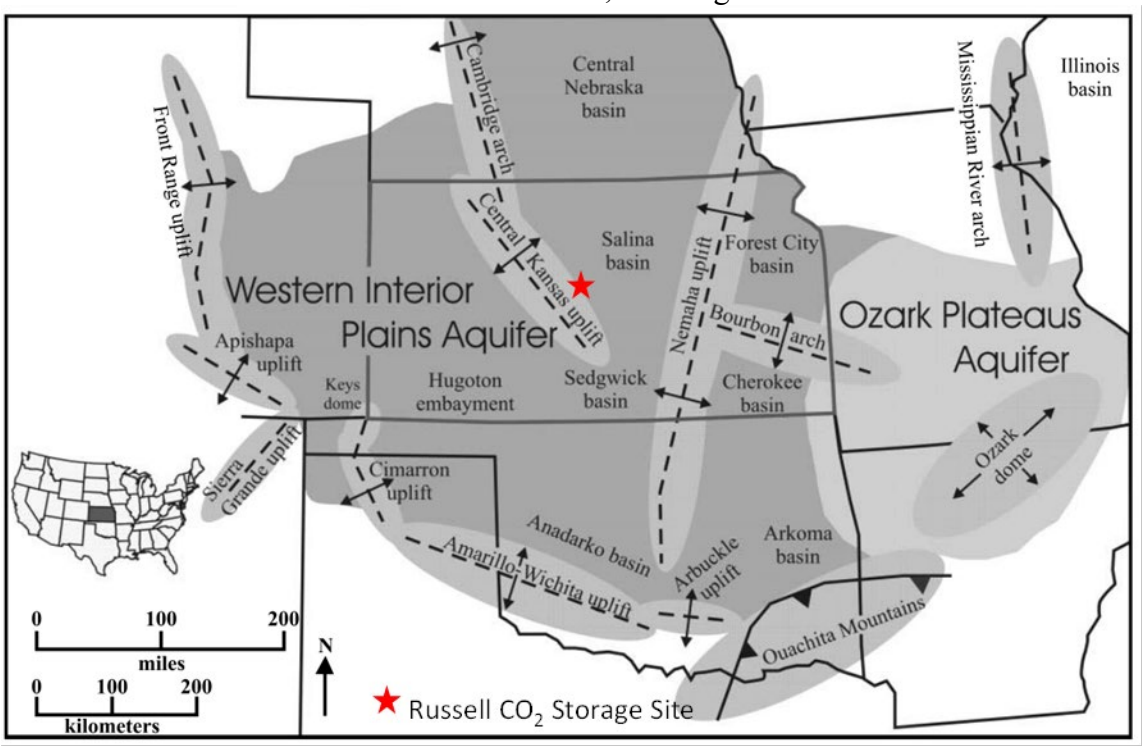

Figure A.I.2-4. Geologic Structure Cross Section through Central Kansas Uplift

From: Franseen 1999

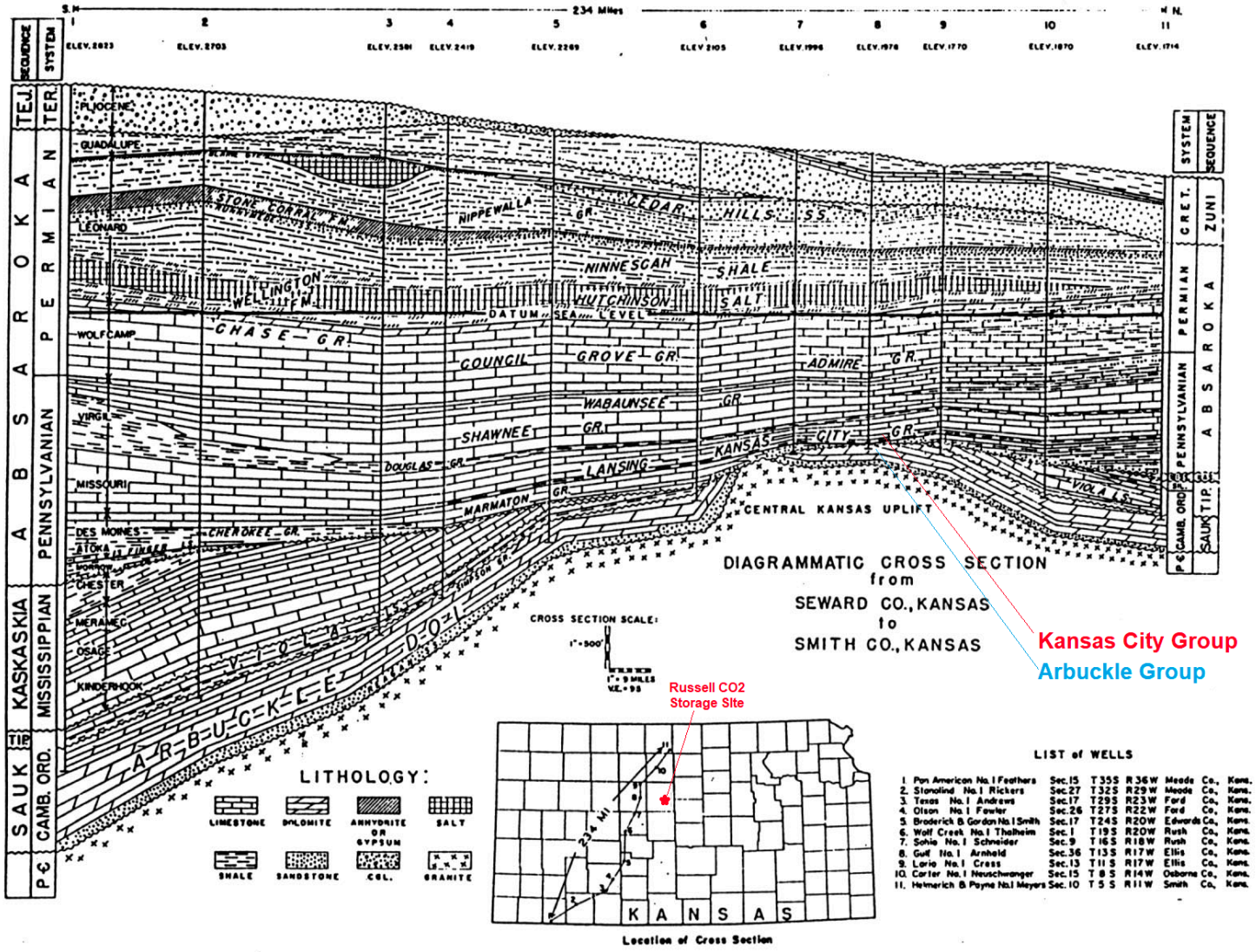

Table A.I.2-1 lists regional stratigraphy, with green boxes identifying geologic layers that are present at the GS site. Quaternary and Tertiary stratigraphic units are generally not present due to erosion and washout in recent geological time. Absent stratigraphic units immediately below the lower Cretaceous are related to regional pinchouts and spatial variability. Absent Mississippian stratigraphic units are due to the CKU that created subaerial exposure and removal, thus forming an unconformity between the Marmaton Group and the Arbuckle Group.

Stratigraphic descriptions are from multiple regional references, including the Kansas Geological Survey, as well as from the lithologic information collected during the drilling of the CSS #1. The surface at CSS #1 is comprised by the Fairport Member of the late Cretaceous Carlile Shale as shown on Figure A.I.2-2. This is generally present to a depth of approximately 20 to 30 ft bgs in the area. It is a calcareous shale with thin beds of chalk. The Greenhorn Limestone underlies the Fairport Member and is comprised of siliceous shale, chalk, and limestone members. The Graneros Shale, a silty shale, underlies the Greenhorn. The Dakota Formation is composed of variegated and gray clay, sandy shale with evenly bedded sandstone, and lenses of cross bedded sandstone. The Kiowa Shale and Cheyenne Sandstone, along with the Dakota Formation above it, comprise the Great Plains Aquifer System. In some literature, these three formations may be identified as just the "Dakota" or the "Dakota Aquifer." Moving down into Upper Permian, the Nippewalla Group is made up of classic red shales with interbedded silts and sands (495 to 769 ft bgs). The Sumner Group (769 to 1,529 ft bgs) beneath the Nippewalla Group contains the Stone Corral Anhydrite, the Ninnescah Shale, and the Wellington, which contains the Hutchinson Salt Member. The Nippewalla through Marmaton stratigraphic units listed in Table A.I.2-1 comprise the Western Interior Plains Confining System in the AoR. Multiple shale layers, along with anhydrite and salt, provide confinement between the Dakota Aquifer and the Arbuckle Group. A portion of the Arbuckle Group will be the injection zone. The Cambrian-age Reagan Sandstone underlies the Arbuckle and overlies the Precambrian basement and provides a dissipation zone. The Reagan Sandstone is also called the Basal sand and the LaMotte Sandstone.

The Precambrian (Proterozoic) basement is present beneath the Reagan Sandstone (Figure A.I.2-5). It is found at shallower depths along structural highs such as the Nemaha anticline and the Central Kansas Uplift. It dips from north to southeast of the Nemaha Ridge and was encountered at a depth of 3,735 ft bgs in the CSS #1. Several different types of basement rock are found in Central Kansas; the basement was found to be quarzitic at the CSS #1 location.

Table A.I.2-1. Stratigraphic Units from the Quaternary/Neogene to the Precambrian/Cambrian Basement Rocks

From: Carr et al. 1986

Geohydrologic unit		Principal stratigraphic unit(s)	Time-stratigraphic unit
High Plains aquifer		Ogallala Formation and unconsolidated deposits	Quaternary and Tertiary
Great Plains confining system		Pierre Shale, Niobrara Formation, Carlile Shale, Greenhorn Limestone, Graneros Shale (includes Lower Cretaceous)	Upper Cretaceous
Great Plains aquifer system	Maha aquifer	Dakota Sandstone, "D" sandstone, "J" sandstone, and equivalent of Newcastle Sandstone	Lower Cretaceous
	Apishapa confining unit	Kiowa Shale and equivalent of Skull Creek Shale	
	Apishapa aquifer	Cheyenne Sandstone and equivalent of Fall River and Lakota Sandstones	
Western Interior Plains confining system		Morrison Formation, Sundance Formation, Entrada Sandstone, Dockum Formation, Elk City Sandstone, Doxey Shale, Big Basin Sandstone, Cloud Chief Formation, Day Creek Dolomite, Whitehorse Sandstone, Nippewalla Group, Sumner Group, Chase Group, Council Grove Group, Admire Group, Wabaunsee Group, Shawnee Group, Douglas Group, Lansing Group, Kansas City Group, Pleasanton Group, Marmaton Group, Cherokee Group, Atokan rocks, Morrowan rocks, and Springer Group	Jurassic through Upper Mississippian (Chesterian)
Western Interior Plains aquifer system	Upper unit	Meramecian, Osagean, and Kinderhookian rocks	Upper Mississippian through Upper Cambrian
	Confining unit	Chattanooga and Woodford Shales	
	Lower units	Hunton Group, Sylvan Shale, equivalent of Galena Dolomite, Viola Limestone, Simpson Group, Arbuckle Group, and Reagan Group	
Basement confining unit		Mostly igneous and metamorphic rocks	Cambrian and Precambrian

General Stratigraphy Present at Location

Figure A.I.2-5. Elevation to Top of Precambrian Basement Complex

Elevation in feet referenced to mean sea level (ft MSL). From: Franseen 2004

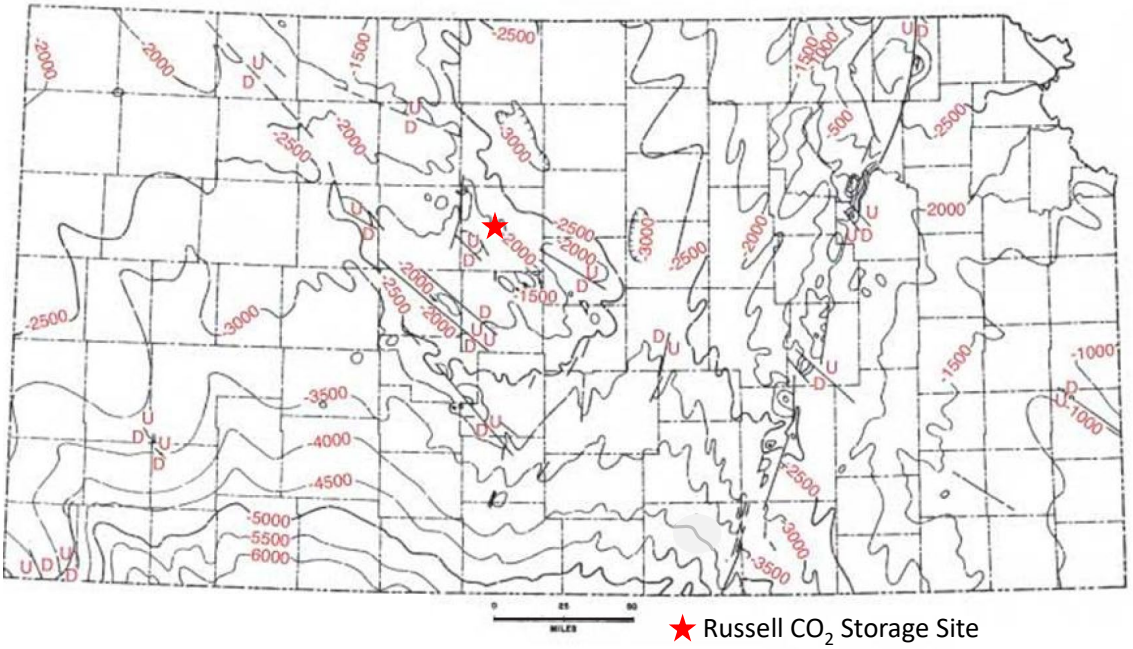

A.I.2.2. Geology and Hydrogeology of the Injection Zone: Arbuckle Group

A porous portion of the Arbuckle Group is planned for CO_2 injection. Other sections of the Arbuckle provide the primary upper and lower confinement in non-permeable lithofacies. This group is described in detail below. Many of the geologic and hydrologic characteristics of the Arbuckle Group, including the structure, salinity, hydraulic head (i.e., pressure), groundwater velocity, and temperature, are inputs to the modeling used to generate the AoR. Thus, this section is referred to in the AoR document presented later in this application.

A.I.2.2.1. Depositional Setting of the Arbuckle Group

The Arbuckle Group includes Upper Cambrian and Lower Ordovician carbonate units. The Arbuckle Group is primarily carbonate deposited about 480 million years ago during the Cambrian and Ordovician periods, and it is composed (top to bottom) of the Jefferson City/Cotter Dolomite, Roubidoux Formation, Gasconade with basal Gunter Sandstone, and Eminence Dolomite (Figure A.I.2-6). The Arbuckle Group was deposited in an epicontinental sea, and the dominant sediment deposited was calcareous mud that later lithified into limestone during periods of sea recession. Post-depositional alteration of Arbuckle limestone to dolomite occurred when freshwaters rich in magnesium and calcium mixed with the local marine waters (Jorgensen et al., 1993).

Arbuckle rocks are a part of the craton-wide Sauk Sequence which is bounded at its base and top by major inter-regional unconformities (Sloss, 1963), The sea-level fall that marked the end of Arbuckle Group deposition resulted in subaerial exposure of platform carbonates. During the early Middle Ordovician, dissolution and karst development formed a regionally extensive karst system over most of the North American craton.

A.I.2.2.2. Geologic Structure of the Arbuckle Group

The geologic structure of the Arbuckle Group is affected by uplift and subsidence that occurred episodically throughout the Phanerozoic, separated by periods of gradual deformation (Newell et al., 1989). While regionally, the location of structural features varied somewhat throughout the Paleozoic, there appear to have been consistent patterns of repeated localized uplift and subsidence (Baars and Watney, 1991). Two prominent structural uplifts that affect the Paleozoic rocks in Kansas; the Nemaha uplift and CKU, represent significant Early Pennsylvanian deformation events likely associated with similarly aged plate convergence along the Ouachita Mountains orogenic belt in Arkansas (Newell et al., 1989). This uplift and erosion locally affected Arbuckle strata, especially on the CKU where Pennsylvanian strata directly overlie Arbuckle strata or basement rocks where Arbuckle strata are absent.

Figure A.I.2-6. Arbuckle Group Units in the Stratigraphic Column

Note: Bonneterre Formation is not Present at the CO_2 Injection Site. From: Franseen 2004.

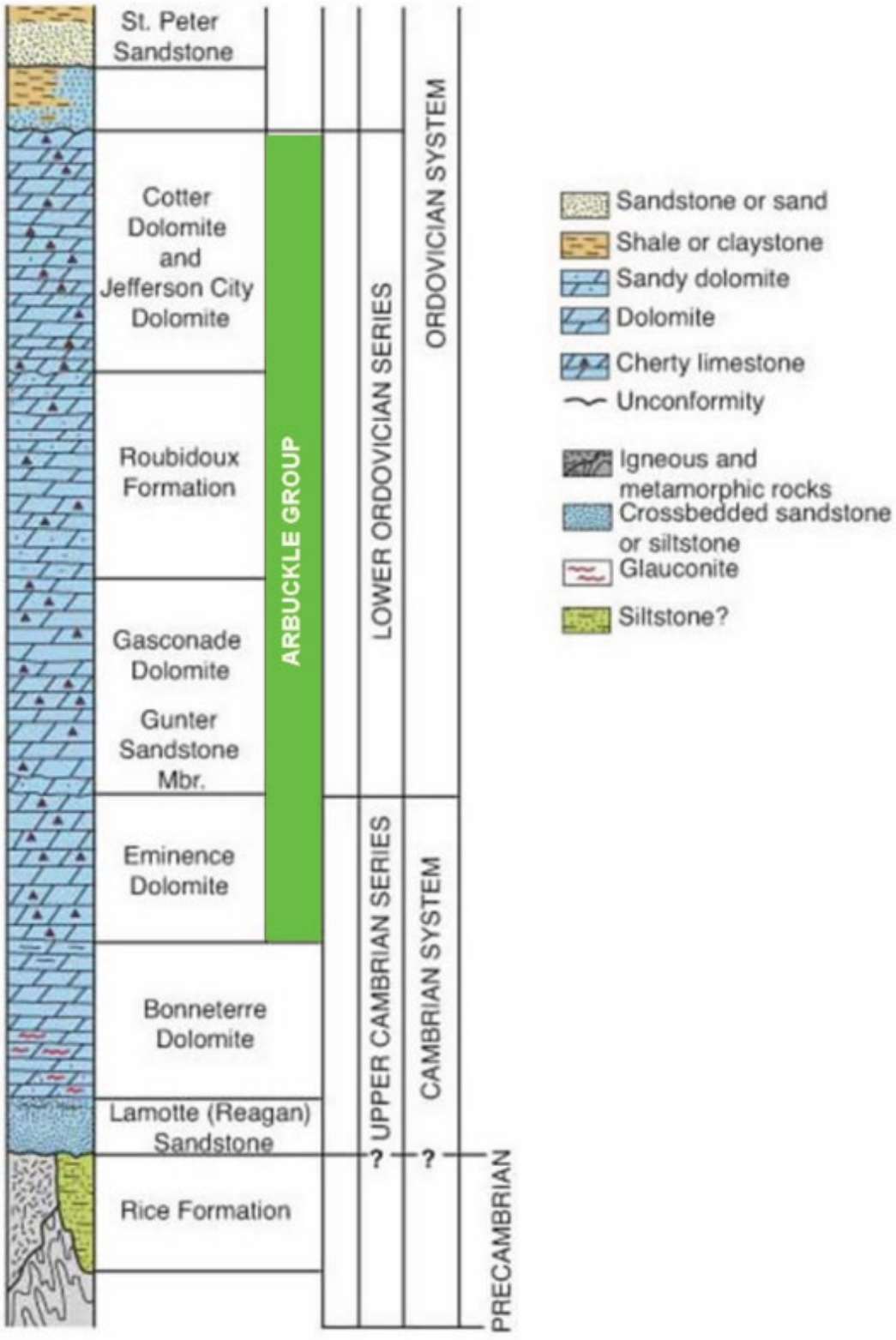

The Arbuckle and the Lansing-Kansas City Groups are the two most prolific hydrocarbon-producing units in the CKU (Gerhard, 2004). The thickness of the Arbuckle Group varies in the area due to erosion along a superjacent unconformity. The thickness of the Arbuckle Group is presented in Figure A.I.2-7. According to the geological regional context, the Arbuckle Group generally thickens as a whole from north to south and is thickest (up to 1,100 ft) in south-central Kansas.

Figure A.I.2-7. Isopach Map of Arbuckle Group Strata from Well Data
Contour Interval 100 ft. Russell Injection Site Represented with a Red Star.
From: Cole 1975

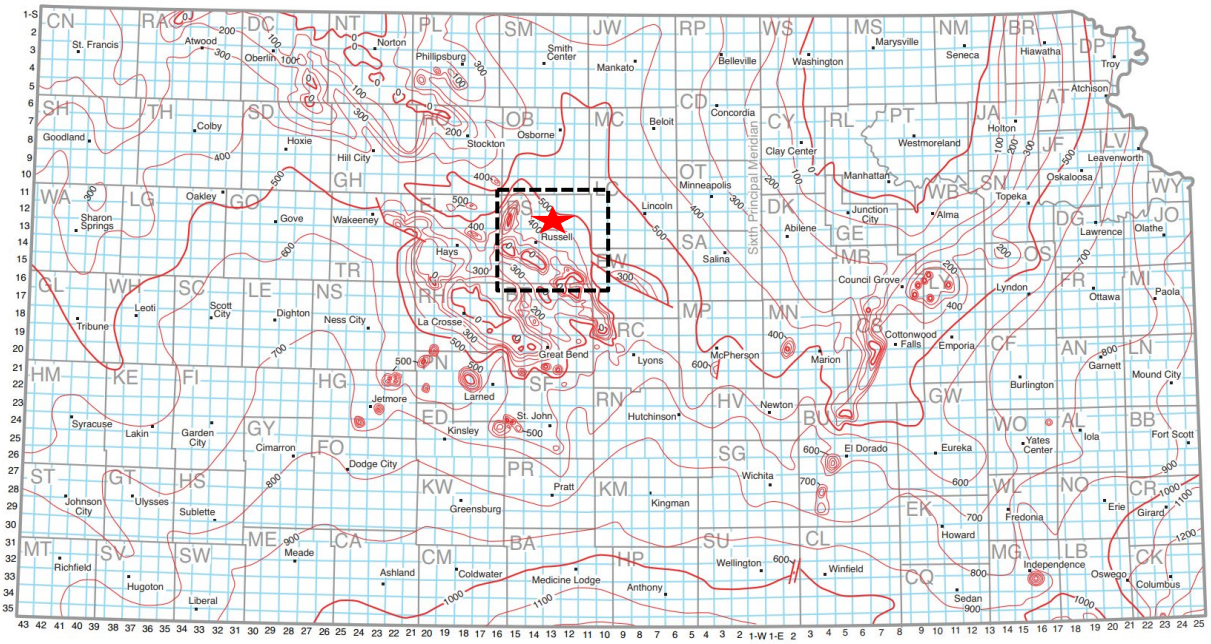

A.I.2.2.3. Regional Aquifer System Associated with the Arbuckle Group

Regionally, the lower Paleozoic aquifer systems in Kansas, Missouri, and Oklahoma comprise one of the largest fresh and saline aquifer systems in North America (Jorgensen, 1989; Jorgensen et al., 1993, 1996). These aquifer systems have been labeled as the freshwater Ozark plateau and saline Western Interior Plains aquifer systems in Kansas, Missouri, and Oklahoma (Jorgensen, 1989; Jorgensen et al., 1993, 1996). However, these two systems have been recognized as a single aquifer system and combined into the Ozark Plateau Aquifer System (Macfarlane, 2000).

The Arbuckle aquifer systems in Kansas, Missouri, and Oklahoma make up one of the largest regional-scale saline aquifer systems in North America and are present in both the Western Interior Plains aquifer system (WIPAS) and the Ozark Plateaus aquifer system (OPAS). The WIPAS, which underlies almost all of Kansas, is similar to the OPAS, which lies to the east in parts of Missouri and southeastern Kansas. Unlike the OPAS, the WIPAS is naturally saline and

yields no freshwater (Faber, 2010). Russell County lies in the WIPAS, and Arbuckle brine concentrations within the county are significantly in excess of 10,000 milligrams per liter (mg/L) salinity as discussed in the next section.

A.I.2.2.4. Salinity of the Arbuckle Group

As described below, the Arbuckle Group in the AoR is saline and not a USDW. Across Kansas, the Arbuckle TDS concentrations vary from relatively low salinity (TDS < 10,000 parts per million [ppm]) to dense brine (TDS > 250,000 ppm) as shown in Figure A.I.2-8. The salinity decreases significantly in the eastern part of the state, where the WIPAS merges with the OPAS. Another key feature of the Arbuckle salinity distribution in Kansas is the general increase in Arbuckle TDS from north to south.

Brine salinity distribution in the Arbuckle is also associated with structural features. Dense brines along the Kansas-Oklahoma border are concentrated in Arbuckle structural lows, particularly in southwestern Oklahoma. Arbuckle brine salinity slowly decreases northward and along the eastern side of the Nemaha anticline. The salinity of the Arbuckle in the vicinity of the GS site ranges from 20,000 to 50,000 ppm (Figure A.I.2-8, Carr et al., 2005). The well was swabbed on May 11, 2023 from perforations in the Arbuckle. The total dissolved solids from laboratory analysis of the water were calculated at 24,900 mg/L.

Figure A.I.2-8. Total Dissolved Solids in Arbuckle Brines

TDS in ppm, overlay is the Structure in ft MSL on Top of Arbuckle. From Carr et al. 2005

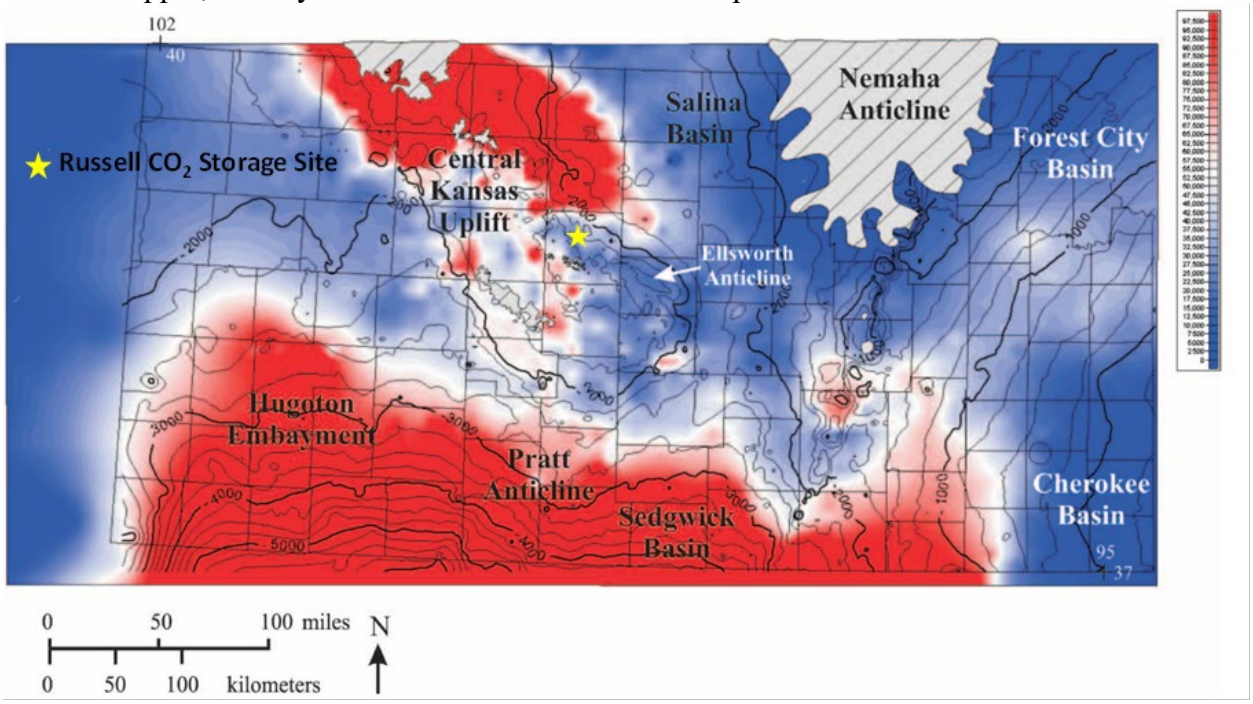

A.I.2.2.5. Hydraulic Head in the Arbuckle Group

The hydraulic head of the Arbuckle Group is relevant to Class VI permitting because the injection pressure must be greater than the hydrostatic pressure so that CO_2 moves into the injection zone. In addition, hydraulic head determines the direction of groundwater flow, which may affect injected CO_2 distribution. Finally, the hydraulic head, closely related to formation pressure, affects the phase of CO_2 (e.g., gas, liquid, or supercritical fluid) and therefore its transport behavior. Regionally, recharge occurs by way of precipitation in the Front Range of the Rocky Mountains (Figure A.I.2-9; Jorgensen et al., 1993). Minimal, if any, recharge occurs vertically from overlying aquifers. As groundwater travels east toward Missouri, bedded halite in the Permian confining unit of WIPAS is dissolved into the aquifer, giving the water its characteristically high salinity (Faber, 2010). The eastward-flowing water discharges into the OPAS, where a number of saline springs and artesian wells have developed in Paleozoic carbonates (Jorgensen et al., 1993).

The boundary between the WIPAS and the OPAS, marked by a low in the equivalent freshwater head (equivalent freshwater head is the height in a column filled with freshwater at the measuring elevation) surface as shown in Figure A.I.2-10, is nearly coincident with the topographic low in eastern Kansas and northeastern Oklahoma (Figure A.I.2-11).

Figure A.I.2-9. Major Geohydrologic Units in the Plains and Ozark Subregions
Section extends from central Colorado to St. Francois Mountains in southeastern Missouri.
From: Jorgensen et al. 1993

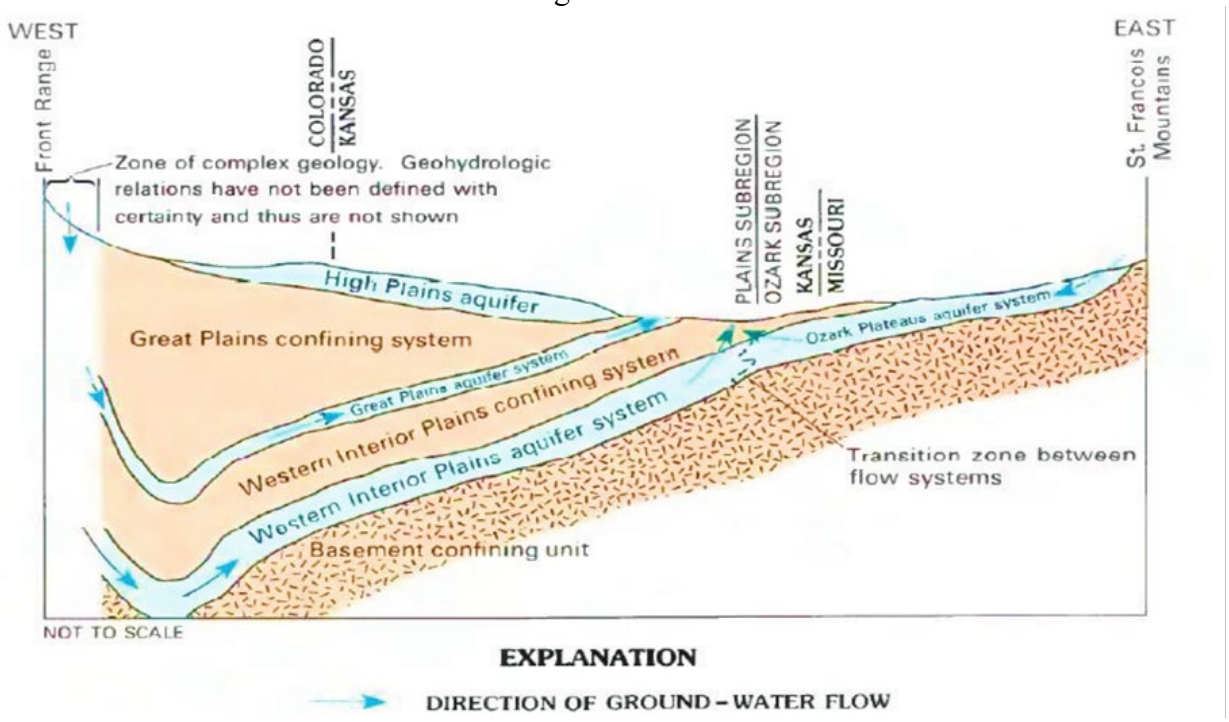

Figure A.I.2-10. Equivalent Freshwater Heads in Cambrian and Ordovician Rocks

From: Jorgensen et al. 1993

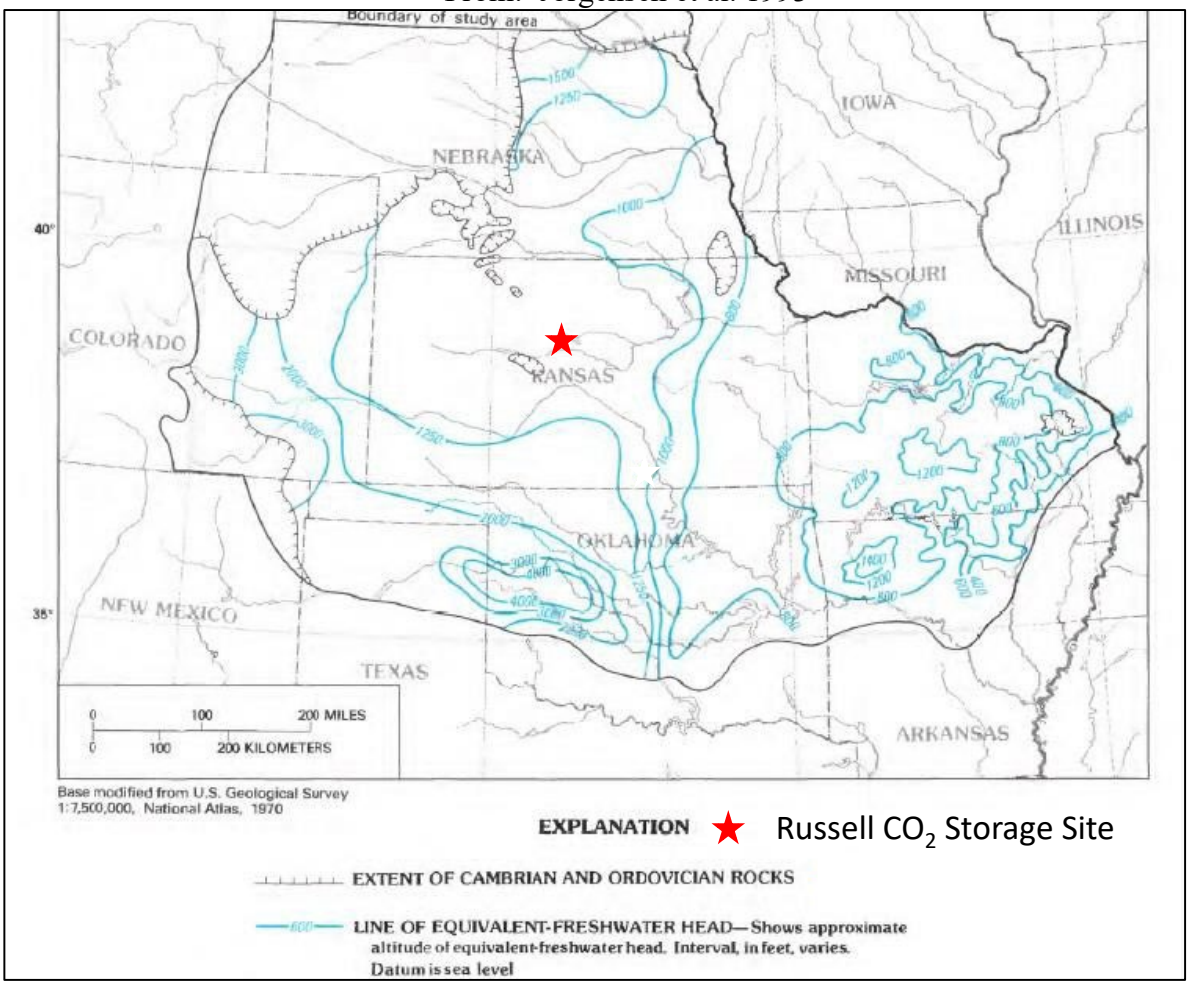

Figure A.I.2-11. Topographic Contours Showing Altitude of Land Surface
Contours in ft MSL. From: Jorgensen et al. 1993

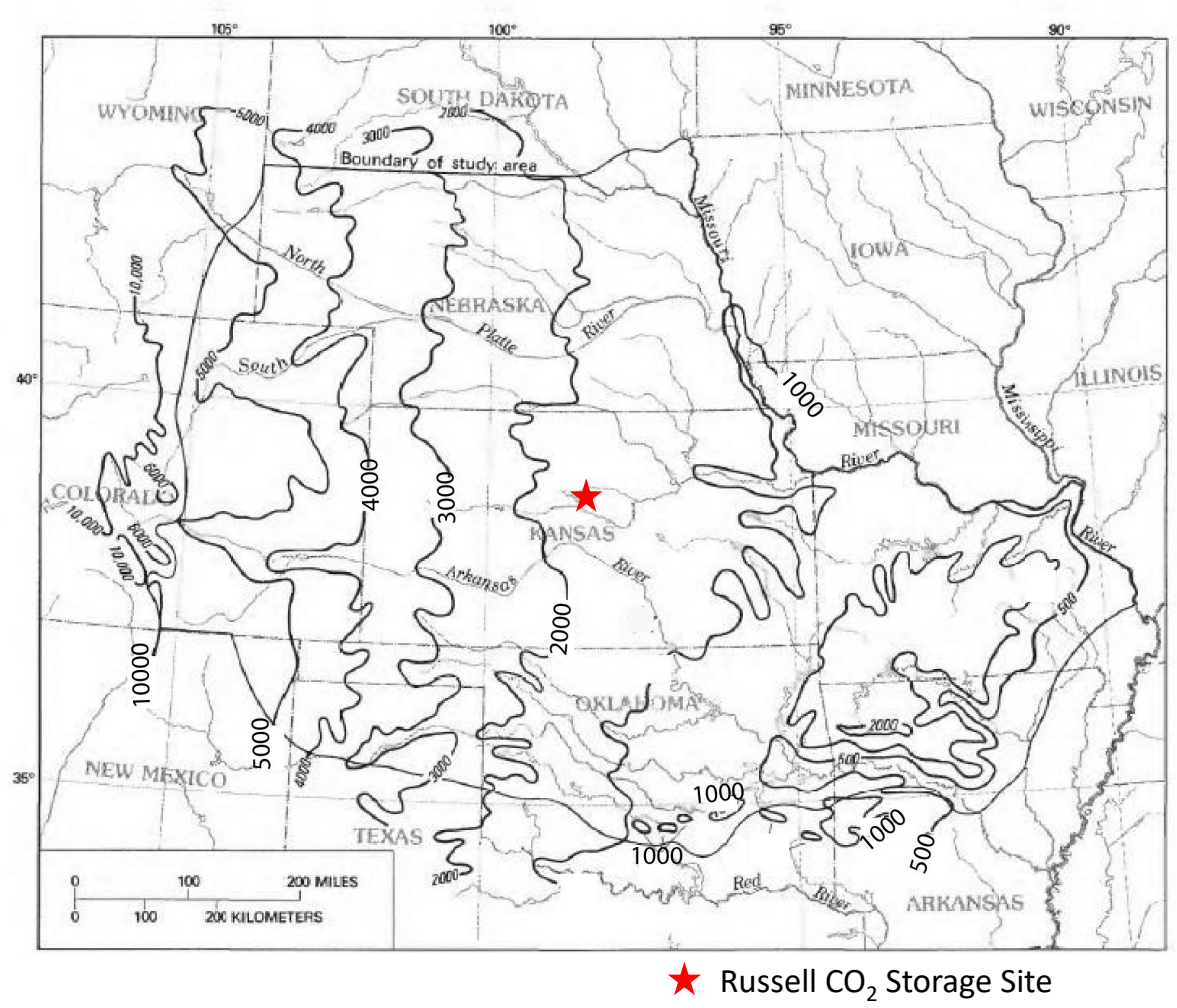

A.I.2.2.6. Groundwater Velocity in the Arbuckle Group

The groundwater velocity of the Arbuckle Group is relevant to Class VI permitting because the injected CO_2 distribution may be affected by groundwater movement. On a regional basis in the Arbuckle Group, groundwater flows from west to east, as shown in the potentiometric surface map presented in Figure A.I.2-12 (Newell et al., 2020). Arbuckle disposal wells in Kansas collectively dispose of roughly 800,000,000 barrels (bbl) (roughly 127,000,000 cubic meters) of wastewater per year, although some of this is recycled from Arbuckle oil production. Declines in oil price since mid-2014 have resulted in reduced oilfield disposal in the Arbuckle since 2015. The number of Class I wells recording annual fluid rises have also declined since 2015, as has the median of their annual change in static fluid level, but overall, more Class I wells are still recording fluid rises. There is a poor correlation between changes in fluid levels in Class I wells and the volume of fluid disposed in them annually, thereby indicating that more regional characteristics may control water movement in the Arbuckle (Newell et al., 2020).

Groundwater velocity is estimated to be very slow. The head in Russell County drops approximately 50 ft over 20 miles (Figure A.I.2-13), resulting in a head gradient of approximately 4.7e-04 feet per foot. Assuming an average large-scale Arbuckle porosity of approximately 6% and an average permeability of 10 millidarcy (mD), the pore velocity in the Arbuckle is approximately 0.2 ft per year, which is fairly small. These numbers are likely on the conservative side.

Figure A.I.2-12. Arbuckle Potentiometric-Surface Map for 2017

Normalization of the thickness of the water columns in an Arbuckle well to water with freshwater fill (i.e., a density of 1.0 grams per cubic centimeter [g/cc]) yields a map that shows direction of movement of Arbuckle Group water from west to east.

Note: Not all Class I and Class II wells within Kansas are displayed on this map.

From: Newell et al. 2020

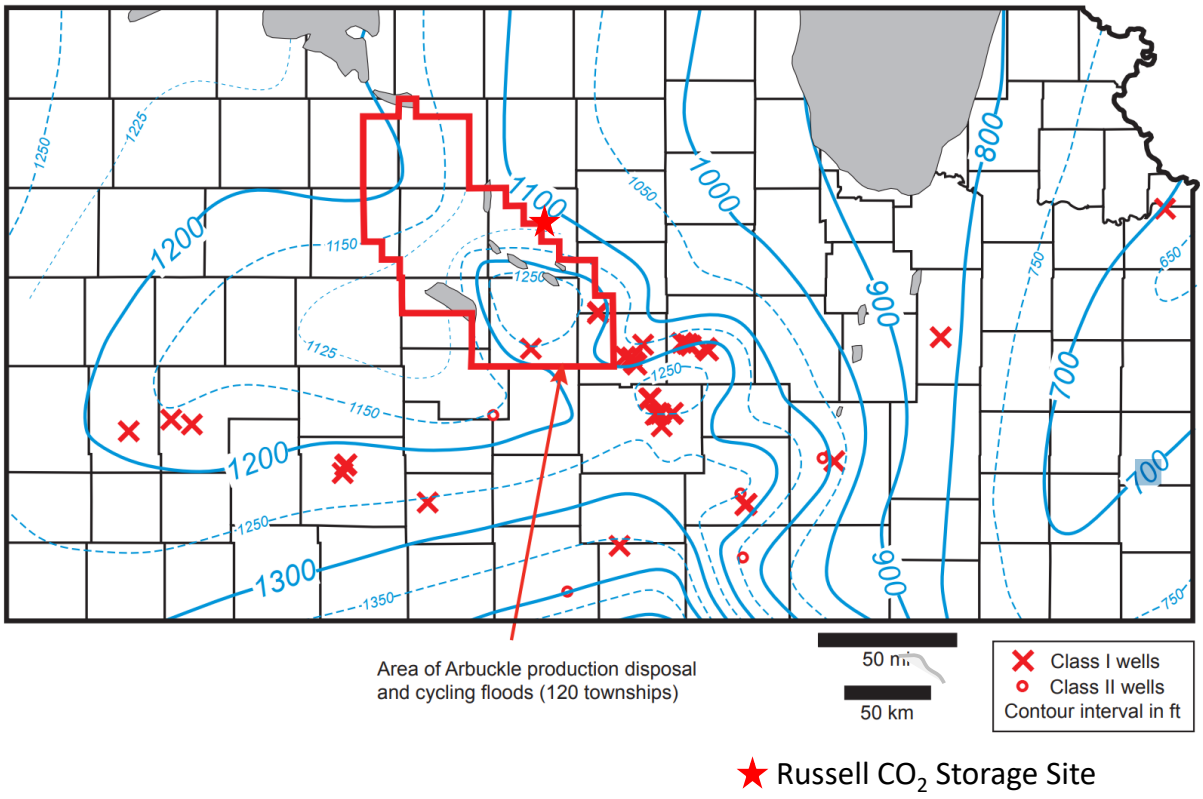

Figure A.I.2-13. Static Fluid Level Elevations for Arbuckle Wells for 2017
The static fluid level is dependent on the density of formation fluid, which markedly varies across Kansas. From: Newell et al. 2020

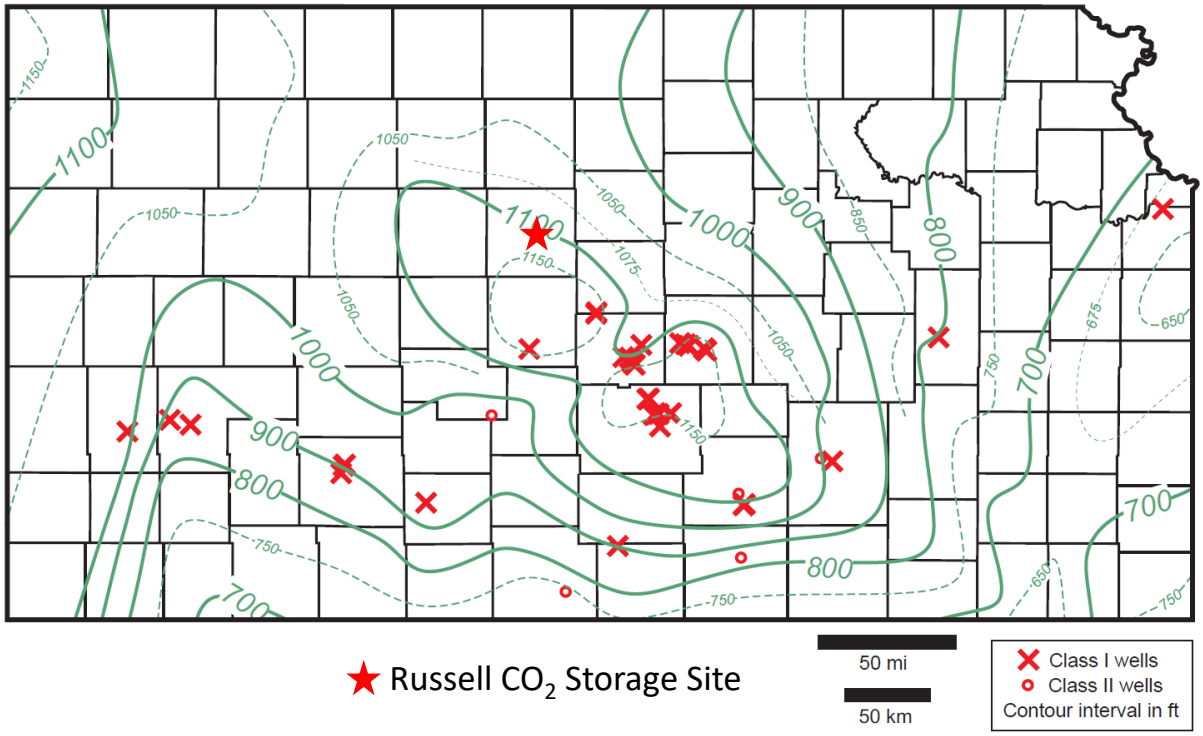

A.I.2.2.7. Arbuckle Groundwater Temperatures

The temperature of Arbuckle Group groundwater is relevant to Class VI permitting because it affects the phase of CO_2 (e.g., gas, liquid, or supercritical) and therefore its transport behavior. Figure A.I.2-14 shows a map of borehole temperatures in the Arbuckle Group along with the measured depth to the top of the Arbuckle. The map shows a strong relationship between temperature and depth.

A temperature gauge with datalogger was installed in CSS #1 for a few months after drilling while the well was configured as a stratigraphic test well. The temperature gauge was installed at a depth of 3,602 ft KB. The reading was a consistent 110 °F. These field results agreed with the regional data presented in Figure A.I.2-14.

Figure A.I.2-14. Map of Borehole Temperatures in Arbuckle Group
Contours represent depth to top of Arbuckle in ft MSL. From: Carr et al. 2005

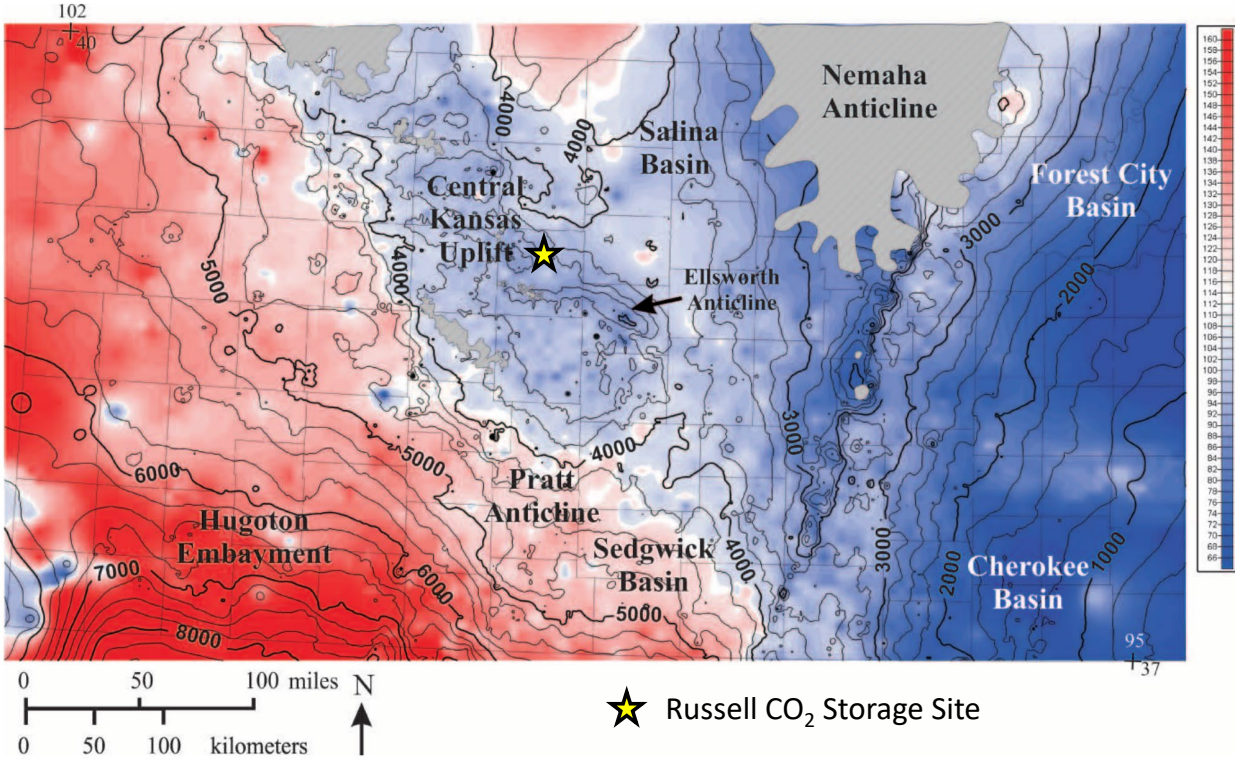

A.I.3. Maps and Cross Sections of the AoR [40 CFR 146.82(a)(2), 146.82(a)(3)(i)]

Data from a combination of CSS #1 well logs, adjacent well logs, and information from the baseline 3D seismic survey were used to create structural cross sections, seismic cross lines, and isopach maps to aid in the evaluation of the AoR and its vicinity. The assessment indicates that both the sequestration interval and the confining units are present and continuous across the AoR, and the site and its vicinity are characterized by uninterrupted flat-lying stratigraphy.

Two structural cross sections of the AoR and vicinity were constructed using well logs from CSS #1, the Kansas Geological Survey's (KGS) type log for Russell County, and several wells with the stratigraphically deepest penetrations in the area. These cross sections are submitted as supporting information in the Geologic Sequestration Data Tool (GSDT) Project Information Tracking module under the file names PBI_StructCrossSection_SN.pdf and PBI_StructCrossSection_WE.pdf. One file contains the South to North structural cross section, the other contains the West to East structural cross section; both cross sections cover from TD to surface of wells adjacent to and through the AoR. The cross sections illustrate the lateral and vertical consistency of confining formations throughout the stratigraphic column. Only a few formations were not present from the type log (located a few townships south) vs. the CSS #1 logs. The stratigraphic column in the AoR and local area is dominated by shale-carbonate depositional sequences. The top of the Arbuckle in the county type log is shown as being on

located on the main carbonate body of the Arbuckle. Several formations are very consistent above the Arbuckle on the type log compared to the CSS #1 logs; however, the main carbonate body of the Arbuckle starts deeper. There is a higher gamma ray section at the top of the group. Regional structural mapping on 25 ft contours by the KGS support placing the top of the group correlative in thickness to the county type log vs dropping it to the top of the blocky carbonate, which is hereby referred to in figures and text as 'main Arbuckle'.

The continuous nature of the formations in the AoR and vicinity is also indicated by a series of seismic cross lines through the AoR, submitted as supporting information in the GSDT Project Information Tracking module under the file name: PBI_SeismicCrossLines.pdf. The first six cross lines are equal spaced parallel West to East lines, the last six are equal spaced parallel South to North lines. Additional discussion of the baseline 3D seismic survey is provided in Section A.I.5.3.

No gross isopach map was generated, as the main Arbuckle is a fairly consistent thickness across the AoR based on both seismic analysis and area well logs. The injection interval isopach, which is approximately 158 feet thick, is shown on Figure A.I.3-1 and ties to the log and interval on the last seismic line provided in PBI_SeismicCrosslines.pdf.

Figure A.I.3-1. Injection Interval Isopach in Arbuckle

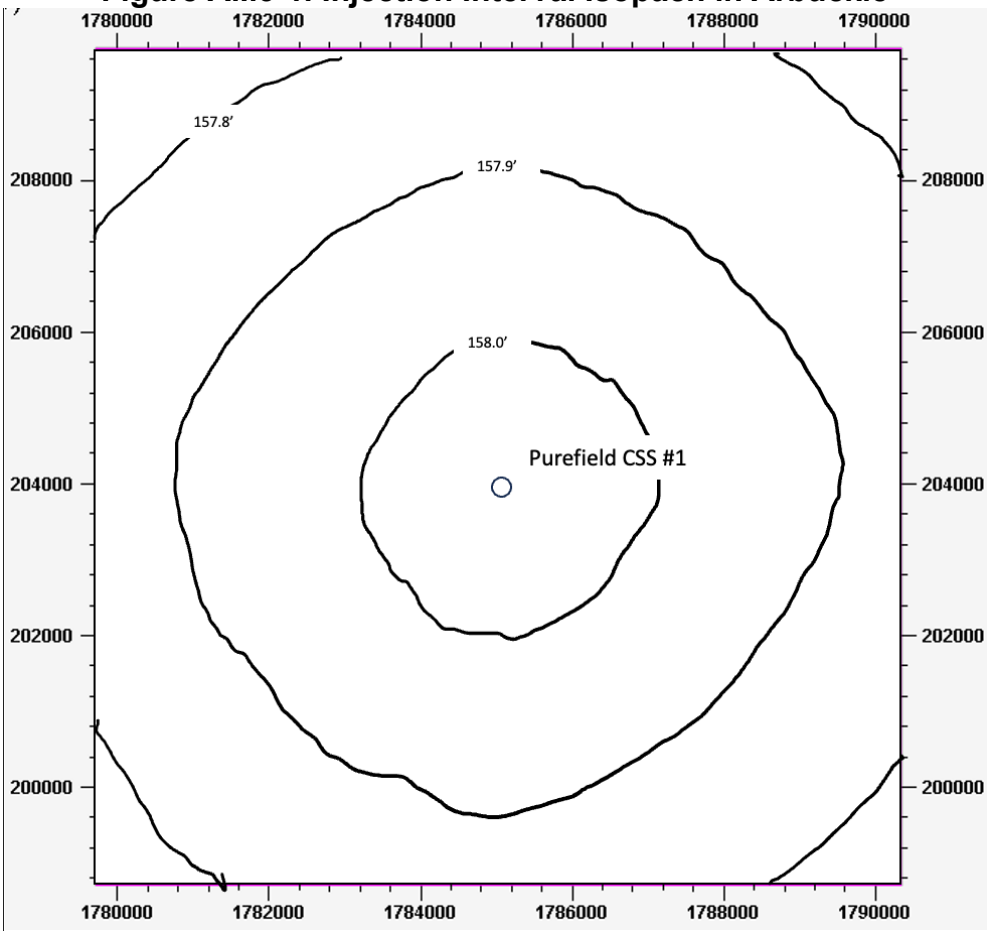

A plan view of the entire Arbuckle in the AoR and surrounding townships along with correlative structural cross sections, is shown on Figure A.I.3-2. This also demonstrates the consistency of the thickness of the Arbuckle and its internal intervals.

Figure A.I.3-2. Main Arbuckle Thickness in Vicinity of CSS #1

Red box indicates area for baseline 3D seismic survey

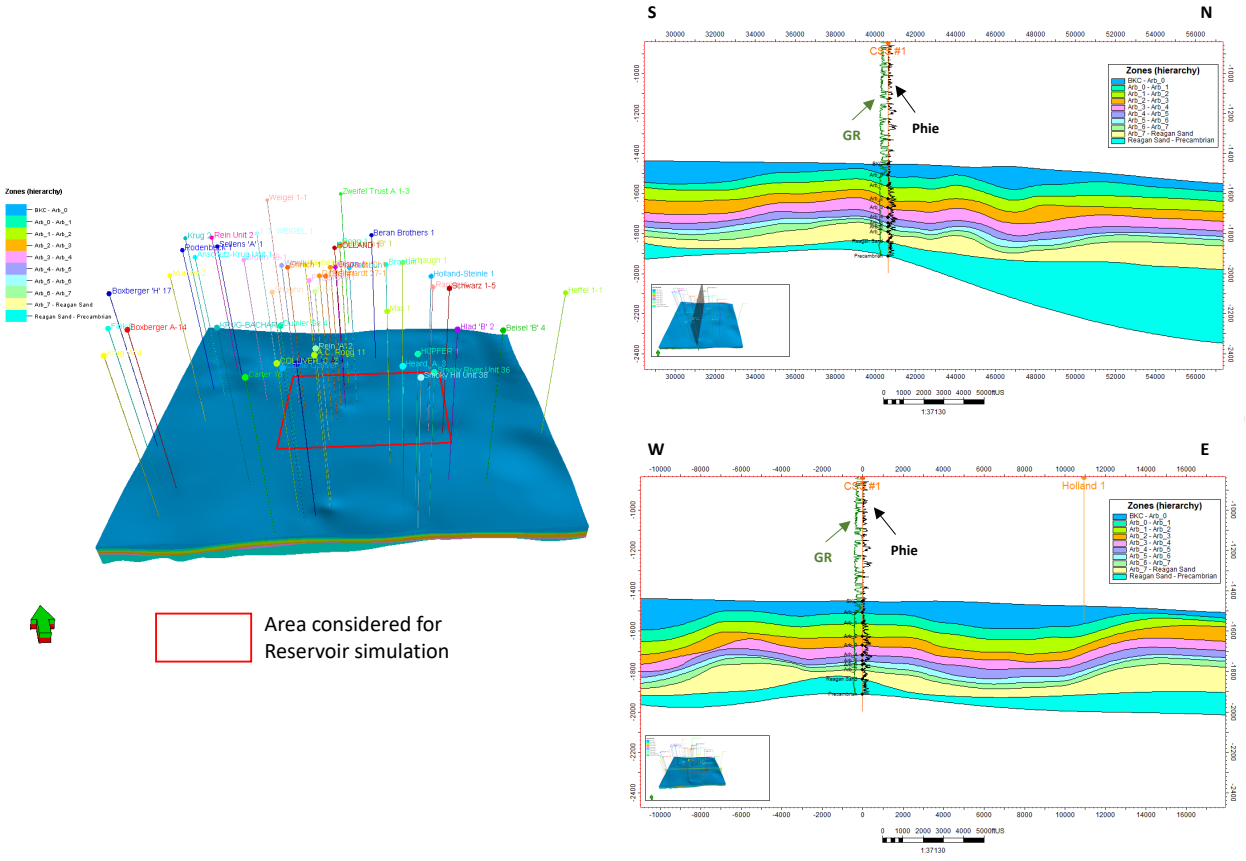

A.I.4. Faults and Fractures [40 CFR 146.82(a)(3)(ii)]

No faults or fractures have been identified in previous studies that are large enough to offset strata within the study area, and none are noted that would likely affect confinement between the Arbuckle injection interval and the USDWs.

Strata in the area were affected by the rejuvenation of basement structures that resulted in fractures, regional uplifts, and minor horst and graben features as shown in Figure A.I-4-1 (Baars and Watney, 1991). The Arbuckle and equivalent reservoirs in the Mid-Continent are generally considered to have favorable reservoir qualities that are directly related to rejuvenated basement structural elements resulting in intraformational fractures, regional uplifts, and minor horst and graben features. Reservoir qualities were modified by karst processes during prolonged and repeated subaerial exposure that began after Arbuckle deposition and continued in some areas until the Pennsylvanian (Franseen et al., 1995).

PCC utilized six different methods to identify faulting and fracturing:

- Literature review for the region.
- Analysis of the site-specific baseline 3D seismic survey conducted by the project.
- Analysis of results obtained from drilling of CSS #1 as a stratigraphic test well.
- Results from the 3D Far-Field Sonic analysis derived from multi-mode array sonic measurements taken in CSS #1 (175 ft radius around wellbore).
- Analysis of results from the Formation Micro-Imager (FMI) log obtained from CSS #1.
- Analyses of core samples taken from CSS #1.

The closest fault found from the literature review is located approximately 4 miles southeast of Russell as shown in Figure A.I.4-1 (the location of CSS #1 is represented with a red star). Stress indicators and seismic hazards are displayed in Figure A.I.4-2a (Levandowski et al., 2018). The Arbuckle and equivalent reservoirs in the Mid-continent are generally considered to have favorable reservoir qualities, some of which are related to rejuvenated basement structural elements (Baars and Watney, 1991).

A baseline 3D seismic survey of the AoR and surrounding area was conducted by PCC in 2022. No faults were identified during the analysis of this data set. More discussion on results from the baseline seismic survey is provided in Section A.I.3 and Section A.I.5.3.

No faulting was noted during the drilling of CSS #1, in the baseline 3D seismic survey, or in the 3D Far-Field Sonic analysis conducted by SLB (formerly Schlumberger); however, analysis of the FMI log conducted by SLB identified a minor fault in the Douglas Group at approximately 2,980 ft bgs with an east-northeast to west-southwest strike orientation. This fault is 450 ft above the gross sequestration interval top in the Arbuckle Group. It is a high angle fault that does not appear to offset the formation. The primary source 3D Far-Field and FMI logs are provided as supporting information submitted through the GSDT Pre-Operational Testing

module. Visual observation of the core indicated slickenside textural features within clay zones that showed no evidence of post-structural fluid migration or alteration.

Natural fractures were interpreted from the FMI log in the Arbuckle Group and the underlying Reagan Sandstone and have an east-west strike orientation. Fracturing was noted in the Arbuckle on the 3D Far-Field Sonic analysis and also showed an east-west orientation. These fractures do not appear to propagate into formations above the Arbuckle, including the overlying Marmaton Group. There is a set of fractures within the gross injection interval (3,448 to 3,606 ft bgs). The top of these is located at 3,448 ft bgs. There are a few found within the upper confining zone from 3,344 ft bgs to 3,358 ft bgs, leaving 90 feet of unfractured confining strata. The bottom perforation is planned for 3,600 ft bgs and the fractures within this zone extend to 3,602 ft bgs. Another small set is found from 3,618 ft bgs to 3,362 ft bgs. Fractures are again found starting at 3,653 ft bgs. The lower confining zone is from 3,647 ft bgs to 3,659 ft bgs. The other predominant set of fractures occurs within the 1,775 to 1,950 ft bgs range within a few different carbonate/shale sequences. A thin set of fractures was also seen within the Lansing-Kansas City Groups which were evaluated as a possible secondary sequestration interval. Please see the CSS #1 Sonic Scanner 3D FF log for additional information and location information, including a 3D view and rose plots. Fractures within the Arbuckle appear to only enhance injectivity, and do not appear to pose any risk to confinement.

See Section A.I.5.5.2 for further information on fracturing found in the core and described as part of the calibration of core data with well log data.

Figure A.I.4-1. Fault Map in Arbuckle Group
From: Baars and Watney 1991

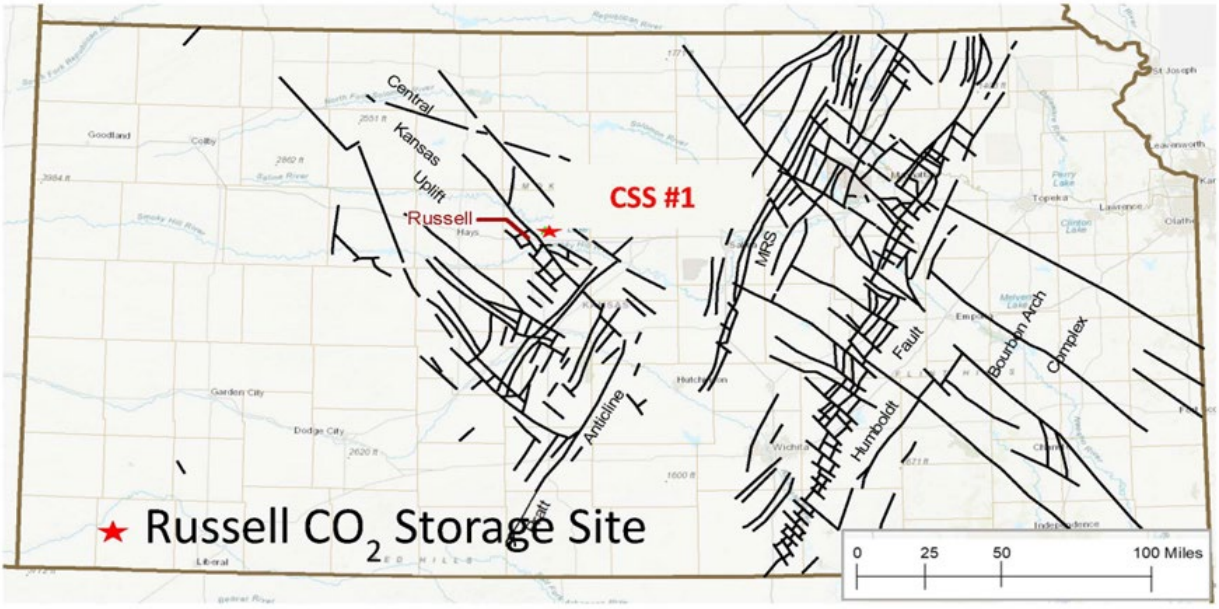

Figure A.I.4-2.a. Stress Indicators and Seismic Hazard. b. Structural Map Showing the Fracture Network within Russell County, KS
Stress indicators. Colored bars: focal mechanisms and in situ indicators for which a stress regime is given; oriented parallel to inferred Seismic Hazard. Black bars: A–C quality in situ indicators averaged over 0.5° bins; lengths reflect data quality.
From: a. Levandowski et al. 2018; b. Baars and Watney 1991

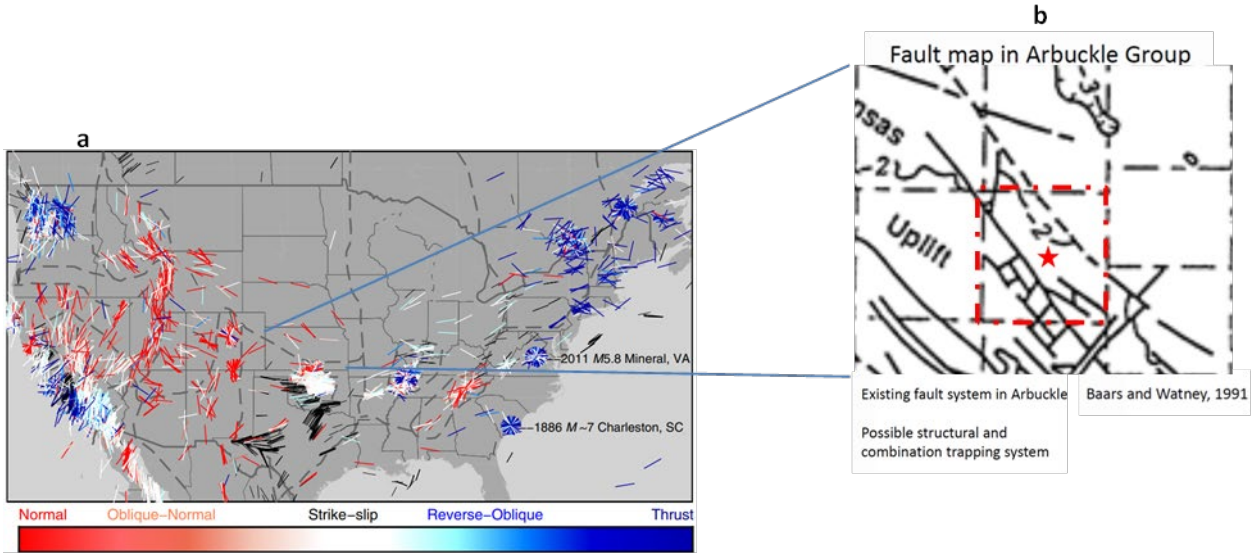

A.I.5. Injection and Confining Zone Details [40 CFR 146.82(a)(3)(iii)]

Data on the depth, areal extent, thickness, mineralogy, porosity, permeability, and capillary pressure of the injection and confining zone and on lithology and facies changes are provided. This information was assembled and evaluated by PCC as part of site characterization from literature and the site-specific pre-operational testing program. There are numerous confining layers separating the Arbuckle Group from the lowermost USDW: over 20 shale layers, the Stone Corral Anhydrite, and the Hutchinson Salt.

The depositional setting, geologic structure, and hydrogeology of the Arbuckle Group were described previously in Section A.I.2.2, with the stratigraphic column summarized in Figure A.I.5-1. Information from core is found in Section A.I.5.5.

A.I.5.1. Properties for Injection Zone

The majority of the Arbuckle Group is composed of dolomite with porosity enhanced by dolomitization, weathering, and ancient tectonic activities (Carr et al. 1986). A karst-like environment with higher porosity and permeability exists in some areas of the Arbuckle (Jorgensen et al., 1993). The storage coefficient of the Arbuckle Group of the WIPAS ranges from 6.8×10^{-5} to 3.2×10^{-3} with an average specific storage of 3.25×10^{-6} ft^{-1} (Jorgensen et al., 1993).

Carr (Carr et al. 1986) estimated the permeability in the Arbuckle to vary from 1 mD to 30 Darcys based on a synthesis of data from drill stem tests and numerical modeling. Carr estimated an average permeability of 50 to 300 mD based on injection test data only. Jorgensen (Jorgensen et al. 1993) developed a map of the intrinsic permeability for the lower units of the WIPAS (Figure A.I.5-2) that includes all units below Devonian rocks and above the basement.

The intrinsic permeability in the AoR nominally equates to about 100 mD. Core data, though, shows that the permeability throughout the overall Arbuckle Group is variable by facies, which is consistent with porosity and permeability in dolomitic carbonates. Intervals/facies identified as confining layers consistently have lower permeabilities and intervals targeted for injection have higher permeabilities. These trends are demonstrated on reservoir property modeling in PBI_Porosity_Permeability Maps.pdf. Confinement is less heterogeneous, as shale facies tend to be more consistent than carbonates; confinement of these formations was verified by differing fluid character (quality, chemistry and pressure), and therefore histories, of targeted and overlying zones. With respect to heterogenic effects on injection, near-well bore data suggest that these will not introduce risk with respect to pressure build-up, which is a primary concern. In general, the permeability estimates of Jorgensen shown on Figure A.I.5.1-2 and of Carr are greater along the CKU as compared to the rest of the basin.

Figure A.I.5-1. Stratigraphic Column at CSS #1

Shows injection and confining zones along with USDW based on log depths from the CSS #1

Geologic Unit	Depth	Hydrogeologic Role
Loess, Carlile Sh, Greenhorn Ls, and Graneros Sh	surface - ~125'	Confining Unit (Great Plains confining system)
Dakota Formation (Upper Dakota Aquifer/Great Plains Aquifer)	~125' - 375'	
Kiowa Fm and Cheyenne Ss (Lower Dakota Aquifer/Great Plains Aquifer)	~375'-495' **BASE OF USDW**	Aquifer (Great Plains aquifer system)
Nippewalla Group (Lower Permian Units)	495'-770'	Confining Unit (Western Interior Plains confining system); some interbedded carbonates have porosity and would be considered minor aquifers
Stone Corral (Anhydrite) - Regional Seal	770'-809'	
Ninnescah Shale	809'-948'	
Wellington	948'-1,124'	
Hutchinson Salt Mbr	1,124'-1,402'	
Geuda Springs Shale Mbr	1402'-1529'	
Shale and Limestone Sequences	1,529-2,909'	
Heebner Shale Member - Secondary Confining	2,909' - 2,927'	
Lansing & Kansas City Groups Potential Secondary Sequestration Interval Iola Limestone Member	2,993' 3,080'-3,128'	First porous interval above Arbuckle
Marmaton Group	3,262'	
Top Primary Upper Confining Zone	3,274'	confining unit
Top of Arbuckle Group	3,277'	
Base Primary Upper Confining Zone	3,438'	
Gross Sequestration Zone	3,448'-3,606'	Aquifer in Western Interior Plains aquifer system
Primary Lower Confining Zone	3,647'-3,659'	confining unit
Top Reagan Sandstone	3,659'	Aquifer
Top of Quartzite Basement	3,735'	Basement confining system

Figure A.I.5-2. Estimated Regional Intrinsic Permeability

Lower units of the Western Interior Plains aquifer system, which includes units below the Devonian rocks and above the basement.

From Jorgensen et al. 1993

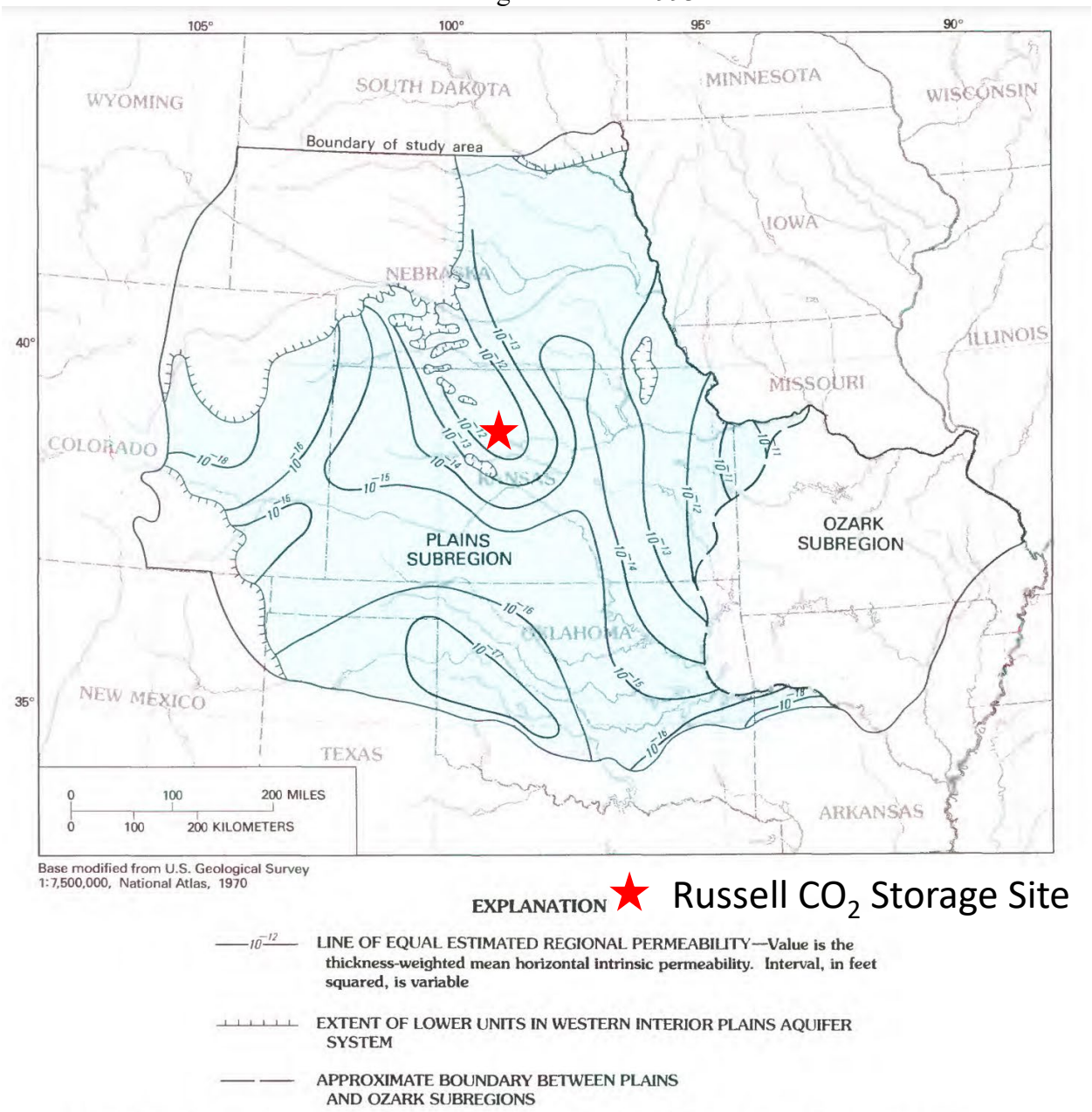

The reason that Arbuckle Group permeability is larger in the CKU may be because rocks were subject to uplift and are probably also more solution enhanced than rocks in the structural basins. Latta states the greatest porosity and permeability are found where the Arbuckle strata have undergone erosion on the top and flanks of uplift areas (Latta 1973). Permeability for the Arbuckle, as indicated by petrophysical analysis only at CSS #1 prior to reconciliation with results from core testing, ranges from 1 mD to 200 mD, with an average of 14 mD across the entire Arbuckle and 90 mD across the injection interval.

Analyses of 76 geophysical logs from wells across Kansas that logged the entire Arbuckle indicate an average porosity of about 12% (Carr et al. 1986). This agrees with the porosity identified in the CSS #1 logs, which ranged from 4% to 20% with an average of 12% across the entire Arbuckle and an injection zone porosity average of 15.2%. Modeling for the area, which includes interpolation of estimated porosities and permeabilities for wells near or within the AoR, indicates a reliable zone of sufficient porosity for injection. Core analysis of the sequestration zone in the Arbuckle showed Klinkenberg permeability ranging from <0.0001 mD to 13,100 mD with an average of 1,560 mD and a median of 210 mD (17 data points), and porosities ranging from 1.2% to 22% with an average of 11.5% and a median of 11.0% (17 data points).

Heterogeneous reservoir properties, such as porosity and permeability, were derived from petrophysical logs and informed by core data from the CSS #1 and seismic attributes from analysis of the 3D seismic dataset and incorporated into the static model using a geostatistical approach of Gaussian random function simulation. This geostatistical distribution populated reservoir properties within the model domain. Eight different layers were modeled, three of which represent the primary confining units (layers 0, 1, and 7). A smaller simulation area was then selected around the injection site. Figure A.I.5-3 is a map of wells utilized for general characteristics of formations including structure, as an overlay of an early-stage delineation of general Arbuckle depositional facies with seismic integration. A total of 34 wells were used in the larger static model to inform petrophysical properties, 12 of which are within the simulation area as shown in Table A.I.5-1. PBI_Porosity_Permeability Maps.pdf contains histograms of porosity and permeability by layer, including the number of well logs utilized along with well log vs individual porosity/permeability value, along with maps of the static model for each layer for clay content, porosity, permeability, and K/PHI Index.

Figure A.I.5-3. Map of Wells Utilized for General Formation Characteristics During Development of the Static Model

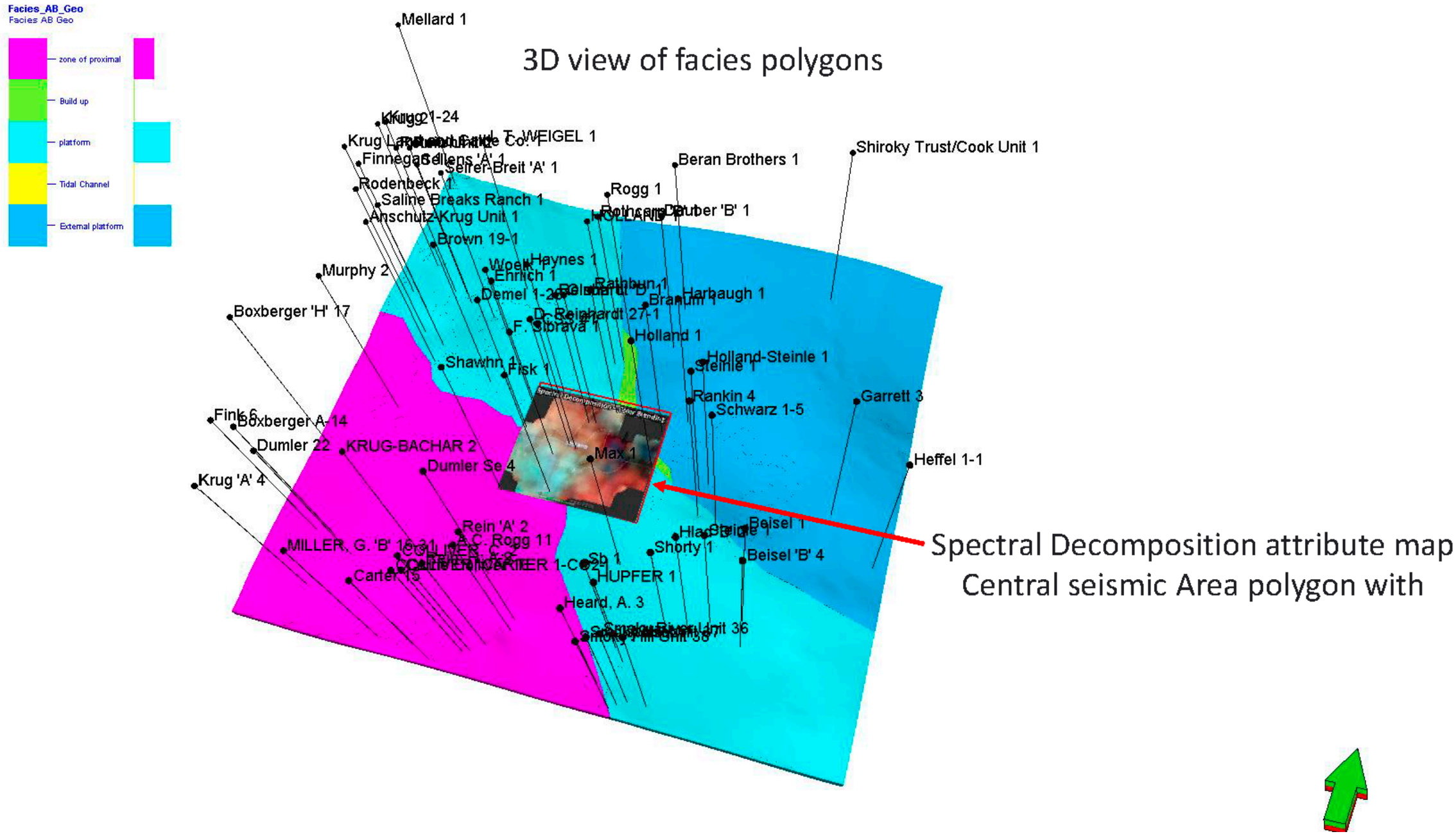

Table A.I.5-1. Wells Utilized in Static Model to Inform Petrophysical Properties

Modeled Area	Simulation Area	Well Name	API #	Location	Spud Date	Total Depth, ft
	x	AC Rogg 11	15-167-24054	T14S R13W, Sec. 27	Feb-23-2017	3,215
x		Amelia 'D' 4	15-167-22761	T14S R14W, Sec. 6	Dec-12-1986	3,397
	x	Anschutz Krug Unit 1	15-167-23721	T13S R14W, Sec. 23	Jun-10-2011	3,350
x		Austin L L 11	15-051-25932	T12S R16W, Sec. 36	Dec-01-2009	3,400
	x	Beran Brothers 1	15-167-23361	T12S R13W, Sec. 15	Jun-25-2006	3,445
x		Beren Trap 1-7	15-167-23819	T12S R13W, Sec. 7	Aug-30-2012	3,450
x		Boxberger 'A' 10-SWD	15-167-22626	T13S R14W, Sec. 32	Dec-19-1985	3,530
x		Brungardt Gary Unit 1	15-051-26648	T13S R16W, Sec. 25	Dec-10-2013	3,490
	x	Carrie Colliver 16	15-167-02515-0001	T14S R13W, Sec. 28	Aug-15-1951/ Apr-15-2003	3,253
	x	CSS #1	15-167-24129	T13S R13W, Sec. 27	Oct-18-2022	3,756
x		Driscoll 4	15-167-23444	T12S R15W, Sec. 20	Jul-02-2007	3,350
x		Driscoll-Maier Unit 1	15-167-23715	T15S R14W, Sec. 4	May-31-2011	3,272
	x	Dumler Se 4	15-167-23447	T14S R13W, Sec. 16	Jul-17-2007	3,450
x		Haberer 'A' 3	15-167-23716	T12S R15W, Sec. 14	Jul-18-2011	3,150
x		Haberer 'A' 4	15-167-23759	T12S R15W, Sec. 14	Jan-17-2012	3,160
x		Haines 1	15-167-23764	T13S R15W, Sec. 25	Feb-06-2012	3,390
	x	Heffel 1-1	15-167-23606	T14S R12W, Sec. 1	Jan-14-2010	3,334
	x	Hlad 'B' 2	15-167-23579	T14S R12W, Sec. 17	Jun-22-2009	3,574
	x	Holland Steinle 1	15-167-23616	T13S R12W, Sec. 29	Mar-03-2010	3,400
x		Keil 11	15-167-23687	T15S R14W, Sec. 5	Jan-12-2011	3,275
x		Krug 2	15-167-23706	T13S R14W, Sec. 3	Apr-20-2011	3,200
x		Miller 'F' 8	15-167-23599	T13S R14W, Sec. 32	Sep-29-2009	3,400
	x	Murphy 2	15-167-21142	T13S R14W, Sec. 35	Mar-01-1978	3,505
x		Rein H A-9	15-167-23701	T14S R13W, Sec. 27	Apr-01-2011	3,300
	x	Rein Unit 2	15-167-23567	T13S R14W, Sec. 11	Apr-13-2009	3,225
x		Rohleder 1	15-167-23719	T13S R15W, Sec. 28	Jun-11-2011	3,407
x		Rohleder 2	15-167-23816	T13S R15W, Sec. 28	Aug-15-2012	3,420
x		Schrant 1	15-167-23757	T14S R15W, Sec. 30	Dec-06-2011	3,504

Modeled Area	Simulation Area	Well Name	API #	Location	Spud Date	Total Depth, ft
x		Schwein 1	15-167-23804	T15S R14W, Sec. 25	May-20-2012	3,400
	x	Smokey Hill Unit 38	15-167-23814	T14S R12W, Sec. 31	Jul-26-2012	3,305
x		Stranger Valley 1	15-167-23815	T13S R15W, Sec. 34	Aug-06-2012	3,430
x		Wieland Unit 2-19	15-167-23602	T12S R15W, Sec. 31	Jan-05-2010	3,420
x		Weiland Unit 6-17	15-051-25936	T13S R16W, Sec. 1	Feb-01-2010	3,525
x		Zweifel Trust A 1-3	15-167-23360	T12S R13W, Sec. 3	Jun-09-2006	3,800

Figure A.I.5-4 demonstrates distinct zones based on porosity within the Arbuckle from petrophysical analysis of the CSS #1 well log. Zones 2-6 are targeted for sequestration. These findings correspond very well with the core results. Figure A.I.5-5 is a representative porosity distribution within the Arbuckle, in particular the porosity distribution for subunit 4. Porosity distributions for the other sequestration interval subunits are similar to subunit 4, and maps for the other subunits are provided in the supporting information submitted through the GSDT Projection Information Tracking module under the filename: PBI_Porosity_Permeability Maps.pdf. CSS #1 has less porosity in zones 0, 1, and 7, which corresponds to the primary confining intervals within the main body of the Arbuckle. Confinement also exists at the top of the Arbuckle Group. Figure A.I.5-6 provides the porosity distribution for the Arbuckle flow units in a west to east cross section, and Figure A.I.5-7 illustrates the porosity distribution in the south to north direction.

Figures A.I.5-8 and A.I.5-9 provide K-Phi maps for the individual Arbuckle subunits and the composite whole.

An isopach map focused on the primary sequestration interval within the Arbuckle was shown previously in Figure A.I.3-2. Figure A.I.5-10 demonstrates the 5 different rock types as characterized by porosity and permeability within the Arbuckle: nano, micro, meso, macro, and mega. The meso, macro, and mega will be utilized for injection; whereas the nano provides internal confinement. The injection interval of the 3 injection rock types is consistent in thickness (~158 ft) across the AoR, which corresponds approximately to Zones 2-6 on Figure A.I.5-4.

Figure A.I.5-4. Distinct Zones in Arbuckle Based on Porosity

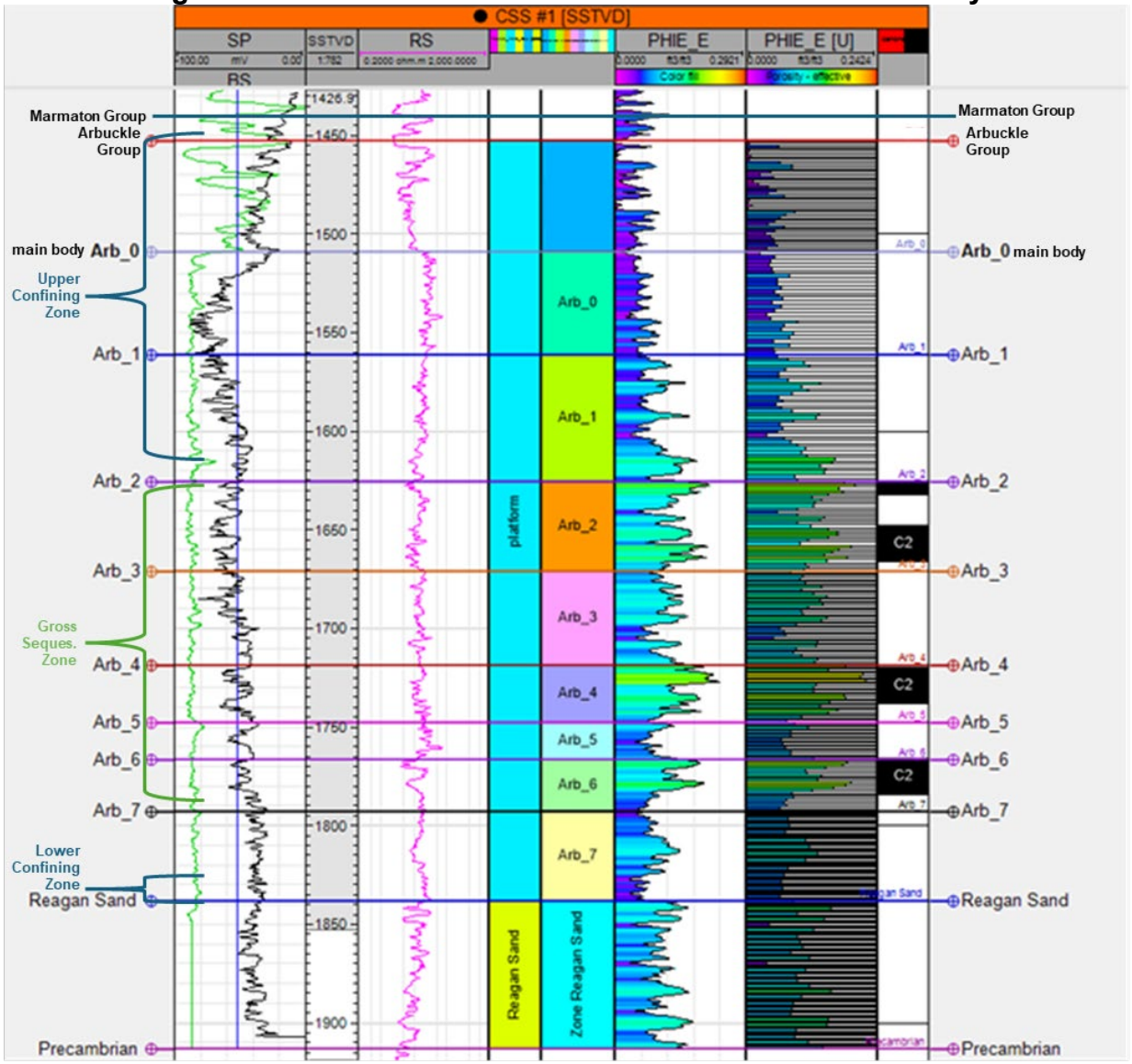

Figure A.I.5-5. Distribution of Porosity in Arbuckle Subunit 4

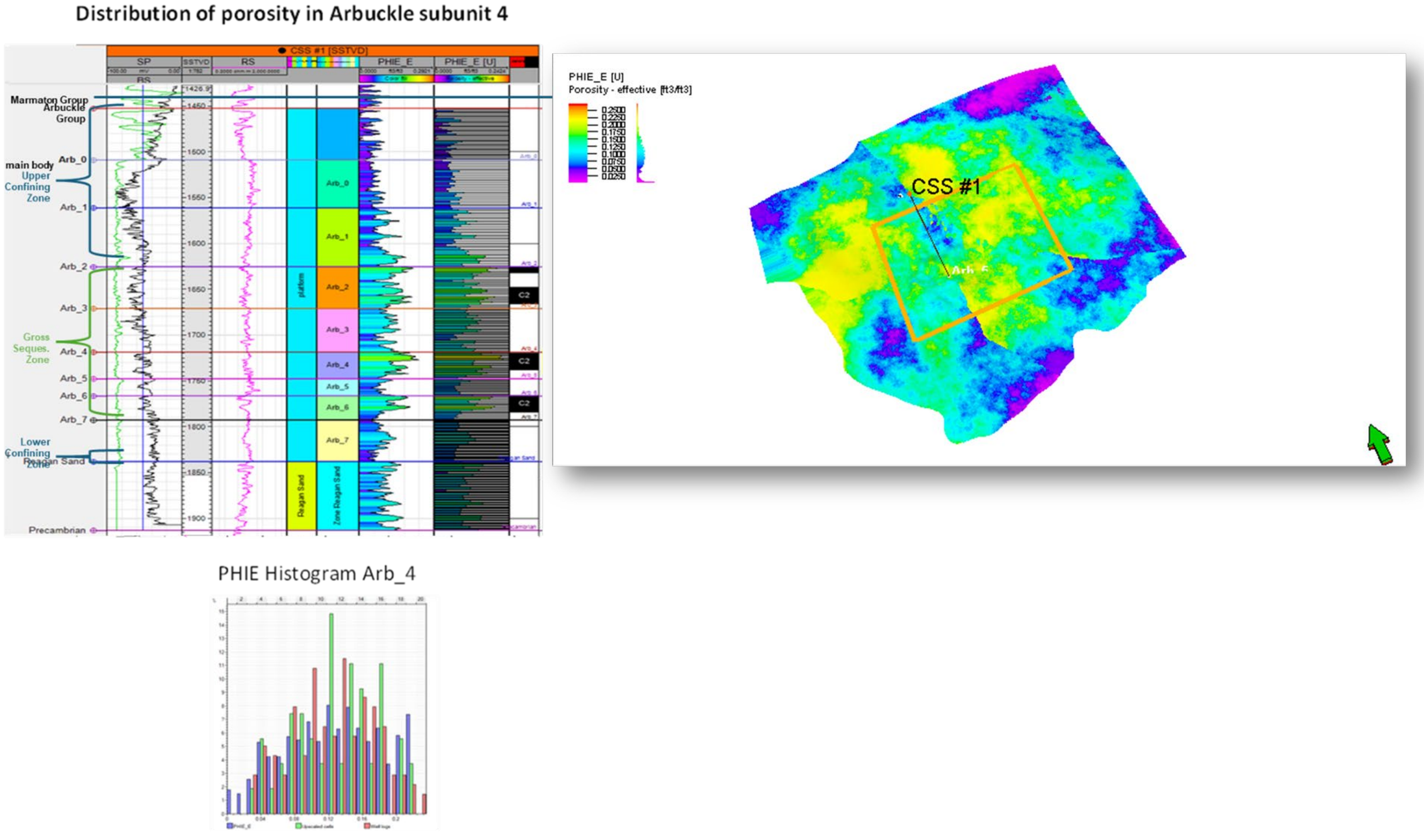

Figure A.I.5-6. West To East Cross Section of Porosity Distribution in Area

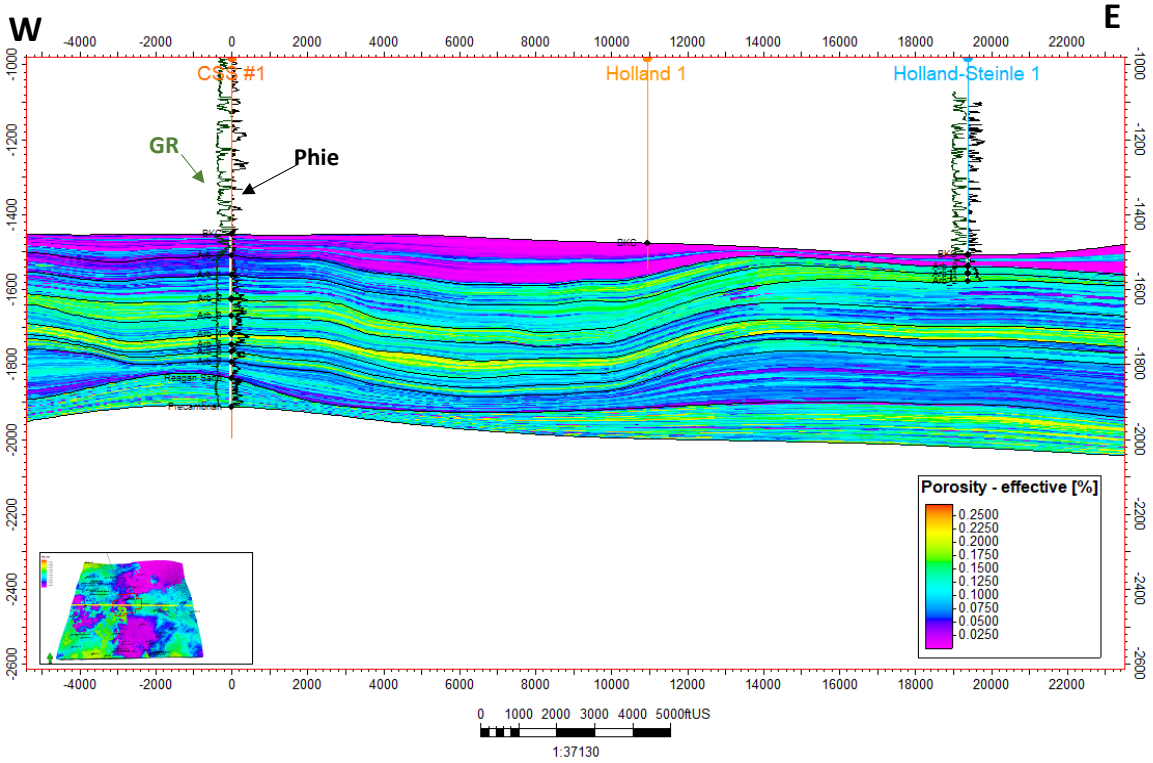

Figure A.I.5-7. South To North Cross Section of Porosity Distribution in Area

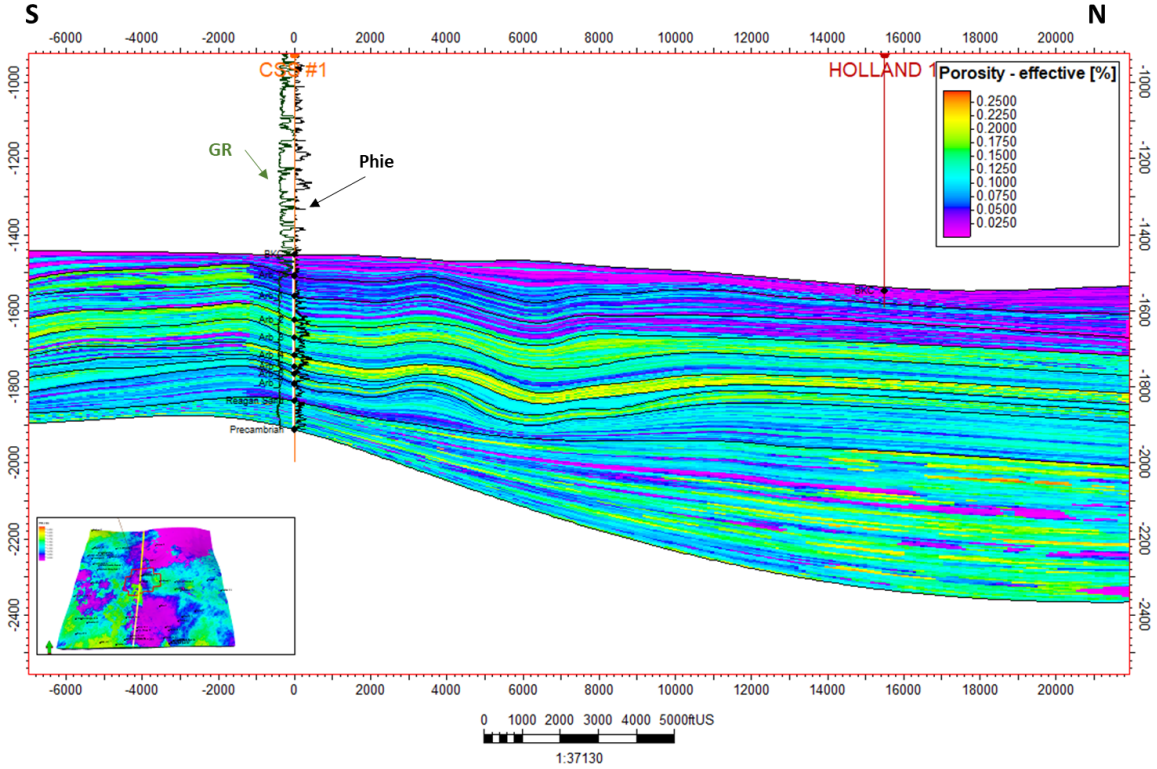

Figure A.I.5-8. K-Phi Distributions by Subunits

Kphi Distribution, Top Arbuckle_0

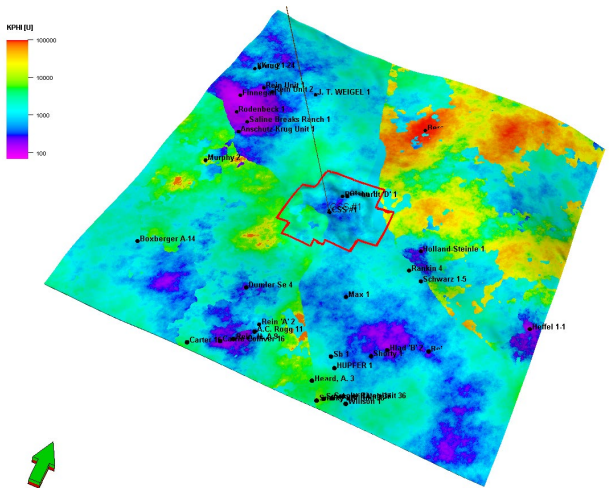

Kphi Distribution, Top Arbuckle_1

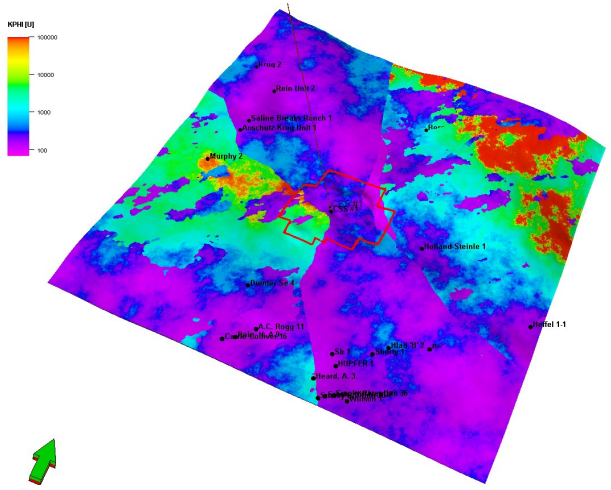

Kphi Distribution, Top Arbuckle_2

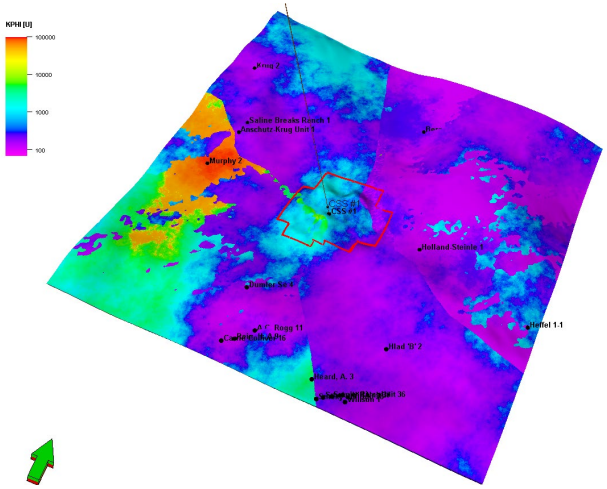

Kphi Distribution, Top Arbuckle_3

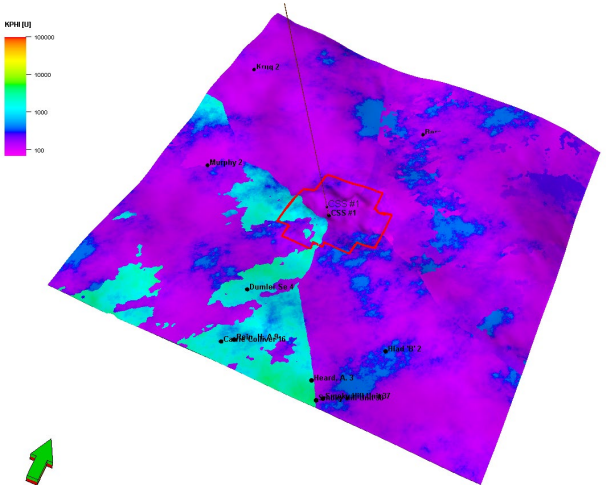

Figure A.I.5-8. K-Phi Distributions by Subunits (con't)

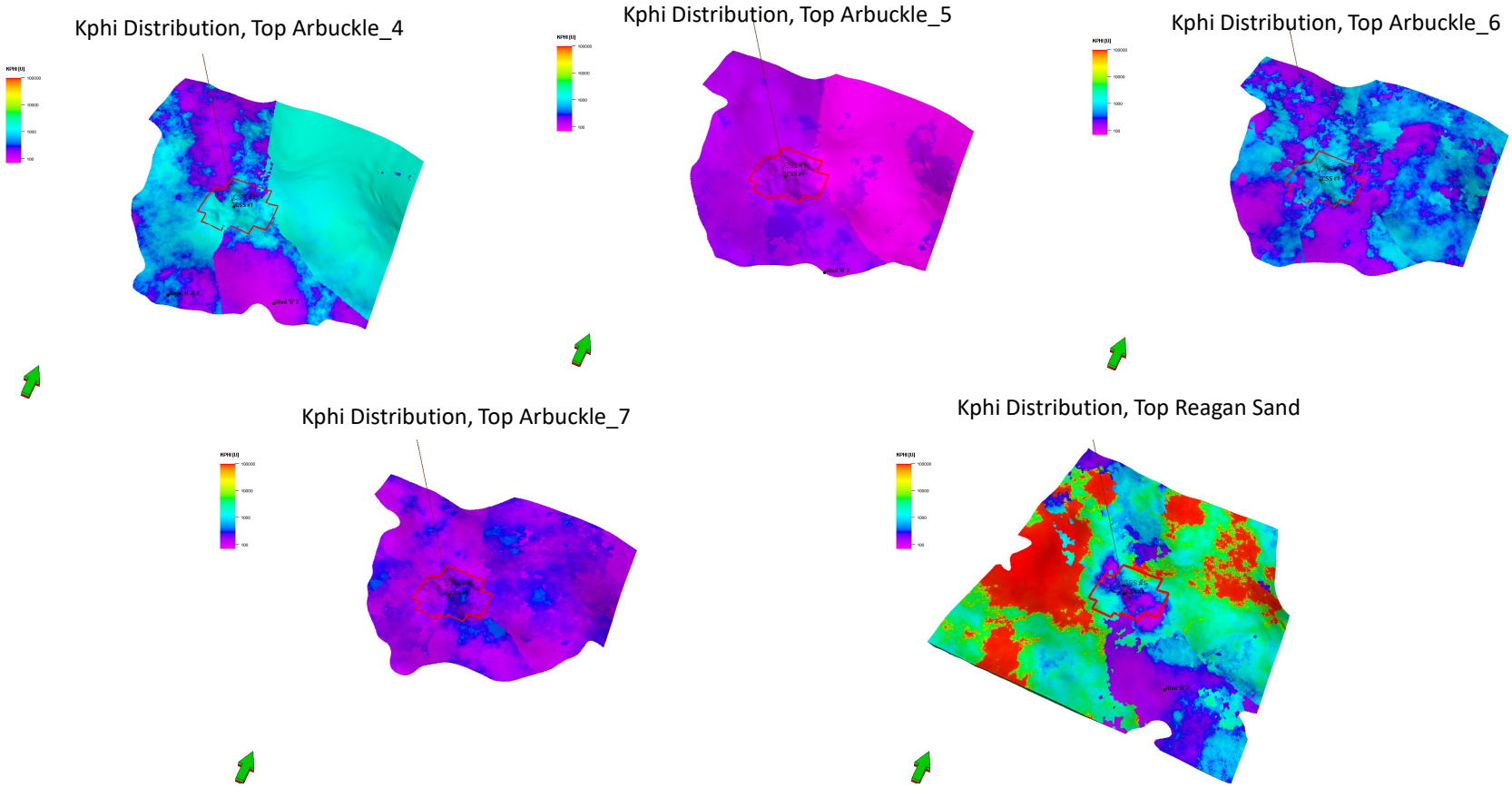

Figure A.I.5-9. Composite K-Phi Distribution for Arbuckle Group

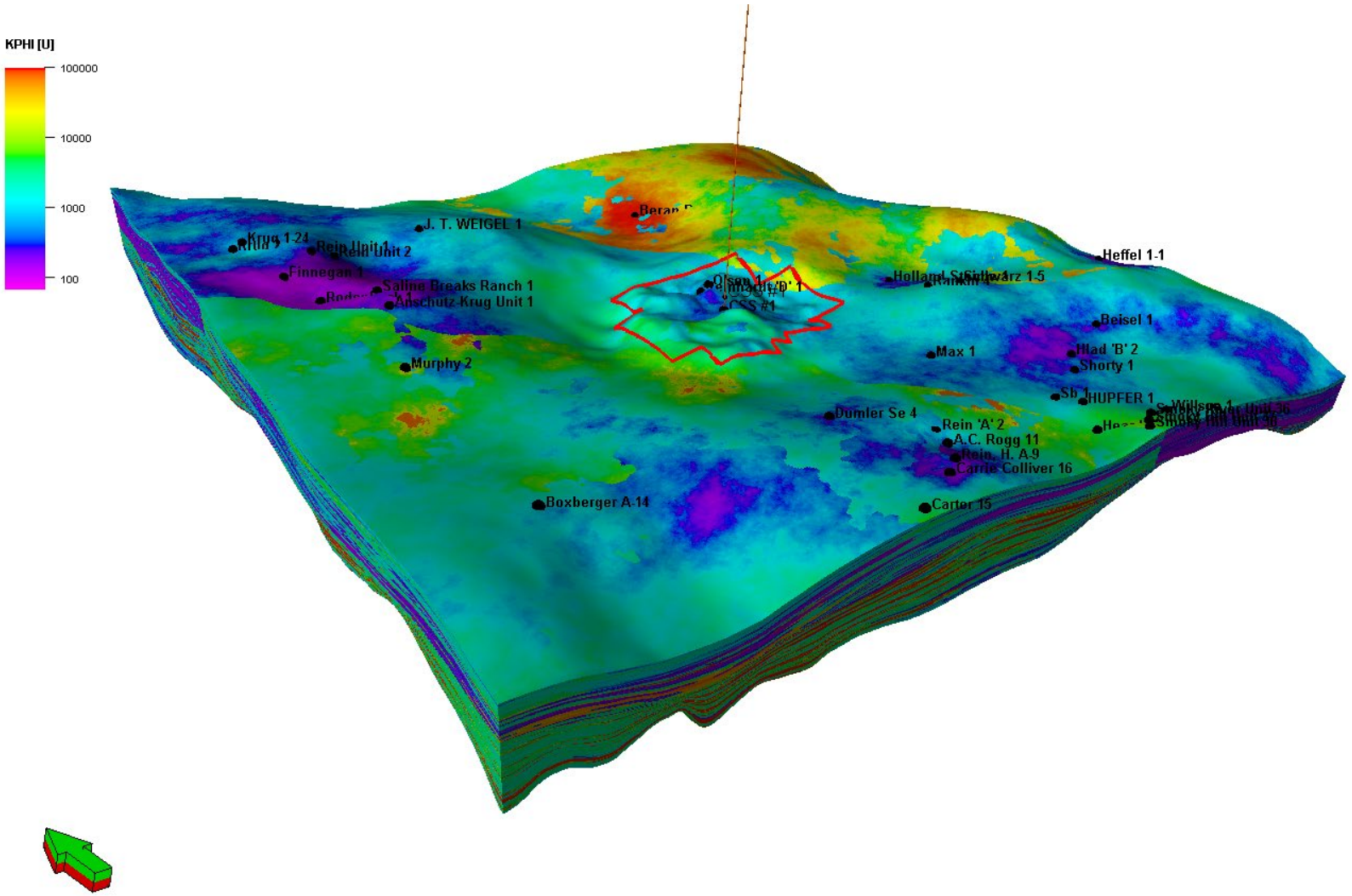

Figure A.I.5-10. Different Rock Types in Arbuckle

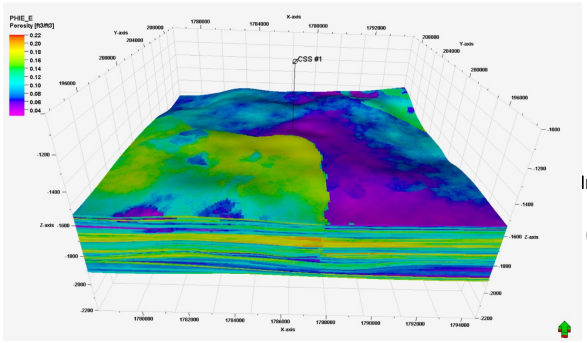

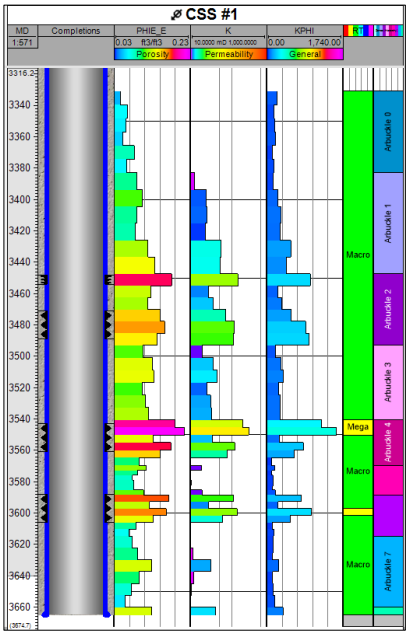

Injection Zone (158 ft.)

3448 – 3454= 6 ft.

3470 – 3488= 18 ft.

3542 – 3560= 18 ft.

3588 – 3606= 18 ft.

Total Perforations (60 ft.)

A.I.5.2. Properties for Confining Zones

Primary confinement for the gross Arbuckle sequestration interval (3,448 to 3,606 ft bgs) is provided by low permeability layers within the Arbuckle. Rock characterization based on petrophysical analysis of porosity and permeability and confirmed through core testing (See Section A.I.5.5) characterizes this interval as a 'nano' rock type within the interval, containing tight limestone with low porosities. See Section A.I.5 and PBI_Porosity_Permeability Maps.pdf for further information on property (i.e. porosity and permeability) distribution generation for modeling. The lower primary confining layer is located between 3,647 and 3,659 ft bgs, and the upper primary confining layer is located between 3,274 and 3,438 ft bgs. Please note that the basal 3 foot shale of the Marmaton Group is included in the upper primary confining layer.

The injection zone is also vertically segregated from the lowermost USDW by multiple confining units including the overlying Marmaton Group, several shales, including the Douglas Group, Heebner, Geuda Springs, and Ninnescah, and thick anhydrite (Stone Corral) and salt (Hutchinson) zones. The Marmaton contains both shales and hard, tight limestones. Several of these shales, including the Douglas Group and Heebner, would provide secondary confinement for sequestration in the Kansas City Group if the GS project evolves to consider additional sequestration intervals in the future.

The base of the Iola Limestone of the Kansas City Group is located 320 feet above the sequestration interval in the Arbuckle. The Iola is the first zone above the Arbuckle with porosity development.

The shale and limestone sequences, which make up a majority of the stratigraphic column, contain over 20 shale layers as correlated to the Type Log for Russell County on the Kansas Geological Survey website (Rocke, 2005). This log is located two townships away in Township 15 South, Range 13 West and starts in the Graneros Shale and has over 70 tops down through the Arbuckle. Lithologic correlation between the type log and CSS #1 log was consistent, aside from one carbonate/shale lithofacies that was not present in the CSS #1 log. This demonstrates that all the additional confining zones are present across a larger area than the AoR. The 76 ft thick Reagan Sandstone, which underlies the Arbuckle, provides a pressure dissipation zone between the Arbuckle and the basement. A fraction of the displaced brine migrates into the dissipation layer, thereby reducing pressure buildup (Zhou, 2008).

Confining zones both within the Arbuckle and overlying formations were not sampled for fluids during pre-operational testing of CSS #1 since they are tight and therefore incapable of flowing water.

A.I.5.2.1 Geological Confinement of CO_2

There are four trapping mechanisms within a CO_2 storage reservoir, with the predominant mechanism varying by both the geologic framework in a basin and time as illustrated in Figure A.I.5-11. This project is characterized as located in a sedimentary basin with

three dominant trapping mechanisms (structural and stratigraphic, hysteresis, and solubility) during the timeframe of interest for the GS project, with a fourth trapping mechanism (mineral) only becoming important during extended timeframes (> 1,000 yr). Nonetheless, the computational model does incorporate mineral trapping calculations as detailed in Appendix B.1 of the Area of Review and Corrective Action Plan.

Figure A.I.5-11. Temporal Evolution of CO_2 Trapping Mechanisms
Left: Sedimentary Basins; Right: Basalt with Mineral Carbonation Trapping
From: National Academies of Sciences 2019

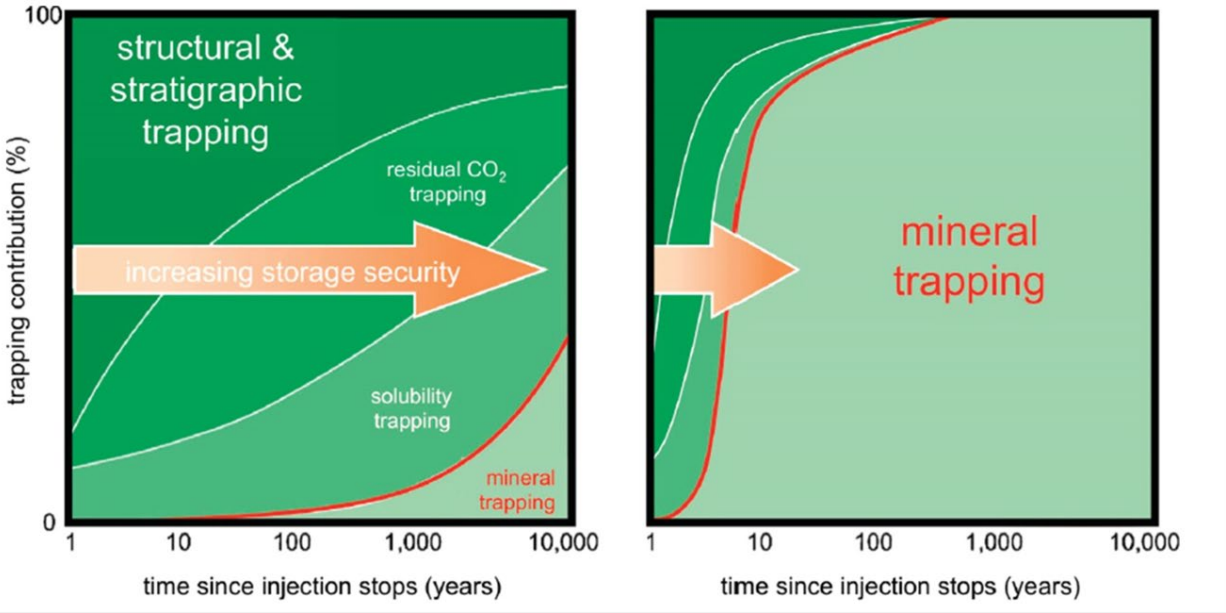

Hydrodynamic Trapping/Structural & Stratigraphic Trapping
Hydrodynamic trapping (aka structural and stratigraphic trapping) is the main CO_2 trapping mechanism at the early phase for this GS sequestration project. Carbon dioxide, being less dense than the formation fluid, will rise buoyantly until it encounters a caprock with a capillary entry pressure greater than the buoyancy or hydrodynamic force. CO_2 will accumulate in a structural or stratigraphic feature with vertical and lateral seals. This mechanism is critical in that it is a prerequisite for any storage site because it prevents the leakage of CO_2 through the caprock during the time required for other trapping mechanisms to come into effect (Bachu 1994).

The trapping efficiency is determined by the structure of the sedimentary basins, which have an intricate plumbing system defined by the location of high and low permeability strata that control the flow of fluids throughout the basin. There are numerous variations of structural and stratigraphic traps, or combinations of both structural and stratigraphic traps, which can be physical traps for geological CO_2 storage. Common structural traps include anticlinal folds or sealed fault blocks – see Figure A.I.5-12.

Figure A.I.5-12. Examples of (a) Structural, and (b) Stratigraphic Traps
From: Zhang and Song 2014

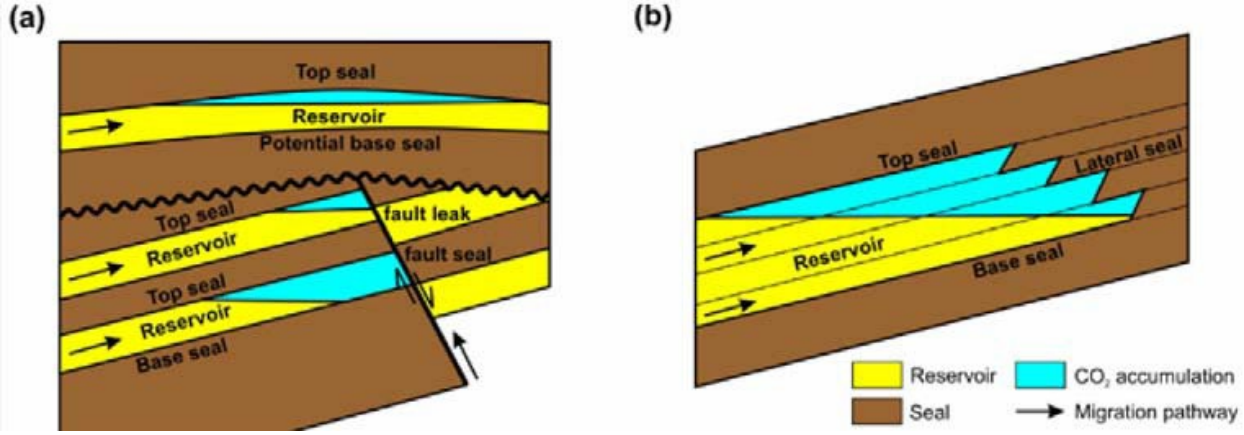

Residual Trapping

Residual trapping (aka capillary trapping, or hysteresis trapping) occurs after cessation of injection. During injection, CO_2 first displaces brine in a co-current fashion throughout the reservoir. But when injection is stopped, due to the density difference between CO_2 and brine, the fluids flow in a counter-current fashion so that CO_2 migrates up towards and the brine flows downwards. Thus, the wetting phase (brine) enters the pores by a less-wetting phase (CO_2). In such a process, the brine displaces CO_2, leading to a significant saturation of CO_2 becoming trapped in small clusters of pores, see Figure A.I.5-13. The disconnected CO_2 is then trapped as an immobile phase.

As this trapping mechanism is expected to have an impact on the CO_2 plume behavior, a combined capillary trapping model using Brooks and Corey (Brooks and Corey 1964) relative permeability model, Land (Land 1968) trapping coefficient, and Akbarabadi and Piri (Akbarabadi and Piri 2013) trapping efficiency for drainage, imbibition, and end points calculations is incorporated into the computational model. The equations are summarized in Figure A.I.5-14.

Figure A.I.5-13. Example of Residual Gas After Density Drift of Plume

From: Juanes et al. 2006

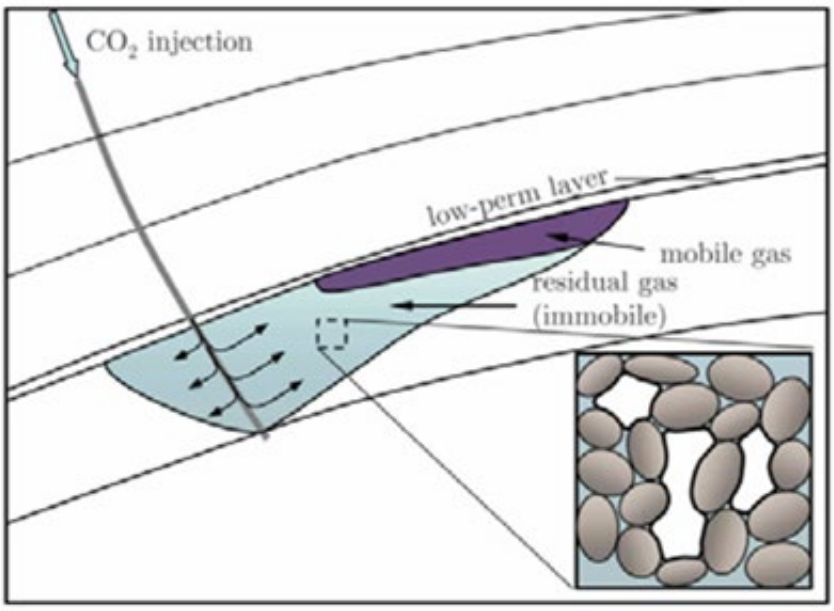

Figure A.I.5-14. Relative Permeability and Trapping Models

Relative Permeability Model
Brooks & Corey 1964

Brooks, R.H., and A. T. Corey. Hydraulic properties of porous media. Hydrology Paper No. 3, Colorado State University, 3:1–27, 1964

CORRELATIONS

$$K_{rb} = K_{rb}^{max}\left(\frac{1 - S_{co2} - S_b^{irr}}{1 - S_{co2}^c - S_b^{irr}}\right)^m \qquad K_{rco2} = K_{rco2}^{max}\left(\frac{S_{co2} - S_{co2}^c}{1 - S_{co2}^c - S_b^{irr}}\right)^n$$

Uncertainty Variables	Drainage
	S_b^{irr}
	K_{rb}^{max}= 1
	K_{rco2}^{max}
	S_{co2}^c = 0
	n and m

Uncertainty Variables	Imbibition
	K_{rb}^{max}
	K_{rco2}^{max}
	S_{co2}^c
	n and m
	S_{co2}^{max} = 1-S_b^{irr}

TRAPPING MODELS

Land's Trapping Coefficient

Land CS. Calculation of imbibition relative permeability for two and three-phase flow from rock properties. Soc. Petr. Eng. J., 1968; 8(2), 149-56.

$$C = \frac{1}{S_{co2}^c} - \frac{1}{S_{co2}^{max}}$$

Trapping Efficiency

Akbarabadi M, Piri M. Relative permeability and capillary trapping characteristics of supercritical CO2/brine systems: An experimental study at reservoir conditions.

$$\frac{S_{co2}^c}{S_{co2}^{max}} = \frac{1}{1 + C * S_{co2}^{max}}$$

Relative permeability and displacement characteristics for the imbibition cycle and trapping efficiency for the four categories of sandstone rocks, based on the analysis of 22 core samples from western Canada (Bachu S., 2013)

Solubility Trapping
Solubility trapping refers to dissolution of CO_2 in formation fluid. Injected CO_2 migrates upwards to the interface between reservoir and caprock and then spreads laterally under the caprock as a separate phase. Mass transfer occurs at the CO_2/brine interface, with the solubility of CO_2 in the brine depend upon salinity, pressure, and temperature.

Mineralization
Mineral trapping refers to the incorporation of CO_2 in a stable mineral phase via reactions with mineral and organic matter in the formation. It is modeled by a set of coupled equilibrium reactions that account for both solid precipitation and solid dissolution depending upon reservoir conditions. The rates for the mineralization equilibrium reactions are generally quite slow in sedimentary basins; thus this mechanism is only a minor contributor to overall CO_2 trapping mechanisms over the timeframe of interest for this geologic sequestration project. Appendix B.1 of the Area of Review and Corrective Action Plan provides additional detail on this trapping mechanism.

A.I.5.3. Baseline 3D Seismic Survey for Project Site

The baseline 3D survey was acquired in 2022 as the first snapshot in the time-lapse surface seismic program to monitor the position of the CO_2 plume over the course the GS project – See Section E.10.2 of the Testing and Monitoring Plan for additional background information on the set-up and processing of data from the baseline seismic survey. The data volume obtained from the baseline survey meets the criteria for quality: adequate frequency content, up to 130 Hertz (Hz), for resolving the inner structure of the reservoir (Arbuckle Group), a good signal to noise ratio and in general, geologically behaving seismic events. Figure A.I.5-15 provides an example West-to-East cross section of the seismic survey results and data quality; this specific cross section will also be used to illustrate how the final results were constructed.

The post-stack seismic volume immediately shows a favorable geology for CO_2 sequestration: continuous and nearly flat layers with no obvious discontinuities or faults through the AoR. The post-stack also shows lateral continuity and consistency of the primary and secondary confining zones, including the Heebner Shale and Marmaton/Upper Arbuckle Groups (Figure A.I.5-16).

The seismic data suggests the Arbuckle Group has a classic carbonate shelf and reef morphology. The shelf morphology is well observed at the upper part of the Arbuckle Group, characterized as a near-flat horizon with possible carbonate buildup morphology limited to the west with transgressive onlaps as seen in Figure A.I.5-17. The western limit of this carbonate shelf is consistent with the northwest-southeast regional lineaments in Central Kansas and is persistent through the entire formation.

Clean gathers with good continuous data were obtained from analysis of the pre-stack data (Figure A.I.5-18).

A model-based simultaneous elastic inversion algorithm was applied to the gathers up to 45 degrees to output P-Impedance, S-impedance, Density, and Vp/Vs ratio volumes. All the volumes show good correlation to the well logs giving high confidence in the inversion results, see Figure A.I.5-19. Elastic properties obtained from the baseline survey are incorporated into the geomechanical computational model for the project.

Figure A.I.5-15. Baseline 3D Seismic Survey West-to-East Survey and Data Quality

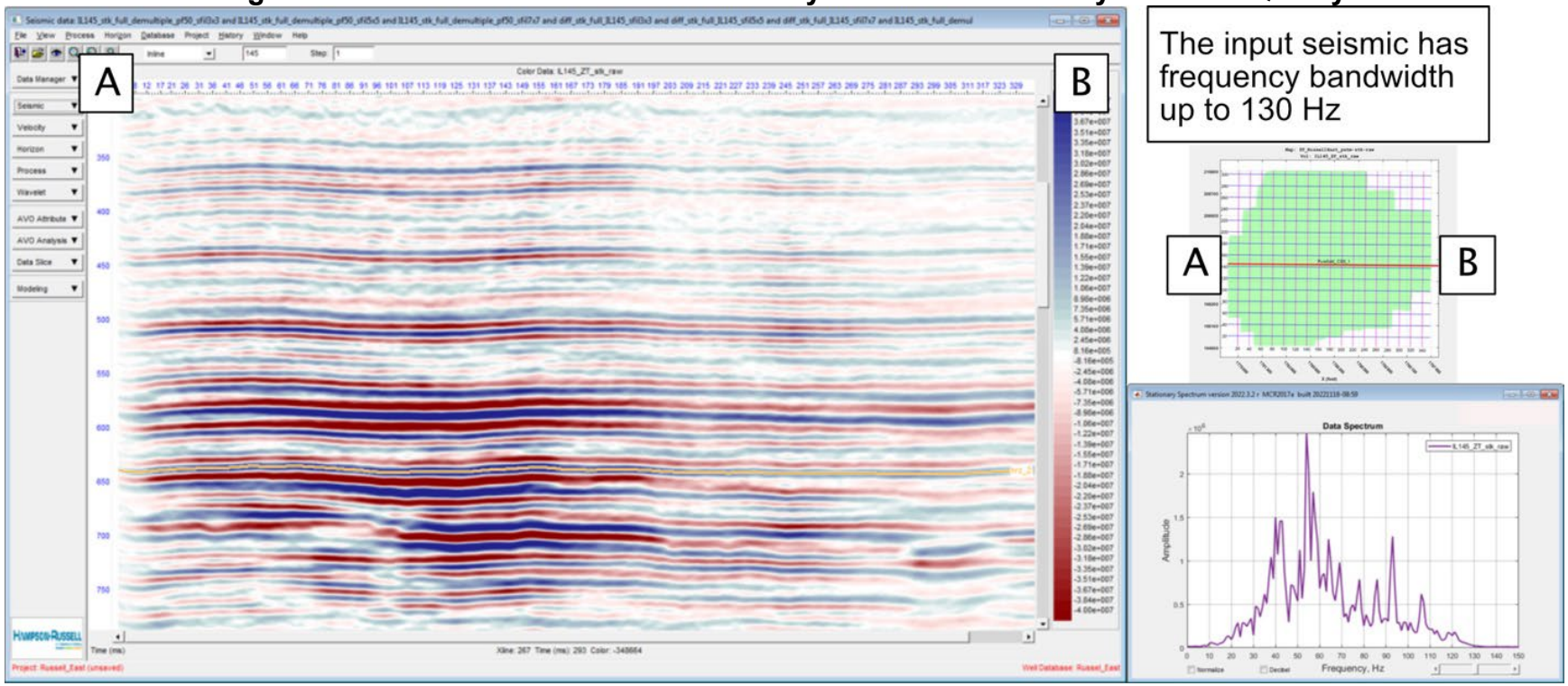

Figure A.I.5-16. Baseline 3D Seismic Survey - Reservoir Image

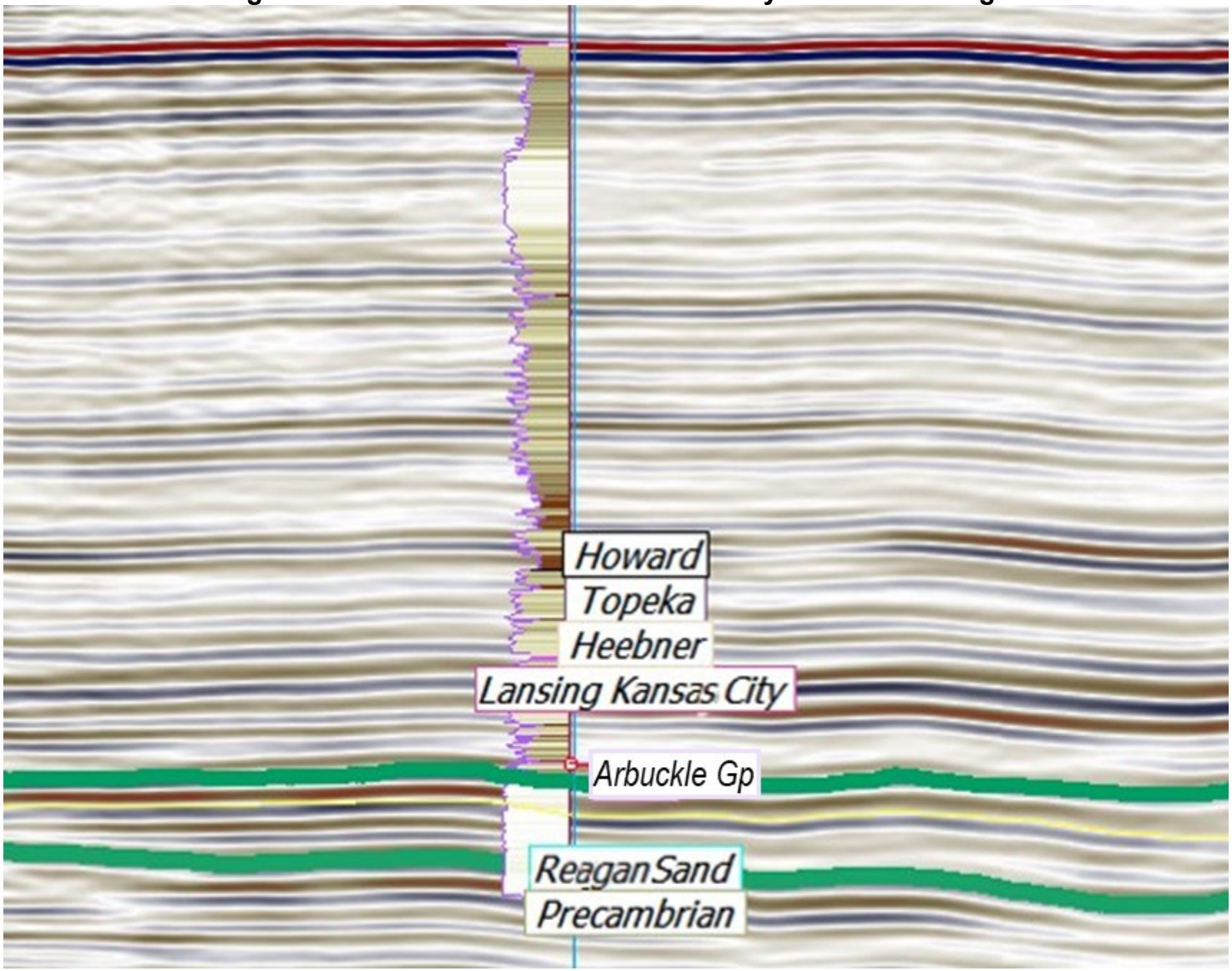

Figure A.I.5-17. Baseline 3D Seismic Survey - Carbonate Shelf and Reef Morphology

Vertical exaggeration: 13 times

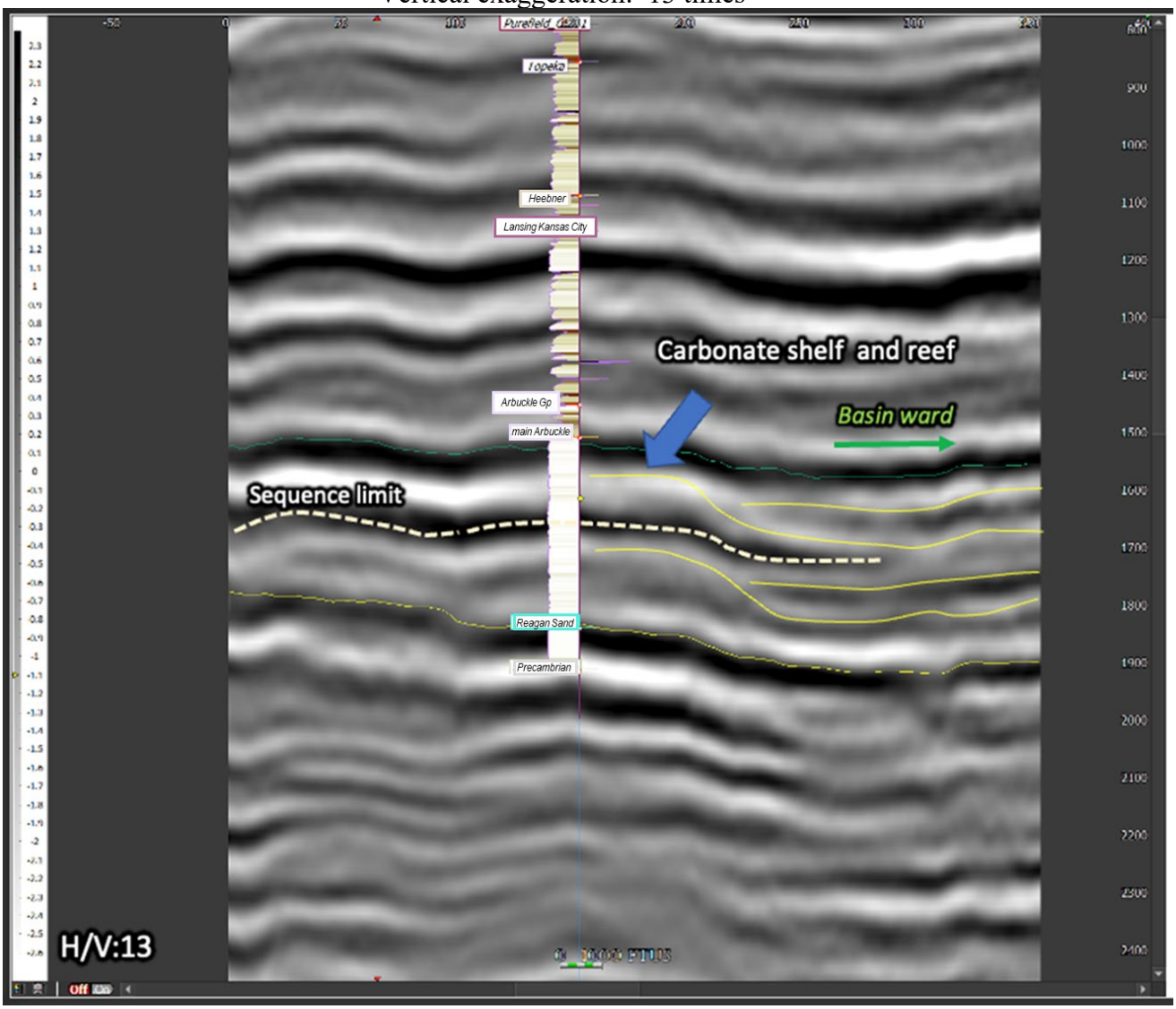

Figure A.I.5-18. Baseline 3D Seismic Survey - Seismic Gathers

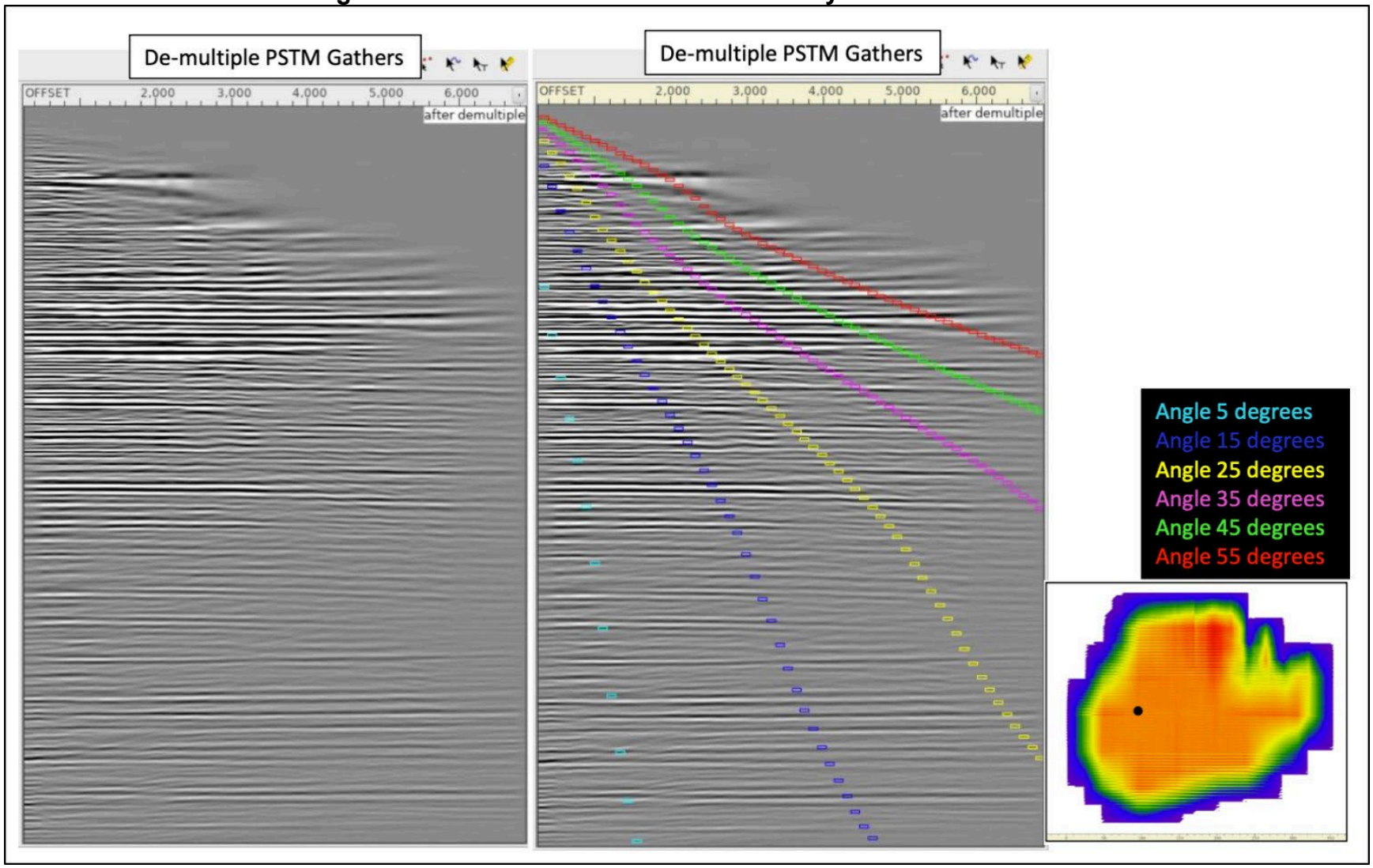

Figure A.I.5-19. Baseline 3D Seismic Survey - Elastic Inversion Results

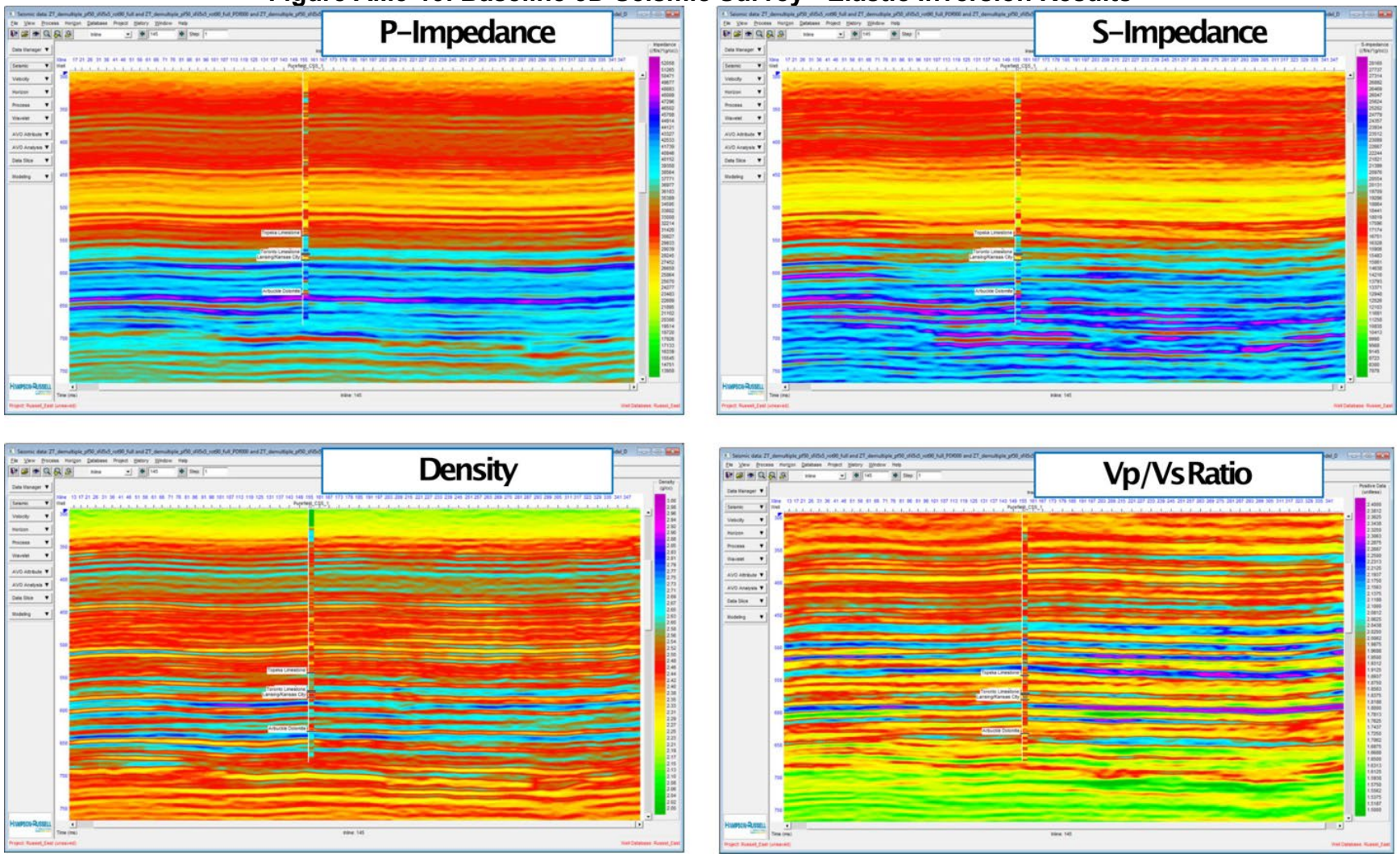

A.I.5.4. Well Logging and Tests [40 CFR 146.87(a)(2) and (3)]

Well logging and testing were conducted to identify appropriate confining and injection zones, and to characterize them before CO_2 injection to confirm that injection fluids will be adequately stored and confined in the injection zone. The logging and testing were conducted on CSS #1 during drilling and completion for stratigraphic well service. The Pre-Operational Testing Program lists the log runs, tests, and dates the work was performed. The primary source files are provided as supporting information submitted through the GSDT Pre-Operational Testing module.

Well logs were first run to identify and/or confirm geological, geomechanical, reservoir data, and well conditions such as:

- Stratigraphic Tops
- Lithology
- Porosity
- Permeability
- Salinity
- Presence of Faults and Fractures
- Wellbore Conditions
- Casing
- Cement Conditions

There were some uncertainties prior to drilling CSS #1, such as the absence or presence of Mississippian-aged rocks (not present), the absence or presence of a formation between the base of the Arbuckle and the Precambrian basement (Reagan Sandstone is present), and the lithology of the basement (quartzite). This information, along with other petrophysical data, has been and will continue to be used to update and confirm and/or reconfigure the geologic model for AoR delineation. Both the Lansing-Kansas City Groups and the Arbuckle Group were evaluated as possible sequestration zones. Based on logging data, there is adequate injection interval and confining zones in the Arbuckle to support current project needs for sequestration. The Lansing-Kansas City Groups remain an option for future injection but are not currently needed for the project.

The following well logging was performed during drilling operations:

- Mudlog
- Borehole Profile/Caliper Logs
- Triple Combo (Density, Neutron, Resistivity Array Induction)
- Litho-Scanner with Chlorine Salinity

- Array Induction
- Formation Micro-Imager
- Combinable Magnetic Resonance
- Dielectric Scanner
- Gamma Ray Spectroscopy
- Sonic Scanner (Borehole Compensated Sonic and Dipole Sonic)

The following well logging was performed during and after casing installation:

- Casing Inspection Logs
  - Isolation Scanner Tool with
    - Casing Integrity Analysis
    - Cement Bond Analysis
    - Variable Density Log
  - Baseline Pulse Neutron
  - Downhole Temperature and Pressure Gauge (after casing installation only). The gauge initially collected measurements once per 1 second. The gauge was later transitioned to collecting measurements once per 5 seconds.

Specialty analyses from the laboratory (SLB) were provided for:

- Cement Bond Logs
- Salinity
  - discussed in the Fluid Analysis section
- FMI
- 3D Far-Field Sonic (175-foot radius around wellbore)

The casing and cementing program requirements as listed in 40 CFR 146.86 (b) were satisfied during the casing and cementing of CSS #1. Surface casing was successfully cemented to the surface (873' to surface). The base of the lowermost USDW is at 495'. The long string casing has overall moderate to high coverage of cement that provides confinement and will not allow for migration of CO_2 behind pipe, although some pockets/channels were noted. SLB and project engineers evaluated Cement Bond Logs. There were two different logs run: one on November 16, 2022, and a second on December 27, 2022. There was an increase in solids noted between the runs. The top of cement for the casing was determined to be within the Hutchinson Salt Member, and the top of 'good' cement within the Geuda Springs Shale Member. The cement of both the surface and long string casing will thereby protect USDWs as required by 40 CFR 146.86 (b).

No faulting was noted during the drilling of the CSS #1, in the 3D seismic analysis, or in the 3D Far-Field Sonic analysis by SLB; however, an analysis of the FMI log by SLB identified a minor fault in the Douglas Group at approximately 2,980 feet below kelly bushing (ft below KB) with an east-northeast to west-southwest strike orientation. This minor fault, located 450 feet above the top of the sequestration interval, is based on hand traced interpreted structural deformation, and these types of faults typically have minimal structural deformation and minor displacement.

Natural fractures were interpreted from the FMI log in the Arbuckle and the underlying Reagan and have an east-west strike orientation, which is correlative to the horizontal maximum stress orientation. Fracturing was noted in the Arbuckle on the 3D Far-Field Sonic analysis and also showed an East-West orientation. These fractures do not appear to be connected with any formations above the Arbuckle, including the overlying Marmaton Group. The other predominant set of fractures occurs within the 1,775 to 1,950 ft depth range within a few different carbonate/shale sequences. A thin set of fractures was also seen within the Lansing-Kansas City Groups which was evaluated as a possible secondary sequestration interval.

Visual observation of the core indicated slickenside textural features within clay zones that showed no evidence of post-structural fluid migration or alteration.

Flow units within the Arbuckle, as well as confining units above and below the gross sequestration interval, were delineated using petrophysical analysis. Porosity for the Arbuckle averages 15.2% and permeability averages 95 mD based on a reconciled combination of core and log data. Core analysis of the sequestration zone in the Arbuckle showed Klinkenberg permeability ranging from <0.0001 mD to 13,100 mD with an average of 1,560 mD and a median of 210 mD (17 data points), and porosities ranging from 1.2% to 22% with an average of 11.5% and a median of 11.0% (17 data points). Wireline log results for the injection and primary confining zones are displayed in Figure A.I.5-20. Additional confinement is provided by the Marmaton Group immediately overlying the Arbuckle Group, and multiple shales, including the Douglas Group, Heebner Shale, Geuda Springs Shale, and Ninnescah Shale and evaporite layers including anhydrite (Stone Corral) and salt (Hutchinson).

Figure A.I.5-20. CSS #1 Wireline Log Results for the Primary Confining and Injections Zones

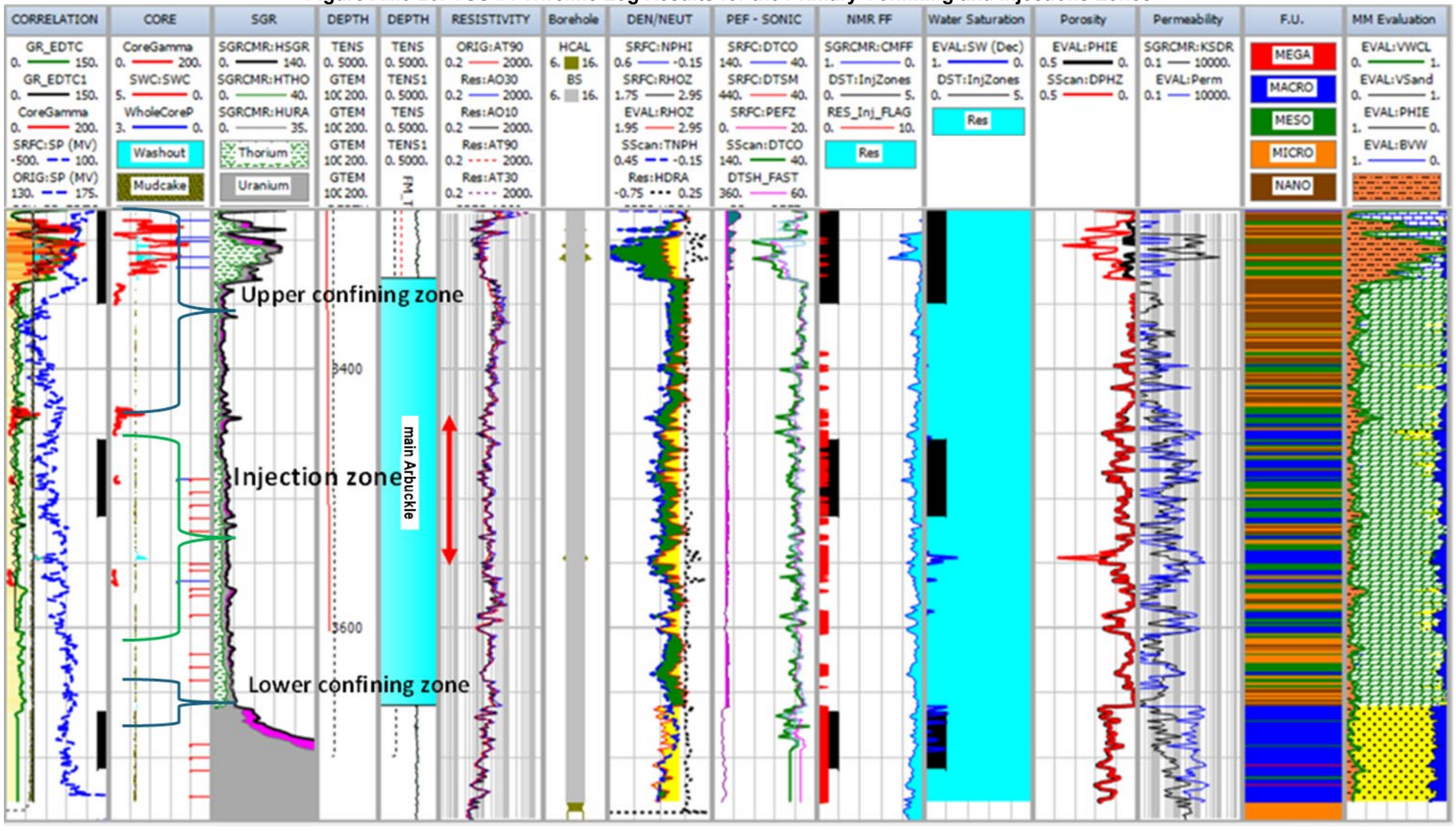

A.I.5.5. Core Analyses [40 CFR 146.87(b)]

Table A.I.5-2 summarize porosity and permeability data on core samples taken from CSS #1. A total of 291 feet of whole core were collected, plus an additional 21 sidewall cores were collected to flesh out the scope of testing for the Arbuckle Group and rocks immediately overlying (Iolat Limestone Kansas City Group, Marmaton Group) and underlying (Reagan Sandstone). Not all of the sidewall cores were deemed to be competent and underwent laboratory analyses. Additional core was collected to support the evaluation of both secondary confining units and potential future sequestration intervals in the Lansing-Kansas City Groups. The collected core catalog sufficiently supports stratigraphic correlation, interpretation of depositional environments, and wireline log calibration. There is no evidence of anomalies in the collected whole core. Visual observation of the core indicated slickensides within clay zones which showed no evidence of post-structural fluid migration or alteration.

The following tests were run on the core samples:

- Routine Core Analysis
  - Dean Stark for fluid saturations
  - Porosity
  - Permeability (including pulse decay permeability in few samples) at Standard and Net Confining Stress
  - Lithologic Description
  - Grain Density
- Geological Core Analysis
  - Thin Section Photographs and Descriptions
  - Scanning Electron Microscopy
  - X-Ray Diffraction for Bulk and Clay Mineral Composition
- Special Core Analysis
  - Relative Permeability
  - Capillary Pressure
  - Geomechanics
  - Rock Mechanics including uniaxial compressive strength and triaxial compressive strength

Table A.I.5-2. Core Data Collected in the Stratigraphic Well CSS #1

Formation	Core Depth (ft KB)	Core Type		Porosity, percent		Permeability, mD	
		Whole	Sidewall	Ambient	NCS 1	To Air	Klinkenberg
Heebner Shale member of Oread Limestone of Shawnee Group	2,923.60	X		0.09	0.08	-	<0.0001
	2,925.15	X		0.35	0.32	-	<0.0001
Toronto Limestone member of Oread Limestone of Shawnee Group	2,927.35	X		0.08	0.07	0.0004	<0.0001
	2,928.45	X		0.06	0.05	0.0004	<0.0001
	2,929.50	X		0.3	0.27	0.0002	<0.0001
	2,935.30	X		0.05	0.05	0.0002	<0.0001
	2,936.60	X		0.13	0.12	0.0004	0.0001
	2,938.30	X		0.13	0.11	0.0008	0.0001
	2,939.55	X		0.23	0.22	0.0003	<0.0001
	2,942.90	X		0.09	0.08	-	<0.0001
	2,943.80	X		0.54	0.52	-	<0.0001
Douglas Group	2,946.65	X		0.23	0.21	-	<0.0001
	2,949.50	X		0.82	0.80	-	<0.0001
	2,950.85	X		0.86	0.84	-	<0.0001
	2,951.50	X		0.34	0.33	-	<0.0001
	2,955.05	X		10.2	9.9	0.0014	0.0003
	2,958.25	X		1.0	0.98	-	<0.0001
	2,959.85	X		0.71	0.70	-	<0.0001
	2,960.95	X		0.15	0.14	-	<0.0001
	2,961.40	X		0.67	0.66	-	<0.0001
	2,963.00	X		1.14	1.11	-	<0.0001
	2,970.55	X		0.46	0.44	0.039	<0.0001
Lansing Group	2,990.25	X		17.9	17.7	0.12	0.072
	2,991.40	X		19.4	19.3	0.388	0.271
	2,992.50	X		5.0	4.9	0.048	0.024
	2,993.60	X		-	19.9	587	552
	2,994.30	X		-	19.3	388	360
	2,996.70	X		4.7	4.5	0.615	0.457
	2,997.40	X		6.7	6.6	0.019	0.0078
	2,998.70	X		3.1	3.0	0.0023	0.0005
	2,999.35	X		4.0	4.0	0.173	0.109
	3,000.65	X		2.3	2.2	0.0017	0.0003
	3,001.50	X		2.3	2.2	0.0022	0.0005
	3,003.00	X		-	17.6	28.1	23.3
	3,006.50	X		-	26.5	540	506
	3,008.50	X		-	27.0	261	240
	3,014.50	X		-	12.8	0.037	0.018
	3,015.50	X		-	12.2	0.024	0.011
	3,017.50	X		-	8.1	0.0078	0.0026
	3,018.50	X		-	16.5	0.029	0.013
	3,019.75	X		-	12.0	0.023	0.01
	3,021.50	X		-	15.5	0.024	0.011
	3,022.50	X		-	21.0	0.14	0.085
	3,023.40	X		-	3.5	0.0044	0.0012
	3,024.55	X		1.1	1.0	0.0034	0.0009
	3,035.50	X		1.2	1.2	0.0014	0.0003
	3,039.30	X		0.9	0.9	0.0049	0.0014
	3,040.50	X		1.4	1.3	0.014	0.0053
	3,041.50	X		-	1.8	0.006	0.0018
	3,042.35	X		1	0.9	0.0022	0.0005
	3,043.50	X		8.4	8.3	0.101	0.059
	3,044.80	X		3.0	2.9	0.0015	0.0003
Hickory Creek Shale Lansing Group	3,045.80	X		1.9	1.8	0.0006	0.0001
Merriam Limestone Lansing Group	3,047.50	X		0.5	0.5	0.0006	0.0001
	3,048.20	X		7.4	7.3	-	-
	3,049.75	X		1.3	1.2	0.0003	<0.0001
	3,051.25	X		3.7	3.6	-	-
	3,052.60	X		9.1	9.0	-	-
Kansas City Group	3,053.50	X		7.2	7.0	0.0026	0.0006
	3,054.45	X		4.0	3.8	0.0026	0.0006
	3,055.75	X		9.4	9.3	0.018	0.0073
	3,057.50	X		10.3	10.2	0.439	0.313
	3,058.50	X		7.0	7.0	0.045	0.023

Formation	Core Depth (ft KB)	Core Type		Porosity, percent		Permeability, mD	
		Whole	Sidewall	Ambient	NCS 1	To Air	Klinkenberg
	3,059.50	X		1.2	1.1	0.0005	0.0001
	3,060.50	X		7.9	7.6	0.077	0.043
Wyandotte Limestone Kansas City Group	3,061.80	X		0.9	0.6	0.0005	0.0001
	3,062.80	X		3.2	3.1	0.0059	0.0018
	3,063.60	X		2.7	2.4	0.0049	0.0014
	3,064.70	X		1.6	1.6	0.0038	0.001
	3,065.35	X		2.7	2.5	0.0082	0.0028
	3,070.25	X		0.9	0.6	0.001	0.0002
	3,071.60	X		2.6	2.5	0.0066	0.0021
	3,074.50	X		-	12.7	0.070	0.038
	3,079.70	X		-	24.6	-	-
Iola Limestone Kansas City Group	3,082.50	X		-	15.0	0.358	0.247
	3,083.50	X		-	11.4	0.060	0.032
	3,084.50	X		1.4	1.3	0.037	0.018
	3,086.50	X		-	18.2	-	-
	3,088.50	X		-	21.8	0.035	0.017
	3,089.50	X		-	12.7	0.043	0.022
	3,090.50	X		-	20.6	0.209	0.135
	3,091.45	X		-	21.7	0.744	0.526
	3,092.50	X		-	20.0	1.03	0.796
	3,093.50	X		-	24.0	0.242	0.159
	3,095.70	X		-	21.5	15.8	13.0
	3,096.50	X		-	13.3	0.169	0.106
	3,097.50	X		-	21.6	0.102	0.059
	3,099.50	X		2.0	1.9	0.0044	0.0012
	3,100.50	X		4.0	3.9	0.011	0.0040
	3,101.50	X		1.8	1.6	0.015	0.0057
	3,104.70	X		2.8	2.7	0.0062	0.0019
	3,105.50	X		1.2	1.1	0.0011	0.0002
	3,106.50	X		2.4	2.2	0.0078	0.0026
	3,107.65	X		1.3	1.3	0.0051	0.0015
	3,108.60	X		3.4	3.2	-	-
	3,109.50	X		5.4	5.3	0.018	0.0076
	3,110.65	X		1.6	1.5	0.0012	0.0002
	3,111.65	X		1.7	1.7	0.0009	0.0001
	3,113.75	X		2.0	2.0	0.0005	0.0001
	3,118.50	X		11	10.9	0.275	0.184
	3,119.50	X		2.2	2.1	0.0012	0.0002
	3,120.50	X		3.9	3.8	0.0020	0.0004
	3,123.80	X		4.4	4.3	0.0023	0.0005
	3,124.50	X		3.2	3.1	0.0021	0.0005
	3,125.10	X		10.9	10.8	0.089	0.05
Marmaton Group	3,275.00		X	-	-	-	-
Arbuckle Group	3,285.00	X		4.9	4.7	0.0021	0.0005
	3,286.45	X		5.2	5.1	0.0055	0.0017
	3,287.25	X		10.8	10.6	15.5	12.7
	3,288.50	X		8.7	8.6	0.073	0.04
	3,292.85	X		0.9	0.9	0.0021	0.0005
	3,310.50	X		0.29	0.21	0.0009	0.0001
	3,314.30	X		0.07	0.06	0.0001	<0.0001
	3,321.00	X		0.8	0.3	-	<0.0001
	3,321.20	X		1.3	0.3	-	<0.0001
	3,323.60	X		16.2	16.2	0.051	0.026
	3,324.25	X		8.7	8.6	0.012	0.0046
	3,326.75	X		9.3	9.3	0.056	0.029
	3,334.50	X		-	4.5	0.103	0.060
	3,335.30	X		-	2.6	0.0015	0.0003
	3,336.20	X		-	3.8	0.075	0.041
	3,338.50	X		-	3.7	0.0095	0.0033
	3,341.50	X		8.2	8.0	0.292	0.197
	3,342.50	X		-	3.4	0.0072	0.0023
	3,343.50	X		3.7	3.6	0.029	0.013
	3,345.50	X		-	10.2	2.9	2.28
	3,346.50	X		-	6.2	38	32.5
	3,347.50	X		-	7.8	6.49	5.19

Formation	Core Depth (ft KB)	Core Type		Porosity, percent		Permeability, mD	
		Whole	Sidewall	Ambient	NCS 1	To Air	Klinkenberg
	3,348.15	X		-	7.8	0.497	0.36
	3,349.75	X		-	8.4	3.65	2.89
	3,430.50	X		13.2	12.9	2.77	2.16
	3,431.50	X		11.7	11.4	1.63	1.25
	3,433.50	X		-	12.0	12.9	10.5
	3,434.50	X		23.3	23.2	3.59	2.79
	3,435.60	X		-	10.7	1.59	1.24
	3,436.50	X		-	8.1	97.6	86.7
	3,438.50	X		-	11.8	1.28	0.997
	3,440.15	X		-	16.2	271	248
	3,447.65	X		-	14	34.2	28.4
	3,483.20	X		-	10.9	1.66	1.3
	3,484.90	X		-	11	168	152
	3,485.10	X		-	17.4	604	568
	3,485.80	X		-	9.8	205	187
	3,486.50	X		13.5	13.2	140	126
	3,487.90	X		-	22	13300	13100
	3,488.15	X		-	6.2	230	210
	3,505.00		X	11.8	11.8	223	204
	3,525.00		X	9.8	9.6	7.61	5.9
	3,556.50	X		-	12.4	7200	7030
	3,557.00	X		-	18.6	2700	2610
	3,558.50	X		-	10.8	569	535
	3,562.35	X		-	16.7	877	832
	3,564.45	X		-	8.0	617	580
	3,564.65	X		-	11.4	398	370
	3,565.65	X		4.4	4.3	10.1	8.19
	3,570.00		X	1.4	1.2	0.0007	0.0001
	3,640.00		X	12.3	12.2	2.66	2.02
Reagan Sandstone	3,700.00		X	4.1	3.9	29.3	24.4

- = test results not reported

A.I.5.5.1. Routine Core Analysis

Routine Core Analysis was collected from whole core and rotary side wall core. The following charts on Figure A.I.5-21 demonstrate the porosity and permeability by depth of core tests for the primary upper confining zone and the injection zone within the Arbuckle Group. The lower confining zone was identified using petrophysical analysis of the CSS #1 which is confirmed by analysis of other well logs in the area as shown on the permeability histogram and rock properties layer for the Arbuckle 7 layer in PBI_Porosity_Permeability Maps.pdf.

Figure A.I.5-21. Routine Core Analysis Data for the Arbuckle Group

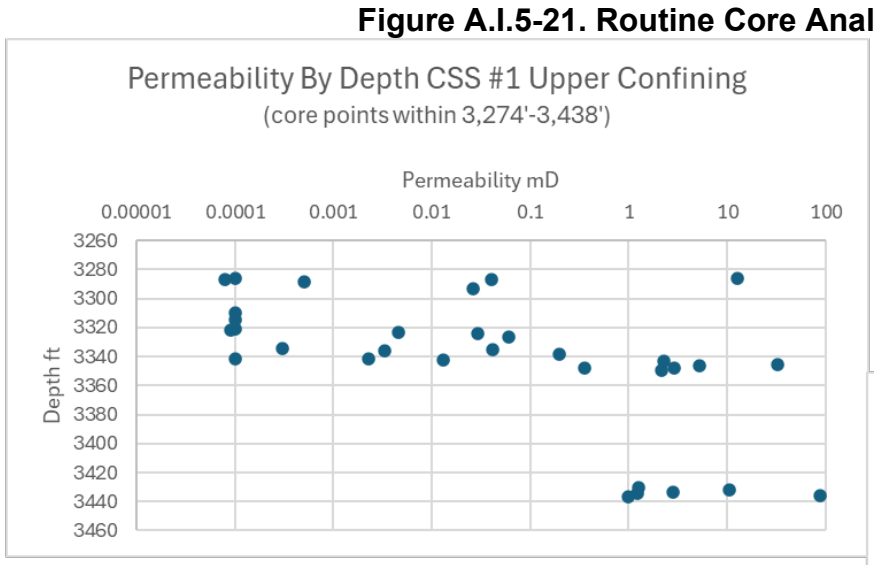

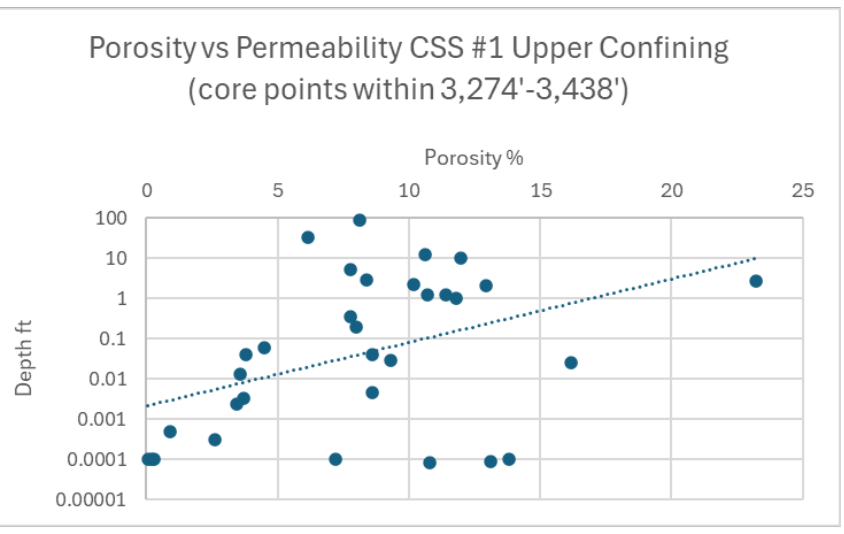

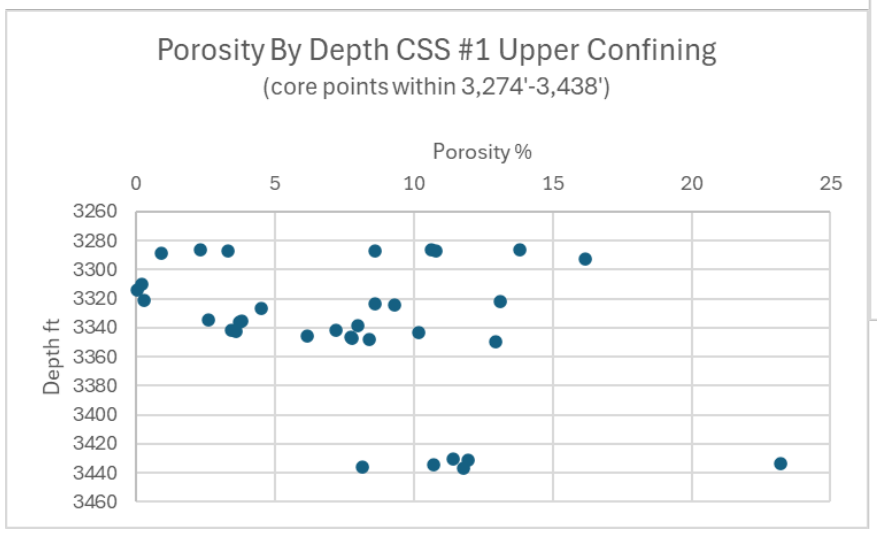

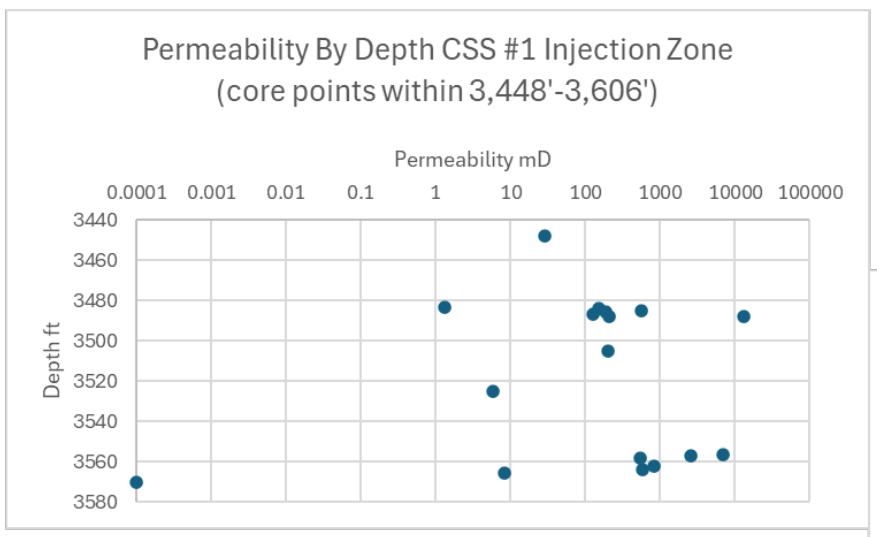

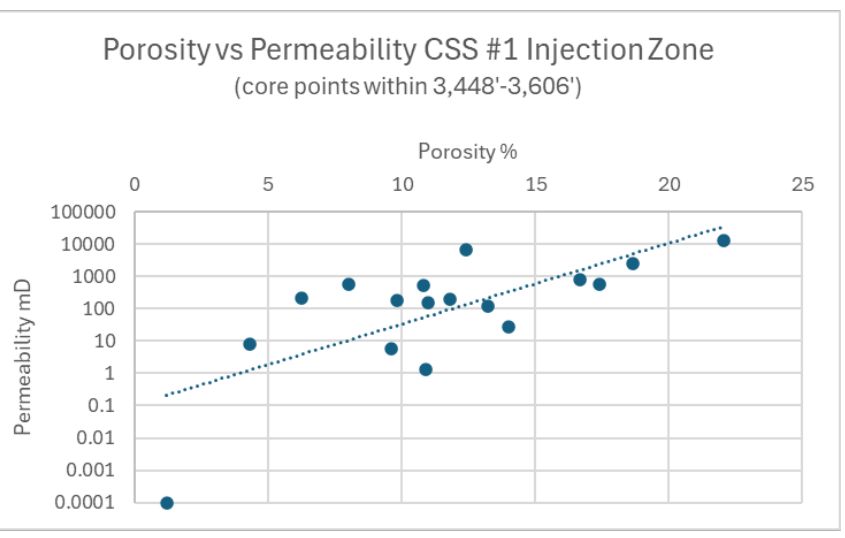

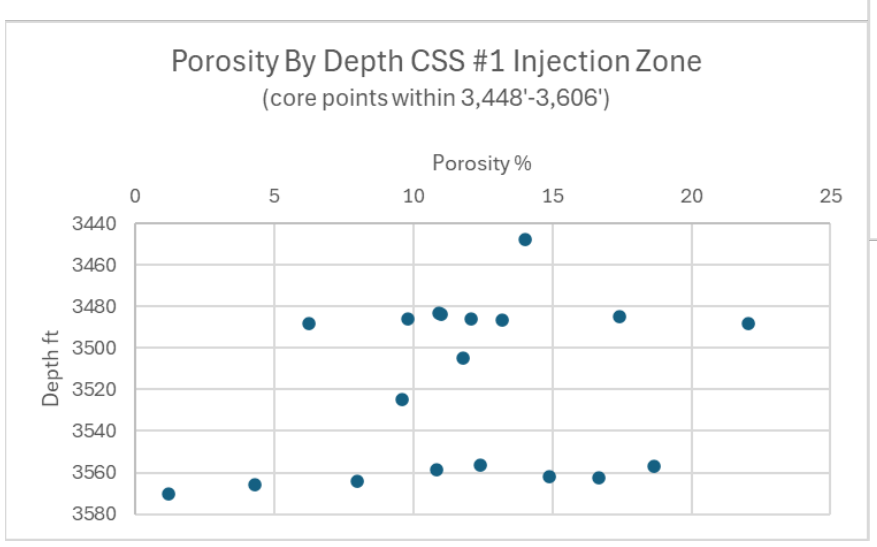

A.I.5.5.2. Rock Geochemical Analysis

Core samples from the well were analyzed for mineralogy, grain and pore architecture, and geochemical properties using a variety of methods including traditional X-ray diffraction (XRD), scanning electron microprobe (SEM), thin section petrography including point counts, and Fourier-transformed infrared spectroscopy (FTIR) analyses were performed on samples at Stratum Reservoir Laboratories. Initial analysis showed that the primary injection target was >80% carbonate, compositional and mineralogical analyses were prioritized. Samples were selected over the entire interval of the core, using well-log data and core observations, to capture and complete the geologic characterization needs for major formations and associated lithofacies, as well as being selected to capture statistically relevant distribution across the targeted formations. Full data and reports are provided as supporting information under the GSDT Pre-Operational Testing module (see PBI_HH-111871ccXRD.pdf, PBI_HH-111871rswcXRD.pdf, PBI_HH-111871_Ci 2879_Purefield CSS_June 2023_FTIR (55).pdf, PBI_HH-111871_Ci 2879_Purefield CSS_June 2023_FTIR (57).pdf, PBI_HH-111871 Thin Section Description – Final.pdf, PBI_HH-111871 Point Count Analysis - Client File.pdf, PBI_HH-111871_SEM_Descriptions.pdf, and folders labeled PBI_HH-111871 SEM Images, Samples 21-43, 48-55, and 56-57). A summary of these analyses is provided herein.

A total of 53 samples were analyzed for XRD (PBI_HH-111871ccXRD.pdf), providing quantitative data on the compositional percentage of four primary mineral types; tectosilicates, carbonates, phyllosilicates and additional minerals – See Figure A.I.5-22. Tectosilicate compositional analysis quantified the percentage of quartz, potassium feldspar and plagioclase. Carbonate compositional analysis quantified the percentage of calcite, dolomite and siderite. Phyllosilicate compositional analysis quantified the percentage of different clay group minerals, and the additional category identifies accessory minerals (PBI_HH-111871ccXRD.pdf). Overlying confining layers of the Heebner and Toronto formations are predominantly composed of clay group minerals (phyllosilicates), mostly illite with some chlorite and kaolinite. Tectosilicates are dominated by quartz with some feldspar; there is no indication of carbonate minerals. The Lansing-Kansas City Groups have mixed compositions, including mixed carbonates and clastic (quartz) carbonates. The carbonates are primarily calcite. Some lithofacies see increased compositions of iron-rich minerals such as hematite and goethite. The Arbuckle Group has dominantly carbonate compositions that are predominantly dolomite; minor compositions of quartz are also observed in some samples and minimal clay or accessory minerals.

Figure A.I.5-22. Total Compositional Analysis of Different Group Minerals Relative to Depth

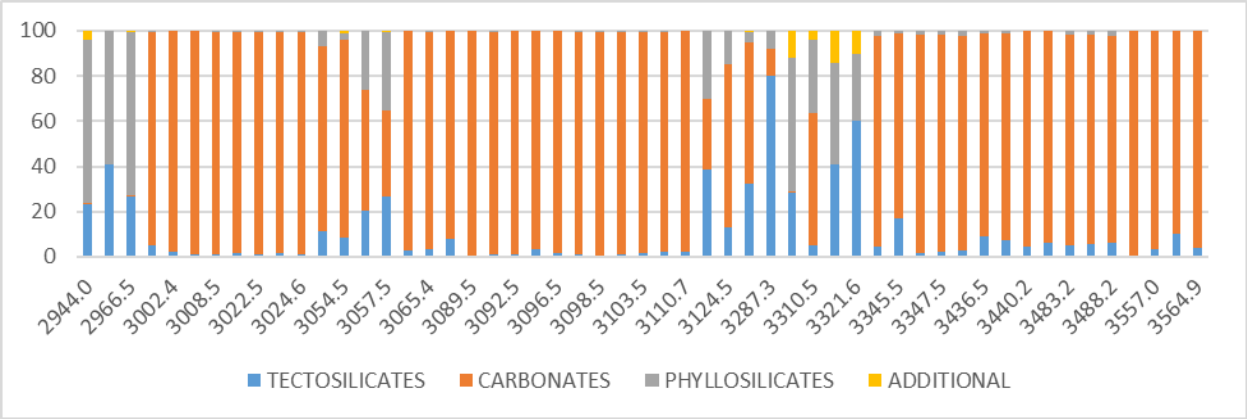

A total of 57 samples were analyzed for FTIR (PBI_HH-111871_Ci 2879_Purefield CSS_June 2023_FTIR (55).pdf, PBI_HH-111871_Ci 2879_Purefield CSS_June 2023_FTIR (57).pdf), to provide additional mineral and compositional data for the whole rock analysis such as total organic carbon. The results for FTIR compositional analysis are comparable to the XRD data; however, this data provided the project with data on the organic and sulfur mineral contents of the formations that could react in the presence of new fluid. Only minor sulfur-bearing minerals and organic contents were observed in the Arbuckle, which is the primary injection zone.

This section analyses were performed on most core samples to describe mineralogy, grain sizes, pore types and distribution, and diagenetic minerals. These data correlate to XRD performed on the samples, and both provided additional support for lithofacies characterization and distribution and pore character. Figure A.I.5-23 shows a typical example from a target injection zone in the Arbuckle Group; a dolostones with high relative porosity and minor accessory minerals. Figure A.I.5-24 highlights the difference with the overlying, low porosity permeability lithofacies in a sample from the Lansing-Kansas City Groups sample. Similarly, Figure A.I.5-25 highlights the distinct difference in carbonate composition between the porous Mg-rich dolostone in the Arbuckle Group and the low porosity calcite-dominate limestone in the Lansing-Kansas City Groups. Figure A.I.5-26 provides an example of the clay- and shale-rich confining zones overlying the injection formations.

SEM was performed on select samples to further strengthen the characterization of core samples with respect to pore architecture, mineral relations, and clay distribution. Figure A.I.5-27 provides an example of SEM imagery and analysis of an Arbuckle Group sample, highlighting the characteristics of dolomite crystals and accessory clay minerals.

Figure A.I.5-23. A Sample of Highly Porous Crystalline Dolostones from the Arbuckle Group

PureField Ingredients LLC
Purefield CSS Whole Core Analysis
Russell County
Onshore Kansas

3640.00 FEET
Sample 11R_P
Dolostone

Project # HH-111871
Rotary Sidewall Core

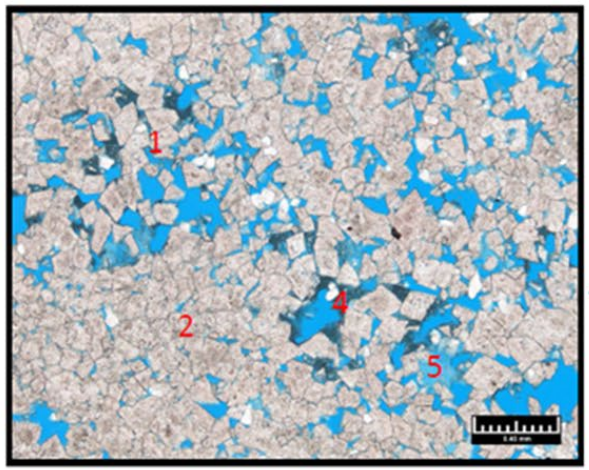

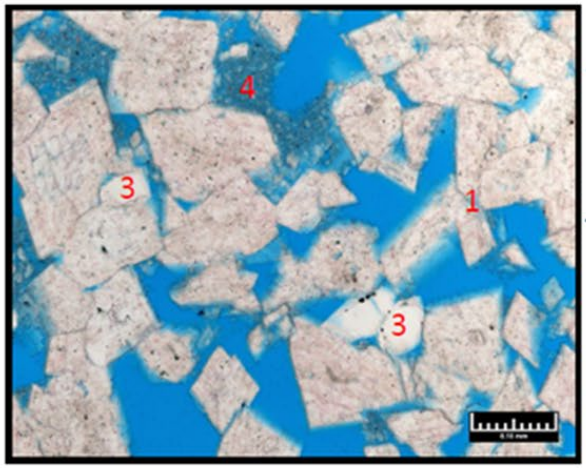

DETRITAL GRAINS/BIOCLASTS:
Est. Avg. Grain Size* = N/A; Range*: N/A
Sorting*: N/A
Compaction: Low to moderate, based on floating to concave/convex crystal contacts, absence of crystal-crushing, and preservation of intercrystalline porosity
*includes sand/silt portion only

MAJOR COMPONENTS:
N/A
MINOR/ACCESSORY:
Monocrystalline quartz, plagioclase
MATRIX:
Rare to minor microcrystalline dolomite mixed with trace remnant, crystal/pore-rimming, undifferentiated clays

DIAGENESIS:

MAJOR:
Dolomite – Abundant very fine (10µm) to coarse (300µm), subhedral to euhedral crystals. Rare to minor recrystallized pore-filling cryptocrystalline microcrystalline dolomite crystals

MINOR:
Quartz Overgrowths – Rare to minor, poorly- to well-developed, and isolated to coalescing overgrowths
Kaolinite – Rare to minor authigenic pore infill
Pyrite – Rare replacement of matrix

PORE TYPES:

Minor to common intercrystalline porosity. Rare to minor secondary porosity from leaching of allochems. Rare possible vuggy porosity.

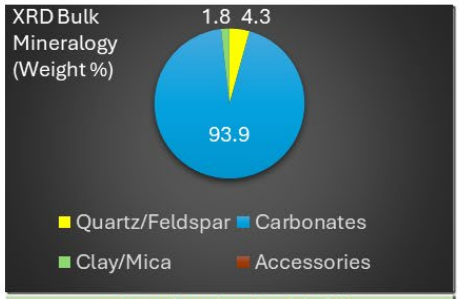

Clay Mineralogy (weight %)			
Chlorite	**Kaolinite**	**Illite/Mica**	**Mx I/S***
0.0	1.0	0.8	Tr

PETROGRAPHIC SUMMARY

Photomicrographs depict a dolostone with a crystalline texture. The fabric is planar and consists mostly of crystal-supported euhedral dolomite rhombs arranged in a planar-e pattern (1) and localized planar-s (2) subhedral to anhedral dolomite crystals. Due to the recrystallized nature of the material, ghosts of the original grains and matrix are impossible to identify. The dolomite crystals consist of very fine (10µm) to coarse (300µm) euhedral to subhedral rhombs likely present as a replacive phase. Minor silt-sized (0.03mm) to fine sand-sized (0.15mm) monocrystalline quartz represents the main detrital constituent (3). Early quartz overgrowth cement developed in some host grains. Minor grain/pore-lining dolomicrite (4) is present likely from precipitation and/or breakage of precursor materials. Rare to minor undifferentiated clays are mixed with the dolomicrite content. Authigenic kaolinite is present as a pore-filling cement (5). A rare amount of fine crystalline, framboidal pyrite replaces the matrix. Patchy porosity (blue epoxy) resulting likely from matrix leaching is distributed throughout the sample slide and is poorly connected by intercrystalline microporosity. Other pore types include secondary intraskeletal molds and possible vugs.

Figure A.I.5-24. Clay-rich Siltstone at top of Arbuckle Group with No Porosity

PureField Ingredients LLC
Purefield CSS Whole Core Analysis
Russell County
Onshore Kansas

3314.30 FEET
Sample 6-5_P
Organic-Rich, Siliceous, Silty Mudstone

Project # HH-111871
Conventional Core

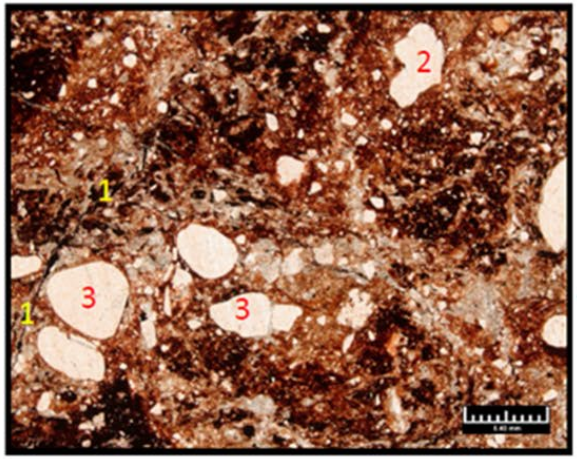

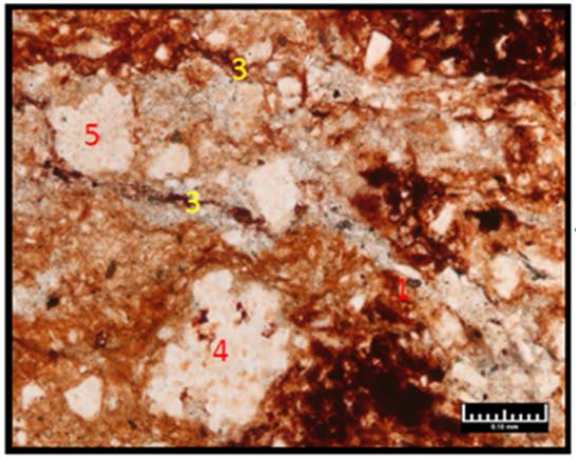

DETRITAL GRAINS/BIOCLASTS:
Est. Avg. Grain Size* = 0.07mm; **Range***: 0.01mm (fine silt) to 0.90mm (coarse sand)
Sorting*: Very poor
Compaction: Moderate, based on floating to longitudinal grain contacts, slightly preferred alignment of some elongated grains, and pressure-solution features on probable burrow traces, and incipient microstylolitization
*includes sand/silt portion only

MAJOR COMPONENTS:
Monocrystalline quartz

MINOR/ACCESSORY:
Chert fragments, chalcedony fragments, polycrystalline quartz, metaquartzite, chert- and quartz-replaced allochems, metamorphic rock fragments, organic fragments, phosphatic fragments, anatase

MATRIX:
Very common pore-filling detrital kaolinite, according to visual examination and XRD analysis

DIAGENESIS:

MAJOR:
Silica – Very common chert replacement of matrix, lenses, burrows, and minor replacement for allochems. Rare equant megaquartz replacement of allochems
Organic Material – Common pore-filling residual hydrocarbon mixed in with detrital, filling microfractures and microstylolites
Hematite – Minor to common replacement of matrix, grains, and organic material

MINOR:
Pyrite – Trace replacement of organic material and matrix

PORE TYPES:
No natural pores were observed under standard petrographic techniques. Plucked grains and open fractures are likely an artifact of the sample preparation process.

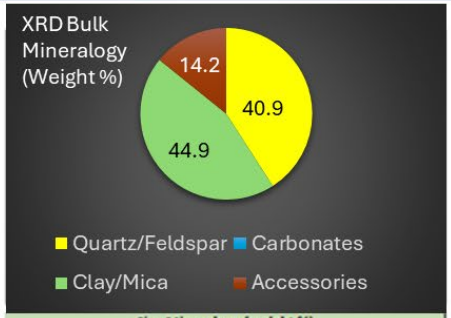

Clay Mineralogy (weight %)				
Chlorite	Corrensite*	Kaolinite	Illite/Mica	Mx I/S**
0.0	0.0	44.9	0.0	0.0

PETROGRAPHIC SUMMARY

Photomicrographs depict an organic-rich, siliceous, silty mudstone. The fabric is massive and chaotic disrupted by soft sediment deformation and burrowing activities. High-angle (?) natural-occurring microfractures have been filled with organic material (1). Organic material-filled incipient microstylolitization is additionally noted (2). The primary detrital component of the sample is monocrystalline quartz (3). Chert, chalcedony fragments, polycrystalline quartz (4), metaquartzite (5), chert- and quartz-replaced allochems, metamorphic rock fragments, organic fragments, phosphatic fragments, and anatase are also present but are rare to minor. The matrix consists of abundant pore-filling detrital kaolinite (brown material) mixed with abundant residual hydrocarbon (dark brown material). Burrow traces are elliptical, with some showing signs of mechanical compaction. Burrow traces and deformed areas have been largely replaced by cryptocrystalline quartz (chert). Chert, chalcedony, and equant megaquartz also occur as minor replacements for allochems. Hematite is an additional common replacement for organic material within the matrix.

Figure A.I.5-25. Fossiliferous Limestone/Calcite in the Lansing/Kansas City Formation

PureField Ingredients LLC
Purefield CSS Whole Core Analysis
Russell County
Onshore Kansas

3054.45 FEET
Sample 4-6
Skeletal Limestone

Project # HH-111871
Conventional Core

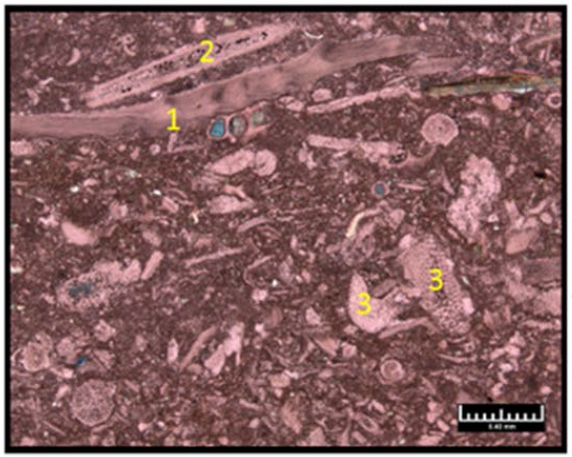

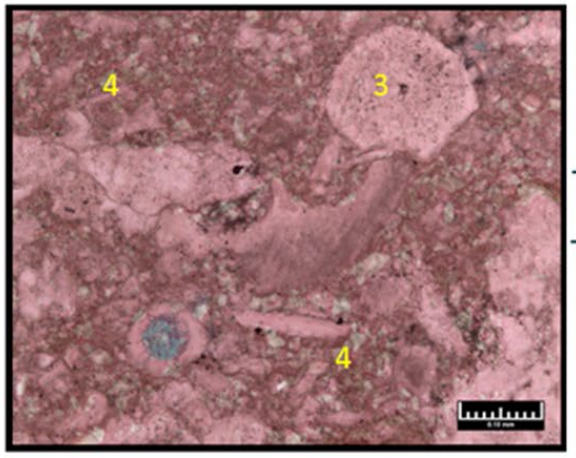

DETRITAL GRAINS/BIOCLASTS:
Est. Avg. Grain Size* = N/A; Range*: N/A
Sorting*: N/A
Compaction: Moderate, based on the preferred orientation of elongated allochems, point to longitudinal allochem contacts, minor to common allochem crushing, and incipient microstylolitization
*includes sand/silt portion only

MAJOR COMPONENTS:
Brachiopod shell fragments, brachiopod spines, echinoderm fragments, undifferentiated thin-walled shell fragments, recrystallized allochems, crushed bioclasts

MINOR/ACCESSORY:
Phosphatic fragments, undifferentiated skeletal debris, calcispheres, bryozoans, monocrystalline quartz

MATRIX:
Common pore-filling microcrystalline calcite mixed with minor detrital clays. Trace allochem-rimming detrital illite

DIAGENESIS:

MAJOR:
Calcite – Very common neomorphosed microspar to pseudospar as interparticle pore infill. Blocky calcite spar as minor intraparticle pore infill and rare interparticle cement. Rare micritization and replacement of allochems

MINOR:
Silica – Minor chert/chalcedony replacement of skeletal debris
Dolomite – Minor fine crystalline replacive phase of the matrix
Organic Material – Rare pore-filling, allochem-coating, and microstylolite-filling residual hydrocarbon
Authigenic Clays – Rare kaolinite and undifferentiated clays filling intraskeletal pores
Pyrite – Trace (visual estimate) replacement of matrix, allochems, and organic material

PORE TYPES:
Rare to minor intraskeletal pores and rare interparticle pores.

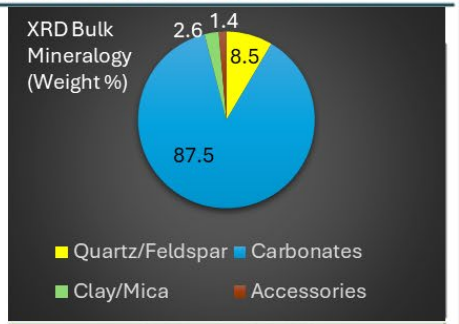

Clay Mineralogy (weight %)				
Chlorite	Corrensite*	Kaolinite	Illite/Mica	Mx I/S**
Tr	0.9	Tr	1.7	Tr

PETROGRAPHIC SUMMARY

Photomicrographs depict a moderately packed, skeletal limestone with a wackestone to packstone texture. Microstylolitization marked by the concentration of pyritized organic material is rare but present. Skeletal debris content is common and includes brachiopod shell fragments (1), brachiopod spines (2), echinoderm fragments (3), undifferentiated thin-walled shell fragments, recrystallized allochems, and crushed bioclasts. The matrix is composed of common pore-filling micrite and very common neomorphosed microspar to pseudospar. Minor detrital clays and organic material filling interparticle pores and rimming allochems are also noted. Minor blocky calcite spar (pink stain) is a minor cement phase occluding intraskeletal pores. Calcite additionally occurs as a replacive phase of skeletal debris. The matrix has been partially replaced by minor fine crystalline dolomite (4). Chert is a minor replacive phase for skeletal debris. The main interparticle porosity has been reduced due to the occurrence of detrital clays and the presence of authigenic pore-filling minerals, resulting only in rare to minor intraskeletal pores (blue epoxy) and rare interparticle pores.

Figure A.I.5-26. Clay-Rich Mudstone in a Sealing Lithofacies at the Study Site

PureField Ingredients LLC
Purefield CSS Whole Core Analysis
Russell County
Onshore Kansas

2944.00 FEET
Sample W/C 1_P
Thin Section C44

Project # HH-111871
Conventional Core

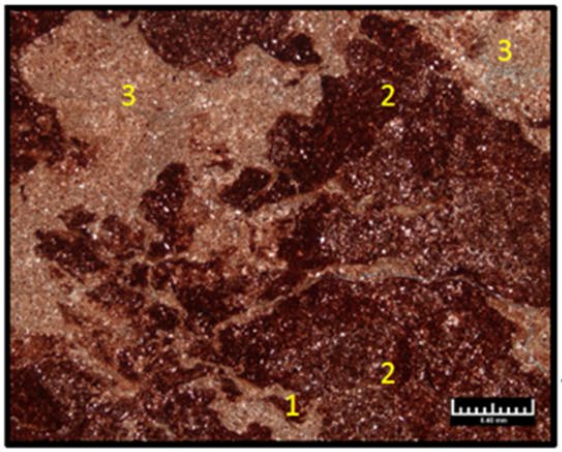

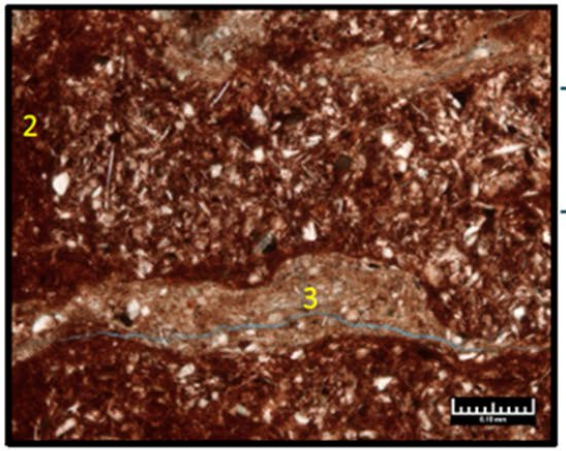

ROCK NAME (Folk): Subarkose
SEDIMENTARY FABRIC: Massive; soft-sediment deformed; burrowed
GRAIN SIZE RANGE*: 0.01mm (fine silt) to 0.05mm (coarse sand)
AVERAGE GRAIN SIZE*: 0.01mm (fine silt)
ROUNDNESS*: Sub-angular to sub-rounded
SORTING*: Very well
COMPACTION: Low to moderate; based on floating grain contacts, mild mechanical deformation on burrow traces, and preferred orientation of elongated/labile grains/allochems

*Sand/silt portion only

FRAMEWORK GRAINS/ALLOCHEMS:

MAJOR: Monocrystalline quartz (18.3%), muscovite (5.7%)
MINOR: Plagioclase (1.0%)
ACCESSORY: Potassium feldspar (0.7%), pseudomatrix from deformed mudstone fragments (0.3%), organic fragments (0.3%), undifferentiated phosphatic fragments (0.3%)
MATRIX: Abundant pore-filling disordered/infiltrated mixed detrital clay (64.0%). Minor to common pore-filling laminar detrital clay (5.3%)

DIAGENESIS:

MAJOR:
N/A

MINOR/ACCESSORY:
Chert – Cryptocrystalline to microcrystalline replacement of the matrix (3.7%)
Iron Oxides - Hematite replacement of the matrix (1.3%)
Pyrite – Fine crystalline replacement of matrix and detrital grains (0.3%)

PORE TYPES:

No natural-occurring porosity visible under plain white. Open fractures are likely an artifact from the sample preparation process.

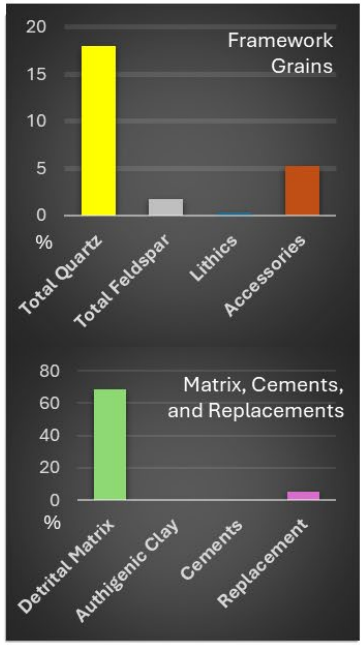

PETROGRAPHIC SUMMARY:

Photomicrographs depict a massive and chaotic, silty mudstone classified by Folk (1968) as a subarkose. The fabric has been altered by soft-sediment deformation, probable dewatering/fluid escape, and clay-filled elliptical burrow traces. Probable flame structures are also present within the deformed areas (1). Detrital constituents include abundant monocrystalline quartz silt and minor to common muscovite. Rare to minor amounts of plagioclase, potassium feldspar, pseudomatrix from deformed mudstone fragments, organic fragments, and undifferentiated phosphatic fragments are also present. The matrix is composed of abundant pore-filling disordered/infiltrated mixed detrital clay and minor to common pore-filling laminar detrital clay. The darker, less susceptible areas within the matrix appear more illitic-rich (2), while the more "flowy" and altered areas within the matrix appear more illite/smectite-rich (3). These illite/smectite-altered zones also show partial replacement by minor chert. Another replacive phases include hematite and fine crystalline pyrite disseminated through the matrix and coating unstable detrital grains. The porosity system has been obliterated by pore-filling clays and authigenic minerals. Open fractures observed in the sample likely occurred during sample preparation.

Figure A.I.5-27. Typical Example of an SEM Image from the Arbuckle Group Showing Annealed, Crystalline Dolomite Crystals and Some Clay Overgrowths

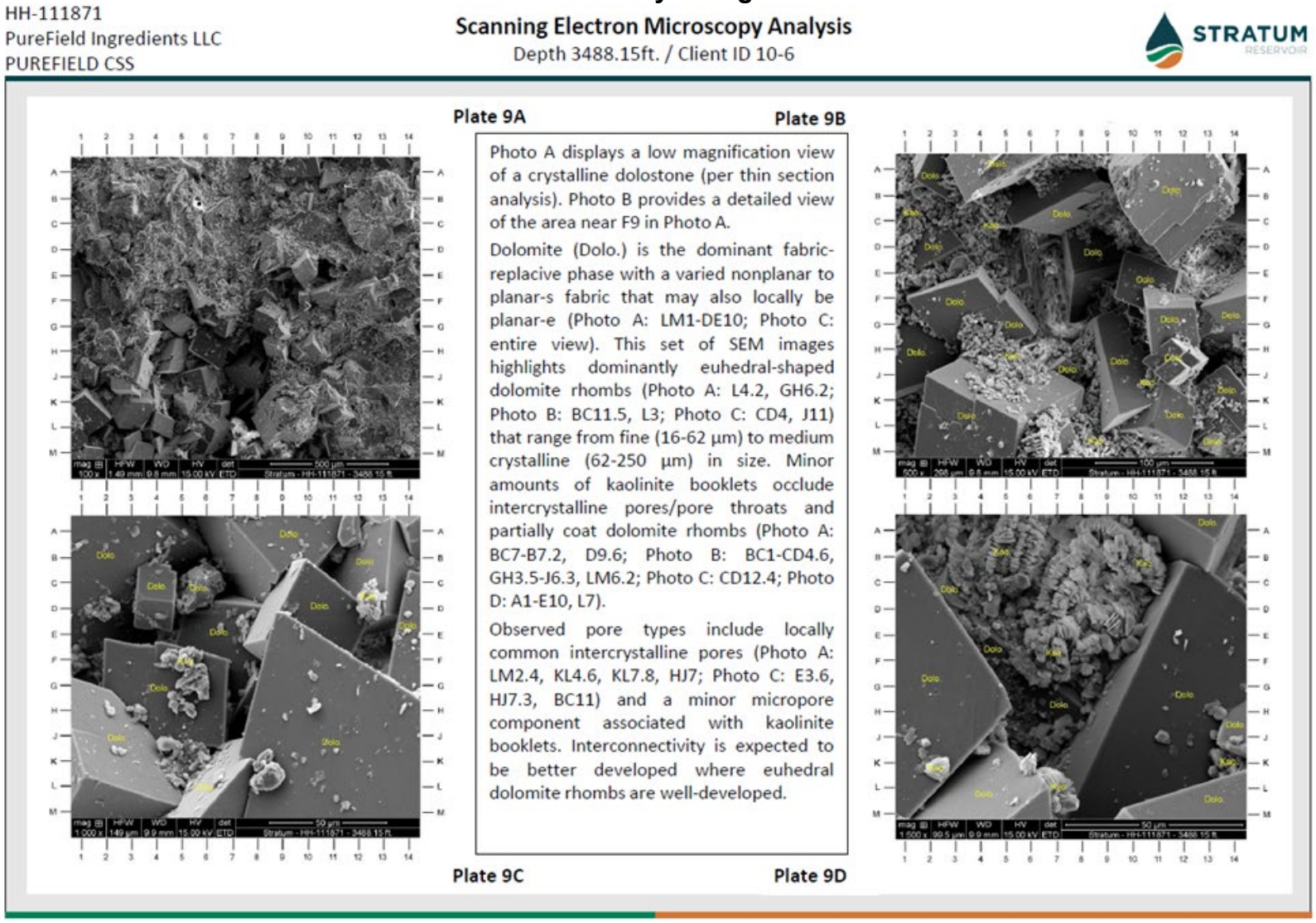

A.I.5.5.3. Log Calibration of Porosity and Permeability Using Core Data

Results from laboratory testing of cores were used to calibrate well logs, especially for porosity and permeability. Core test results correlated consistently with well logs, increasing confidence in both. The relationship between porosity and permeability assists in discriminating different types of fractures and vugs present in the Arbuckle, as well as the secondary potential sequestration interval of the Lansing-Kansas City Groups, as shown in Figure A.I.5-28 and Figure A.I.5-29. Although karst features and vuggy porosity were observed, these are isolated occurrences that contribute to storage capacity and do not play a negative role in sequestration integrity. This concurs with other data collected on fracturing in the testing program.

Figure A.I.5-28. K-Phi Relationships Based on Laboratory Fractures and Vug Observations

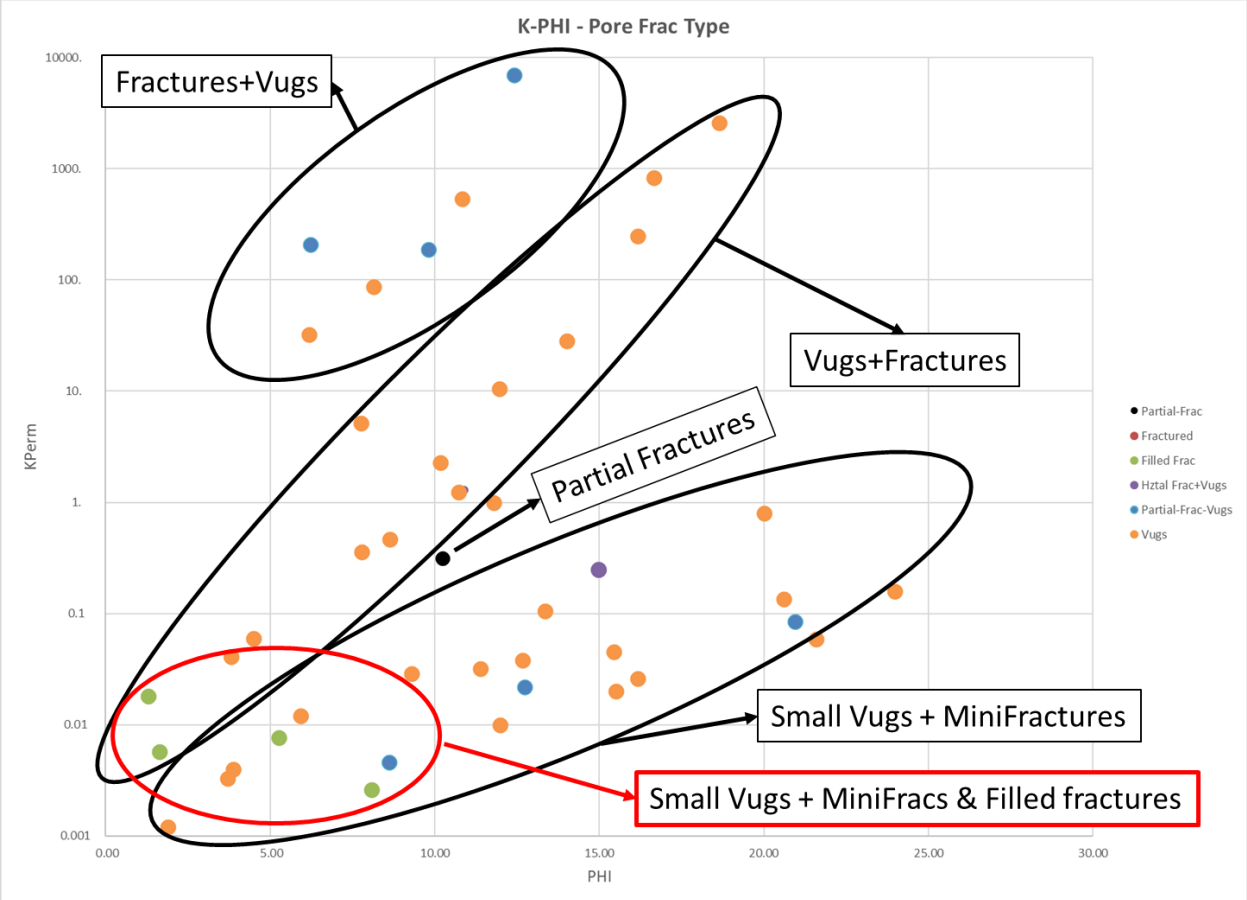

Figure A.I.5-29. Cross Plot of Porosity and Permeability for Carbonate Samples from the Lansing-Kansas City and Arbuckle Groups

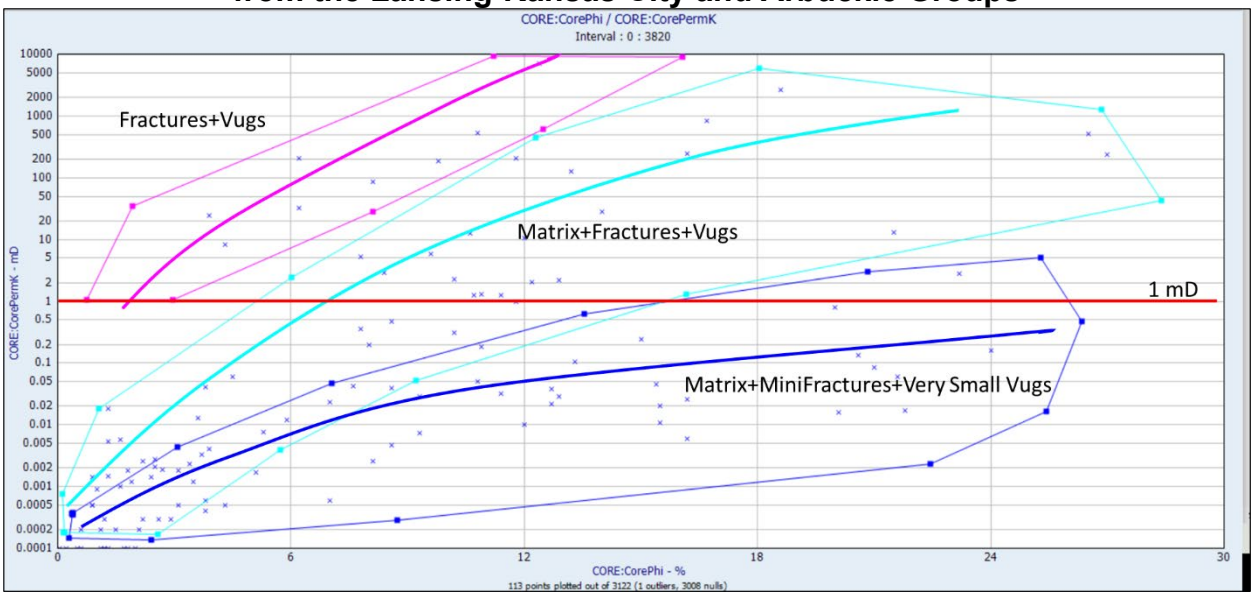

A.I.5.5.4 Capillary Pressure of Primary and Secondary Confining Zones vs. Sequestration Interval

Figures A.I.5-30 through A.I.5-32 demonstrate the contrast in capillary pressures between the Marmaton and Upper Arbuckle upper confining zones (1,315 psi) vs the main storage reservoir interval in the Arbuckle (5-50 psi).

Figure A.I.5-30. Capillary Pressure Seal and Storage Reservoir Properties

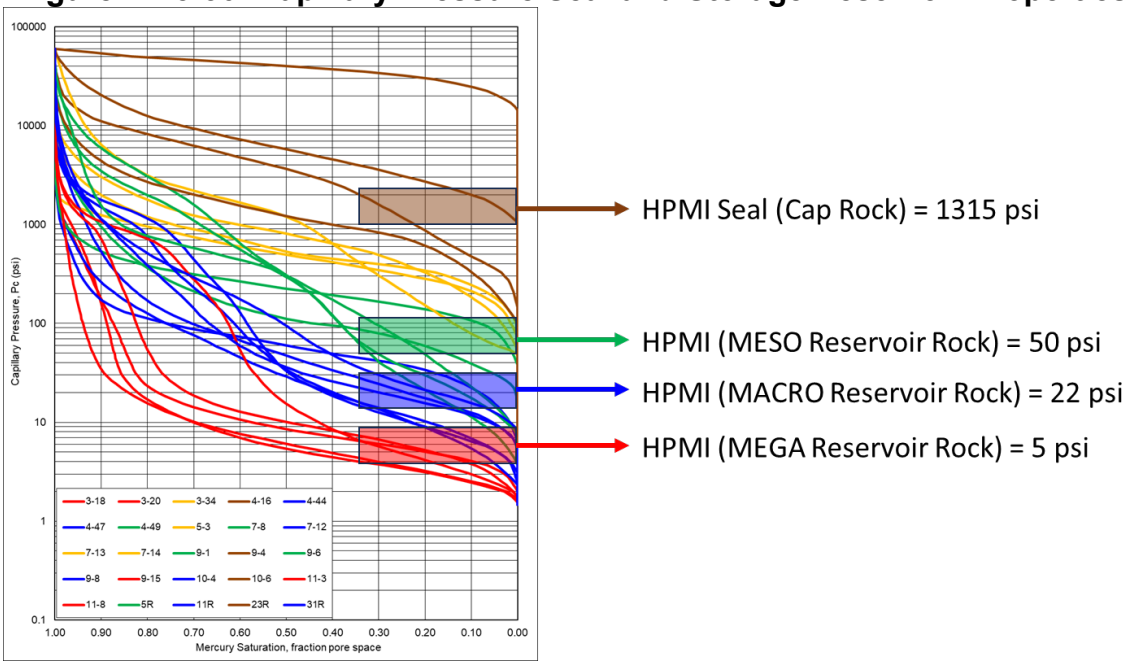

Figure A.I.5-31. Capillary Pressure Seal and Storage Reservoir Properties Calculation

SEAL CAPACITY CO2 INJECTION

							Mega	Macro	Meso
						Seal	Reservoir	Reservoir	Reservoir
	Pc A/Hg	Capillary Pressure air-mercury				1315	5	22	50
	IT (b/air)*Cos(a)b/air	Interfacial Tension B/gas*Cos(a)b/gas				72	72	72	72
	IT (a/Hg)*Cos(a)a/Hg	Interfacial Tension a/Hg*Cos(a)a/Hg				367	367	367	367
	Cos(a)b/hc	Cosine contact angle b/Hc				1	1	1	1
	Cos(a)a/Hg	Cosine contact angle air-mercury				0.765	0.765	0.765	0.765

		Brine / Gas Capillary Pressure			
		SEAL	RES-MEGA	RES-MACRO	RES-MESO
Pc b/gas	MEGA	258.0	1.0		
Pc b/gas	MACRO	258.0		4.3	
Pc b/gas	MESO	258.0			9.8

hmax	Max height seal capacity			Denw	1
Pds	PC b/hc seal			Est. Dengas	0.355
Pdr	PC b/hc reservoir Rock				
			MEGA	MACRO	MESO
	Seal capacity	hMax	920.22	908.27	888.61

Figure A.I.5-32. Capillary Pressure Seal and Storage Reservoir Properties Results

1)- AVG. Hg Capillary Pressure for Cap Rock and Quality Reservoirs are:
- Cap Rock = 1315 psi
- MEGA Reservoir = 5 psi
- MACRO Reservoir = 22 psi
-MESO Reservoir = 50 psi

2)- Using required parameters and dominant reservoir quality for injection zone as shown in calculation inputs, the height for seal capacity in the Arbuckle for a column of approximately 920 ft, enough for the CO_2 volumes to be injected, according to the preliminary simulation, storage and seal capacity are maintained.

A.I.5.5.5 CO_2-Brine/Rock Reactions

Water composition, geochemical logs, core samples composition, and thin sections were analyzed to enable equilibrium and reaction kinetics modeling and determining the potential for dissolution reactions, mineralization, and investigate plugging pore space due to mineral precipitation or halite precipitation due to dissolution of CO_2 in water caused by CO_2 injection. Equilibrium and kinetic geochemical modeling were performed using PHREEQC version 3.0[1], and reservoir geochemical modeling was performed using CMG GEM™[2]. Reservoir water compositions and properties were adjects to in-situ reservoir temperatures and pressures. The mineral spatial composition of the reservoir was adjusted based on the geochemical log and core mineralogy concentrations using rock-type distributions. Geochemical modeling of CO_2-water-rock interactions helped clarify the following potential issues: 1) does the risk of formation damage pore-space clogging exist that can potentially increase downhole injection pressure? 2) does the risk of mineral dissolution exist that can potentially influence CO_2 upwards or lateral migration? 3) does mineral precipitation increase CO_2 trapping in the reservoir? Equilibrium and kinetic geochemical models have indicated that:

1. Due to the relatively small-scale nature of the project, mineral precipitation is not expected during an active phase of CO_2 injection, and pore-space clogging, which may reduce permeability and negatively impact injectivity, is not forecasted. Also, due to the relatively low injection rate of CO_2 and unfavorable concentrations of Na and Cl ions, the halite precipitation rate is projected to be low, and the forecast does not exceed 1% of all available pore space strictly around the wellbore.
2. CO_2 injection process creates such pressure and temperature conditions, that only mild dissolution of calcite and dolomite is thermodynamically favorable. The reservoir porosity is projected to increase by about 1% around the wellbore and up to 300 ft radius around the injection zone.
3. Geochemical primary caprock integrity is not compromised by the introduction of CO_2 into the reservoir.
4. Any mineral storage that may occur will only result in faster stabilization of the CO_2 plume and make projections presented in this model somewhat more conservative concerning the extent of plume migration and CO_2 concentrations.

[1] PHREEQC Version 3, 2021. See: https://www.usgs.gov/software/phreeqc-version-3
[2] GEM is a trademark of Computer Modelling Group Ltd. see: https://www.cmgl.ca/gem

A.I.6. Geomechanical Information Within Confining Zones [40 CFR 146.82(a)(3)(iv)]

Geomechanical characterization within confining zones plays a critical role in subsurface injection and storage of CO_2. These operations change the in-situ state of the pore pressure; the integrity of the confining zones may be compromised depending on the injection rate and the level of pressure perturbation in the subsurface. Consequently, new potential fractures or reactivation of existing discontinuities (faults or natural fractures) can be induced. It is vital to provide a geomechanics characterization and evaluation of the confining zones integrity including the potential fractures, stress, ductility, rock strength and in-situ fluid pressures to ensure the injected CO_2 remains safely confined in the injection zone.

The characterization on fractures, stress, ductility, rock strength, and in situ fluid pressures was assembled from literature and site-specific data obtained from pre-operational testing of CSS #1 (e.g., well logs, laboratory rock mechanics tests on core samples). The characterization resulted in an estimated fracture gradient of 0.78 to 0.82 psi/ft for the top of the Arbuckle Group injection zone, consistent with the results from the geomechanics model based on dynamic elastic properties (Young's modulus, Poisson's ratio) estimated from the density log and compressional and shear interval transit time logs from CSS #1 with confirmation of elastic properties from triaxial compressive strength testing of CSS #1 core samples. A failure envelope was also defined to evaluate the confining zone and injection zone integrity after CO_2 injection.

Locations for the specific information required under 40 CFR 146.82(a)(3)(iv) are as follows:

- **Fractures** See Section A.I.4 and A.I.5.4.
- **Stress** See Section A.I.6.2.
- **Ductility** See Section A.I.6.1.
- **Rock Strength** See Section A.I.6.1.
- **In Situ Fluid Pressures** See Section A.I.6.2.

A.I.6.1. Rock Strength and Ductility

Triaxial compressive strength tests of core samples were performed at different confining pressures to estimate the rock strength of the confining zones and injection zone. This type of test defines the shear failure of the rock. A total of eight (8) core samples at different depths were tested. The samples "6-12V" and "11-10V" represent the confining zone (lower part of Marmaton and upper portion of Arbuckle Group) and the injection zone (Arbuckle Group), respectively. Stress-strain curves were defined to evaluate the rock ductility and estimate the elastic properties (Young's modulus and Poisson's Ratio). Table A.I.6-1 and Figure A.I.6-1 show the triaxial compressive strength test results and the strain/strain curve that define the rock ductility, respectively.

Table A.I.6-1. Triaxial Compressive Strength Test Results

Sample Number	Sample Depth	Loading Strain Rate	Confining Pressure	Compressive Strength & Elastic Moduli		
				Peak Compressive Strength	Static Young's Modulus	Static Poisson's Ratio
[-/-]	[ft]	[sec^{-1}]	[psi]	[psi]	[$x10^6$ psi]	[-/-]
1-36-1V	2955.05	5.00E-06	1500	4869.50	0.57	0.29
2-14-2V	2978.00	5.00E-06	1500	19030.90	5.15	0.22
3-5V	2993.60	5.00E-06	1500	5075.02	2.15	0.18
3-15-1V	3003.00	5.00E-06	1500	4968.45	2.01	0.21
4-43V	3091.45	5.00E-06	1500	5648.88	3.20	0.16
5-1V	3285.00	5.00E-06	1500	10565.38	1.41	0.62
6-12V	3321.00	5.00E-06	2000	6336.64	1.64	0.20
11-10V	3564.45	5.00E-06	2000	9049.11	4.04	0.18

Figure A.I.6-1. Rock Ductility

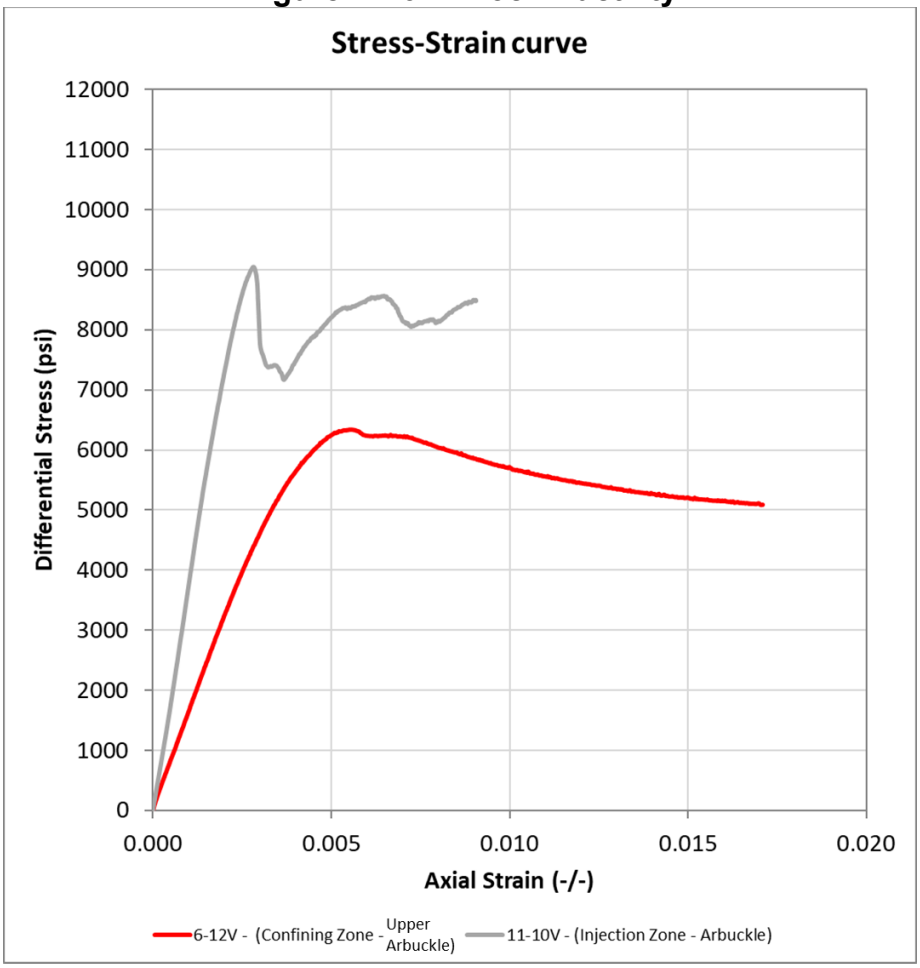

Figure A.I.6-1 shows a mostly plastic deformation (ductile behavior) is observed in the confining zone (Upper Arbuckle), which is expected for rocks with higher clay content. However, mostly brittle behavior is observed in the injection zone Arbuckle Group, which is expected for rocks

with higher carbonate content. Note the maximum peak of compressive strength with 2,000 psi of confining pressure is ~6,337 psi and ~9,049 psi in the confining zone and injection zone, respectively. From a rock mechanics standpoint, the confining zone exhibits a plastic behavior that is beneficial as a cap rock seal because additional energy beyond the elastic state is needed to induce permanent deformation and post-failure. Also, plastic rock material can contain more potentially induced fracture growth compared with brittle rock material.

Brazilian tensile strength tests were also performed to estimate the tensile failure of the confining and injection zones. A total of thirteen (13) core samples at different depths were tested. The samples "10-2-3" and "11-10-1" represent the confining zone (Upper Arbuckle) and the injection zone (Arbuckle Group), respectively. Table A.I.6-2 presents the Brazilian tensile strength test results.

Table A.I.6-2. Brazilian Tensile Strength Test Results

Sample Number	Well Name	Sample Depth	Bedding Orientation	Saturation State	Sample Dimensions		Diameter to Thickness Ratio	Bulk Density	Maximum Load	Brazilian Tensile Strength
					Thickness	Diameter				
[-/-]	[-/-]	[ft]	[-/-]	[-/-]	[in]	[in]	[-/-]	[g/cc]	[lbf]	[psi]
6-1RM	CSS WCA	3310.50	Perpendicular	As-received	0.716	1.504	2.10	2.61	655	387
6-5RM	CSS WCA	3314.30	Perpendicular	As-received	0.711	1.503	2.12	2.58	507	302
1-32-2	CSS WCA	2955.15	Perpendicular	As-received	0.536	1.001	1.87	2.31	298	353
1-35-1	CSS WCA	2954.95	Perpendicular	As-received	0.783	1.499	1.91	2.45	291	158
2-14	CSS WCA	2978.50	Perpendicular	As-received	0.520	1.012	1.94	2.49	830	1004
3-5-1	CSS WCA	2993.90	Perpendicular	As-received	0.537	1.015	1.89	2.05	296	346
3-15-2	CSS WCA	3003.50	Perpendicular	As-received	0.753	1.480	1.97	1.97	340	194
4-43-1	CSS WCA	3091.90	Perpendicular	As-received	0.769	1.494	1.94	2.16	609	337
5-1-2	CSS WCA	3285.85	Perpendicular	As-received	0.499	1.009	2.02	2.50	836	1058
6-4-1	CSS WCA	3313.65	Perpendicular	As-received	0.519	1.014	1.95	2.51	271	328
6-12-1	CSS WCA	3321.60	Perpendicular	As-received	0.767	1.508	1.97	2.26	377	208
10-2-3	CSS WCA	3484.85	Perpendicular	As-received	0.779	1.503	1.93	2.03	469	255
11-10-1	CSS WCA	3564.90	Perpendicular	As-received	0.783	1.524	1.95	2.50	1437	766

Note: CSS WCA = CSS #1 Whole Core Analysis

The dynamic elastic properties, Young's modulus and Poisson's ratio, that describe the stiffness of the rock and its capacity to be deformed under subsurface stress conditions were estimated from the density log and compressional and shear interval transit time logs from CSS #1, and the estimates were confirmed by triaxial compressive strength testing of CSS #1 core samples as shown in Figure A.I.6-2.

The following equations were applied to estimate Young's modulus and Poisson's ratio:

$$YMOD = (RHOB/Dts^2) * ((3Dts^2 - 4Dtc^2)/(Dts^2 - Dtc^2)) \cdot 13400$$

$$Poisson\_Ratio = (1/2 * (Dts/Dtc)^2 - 1)/((Dts/Dtc)^2 - 1)$$

where YMOD is the dynamic Young's modulus in Mpsi; Poisson's ratio in unitless; Dts, Dtc are the compressional and shear interval transit time in us/ft, respectively; and RHOB is the formation density in gr/cc.

Figure A.I.6-2. Elastic Properties and Rock Compressibility at CSS #1

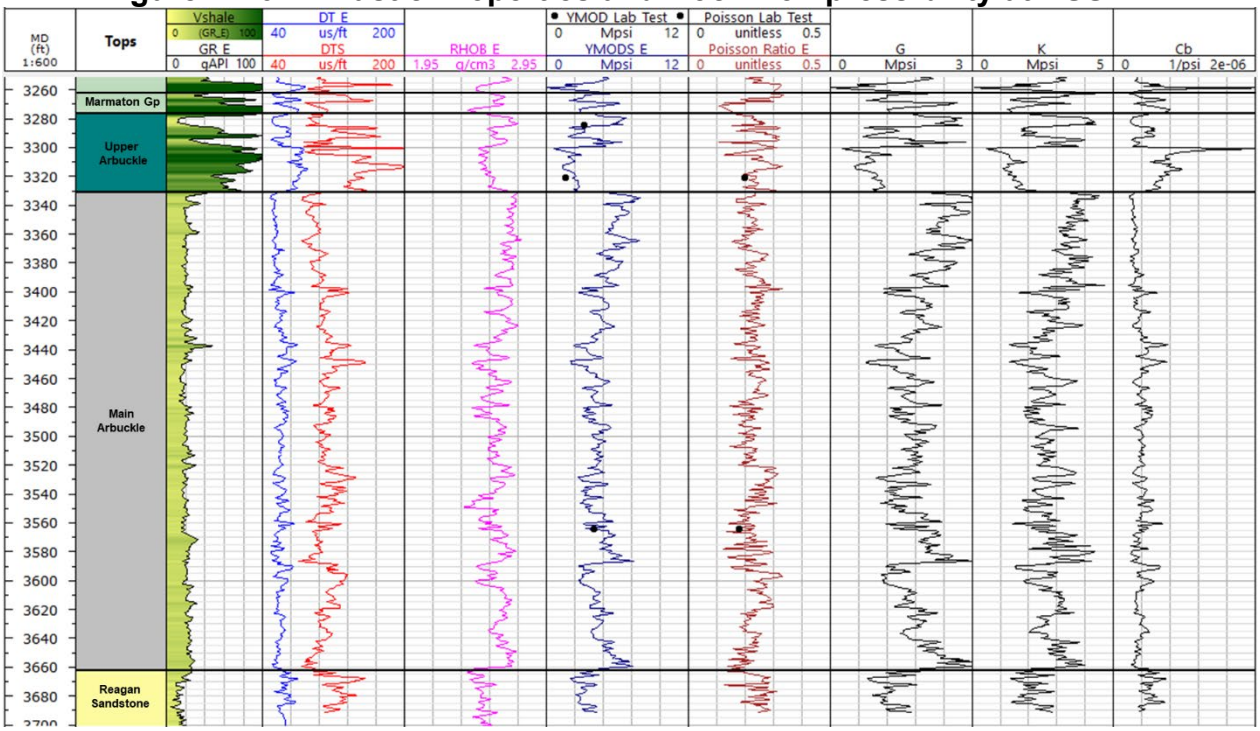

The matrix rock compressibility (Cb) was estimated with the bulk modulus (K), which is a function of the elastic properties. The following equations were used to calculate the bulk modulus and matrix rock compressibility:

$$K = YMOD/(1 - Poisson\_Ratio)$$

$$Cb = 1/K$$

The rock failure envelope was defined with Morh's circle plotting the shear stress (τ) versus the effective normal stress (σ') based on the rock compressive strength and tensile tests. This envelope defines the rock failure limit under compression and tension at a particular state of stress. Figures A.I.6-3 and A.I.6-4 illustrate the failure envelope in the confining zone (Upper Arbuckle) and injection zone (within main Arbuckle), respectively. Note that the area above the failure envelope in the positive scale of the horizontal axis defines the "shear failure zone" and the negative scale defines the "tensile failure zone". Meanwhile, the area below the failure envelope is the "no failure zone". This envelope is critical to evaluate the integrity of the confining and injection zones after perturbating the in-situ state of stress and fluid with the CO_2 injection.

Figure A.I.6-3. Failure Envelope in the Upper Confining Zone (Upper Arbuckle) at CSS#1

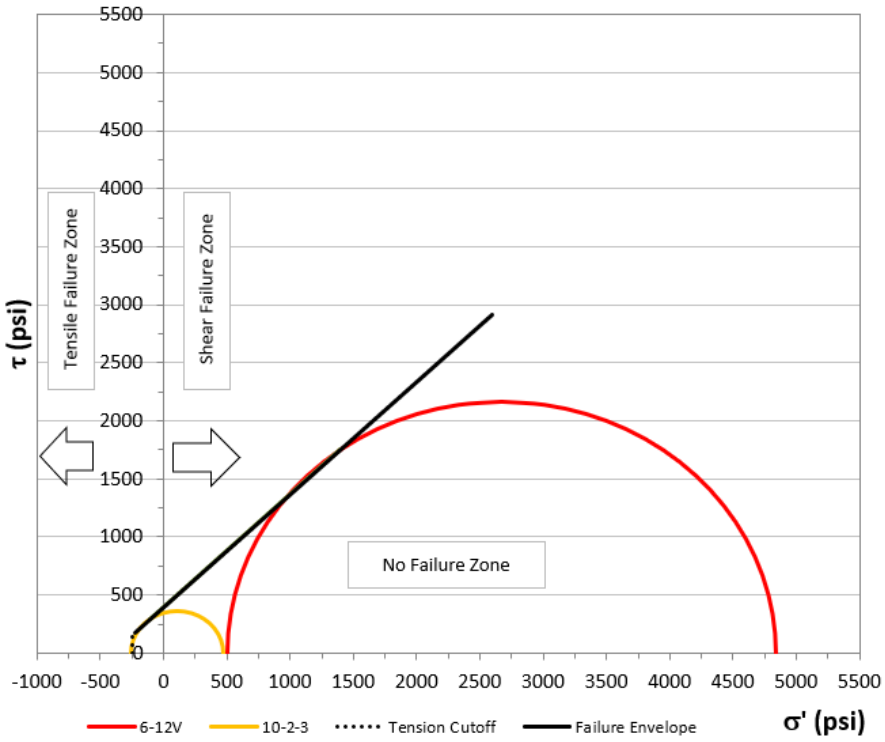

Figure A.I.6-4. Failure Envelope in the Injection Zone (Arbuckle) at CSS#1

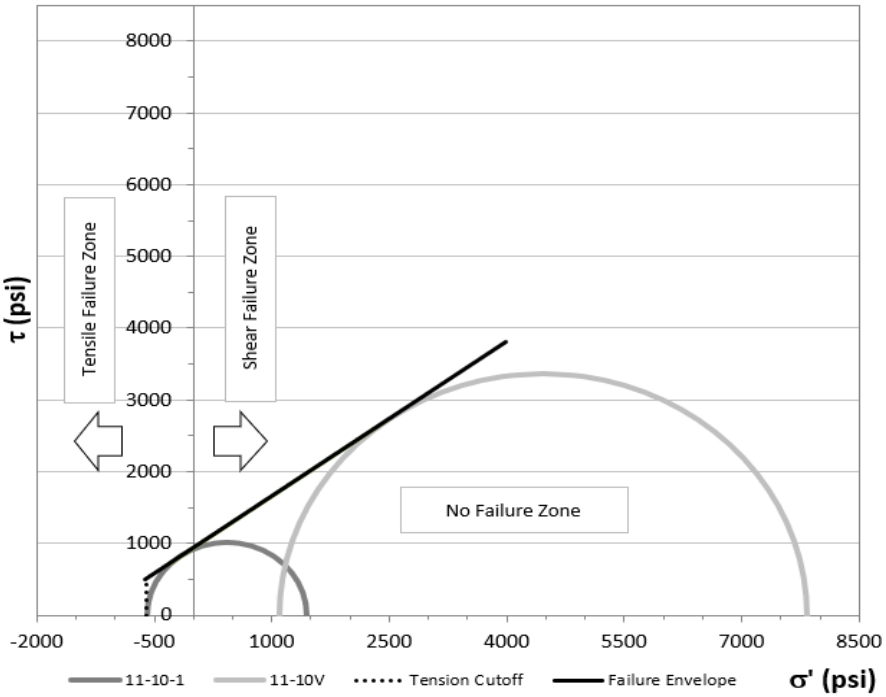

A.I.6.2. In Situ Fluid Pressures and Stress

The initial in-situ fluid pressure and stress state are among the key parameters that control the extent to which a rock mass can sustain stress perturbations. This distance from the rock failure envelope is essential for determining upper bounds to acceptable fluid pressure changes in both the injectivity at the well(s) and the storage capacity. A geomechanics data review of nearby counties was conducted to provide a reference point for comparison of results derived from site-specific data. Schwab (Schwab et al. 2017) provides detailed analyses for a US DOE sponsored pilot-scale GS project that injected 40,000 metric tons of CO_2 into the Wellington Field Arbuckle Group in Sumner County, KS, approximately 160 miles southeast of CSS #1. Schwab reports a pore pressure of 14.5 MPa (2,103 psia = 2,088 psig) at a depth of 1,484 meter (4,869 ft) based on a pump test at their KGS 1-32 (API: 15-191-22591) well, giving a pore pressure gradient of 0.43 psi/ft.

Figure A.I.6-5 reports on geomechanics studies for the Wellington Field in Sumner County, KS. Analysis of drilling-induced fracture orientation and drilling-related wellbore breakouts from the FMI log were used to determine dominant stress orientations. These show the maximum horizontal stress is East-West and minimum horizontal stress is oriented approximately North-South.

Figure A.I.6-5. SHmax Orientation from Sumner County

From: Schwab et al. 2017

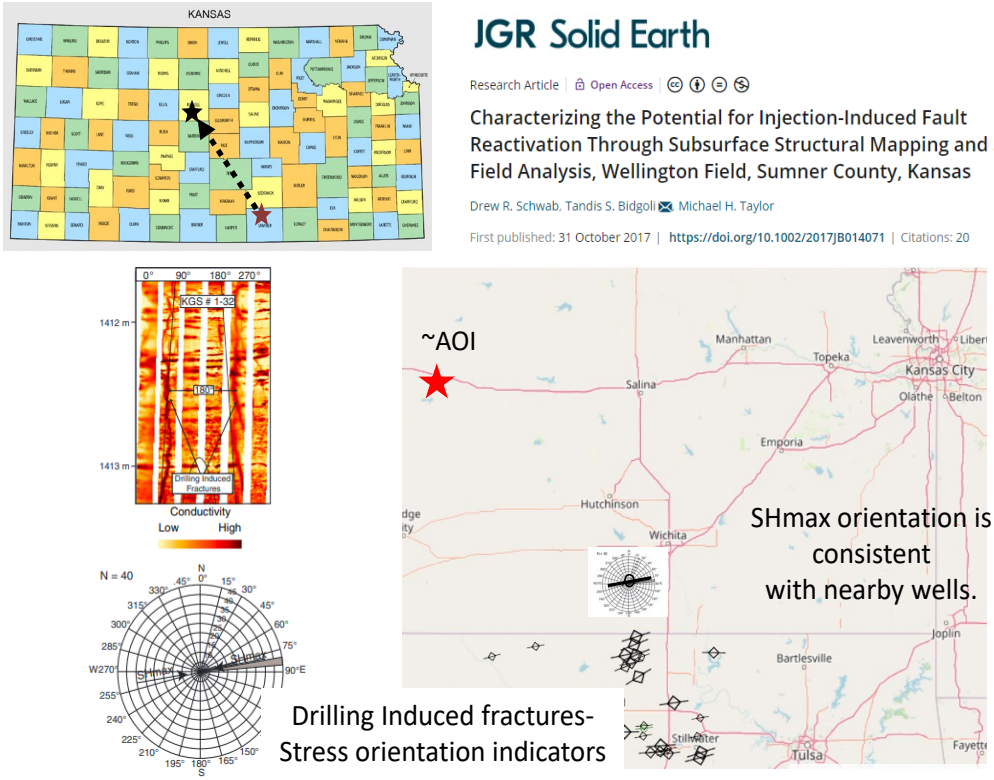

Geomechanical and pressure analysis did not identify overpressure intervals in the formations at CSS #1 (e.g., mechanical compaction or hydrocarbon generation). Two pore pressure scenarios were included: a normal pore pressure in the confining zone (0.445 psi/ft), and a depleted pore pressure (0.35 psi/ft) in the injection zone of the Arbuckle Group based on field measurements at CSS #1 of 1,245 psig at 3,560 ft during a drill stem test with later confirmation by several months of data obtained from a temporary downhole gauge.

The vertical stress (OB) was estimated with the density log. It represents at any given depth the sum of the weight of sediments from ground level to the depth of interest. It depends on the formation density, which changes from bottom to top.

$$OB = \int_{TVD_{\text{int}erest}}^{TVD_{GL}} \rho_{sed} * g * dTVD$$

The poroelastic horizontal strain model was used to estimate the horizontal stresses based on the well logs elastic properties and vertical stress. Figure A.I.6-6 shows the vertical, maximum, and minimum horizontal stresses (Sv, SHmax, and Shmin, respectively) as well as the pore pressure corresponding to the Arbuckle Group at CSS #1. Table A.I.6-3 summarizes the average of in-situ fluid pressure and stress.

Table A.I.6-3. Average In-Situ Fluid Pressures and Stress at CSS#1

Formation	Depth (ft)	SV (psi/ft)	Shmin (psi/ft)	SHmax (psi/ft)	Pore Pressure (psi/ft)
Confining Zone (Upper Arbuckle)	3300 - 3320	1.06	0.68	0.83	0.445
Injection Zone (Main Arbuckle)	3448 - 3588	1.06	0.59	0.73	0.35

Figure A.I.6-6. In-Situ Fluid Pressures and Stress at CSS#1

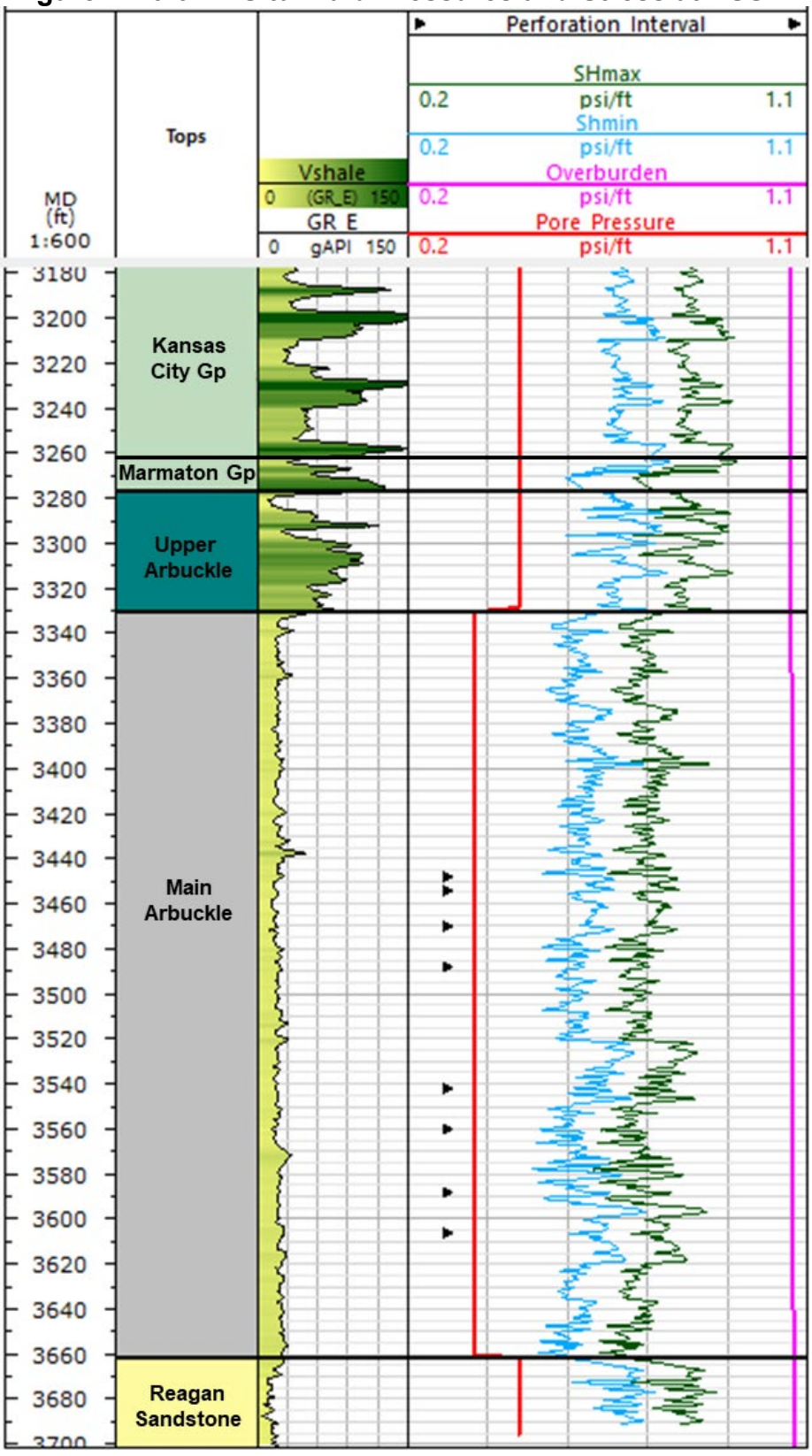

A.I.6.3. Fracture Pressure and Fracture Gradient

Fracture gradient and fracture pressure in the confining zone and injection zone are estimated based on the poroelastic solution using Eaton's method as a function of the elastic properties, overburden, and pore pressure. Fracture pressure is defined as the minimum pressure to break the rock once the minimum horizontal stress and tensile stress of the rock is exceeded. This is estimated with the following equation:

$$F_P = P_P + (OB - P_P) * (Poisson\_Ratio/(1 - Poisson\_Ratio))$$

Figure A.I.6-7 presents the elastic properties, in-situ fluid, stress, and fracture gradient estimate. Note that the confining zone (Upper Arbuckle) exhibits a thicker fracture gradient with higher values ranging between ~0.78 psi/ft and ~0.82 psi/ft. Meanwhile, the injection zone in the main carbonate part of the Arbuckle Group presents thinner interlayers with fracture gradient ranging between ~0.66 psi/ft and ~0.81 psi/ft. Table A.I.6-4 summarizes the range of fracture gradient in the confining zone (Upper Arbuckle) and injection zone (Main Arbuckle).

Table A.I.6-4. Fracture Gradient Estimate at CSS#1

Formation	Depth (ft)	Fracture Gradient Range (psi/ft)	Fracture Pressure Range (psig)
Confining Zone (Upper Arbuckle)	3300 - 3320	~ 0.78 – 0.82	~ 2590 - 2722
Injection zone (Main Arbuckle)	3448 - 3588	~ 0.66 – 0.81	~ 2362.8 - 2900

Figure A.I.6-7. Elastic Properties, In-Situ Fluid, Stress and Fracture Gradient

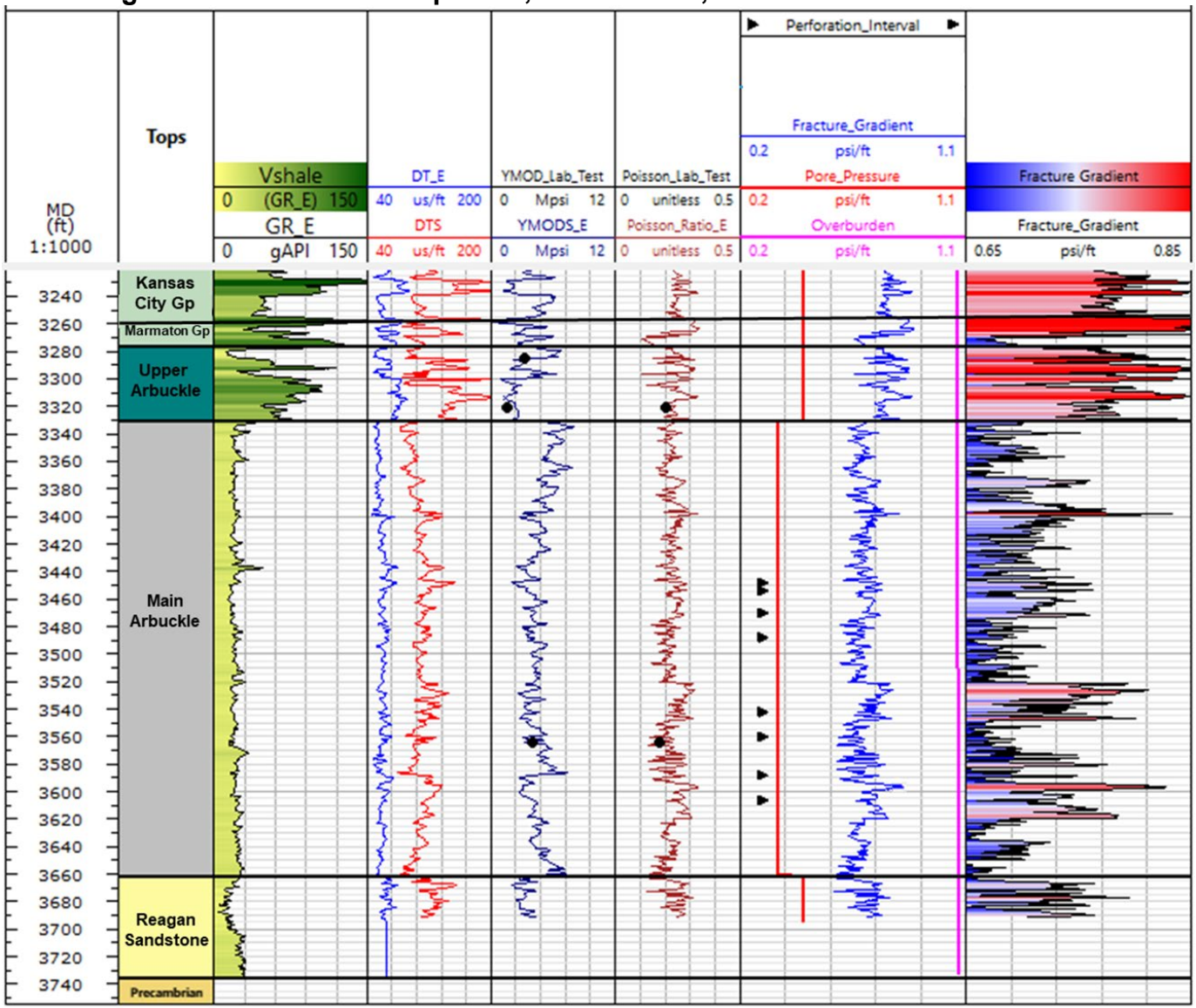

A.I.6.4. Confining Zones Integrity Before/During CO_2 Injection

Integrity of the confining zones was evaluated with the condition of the in-situ effective stress before/during the CO_2 injection and its relative state concerning the rock failure envelope which represents the bounds to acceptable fluid pressure changes in both the injectivity at the well(s) and the storage capacity to prevent potential shear/tensile failure. The effective stresses decrease as the CO_2 is injected. Based on the reservoir simulation model, a maximum pressure of ~2,081 psig and 2,116 psig were observed during the worst-case scenario of the injection period (first month of injection) within the upper confining zone (Upper Arbuckle) at a depth of 3,330 ft and at the top of the first perforations in the Arbuckle Group at a depth of 3,448 ft, respectively. As observed in Figure A.I.6-8 and Figure A.I.6-9, the state of effective stress decreased during the injection. Note that it is maintained in the "no failure zone"; thus, shear or tensile failure are not expected in both confining zones and injection zone.

Table A.I.6-5 summarizes the results of the confining zones integrity after the injection for the worst-case scenario of maximum pressure. Note that the maximum differential pressure induced during the injection is lower than the critical differential pressure. A maximum of ~59.8% of the critical differential pressure was observed in the base of the confining zone and ~65.99% in the top of the first perforations of the Arbuckle Group. Thus, no risk of inducing shear or tensile failure is expected.

Figure A.I.6-8. Failure Envelope and State of Stresses at Top of Arbuckle Group

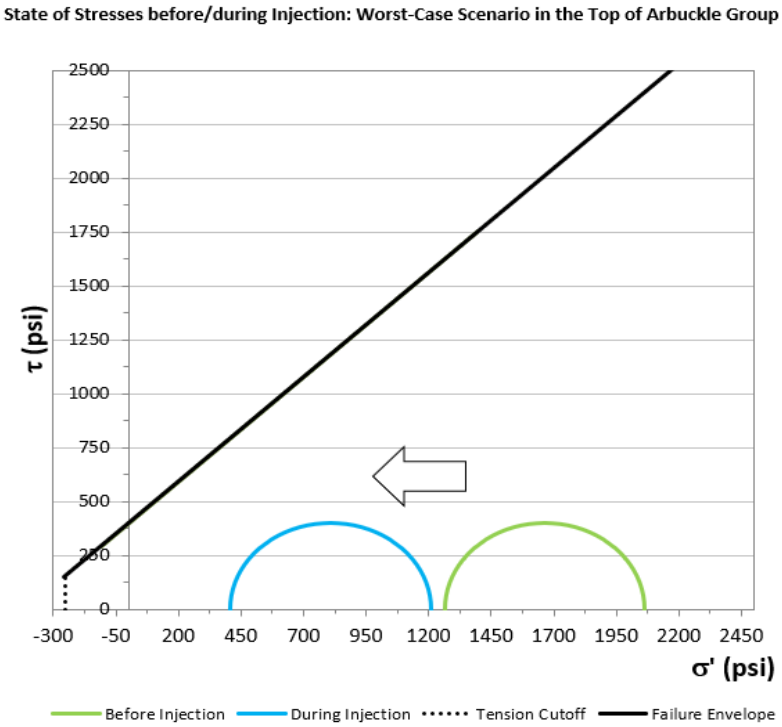

Figure A.I.6-9. Failure Envelope and State of Stresses at Top of Perforations

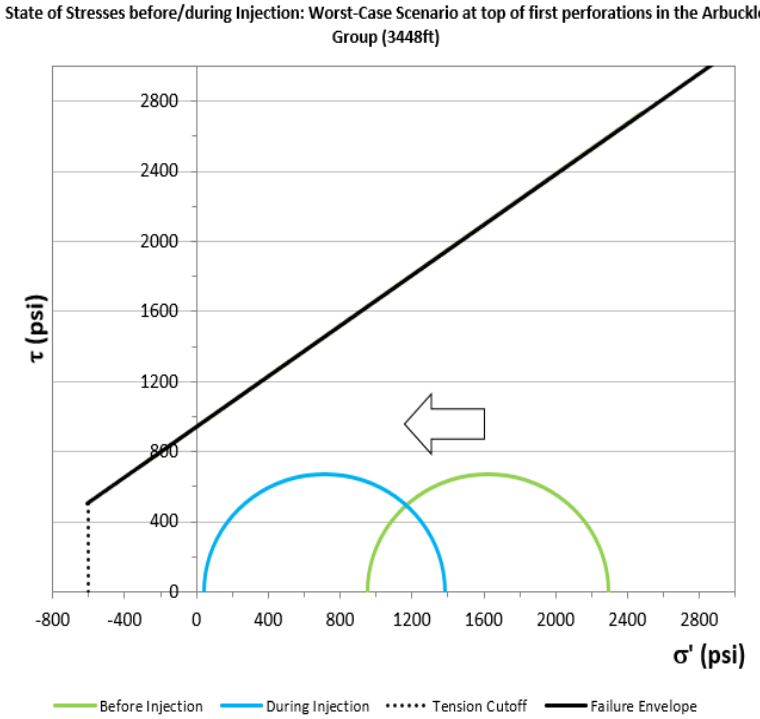

Table A.I.6-5. Confining Zones Integrity Results at CSS#1

Formation	Depth, ft	Initial Pressure Before Injection, psig	Max. Pressure During Injection, psig	Max. Differential Pressure During Injection, psi	Average Fracture Pressure, psig	Critical Differential Pressure, psi		Confining Zones Integrity
						From Fracture Pressure	From Mohr's Coulomb Circle	
Within upper confining zone (Upper Arbuckle)	3330	1225	2081	856	2664	1439	~1421	Max differential pressure during the injection < critical differential pressure. Thus, no risk of inducing rock failure in the confining zones
Injection zone at top of first perforations (Main Arbuckle)	3448	1205	2116	911	2534	1329	~1432	

A.I.7. Seismic History [40 CFR 146.82(a)(3)(v)]

PCC believes the risk of a seismic event occurring with sufficient intensity to interfere with containment for the GS project is low, mitigated by the following factors:

- Favorable Seismic History – Records show little evidence of past events in the area with sufficient intensity to damage infrastructure.
- Favorable Site Stratigraphy – The stratigraphic column at CSS #1 provides confining layers both above and below the injection zone, plus the Reagan Sandstone layer beneath the lower confining layer serves as a dissipation interval to further mitigate the impact of seismic events on containment.
- Modest Injection Rate – The GS project injection rate is up to 150,000 metric ton per year = 3,200 bpd, which is modest when compared to total injection rates for existing Class II wells within Russell County.
- Integrated Testing and Monitoring Plan – The plan contains integrated mechanical integrity testing and monitoring elements to assure the GS project wells are in suitable mechanical condition to withstand expected seismic intensities over their service life. The plan also integrates elements for continuous monitoring of two regional earthquake monitoring networks and a dedicated passive seismic system to track micro-seismic events across the GS site, which together provide timely information to properly manage GS project operations.
- Aligned Emergency and Remedial Response Plan – The Emergency and Remedial Response Plan defines suitable actions to be followed in case of a seismic event and is aligned with the response plan delineated in the Kansas Seismic Action Plan that state-level agencies follow for regulation of Class I through V wells in Kansas.

The Kansas Geological Survey (KGS) cites the largest recorded earthquake in Kansas occurred in 1867, located near Wamego, KS approximately 150 miles away from the GS project site, measuring VII on the Modified Mercalli scale with an estimated intensity between magnitude 5.0 and 5.5 (Steeples and Brosius 2024). At least 25 additional earthquakes occurred in Kansas between 1867 and 1976 that were felt by human inhabitants, none of which had epicenters located in Russell County. KGS operated a network of seismometers throughout the state for twelve years from 1977 to 1989, recording more than 100 events of which most were microearthquakes too small human inhabitants to feel.

KGS resumed state-wide seismic monitoring in 2015 and currently operates a network with 18 stations spread across Kansas as shown in Figure A.I.7-1. The closest station on the KGS network is the Saline State Fishing Lake station, roughly 60 miles east of the GS project site. KGS also maintains the Kansas Earthquake Database that provides historical information, both as text records and an interactive map of past seismic events, with event records documenting the time, location, and magnitude for each cataloged event. Events with magnitude equal to or greater than 2.0 M_L are reported, using the M_L scale (aka magnitude long or Richter scale) as this scale is utilized by the KGS regional seismic network. No information on event depth is provided to the public in the Kansas Earthquake Database.

Figure A.I.7-1. Seismic Station Locations (2023) in the KGS Network

From: https://www.kgs.ku.edu/Geophysics/Earthquakes/network.html

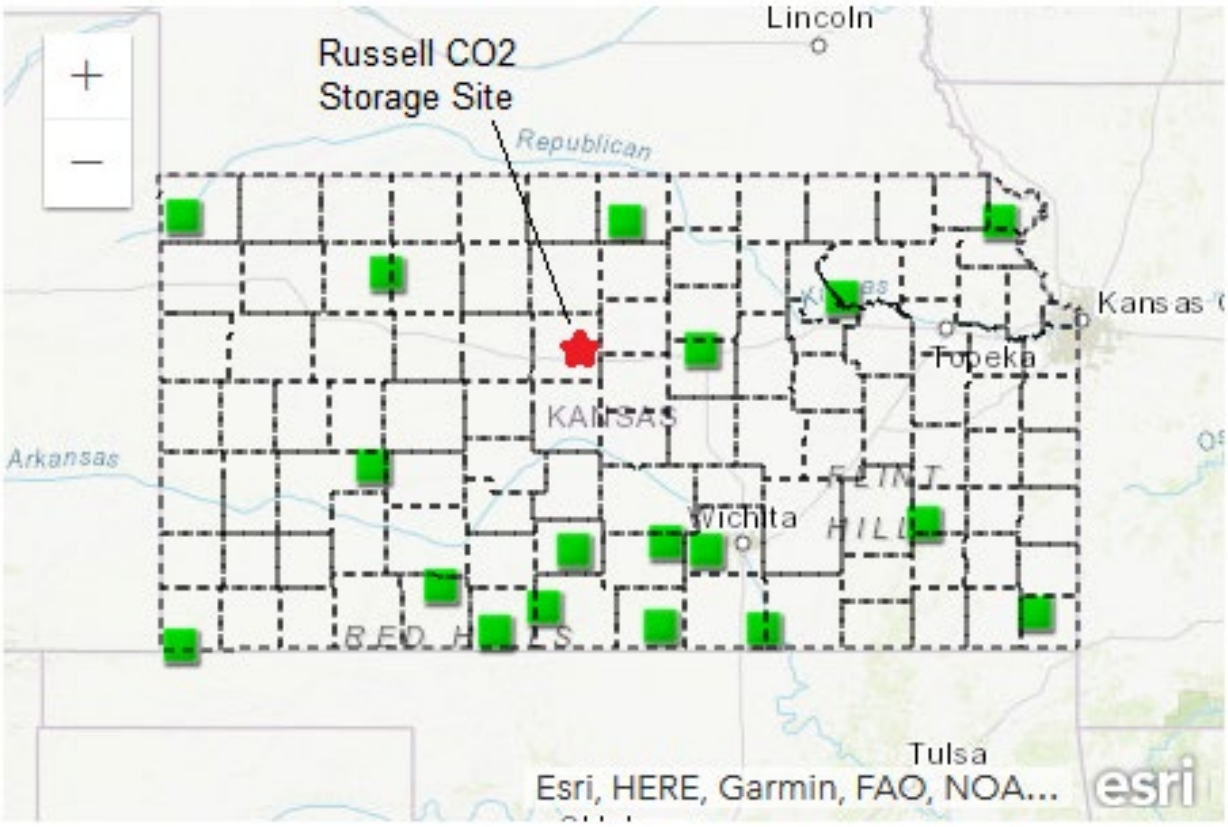

Figure A.I.7-2. Seismic Station Locations (2023) for USGS ANSS

From: https://earthquake.usgs.gov/monitoring/operations/network.php?virtual_network=ANSS

The United States Geological Survey also monitors and catalogs seismic activity in Kansas. Figure A.I.7-2 shows locations of seismic stations in the USGS Advanced National Seismic System (ANSS). Two stations are on the United States (US) Network, US CBKS at Cedar Bluff Reservoir roughly 70 miles west of GS project site and US KSU1 at the Konza Prairie Biological Station roughly 120 miles east of GS project site. A third station is on the N4 Network, this station is N4 R32B near Great Bend, Kansas roughly 40 mile south of GS project site. The ANSS Comprehensive Earthquake Catalog (ComCat) provides historical information as text records and an interactive map for past seismic events. In practice, there are considerably fewer seismic event records in the ANSS ComCat database than the Kansas Earthquake Database. The ANSS ComCat database provides event records for time, location, magnitude, and depth. Records are given for events equal to or greater than 2.5 mb_lg, with reporting most often in the mb_lg scale (the short-period surface wave magnitude scale) as this is the scale used by the ANSS network. For the same event, magnitude numbers expressed in the mb_lg scale are roughly 0.2 units larger than magnitude numbers expressed in the M_L scale (e.g., 2.7 mb_lg ≈ 2.5 M_L). Although the data set in the ANSS ComCat database base is comparatively sparse, the reporting of event depth is very useful for assessing whether an event is attributable to natural or induced seismicity.

Figures A.I.7-3 and A.I.I.7-4 display seismic events maps for Kansas using data since 1970 from the Kansas Earthquake Database and ANSS ComCat, respectively. Events in the general area around the GS project site tend to occur along faults associated with the CKU. Examination of in the ANSS ComCat database shows the majority of these events are deep into the bedrock (typically 5 kilometers [km] = 16,404 ft), suggesting natural seismicity as the underlying cause. Unfortunately, the KGS network does not have sufficient vertical resolution to provide reliable event depths (Personal Communication - Peterie 2023), preventing correlation of event depths between the Kansas Earthquake Database and ANSS ComCat.

The cluster of seismic events in south-central Kansas is centered in Harper County and Sumner County, about 160 miles from the GS site. This cluster is a relatively new phenomena, with an uptick starting in the 2010's of event magnitude and frequency vs. the historical baseline. Extensive study has been conducted correlating this uptick to the rise of saltwater injection into Class II wells in the area. While correlation does not prove causation, in Harper County the annual saltwater disposal volume increased from roughly 10 million bbl in 2011 to more than 100 million bbl in 2015, suggesting induced seismicity as contributing factor in the uptick of seismic event magnitude and frequency.

The situation in south-central Kansas led to a collaborative effort between the Kansas Department of Health and Environment, the Kansas Corporation Commission, and KGS to develop and implement the Kansas Seismic Action Plan (Kansas 2015). This plan established the KGS seismic monitoring network described earlier in this subsection, and also established a uniform response plan for agency regulation of Class I through Class V wells with respect to seismic events. The response plan portion of the Kansas Seismic Action Plan is described more fully in Section E.15 of the Testing and Monitoring Plan, and Section H.4.5 of the Emergency and Remedial Response Plan implements an action plan for seismic events that is aligned with the plan that state-level agencies follow for regulation of Class I through V wells in Kansas.

Figure A.I.7-3. Seismic Event Map for Kansas, 1970-2022

From: Kansas Earthquake Database, https://www.kgs.ku.edu/Geophysics/Earthquakes/

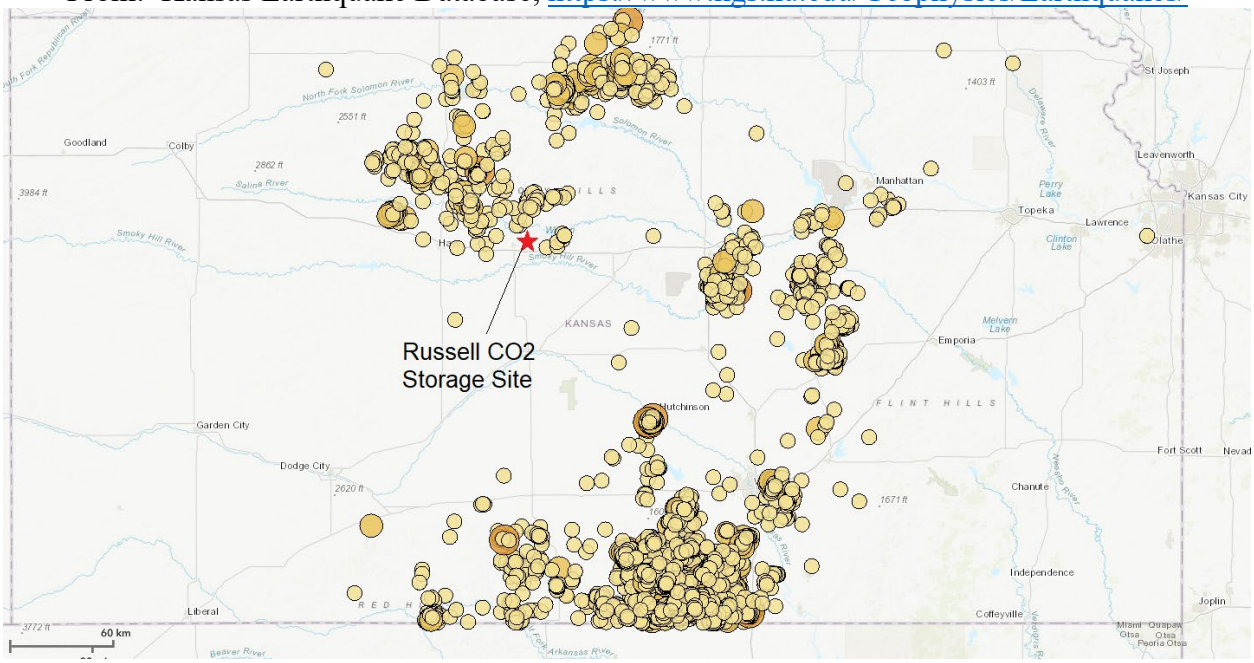

Figure A.I.7-4. Seismic Event Map for Kansas, 1970-2022

From: ANSS ComCat database, https://earthquake.usgs.gov/earthquakes/search/

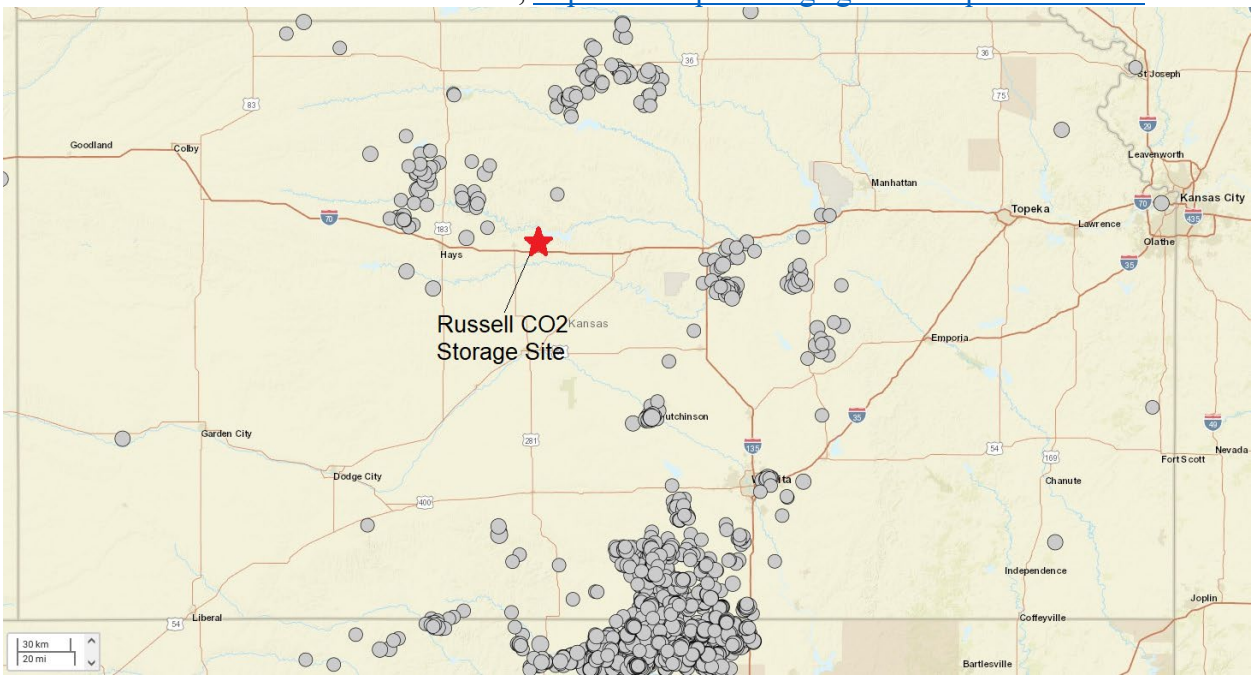

PCC searched the Kansas Earthquake Database and the ANSS ComCat database and found three recorded events of 2.7 M_L or greater in Russell County – two 2.8 M_L events located more than 16 miles from CSS #1, and one 2.7 M_L event located approximately 11.4 miles away from

CSS #1. PCC found over 40 additional records for seismic events less than 2.7 M_L in Russell County in the Kansas Earthquake Database. Figures A.I.7-5 and A.I.7-6 provide maps for these events in Russell County. Tables A.I.7-1 and A.I.7-2 provide summaries of the event records.

Two items of note on the search results:

- All but one of the records are sourced from the Kansas Earthquake Database, with the events occurring after the installation of the KGS network in 2015. A likely explanation for the preponderance of results from the Kansas Earthquake Database is that event detection by the ANSS seismic network may not be sufficient to catch all events of 2.5 M_L or greater across Russell County.
- The majority of seismic events occur in the northern portion of Russell County, distant from the GS project site, and also distant from oil & gas operations elsewhere in the county.

PCC believes the risk of damage to CSS #1 and MW #1 from seismic activity is low. The largest magnitude of past recorded events in Russell County is 2.8 M_L, which typically corresponds to an event intensity of II or III on the Modified Mercalli Intensity (MMI) scale, meaning the event can be noticed by persons indoors but structural damage to infrastructure is uncommon. For comparison, the Coalinga California Earthquake of 1983 was a 6.7 M_L event with VIII MMI that occurred near an oilfield (Rymer & Ellsworth 1990). While there was considerable damage to ordinary buildings, the damage to subsurface well bores was slight with damage to only 26 of 1,720 of the active wells in the field. Well damage occurred in a random geographical pattern, with most damage attributed to the earthquake inducing failures in corroded casings. Sections E.4 and E.7 of the Testing and Monitoring Plan describes the external mechanical testing and corrosion monitoring programs for the GS project, respectively, which are specifically designed to mitigate risk of structural failures of the CSS #1 and MW #1 wellbores.

Figure A.I.7-5. Seismic Event Map for Russell County, 1970-2022

From: Kansas Earthquake Database, http://maps.kgs.ku.edu/earthquake_mini_viewer/

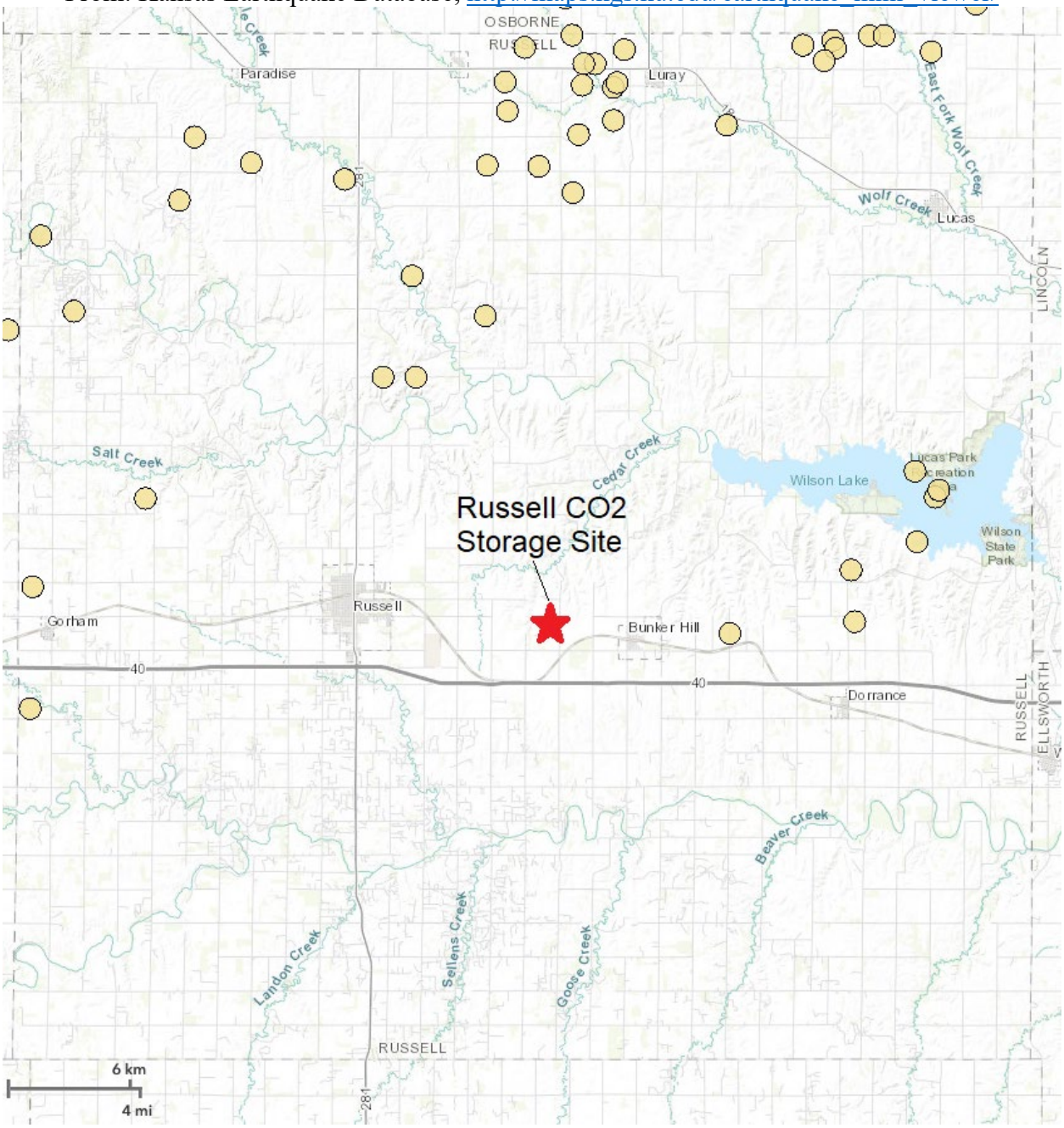

Figure A.I.7-6. Seismic Event Map for Russell County, 1970-2022
From: USGS ANSS ComCat, https://earthquake.usgs.gov/earthquakes/search/

Table A.I.7-1. Seismic Event Records for Russell County, 1970-2022

From: Kansas Earthquake Database, https://www.kgs.ku.edu/Geophysics/Earthquakes/data.html

Quake ID	UTC Time	Magnitude (M_L)	Event Location		Approximate Distance from CSS #1 (miles)
			Latitude	Longitude	
Events ³ 2.7 Magnitude					
1001454021	9/26/2018 17:50	2.8	39.12139	-98.5987	18.2
1001471409	12/2/2021 4:22	2.8	39.02387	-98.63667	11.4
1001475623	8/27/2022 6:01	2.7	38.97349	-99.03571	16.5
Events < 2.7 Magnitude					
1001457560	7/1/2019 19:25	2.6	39.0534	-98.93572	15.3
1001462981	3/30/2020 14:27	2.5	39.09373	-98.75308	14.4
1001462993	3/31/2020 12:17	2.5	39.09158	-98.74797	14.3
1001465602	10/23/2020 0:39	2.5	38.91322	-98.61393	7.6
1001471157	11/18/2021 17:39	2.5	38.98996	-98.77918	7.4
1001475795	8/31/2022 21:47	2.5	38.89784	-99.0316	15.1
1000270608	9/3/1982 10:55	2.5	38.7905	-98.8925	10.1
1001462973	3/30/2020 0:36	2.4	39.05566	-98.74829	11.8
1001462980	3/30/2020 11:37	2.4	39.09179	-98.74928	14.2
1001457229	6/5/2019 23:05	2.3	39.06211	-98.95135	16.3
1001463265	4/14/2020 7:55	2.3	39.06548	-98.74052	12.4
1001465099	9/1/2020 19:06	2.3	38.93942	-98.55387	11.2
1001468008	5/28/2021 7:27	2.3	39.10095	-98.61278	16.6
1001477037	12/31/2022 2:46	2.3	39.0854	-98.65388	14.8
1001449328	4/29/2018 2:21	2.2	39.08607	-98.73952	13.9
1001462198	1/16/2020 23:55	2.2	38.85738	-98.56502	10.2
1001465627	10/24/2020 21:19	2.2	38.83964	-98.58537	9.4
1001466156	12/2/2020 13:14	2.2	38.9158	-98.55434	10.8
1001470575	10/3/2021 6:03	2.2	39.06416	-98.73441	12.4
1001408051	7/23/2017 13:45	2.1	39.06536	-98.73615	12.4
1001454441	8/22/2018 9:42	2.1	39.12793	-98.61034	18.4
1001457276	6/8/2019 9:53	2.1	38.97517	-98.82007	7.2
1001461330	6/29/2019 15:04	2.1	38.93545	-98.96989	12.3
1001467067	2/3/2021 13:33	2.1	38.94888	-98.5452	11.9
1001408014	7/23/2017 13:27	2.0	39.07651	-98.75481	13.2
1001407985	7/23/2017 13:33	2.0	39.02374	-98.75275	9.6
1001457329	6/13/2019 20:27	2.0	39.06051	-98.95541	16.4
1001460427	9/7/2019 7:53	2.0	39.02039	-98.84084	10.5
1001464264	6/23/2020 7:21	2.0	38.94432	-98.54364	11.8

Quake ID	UTC Time	Magnitude (M_L)	Event Location		Approximate Distance from CSS #1 (miles)
			Latitude	Longitude	
1001466157	12/2/2020 17:26	2.0	38.87805	-98.65025	5.4
1001469545	3/18/2021 6:14	2.0	39.12516	-98.54013	20
1001469849	5/21/2021 18:04	2.0	39.1266	-98.59248	18.7
1001472836	8/1/2021 10:39	2.0	39.09216	-98.74586	14.3
1001470287	9/1/2021 3:27	2.0	39.12278	-98.58463	18.6
1001473332	12/31/2021 7:07	2.0	39.12006	-98.7302	16.2
1001474263	3/19/2022 18:57	2.0	39.07994	-98.84611	14.4
1001473891	3/23/2022 1:49	2.0	39.12698	-98.76246	16.7
1001474942	6/11/2022 20:04	2.0	39.13221	-98.73662	17.1
1001475290	7/21/2022 19:37	2.0	39.1124	-98.77326	15.7
1001476173	10/4/2022 21:09	2.0	39.11527	-98.74711	15.9

Table A.I.7-2. Seismic Event Records for Russell County, 1970-2022

From: USGS ANSS ComCat https://earthquake.usgs.gov/earthquakes/search/

Event ID	Time	Magnitude		Depth (km)	Location		Approximate Distance from CSS #1 (miles)
		mb-lg as reported	M_L Approximate		Latitude	Longitude	
us6000d4a9	2020-12-28 T04:17:44.594Z	2.6	2.4	5	38.9776	-99.0286	16.2

PCC believes the risk is low for the GS project to cause induced seismicity within Russell County. The sole historical event listed in the ANSS ComCat database for Russell County was an event reported in 2020 with magnitude 2.4 M_L at 5 km depth located approximately 16.2 mi west of CSS #1. The depth was deep into the bedrock suggesting natural seismicity as the likely cause. Informal searches in the ANSS ComCat database by PCC for events in counties bordering Russell County likewise found the majority of those events were deep in the bedrock.

Unfortunately, seismic event records from the Kansas Earthquake Database do not provide event depth, so a bit more analysis is needed to attribute the likely cause for seismicity in Russell County. Figure A.I.7-5 illustrates locations for Class II wells and enhanced oil recovery (EOR) operations in Russell County. The majority of these wells and operations are in the south and western portions of Russell County, while the majority of seismic events displayed in Figure A.I.7-5 (several pages back) are in the northern portion of Russell County, thus there is little geographic overlap between the two activities. While by no means conclusive since studies on the situation in Harper and Sumner suggested induced seismicity can be triggered as far as 90 km away from injection activities (Peterie et al. 2018), the lack geographic overlap at the site

of injection activities suggests the majority of seismic events detected by the KGS network in Russell County attributable as natural rather than induced seismic events.

Table A.I.7-3. Annual Injection Rates for Class II Wells in Russell County

From: Kansas Geological Survey, https://www.kgs.ku.edu/Magellan/Qualified/class2_db.html

Reporting Year	Annual Injection by Activity, barrel per year			
	Saltwater Disposal	EOR	Other	Total
2016	45,294,040	30,525,921	245,084	76,065,045
2017	46,364,762	28,014,344	247,105	74,626,211
2018	43,377,031	29,814,075	277,925	73,469,031
2019	44,319,289	28,049,350	310,914	72,679,553
2020	38,735,097	24,930,986	253,558	63,919,641
2021	42,662,544	25,879,576	217,634	68,759,754

Table A.I.7-3 summarizes annual injections by activity into Class II wells across Russell County. Saltwater disposal was relatively constant over the reported timeframe, averaging 43.4 million barrels per year, equivalent to a specific injection rate of 18,600 barrels per year per squared kilometer (bbl/yr per km^2) using 2,330 km^2 as the area for all of Russell County. For comparison, the specific injection rate for Harper County was approximately 48,000 bbl/yr per km^2, or 2.6 times the specific injection rate for Russell County. Furthermore, the injection rate for CSS #1 is roughly 3,200 bpd, which is modest in comparison to the situation in Harper County that involved 47 high-volume wells with injection rates of 10,000 bpd or more.

Figures A.I.7-8 and A.I.7-9 provide the 2018 Long-term National Seismic Hazard Map and the 2014 National Seismic Hazard Model for Kansas, respectively. These maps show peak ground accelerations that have a 2% probability of being exceeded in 50 years for a firm rock site. The models are based on seismicity and fault-slip rates and consider the frequency of earthquakes of various magnitudes. This type of information is used for seismic provisions in building codes and for risk models in insurance rate structures.

Figure A.I.7-7. Map of Class II Wells and EOR Operations in Russell County

From: Kansas Geological Survey, https://maps.kgs.ku.edu/oilgas/index.html

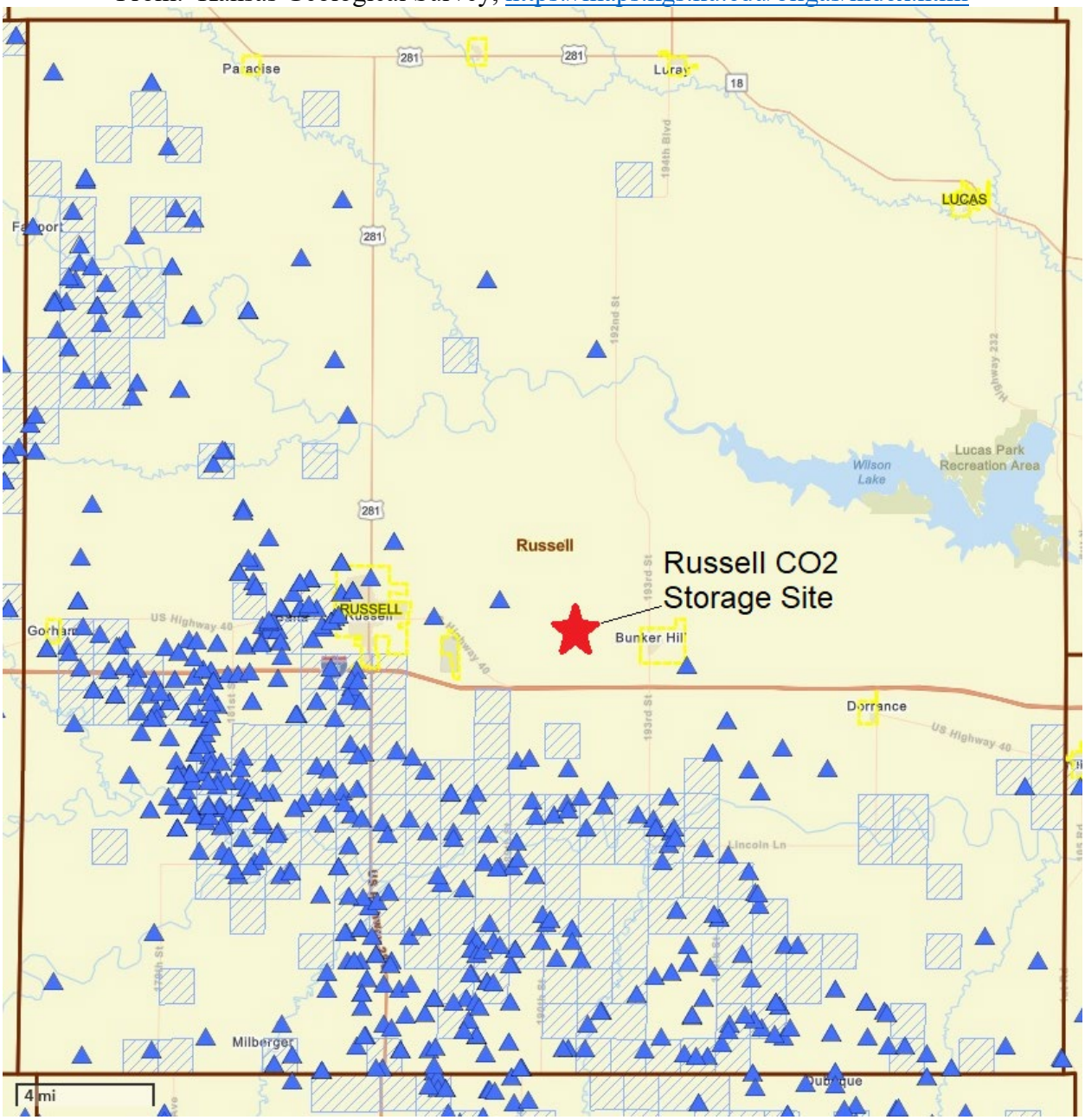

Figure A.I.7-8. 2018 Long-term National Seismic Hazard Map

From: https://www.usgs.gov/media/images/2018-long-term-national-seismic-hazard-map

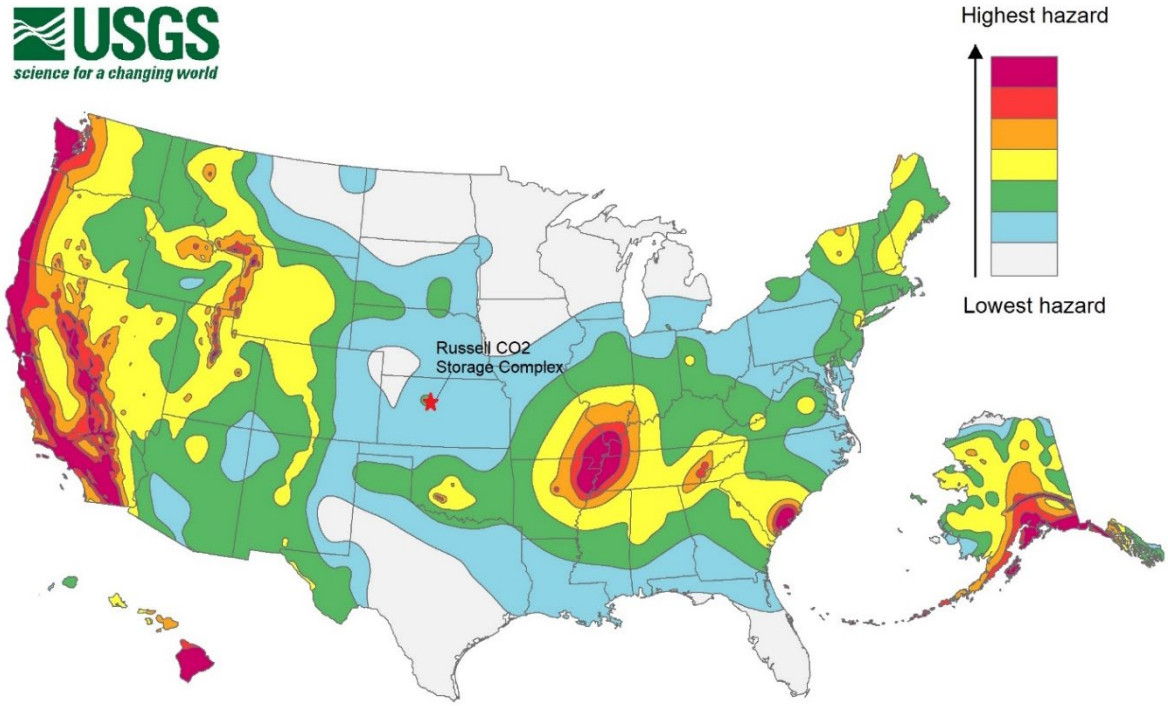

Figure A.I.7-9. 2014 National Hazard Model for Kansas

From: https://www.usgs.gov/media/images/2014-seismic-hazard-map-kansas

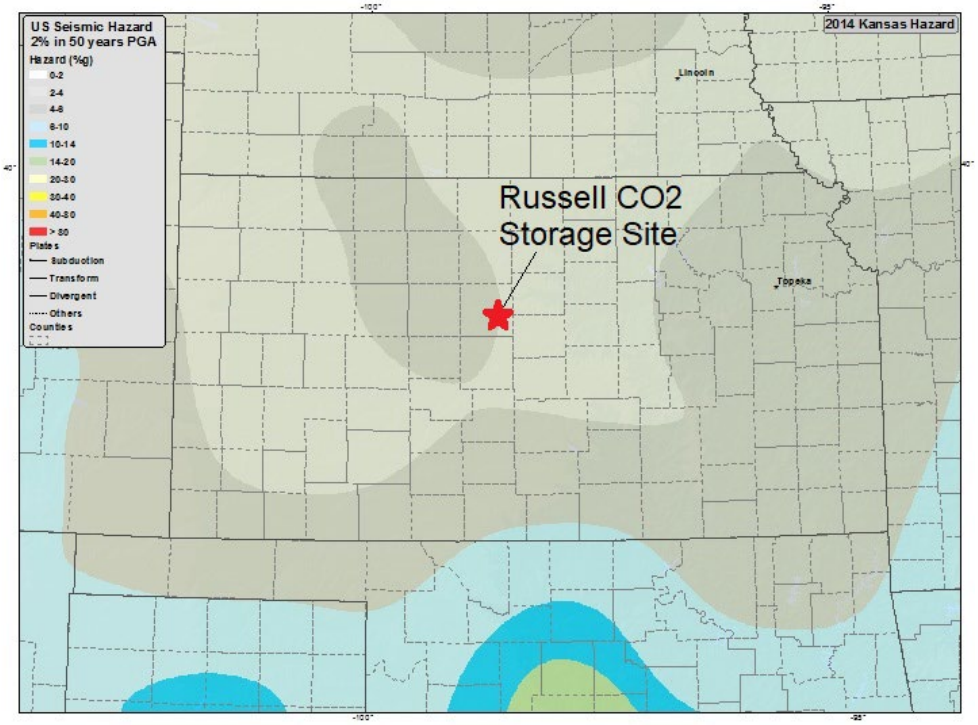

A.I.8. Hydrologic and Hydrogeologic Information [40 CFR 146.82(a)(3)(vi), 146.82(a)(5)]

Section A.I.2.2 presents detailed hydrologic and hydrogeologic information for the planned injection interval (Arbuckle Group), showing the predominant direction of water movement is from west to east across the state. Figure A.I.8-1 (next page) provides a map of water wells within the AoR and the maximum monitoring area (MMA), and their positions relative to CSS #1. The predominant direction of surface and shallow groundwater is to the north and east towards Cedar Creek. The depths of all water wells within the AoR are comparatively shallow, with the bottom of the deepest water well vertically separated from the injection zone by multiple confining units with total thickness of several thousands of feet. A search by PCC of public records (USGS National Hydrography Dataset 2023, Buchanan et al. 2008) in 2023 found no records of springs within the areal extent of the AoR, MMA, and immediate vicinity. Literature suggests small un-recorded springs or seeps are somewhat common in the region and may occur in low-lying areas near the tributaries to Cedar Creek.

The shallow (less than 800 ft bgs) hydrology and hydrogeology are discussed in this subsection, with an emphasis on determination of the lowermost USDW. Shallow groundwater is present in two depths in the project area based on preliminary characterization. Surficial groundwater, at top depths ranging from approximately 50 to 120 ft bgs, depending on location, is present within low permeability Greenhorn or Graneros strata. This groundwater is not typically used as a drinking water source. Fall 2022 sampling indicated that the surficial groundwater was characterized by high ion content (conductivity greater than 1,000 microsiemens per centimeter [mS/cm]) and low achievable extraction rates (less than 0.1 gallons per minute [gpm]). Below the surficial groundwater is groundwater generally corresponding to the Dakota Formation at top depths ranging from 153 to 214 ft bgs. This is also a low permeability formation in this area and not typically used as a drinking water source. Fall 2022 sampling indicated that this groundwater was characterized by high turbidity, high conductivity (generally in the 1,000 to 16,000 mS/cm) and low achievable extraction rates (less than 0.1 gpm).

The Dakota Formation includes the drinking water Dakota Aquifer in portions of Kansas (Whittemore et al. 2014). However, the City of Russell, Kansas currently relies primarily on alluvial wells adjacent to the Smoky Hill River approximately 23 miles southwest of the city, and surface water from the Big Creek (https://www.russellcity.org/199/Water-Production). Approximately 50% of the municipal water supply for the City of Russell Kansas comes from groundwater water originating from the shallow, undifferentiated Pleistocene alluvial deposits adjacent to the Smoky Hill River near Pfiefer in Ellis County (approximately 23 miles southwest of the City of Russell). The comprehensive plan for the City of Russell involves purchasing water rights from the Great Bend Prairie aquifer in a cooperative project with the City of Hays to the west (Russell City Planning Commission 2016). Additionally, the City of Bunker Hill Kansas municipal water supply is comprised 100% of ground water originating from a water supply well completed into Dakota Formation (Dakota Aquifer).

The two other most common water supply sources for potable, commercial, and agricultural uses in this part of Kansas include the installation of use of private wells or connection to one of

several rural water district water supply entities that operate in Russell County. In the vicinity of the GS project site and CSS#1, these wells are typically completed into the Dakota formation (Dakota Aquifer) or occasionally shallower unconfined aquifers (e.g., Greenhorn Limestone or undifferentiated alluvial deposits). There are 12 shallow water wells within a 2-mi distance of CSS #1. The predominant use for water from wells in the general vicinity is for cattle though some may be used for domestic purposes other than cattle (KGS 2022).

Figure A.I.8-1. Map of Water Wells at the GS Site

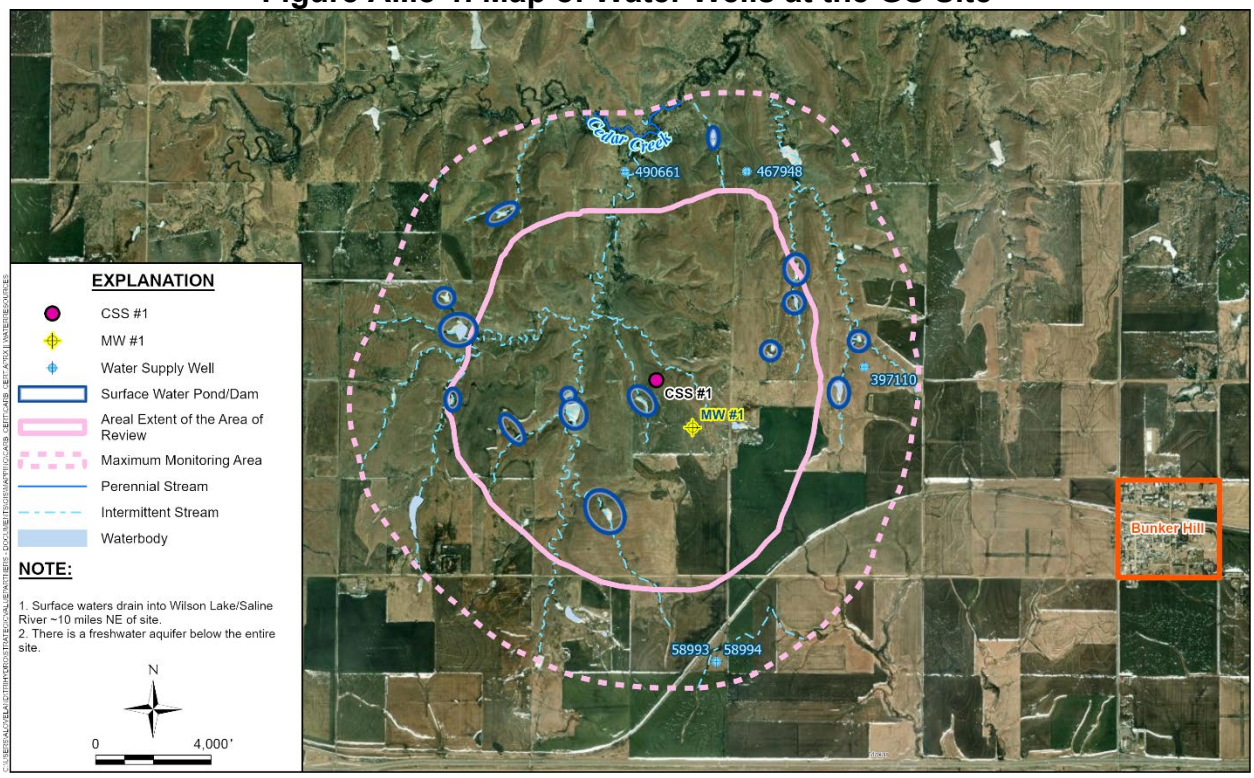

A.I.8.1. Determination of the Lowermost USDW

The Dakota Aquifer is the lowermost USDW for the proposed GS site. As shown in Figure A.I.8-2, the Lower Cretaceous Dakota Formation outcrops in portions of Russell County, both to the north and south of the proposed GS site.

Figure A.I.8-2. Dakota Formation Outcrop Locations
From: MacFarlane et al. 1988

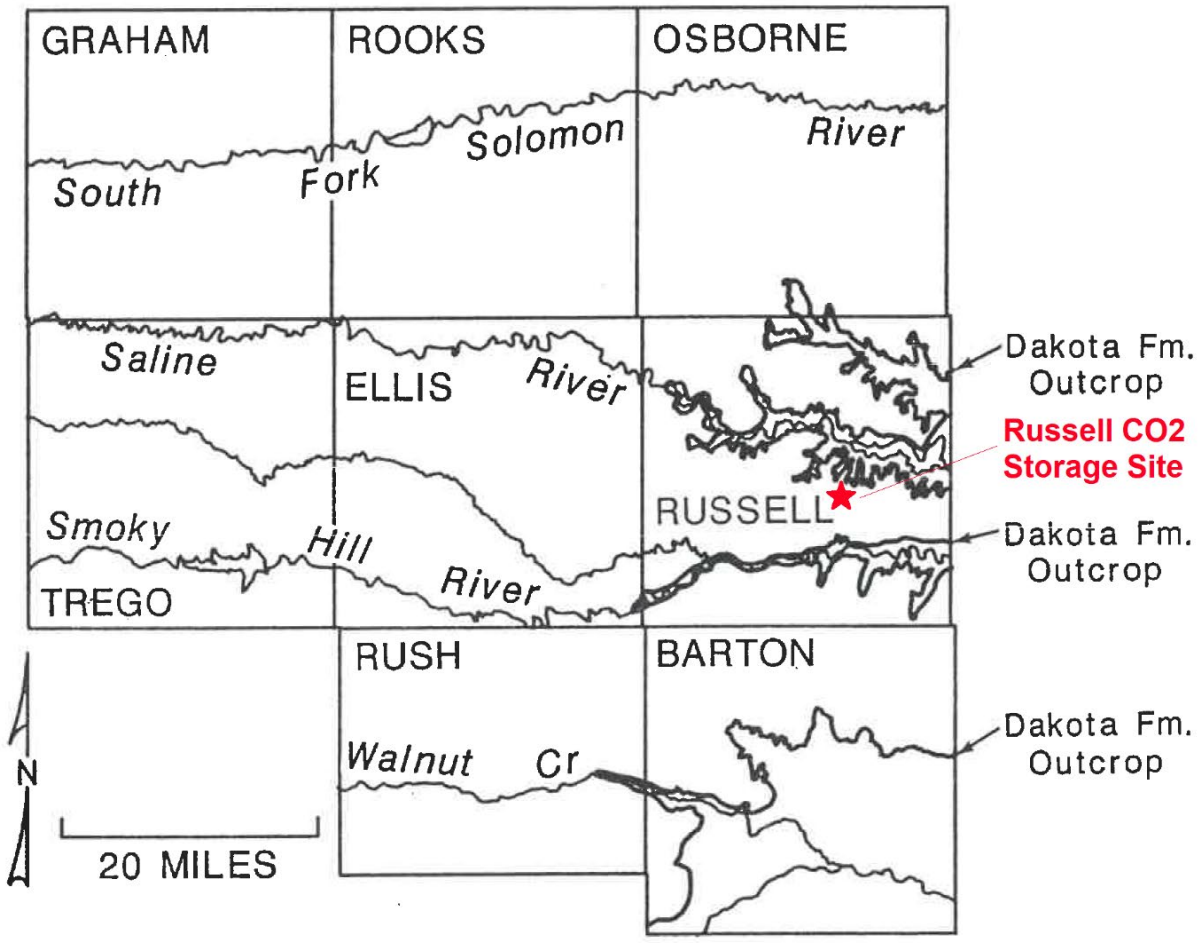

At the proposed GS site, the Dakota Formation is overlain by Upper Cretaceous Carlile Shale, Greenhorn Limestone, and/or Graneros Shale. These formations are shown in Figure A.I.8-3 (next page) using site-specific drilling information at the previously installed monitoring stations, and accounting for varying ground surface elevations in the area. The wells shown below screened in the Greenhorn Limestone and Graneros Shale produce water at relatively low flowrates (less than 0.1 gpm) and are considered to be the "water table" aquifer. The wells screened in the Dakota Formation also produce water at relatively low flowrates (less than 0.1 gpm) and are considered to be the lowest zone from which drinking water could theoretically be obtained.

Figure A.I.8-3. Site-Specific Stratigraphy Above the Dakota Formation

Based on drilling for shallow subsurface monitoring stations[3]

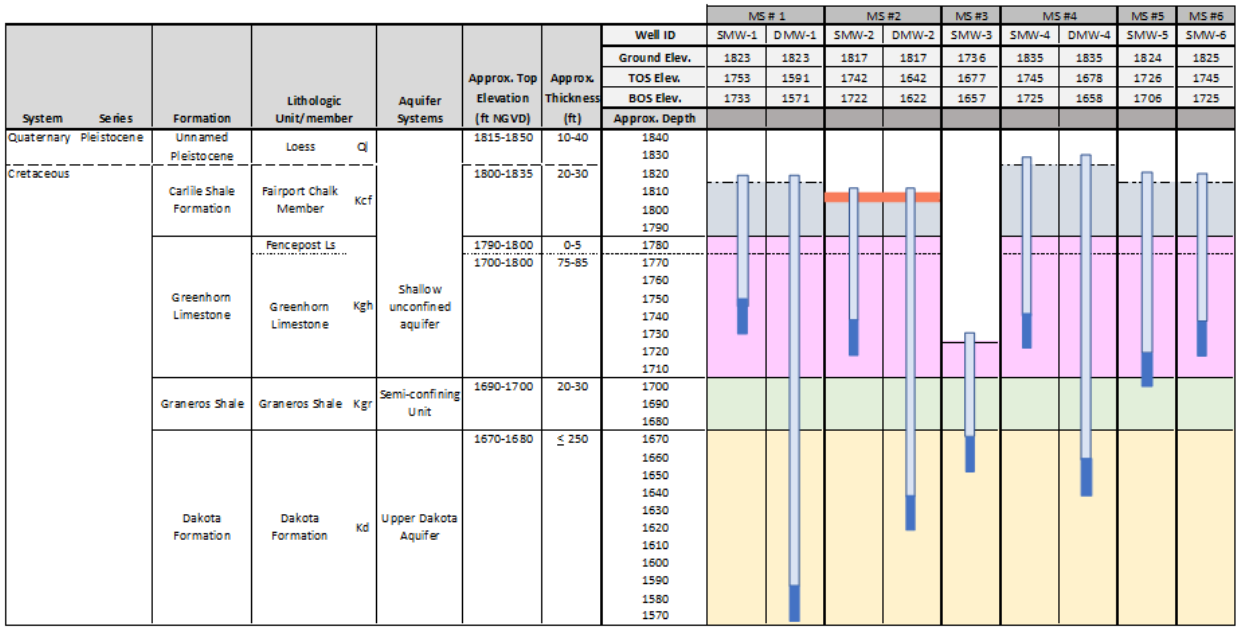

Figure A.I.8-4 provides a shallow stratigraphic column for central Kansas. The geologic units that comprise the Dakota Aquifer include the Dakota Formation and the underlying Kiowa Formation and the Cheyenne Sandstone. These are sometimes grouped with the Dakota Formation as comprising the Dakota Aquifer. Based on data from OFR 88-39 (MacFarlane et al. 1988), the Jurassic-aged Morrison Formation and Upper Permian-aged undifferentiated Permian unit are not present beneath the PCC project site location in central Russell County. However, the Lower Permian-aged units may include different formations within the Nippewalla Group. The Stone Corral Anhydrite, an evaporite-anhydrite unit that serves as a regional confining unit, underlies these lower Permian-aged units.

[3] Note: DMW-3 does not exist. SMW-3 is located in a valley that allows a shallow monitoring well to directly monitor the Upper Dakota Aquifer, eliminating the need for a deep groundwater monitoring well at MS #3.

Figure A.I.8-4. Shallow Stratigraphy for Central Kansas

From: MacFarlane et al. 1988

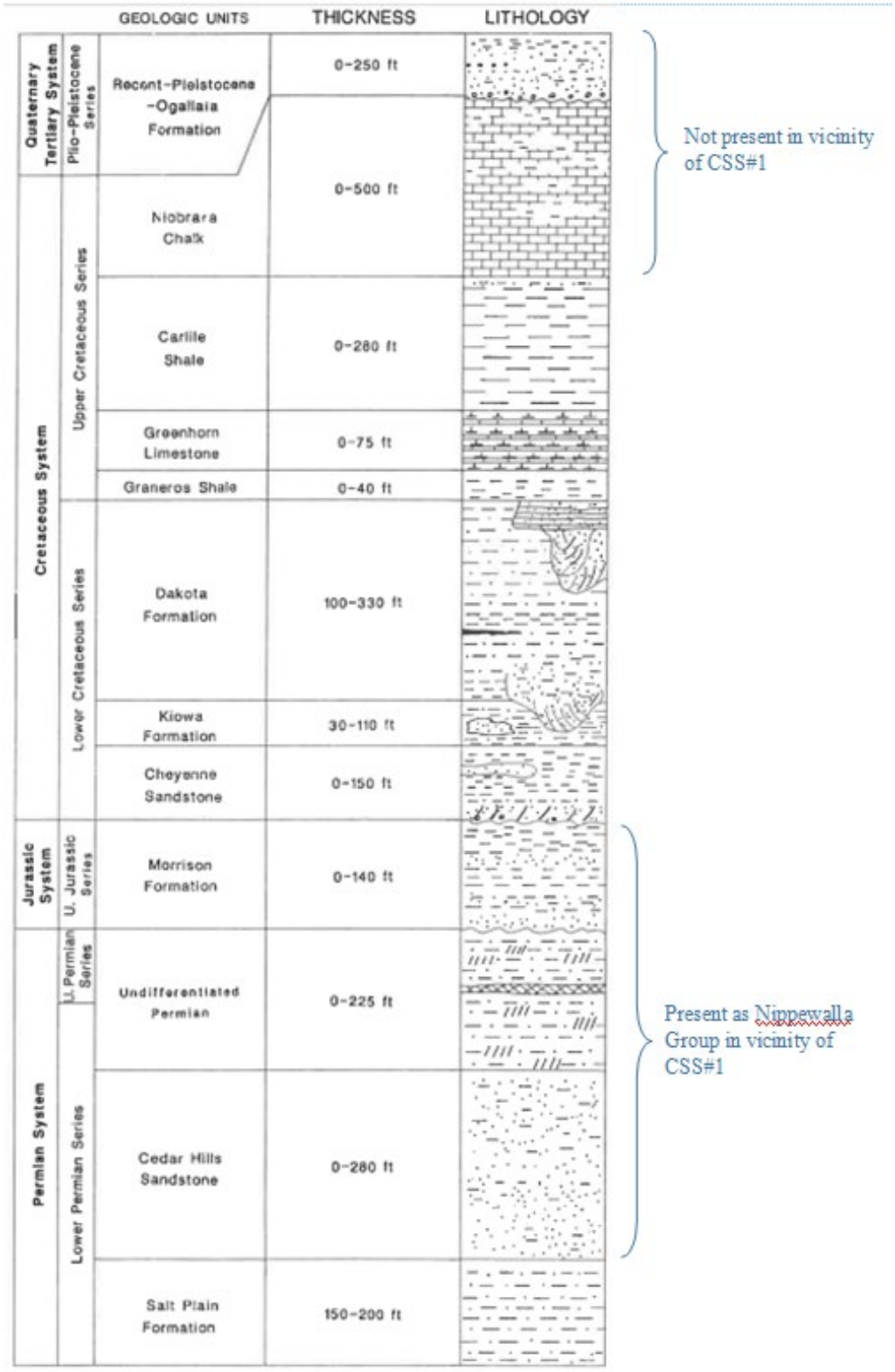

According to the Kansas Geologic Survey (MacFarlane et al. 1988 and Whittemore et al. 2014), Russell County Kansas experiences some of the greatest spatial variations exhibited in salinity and TDS within the Dakota aquifer across all of Kansas (KGS Bulletin 260 – Figure 32). The main constituents influencing groundwater salinity and TDS are sodium and chloride. In western Russell County, the Dakota Aquifer has its most saline concentrations where this unit overlies saline zones within the Permian Nippewalla Group. However, in eastern Russell County, where the overlying confining units are thin or absent near outcrop locations (e.g., valleys), local recharge and discharge have flushed much of the saline water in the upper portion of the aquifer. In general, the freshest water quality occurs in the upper portions of the Dakota Aquifer, and the salinity and associated TDS concentrations increase with depth. The presence of low permeability units vertically through the aquifer may play an important part in separating low and high salinity zones.

Figure A.I.8-5. Groundwater Quality Profile for Russell County, KS (1945)
From: Figure 2 of MacFarlane et al. 1988

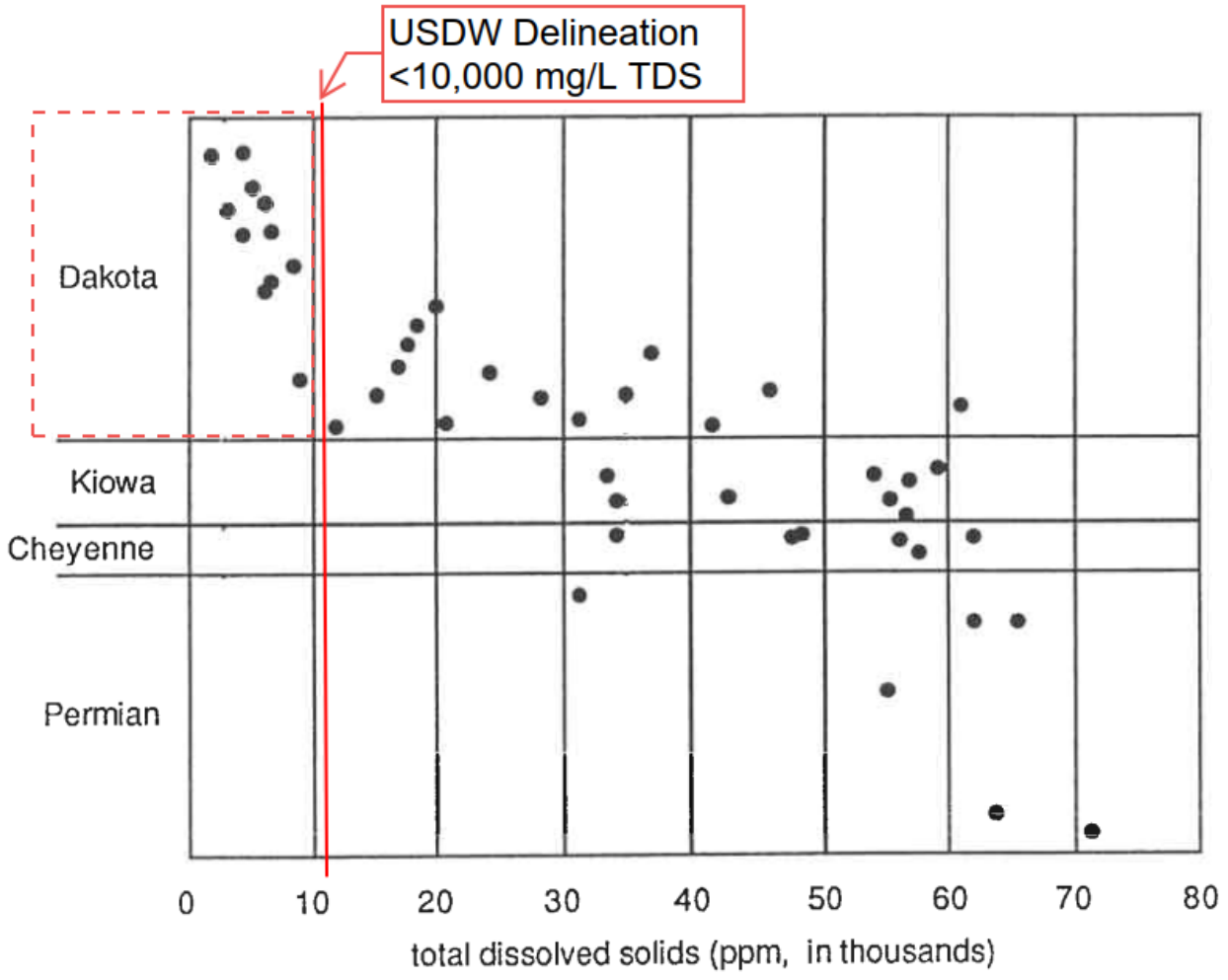

Figure A.I.8-5 shows groundwater quality data in Russell County from 1945. In the 1940s, several investigations were conducted into the Lower Cretaceous and Lower Permian units in

Russell County (MacFarlane et al. 1988 – Figure 2). These investigations found that the TDS and chloride concentrations progressively increase with depth in these formations. The TDS concentrations from the lower portion of the Dakota Formation ranged between 9,000 to 60,000 mg/L. Within the Kiowa and Cheyenne Formations, the TDS concentrations ranged from 33,000 to 62,000 mg/L, and within the Permian section the TDS concentrations reportedly ranged from 31,000 to 71,000 mg/L.

More recently in the early 1990s, the City of Russell drilled a series of test wells in the east and southeast portions of the county while exploring the area for a new potential water supply (Whittemore et al. 2014 - Tables 16 & 17, Figure 65). These data also indicated that the salinity and TDS concentration generally increase with depth. Three groundwater samples were collected from one test well (TH 4-93), near Dorrance KS, located approximately nine miles to the east-southeast of the proposed GS site. The deepest of these three samples was taken from a depth interval of 220 to 230 ft bgs which corresponds to an elevation of 1,505 to 1,515 ft referenced to the National Geodetic Vertical Datum of 1929. This well and deep sampling interval depth occur within the Dakota aquifer system. The TDS concentration of the groundwater sample collected from this depth interval at test well TH 4-93 was 12,307 mg/L. This TDS concentration also exceeds the 10,000 mg/L threshold used to delineate the USDW for the Underground Injection Control (UIC) program. This sample interval was within the Dakota Aquifer system, and it occurs at an elevation only slightly below (roughly 70 to 150 ft lower in elevation) the recently drilled wells at shallow monitoring stations near CSS#1 that penetrate into the upper portion of the Dakota Aquifer.

Finally, the USGS Produced Water Database was mined for samples collected in the subsurface in Russell County, Kansas. Only 7 of 319 samples for TDS had concentrations less than 10,000 mg/L. Those seven samples were collected in the Dakota or Cheyenne Formations (or "unknown") and all lower sample depths were less than 500 ft bgs.

Based the evaluation of these relevant lithologic and hydrogeologic data and in consideration of the site-specific testing and monitoring program, the bottom of the USDW beneath the PCC project site near Russell Kansas is within the lower portion or near the bottom of the upper portion of the Dakota Aquifer system (less than or equal to 500 ft bgs). As described above, the groundwater testing and monitoring program implemented for the PCC project includes the Dakota Aquifer system, and thus are monitoring the lowest USDW.

A.I.8.2. Water Supply Wells In Proximity To The Project Site

A search of the active KGS well record database (KGS 2023) in February 2023 found there were fewer than 25 active (non-plugged) water wells located within all of Township 13 South, Range 13 West and the northeast portion of Township 14 South and Range 13 West that includes CSS #1 and the entire AoR. All identified water wells in proximity to the project site are comparatively shallow; none penetrate confining layers for the GS project. Of the identified water wells, one is located within the areal extent of the AoR at a depth of 65 ft bgs, five are located within the ½-mi buffer zone of the MMA with depths ranging from 20 to 377 ft bgs, and

six are located outside the MMA but within 2-mi of CSS #1 at depths ranging from 15 to 106 ft bgs. See Section B.5.1 of the Area of Review and Corrective Action Plan for a complete tabulation of wells in proximity to the project site.

Based on information obtained from the State of Kansas Department of Health and Environment (https://dww.kdhe.ks.gov/DWW/JSP/WaterSystemDetail.jsp), the City of Russell, Kansas municipal water supply is comprised of roughly 50% ground water and 50% surface water. The groundwater water source is the shallow, undifferentiated Pleistocene alluvial deposits adjacent to the Smoky Hill River near Pfiefer in Ellis County (approximately 23 miles southwest of the City of Russell) (https://www.russellcity.org/199/Water-Production). The surface water source comes from an intake structure on the Big Creek within the Big Creek watershed, also located west to southwest of the City (https://www.russellcity.org/199/Water-Production).

Based on information obtained from the State of Kansas Department of Health and Environment (https://dww.kdhe.ks.gov/DWW/JSP/WaterSystemDetail.jsp), the City of Bunker Hill, Kansas municipal water supply is comprised 100% of ground water. The groundwater water source is a water supply well completed into Dakota Formation (Dakota Aquifer). The precise location of this supply well is not shown in the active KGS well record database (KGS 2023) or on its associated mapping tool, but it is assumed to be located within the city boundaries which are outside of the AoR.

A.I.9. Geochemistry [40 CFR 146.82(a)(6)]

Site-specific baseline geochemistry data have been collected for the Dakota Formation groundwater (lowermost USDW), the Water Table aquifer groundwater, the vadose zone, and at ground surface since the Fall of 2022. Collectively, these are referred to as the "Shallow Zones" in Section A.I.9.1 below. Groundwater in the Dakota is relatively hard, has a high TDS, and exhibits variable salinity content. "Deep Zones" are considered in Section A.I.9.2 as those below the Dakota Formation (lowermost USDW), for which data collection started with pre-operational testing of CSS #1. These data will be used as a baseline for comparison of groundwater samples taken during the Injection and PISC periods to monitor for changes in groundwater quality that could warn of unanticipated movement of formation fluids or non-containment of CO_2.

Solid phase geochemistry for CO_2-Brine/Rock Reactions is discussed in Section A.I.5.5.4.

A.I.9.1. Geochemistry in Shallow Zones

The purpose of the baseline environmental testing and monitoring program (BETM) was to characterize geochemical conditions, spatial variability, and temporal (e.g., seasonal and more frequent) variability with the lowermost USDW and shallower environment. The following sections review data collected through July 2023, sequencing from the lowermost USDW upwards. The results, detailed in Appendix A.I-1, are summarized as follows:

- General Observations/Comments
  - The Year 1 geochemical monitoring data collected from the Dakota Aquifer exhibited minimal temporal variation but did vary spatially, both concentration levels and primary constituents, across the project site and different monitoring stations.
  - Except for Monitoring Station 6 (SMW-6), the Year 1 geochemical monitoring data collected from the Water Table aquifer exhibited relatively little spatial or temporal variation.
  - The graphical and statistical methods of data analyses performed on these groundwater monitoring results will help geochemically characterize ("fingerprint") the groundwater quality data collected from each monitoring station and aquifer interval being monitored across the project site.
  - Furthermore, these manner of data analyses should improve the future ability to monitor for anomalous change detection potentially created from the subsurface migration of CO_2 into these monitored aquifer intervals.
- Dakota Formation groundwater (lowermost USDW)
  - Temperatures were steady over time and consistently approximately 15 ºC across monitoring wells. Salinity was more variable between wells ranging from less than 0.5 parts per thousand to greater than 10 parts per thousand. The depths to groundwater at the majority of wells (DMW-2 was the exception) were demonstrably affected by groundwater sampling, sometimes resulting in multi-day periods of recharge.
  - The DMW-1 and DMW-4 groundwater are geochemically similar, with sodium and potassium as the dominant cations and chloride as dominant anion. The DMW-2 and SMW-3 groundwater have more even mixes of other cations and/or anions.
  - Over time, the geochemistry of groundwater at any given well was relatively stable, indicating consistent conditions over time.
- Water Table aquifer
  - Temperatures were steady (approximately 15 ºC). Versus Dakota Formation groundwater, salinity was measured within a tighter range (2.34 to 4.35 parts per thousand as averages for the five wells). The depths to groundwater at all wells were demonstrably affected by groundwater sampling, sometimes resulting in multi-day periods of recharge.
  - The Water Table aquifer geochemistry was similar across monitoring wells. Sodium and potassium were the dominant cations and chloride was the dominant anion.
  - Over time, the geochemistry of groundwater was stable, with the exception of SMW-6. At that location, there was variability between sample events, including a switch from chloride as the dominant anion in October 2022, January 2023, and July 2023 to bicarbonate/carbonate as the dominant anion in April 2023.

- Soil gas CO_2
  - CO_2 concentrations were elevated above atmospheric levels at all stations and both depths (5 ft bgs and 10 ft bgs), indicating subsurface sources of CO_2.
  - Both 5 ft bgs and 10 ft bgs CO_2 concentrations exhibited increasing trends beginning approximately in April 2023. In addition to these general trends, the 5 ft bgs CO_2 concentrations varied on shorter time periods. The most extreme variation was at SVP-4, where multiple episodes of CO_2 concentration decrease to near atmospheric concentrations were followed by longer term elevated values.
  - Stable carbon isotopes in soil gas CO_2 were within an -11 to -21 ‰ range across measurement locations for all sample events.
- CO_2 effluxes
  - Mean CO_2 effluxes were similar in October 2022 and April 2023, with values in the 0.8 to 2.2 micromoles per square meter per second ($\mu mol\ m^{-2}\ s^{-1}$) range.
  - July 2023 mean CO_2 effluxes were relatively high across all stations, with values in the 5.9 to 11.3 $\mu mol\ m^{-2}\ s^{-1}$ range.

A.I.9.2 Geochemistry in Deep Zones

Ground water samples from the deep zones were collected as follows:

- Drill Stem Testing (DST)
  - Six DSTs were conducted during drilling of CSS #1
- Swab Fluid Testing
  - Fluid was swabbed from CSS #1 Arbuckle perforations in 2023.

Specialty analysis from SLB provided salinity, confirming there were no fresh waters below 1,500 ft below KB. This tied into the DST results for both the Oread Limestone at 2,874 ft below KB (78,900 mg/L TDS) and Reagan Sandstone at 3,665 ft below KB (25,800 mg/L TDS). DST fluids that were deemed representative of formation fluids were analyzed. Full DST results and associated fluid laboratory results are provided separately. Fluid samples from the Arbuckle were collected via swabbing on May 11, 2023 and showed a salinity of 24,900 mg/L.

The literature for the Arbuckle Group indicates chloride is a major anion present in groundwater. As shown on Figure A.I.9-1, the chloride concentration is approximately 25,000 mg/L in the AoR and vicinity.

Figure A.I.9-1. Chloride concentrations in the Arbuckle Group
From: Carr et al. 1986

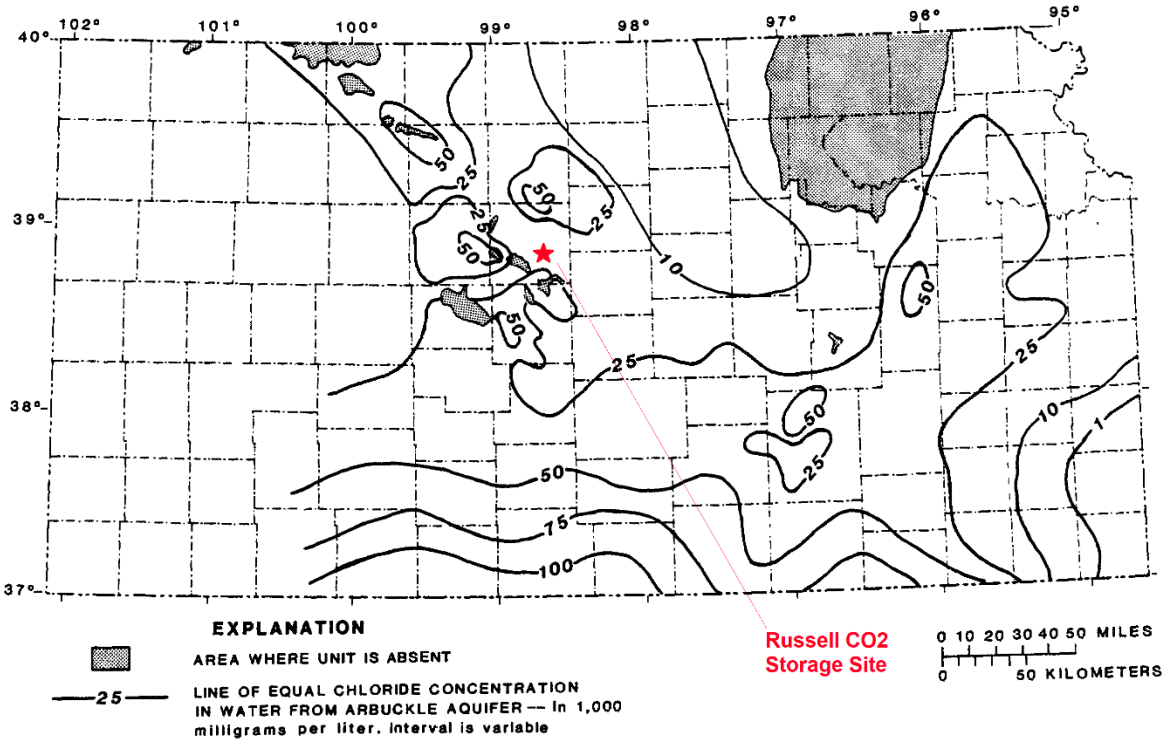

Lithologic core analysis and groundwater sampling of the Arbuckle Group from CSS#1 have been performed. At present, a useful resource on Arbuckle geochemistry is for Sumner County, Kansas. Scheffler (Scheffler 2012) processed groundwater data from ten samples collected within the Arbuckle, with results displayed in Table A.I.9-1. Calcium and magnesium were identified at high concentrations (61 to 280 millimoles per liter [mmol/L] and 22 to 86 mmol/L, respectively), consistent with the dolomitic makeup of the formation. High concentration of chloride, sodium, and potassium were also observed, suggesting reservoir salt accumulation.

Table A.I.9-1. Literature Results on Groundwater Geochemistry

Drill stem test samples within the Arbuckle Group in Sumner County, KS

From: Scheffler 2012

Brine data

Depth (Ft)	T °c	pH (field)	HCO_3	DOC	CH_4	Br	Cl	N/NO_3	P/PO_4	SO_4
4188	43.9	7.1	6.2	12	7.E-01	1.1	969	0.07	8.42E-05	8.4
4335	46.0	6.9	6.6	11	7.E-01	0.9	889	0.09	1.05E-04	15.3
4370	**	6.7	4.0	**	**	1.2	1332	**	**	8.6
4520	50.3	6.4	4.2	1	6.E-02	1.5	1802	0.16	7.37E-05	9.5
4875	**	6.2	2.8	**	**	2.1	2873	**	**	3.8
4927	53.3	6.3	1.9	9	6.E-01	2.1	2646	0.25	6.84E-04	3.8
4928	**	6.2	2.6	**	**	2.3	2894	**	**	3.2
5010	**	5.7	1.6	14	**	2.8	3326	0.18	**	3.1
5037	54.4	6.0	1.1	19	9.E-01	2.7	3114	0.24	5.05E-04	2.8
5191	54.3	6.8	1.9	3	**	2.6	2507	0.32	1.05E-03	2.6

Depth (Ft)	Ca	K	Mg	Na	B	Si	Fe^{2+}	Fe total	Al	Sr
4188	61	6	22	805	12	0.1	0.4	0.2	0.1	3.7
4335	70	7	25	758	12	0.1	0.5	0.2	0.1	3.2
4370	94	9	37	1071	**	**	0.5	*	*	1.4
4520	132	12	48	1406	24	0.3	3.0	0.4	0.2	6.7
4875	230	19	73	2152	**	**	0.4	*	*	3.4
4927	217	17	68	1974	48	0.3	2.1	0.5	0.4	8.3
4928	237	19	74	2215	**	**	0.5	*	*	3.5
5010	280	22	86	2584	48	0.4	2.0	0.5	0.4	9.0
5037	258	20	76	2209	48	0.3	2.0	0.5	0.4	8.8
5191	226	17	68	1921	48	0.3	6.3	0.4	0.5	7.4

All values presented in mmol/L

*Not detected

**Not analyzed for.

Redox indicator species for the Scheffler groundwater samples are presented on Figure A.I.9-2 below. Ferrous iron concentrations increased with depth, suggesting oxygen-limited iron reduction within the deeper portions of the Arbuckle. This inference is supported by decreasing sulfate concentrations with depth that suggest sulfate reduction to sulfides.

Figure A.I.9-2. Literature Result on Groundwater Redox Indicators
Drill stem test samples within the Arbuckle Group in Sumner County, KS
From: Scheffler 2012

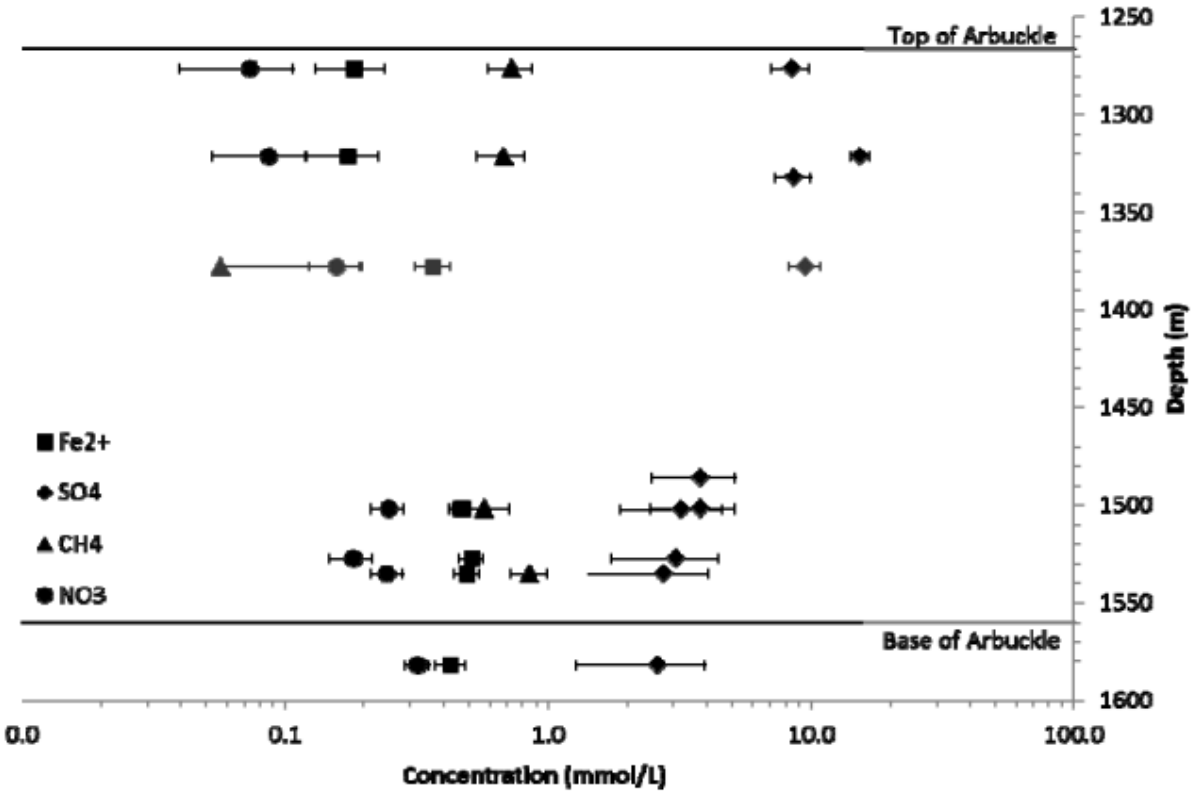

The Scheffler study also characterized solid-phase geochemistry of the Arbuckle in Sumner County, Kansas via wireline logging. The analysis identified primarily cherty dolomite (silicon dioxide and dolomite), with calcium (average of 20.1% by weight), magnesium (average of 8.1%), and silicon (average of 7.5%) at the highest elemental abundance. In chert-rich zones, silicon makes up the primary component of the rock at 43.4%. Aluminum content varied between 0 to 5.3%, iron from 0 to 1.2%, potassium from 0.6 to 2.2%, and sulfur from 0 to 2.7%.

Table A.I.9-2 shows the water sample results for the Arbuckle Group that were collected on May 11, 2023 from well swabbing and a Piper diagram is shown as Figure A.I.9-3 comparing swab results from other Arbuckle samples.

Figure A.I.9-3. Arbuckle Group Piper Diagram
CSS #1 Arbuckle Swab Sample ("UIC Well") and Arbuckle Samples in Sumner County
From: Scheffler 2012

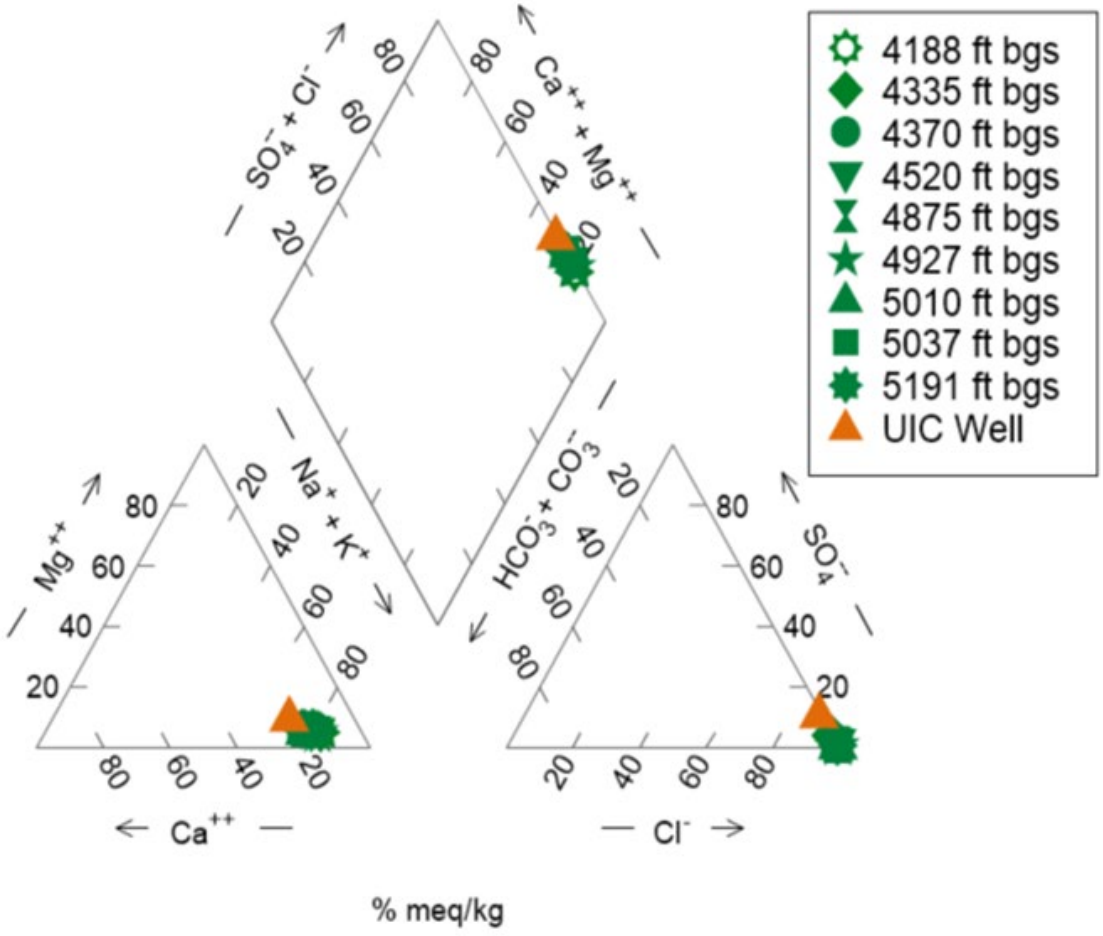

The CSS #1 Arbuckle swab sample plots adjacent to the Arbuckle samples collected from Sumner County, despite the sampling locations being more than 100 miles apart. Each of the Arbuckle samples is indicative of sodium and potassium as the dominant cation component and sulfate and chloride as the dominant anion component. The Stiff diagram presented in Figure A.I.9-4 provides additional resolution on the CSS #1 geochemistry. The dominant anion is chloride, further aligning with the results for the Arbuckle water in Sumner County (Table A.I.9-1).

Figure A.I.9-4. CSS #1 Arbuckle Swab Sample Stiff Diagram

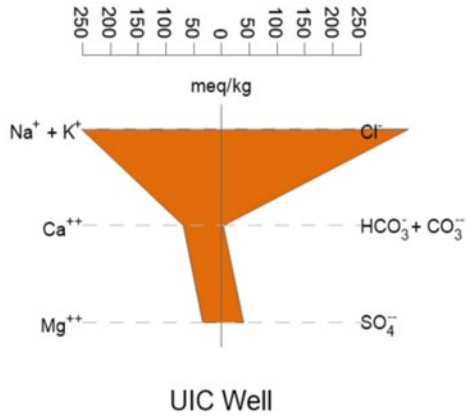

In addition to the major cations identified above, strontium was detected at a concentration of 32.8 mg/L, iron at 21.3 mg/L, and silicon at 10.9 mg/L (Table A.I.9-2). Other cations were either not detected or were measured at concentrations less than 10 mg/L. Additional detected anions included bromide (32.9 mg/L), fluoride (1.8 mg/L), and sulfide (0.57). The measured TDS concentration was 24,900 mg/L.

Table A.I.9-2. Water Sample Data for CSS #1 Arbuckle Group Swab Sample

Analyte	Concentration (mg/L)	Analyte	Concentration (mg/L)
Aluminum	ND(0.075)	Manganese	0.634
Ammonia as N	11.6	Mercury	ND(0.0002)
Antimony	ND(0.015)	Nickel	0.0212
Arsenic	0.0114	Nitrate as N	ND(1)
Barium	0.102	Nitrite as N	ND(5)
Beryllium	ND(0.001)	Oil and Grease	17.2
Boron	4.87	pH	6.8 standard units
Bromide	32.9	Phenol	ND(0.010)
Cadmium	ND(0.005)	Selenium	ND(0.015)
Chromium	0.0233	Silica	23.4
Cobalt	ND(0.005)	Silicon	10.9
Copper	0.0196	Silver	ND(0.007)
Cyanide	ND(0.005)	Strontium	32.8
Fluoride	1.8	Sulfide as H_2S	ND(1)
Iron	27.3	Sulfide, Total	0.57
Iron, Ferric	6	Vanadium	ND(0.010)
Iron, Ferrous	21.3	Total Dissolved Solids	24,900
Lead	ND(0.010)	Total Organic Carbon	ND(2)

Overall, the 2023 CSS #1 Arbuckle swab sample results aligned more closely with Arbuckle sampling results elsewhere in Kansas than with shallow groundwater (including the lowermost USDW) in the AoR for planned injection.

Table A.I.9-3 presents the details from the drill stem testing.

Table A.I.9-3. Drill Stem Test Analytical Results from CSS #1

Formation		Oread Limestone/ Heebner Shale (DST1)	Missourian Series/ Lansing (DST2)	Iola Limestone (Kansas City Group) (DST3)	Marmaton Group/ Arbuckle Group (DST4)	Arbuckle Group (TBD)	Reagan Sandstone (DST5)	Reagan Sandstone DUP (DST7)
Sample Interval (ft below KB)		2,874-2,920	3,025-3,050	3,080-3,100	3,270-3,350	3,456-3,515	3,665-3,710	3,665-3,710
Sample Date		10/25/2022	10/28/2022	11/2/2022	11/5/2022	TBS	11/10/2022	11/11/2022
Analytes	Units							
Aluminum	ug/L	255,000	NA	NA	NA	TBS	6,480	2,830
Antimony	ug/L	ND(75.0)	NA	NA	NA	TBS	ND(300)	ND(300)
Arsenic	ug/L	159	NA	NA	NA	TBS	ND(200)	ND(200)
Barium	ug/L	1,480	NA	NA	NA	TBS	214	136
Beryllium	ug/L	21.7	NA	NA	NA	TBS	ND(20.0)	ND(20.0)
Boron	ug/L	1,410	NA	NA	NA	TBS	6,520	6,100
Cadmium	ug/L	32.2	NA	NA	NA	TBS	ND(100)	ND(100)
Calcium	ug/L	9,010,000	NA	NA	NA	TBS	1,740,000	1,620,000
Chromium	ug/L	421	NA	NA	NA	TBS	ND(100)	ND(100)
Cobalt	ug/L	187	NA	NA	NA	TBS	ND(100)	ND(100)
Copper	ug/L	519	NA	NA	NA	TBS	ND(200)	ND(200)
Iron	ug/L	458,000	NA	NA	NA	TBS	10,200	4,190
Lead	ug/L	13,600	NA	NA	NA	TBS	ND(200)	ND(200)
Lithium	ug/L	2,370	NA	NA	NA	TBS	3,100	2,810
Magnesium	ug/L	1,220,000	NA	NA	NA	TBS	580,000	537,000
Manganese	ug/L	15,500	NA	NA	NA	TBS	569	452
Nickel	ug/L	510	NA	NA	NA	TBS	ND(100)	ND(100)
Potassium	ug/L	128,000	NA	NA	NA	TBS	113,000	102,000
Selenium	ug/L	17.5	NA	NA	NA	TBS	ND(300)	ND(300)
Silica	ug/L	151,000	NA	NA	NA	TBS	54,600	39,900
Silicon	ug/L	70,500	NA	NA	NA	TBS	25,500	18,600

Formation		Oread Limestone/ Heebner Shale (DST1)	Missourian Series/ Lansing (DST2)	Iola Limestone (Kansas City Group) (DST3)	Marmaton Group/ Arbuckle Group (DST4)	Arbuckle Group (TBD)	Reagan Sandstone (DST5)	Reagan Sandstone DUP (DST7)
Sample Interval (ft below KB)		2,874-2,920	3,025-3,050	3,080-3,100	3,270-3,350	3,456-3,515	3,665-3,710	3,665-3,710
Sample Date		10/25/2022	10/28/2022	11/2/2022	11/5/2022	TBS	11/10/2022	11/11/2022
Silver	ug/L	ND(7.0)	NA	NA	NA	TBS	ND(140)	ND(140)
Sodium	ug/L	100,900,000	NA	NA	NA	TBS	9,220,000	8,570,000
Strontium	ug/L	114,000	NA	NA	NA	TBS	59,500	56,000
Vanadium	ug/L	321	NA	NA	NA	TBS	ND(200)	ND(200)
Zinc	ug/L	5,800	NA	NA	NA	TBS	ND(1,000)	ND(1,000)
Sodium Adsorption Ratio	unitless	28.7	NA	NA	NA	TBS	48.9	47.2
Mercury	ug/L	ND(0.20)	NA	NA	NA	TBS	ND(0.20)	ND(0.20)
Phenol	ug/L	ND(15.6)	NA	NA	NA	TBS	ND(9.6)	ND(9.6)
Nitrate as Nitrogen	mg/L	45.4	NA	NA	NA	TBS	ND(1.0)	ND(1.0)
Nitrite as Nitrogen	mg/L	ND(2.0)	NA	NA	NA	TBS	ND(2.0)	ND(2.0)
Specific Conductance @ 25°C	umhos/cm	84,800	NA	NA	NA	TBS	43,200	44,000
Oil and Grease	mg/L	NS	NA	NA	NA	TBS	7.5	8.8
Alkalinity, Total as CaCO3	mg/L	ND(20.0)	NA	NA	NA	TBS	278	255
Total Dissolved Solids	mg/L	78,900	NA	NA	NA	TBS	25,800	21,900
Iron, Ferric	mg/L	456	NA	NA	NA	TBS	10.1	4.2
Iron, Ferrous	mg/L	2.3	NA	NA	NA	TBS	ND(0.20)	ND(0.20)
pH, Laboratory	Std. Units	7.9	NA	NA	NA	TBS	7.1	7.3
Sulfide as H2S (calculation)	mg/L	ND(1.0)	NA	NA	NA	TBS	ND(1.0)	ND(1.0)
Sulfide, Total	mg/L	ND(0.5)	NA	NA	NA	TBS	ND(0.050)	ND(0.050)
Bromide	mg/L	83.6	NA	NA	NA	TBS	55.3	57.4
Chloride	mg/L	59,000	NA	NA	NA	TBS	17,100	16,800
Fluoride	mg/L	ND(0.20)	NA	NA	NA	TBS	ND(0.20)	ND(0.20)

Formation		Oread Limestone/ Heebner Shale (DST1)	Missourian Series/ Lansing (DST2)	Iola Limestone (Kansas City Group) (DST3)	Marmaton Group/ Arbuckle Group (DST4)	Arbuckle Group (TBD)	Reagan Sandstone (DST5)	Reagan Sandstone DUP (DST7)
Sample Interval (ft below KB)		2,874-2,920	3,025-3,050	3,080-3,100	3,270-3,350	3,456-3,515	3,665-3,710	3,665-3,710
Sample Date		10/25/2022	10/28/2022	11/2/2022	11/5/2022	TBS	11/10/2022	11/11/2022
Sulfate	mg/L	2,880	NA	NA	NA	TBS	3,780	2,130
Nitrogen, Ammonia	mg/L	12.1	NA	NA	NA	TBS	5.1	5.1
Cyanide	mg/L	ND(0.030)	NA	NA	NA	TBS	ND(0.0050)	ND(0.0050)
Carbon Dioxide (calculation)	mg/L	ND(20.0)	NA	NA	NA	TBS	289	251
Total Organic Carbon	mg/L	3.9	NA	NA	NA	TBS	2.0	1.5

DUP = duplicate sample
NA = Not analyzed due to drilling mud comingling with sample
ND = Nondetected at the reporting limit. Reporting limit provided in parentheses
NS = Not sampled, Oil and Grease was not included in this analytical suite
Std. Units = Standard Units
TBD = to be determined
TBS = to be sampled in 2023
ug/L = micrograms per liter
umhos/cm = micromhos per centimeter

A.I.10. Other Information (Including Surface Air and/or Soil Gas Data, if Applicable)

Soil gas probes have been installed at 5 and 10 ft bgs at 6 monitoring stations for preliminary characterization. Sampling of these probes in Fall 2022 indicated oxygen (generally 20 to 21%) and nitrogen concentrations (78%) similar to atmospheric conditions at both depths. CO_2 concentrations for 5 ft bgs ranged approximately 0.2% to 0.6%, higher than atmospheric concentrations potentially indicative of natural soil respiration processes and/or sedimentary rock weathering and CO_2 generation. Elevated CO_2 was also detected in several of the 10 ft bgs probes, with a maximum value of approximately 1.2%. This potentially supports an inference of sedimentary rock weathering.

CO_2 effluxes were measured at each of the 6 monitoring stations for preliminary characterization in Fall 2022, with 16 soil collars per station. For the 6 monitoring stations, average CO_2 effluxes ranged from 1.3 to 2.2 micromoles per square meter per second (mmol m^{-2} s^{-1}). This is similar to, or slightly higher than, measurements collected elsewhere for temperate grasslands (Apostolakis et al. 2022, Peng et al. 2011). Coefficients of variation ranged from 0.3 to 0.7 mmol m^{-2} s^{-1}, providing a preliminary estimate of variability for a given station.

A.I.11. Site Suitability [40 CFR 146.83]

PCC believes the site is well-suited for the GS project. The specific requirements of 40 CFR 146.83 are addressed below:

A.I.11.1. Ability to Receive the Total Anticipated CO_2 Stream

The injection zone is of sufficient areal extent, thickness, porosity, and permeability to receive the total anticipated volume of the carbon dioxide stream. The computational model predicts the AoR is an inverted irregular circular cone with an areal extent of 3.1 mi^2 for a total injection of 1.8 million metric ton CO_2, resulting in a storage capacity of 580,000 metric ton CO_2/mi^2. This footprint for the GS project is based upon site-specific values for injection zone thickness, porosity, permeability, and other parameters incorporated into the computational model. The predicted plume is well within the lateral limits of the Arbuckle Group at CSS #1. See Section A.I.3. for further discussion of the lateral extent of the Arbuckle Group injection zone across the AoR and vicinity, Section A.I.3 for further discussion of the thickness of the injection zone across the AoR and vicinity, Section A.I.5.1 for further discussion of porosity and permeability across the AoR and vicinity, and Section B.4.2 of Area of Review and Corrective Action Plan for further discussion of storage capacity predictions from the computational model.

A.I.11.2. Confining Zone Properties

The Arbuckle Group will provide the entirety of the injection zone (3,448 to 3,606 ft bgs) for the GS project, and also provide the primary upper confining layer (3,277 to 3,330 ft bgs), along

with the lower portion of the Marmaton Group (3,274 to 3,277 ft bgs) and a lower confining unit (3,647 to 3,659 ft bgs).

The confining zones are of sufficient areal extent and integrity to contain the injected carbon dioxide stream and displaced formation fluids and allow injection at proposed maximum pressures and volumes without initiating or propagating fractures in the confining zone. Section A.I.4 provides discussion on identified faults and fractures, which do not pose a concern for confinement. Integrity of the confining zones is examined in Section B.5 of the Area of Review and Corrective Action Plan, where legacy wellbores within the AoR are identified and a phased corrective action plan is provided. The computational model presented in the Area of Review and Corrective Action Plan shows pressure at the top of the injection zone should never exceed 80% of fracture pressure at the permit injection rate, thus preventing initiation or propagation of fractures during injection operations.

A.I.11.3. Properties of Additional Zones

The GS site has additional zones that will impede vertical fluid movement, allow for pressure dissipation, and provide additional opportunities for monitoring, mitigation and remediation. Secondary confining zones that will impede vertical fluid movement above the injection zone are the Marmaton Group, as well as several shale sequences plus thick anhydrite and salt zones as discussed in Section A.I.5.2. PCC has found no evidence to date of any faults or fractures that may interfere with containment within the AoR (see Section A.I.4 for further discussion). The Reagan Sandstone provides a pressure dissipation zone below the injection zone, see Section A.I.7 for further discussion. Additional opportunities for monitoring, mitigation, and remediation are discussed in monitoring well plans.

A.I.12. References

Akbarabadi, M. and Piri, M., 2013, Relative permeability hysteresis and capillary trapping characteristics of supercritical CO2/brine systems: An experimental study at reservoir conditions, Advances in Water Resources, Volume 52, Pages 190-206. https://doi.org/10.1016/j.advwatres.2012.06.014.

Apostolakis, A., Schoning, I., Michalzik, B., Klaus, V. H., Boeddinghaus, R. S., Kandeler, E., Marhan, S., Bolliger, R., Fischer, M., Prati, D., Hansel, F., Nauss, T., Holzel, N., Kleinebecker, T., and Schrumpf, M., 2022. Drivers of Soil Respiration Across a Management Intensity Gradient in Temperate Grasslands Under Drought. *Nutrient Cycling in Agroecosystems*, 124, 101-116. https://doi.org/10.1007/s10705-022-10224-2.

Baars, D. L. and Watney, W. L., 1991. Paleotectonic control of reservoir facies. Kansas Geological Survey Bulletin, 233, 253–262. https://www.kgs.ku.edu/Publications/Bulletins/233/Baars/baars.pdf.

Bachu, S., Gunter, W.D., and Perkins, E.H., 1994. Aquifer disposal of CO_2: Hydrodynamic and mineral trapping. Energy Conversion and Management, 35: 269-279.

Birdie, T., Watney, L., Gerlach, P., Killion, M., Raney, J., Holubnyak, E., Bidjoli, T., Williams, G., Nguyen, M., & Wilson, B. (2014). The Impacts of Carbon Dioxide Storage in the Saline Arbuckle Aquifer on Water Quality in Freshwater Aquifers in Kansas. *Midwest Groundwater Association Conference.* https://www.kgs.ku.edu/PRS/Ozark/Reports/2014/MGWA_2014_Arbuckle_Freshwater_Aquifers_TBirdie.pdf.

Brooks, R.H., and Corey, A.T., 1964. Hydraulic properties of porous media. Hydrology Paper No. 3, Colorado State University, 3:1–27.

Buchanan, R., Swain, R., Lebsack, W., 2008. Kansas Springs, Kansas Geological Survey, Public Information Circular II, Oct. 1998, Revised May 2008. Available at: https://kgs.ku.edu/sites/kgs/files/files/PICpdfs/PIC11KansasSprings.pdf.

Carr, J. E., McGovern, H. E., and Gogel, T. 1986. Geohydrology of and Potential for Fluid Disposal in the Arbuckle Aquifer in Kansas. U. S. Geological Survey, Open File Report 86-491. https://doi.org/10.3133/ofr86491.

Carr, T.R., Merriam, D.F., Bartley, J.D. 2005. Use of Relational Databases to Evaluate Regional Petroleum Accumulation, Groundwater Flow, and CO2 Sequestration in Kansas, AAPG Bulletin, Vol. 89, No. 12 (December 2005), pp.1607-1627. https://doi.org/10.1306/07190504086.

City of Russell, 2022. Water Production. Available from: https://www.russellcity.org/199/Water-Production#:~:text=The%20City%20of%20Russell%20has,the%20City%20along%20Big%20Creek.

Chang, Y., Coats, B., and Nolen, J., 1996. A compositional model for CO_2 floods including CO_2 solubility in water, Society of Petroleum Engineers 35164.

Cole, V. B., 1975. Subsurface Ordovician-Cambrian rocks in Kansas: Kansas Geological Survey, Subsurface Geology Series 2, 18 p. https://www.kgs.ku.edu/Publications/Bulletins/Sub2/.

Faber, Z., 2010. Injection of waste fluids into the Arbuckle group of the Western Interior Plains Aquifer System in Kansas: M.S. thesis, Emporia State University, Emporia, Kansas.

Fazelalavi, M., 2015. Fracture Pressure in Arbuckle Based on Step-Rate Test. Kansas Geological Survey Open-File Report 2015-19. https://www.kgs.ku.edu/Publications/OFR/2015/OFR2015_19.pdf.

Franseen, E.K., 1999. A Review of Arbuckle Group Strata in Kansas from a Sedimentologic Perspective. KGS Open-field Report 1999-49. https://www.kgs.ku.edu/Publications/OFR/1999/OFR99_49/.

Franseen, E.K., Enos, P., Farr, R.M., Goldstein, R. and Olea, R.A., 1995. Technical Proposal: Depositional, structural, and diagenetic controls on fractured reservoirs, Arbuckle Group, Kansas: Kansas Geological Survey through the University of Kansas Center for Research, Inc., 74 p.

Franseen, E. K., Byrnes, A.P., Cansler, J.R., and Carr, T., 2004. Geology of Kansas: Arbuckle Group: Current Research in Earth Sciences Bulletin A, 250, part 2. https://www.kgs.ku.edu/Current/2004/franseen/franseenarbuckle.pdf.

Gerhard, Lee C., 2004. "A New Look at an Old Petroleum Province". Midcontinent Geoscience, no. 250 (September):1-27. https://journals.ku.edu/mg/article/view/11808.

Johnson, W.C. and Arbogast, A.F., 1996. Geologic Map of Russell County, Kansas, Kansas Geological Survey/The University of Kansas - Map M-37. https://www.kgs.ku.edu/General/Geology/County/rs/russellLarge.html.

Jorgensen, D. G., 1989. Paleohydrology of the central United States: U.S. Geological Survey Bulletin, v. 1989-D, 32 p. https://doi.org/10.3133/b1989D.

Jorgensen, D.G., Helgesen, J.O., and Imes, J.L. (eds.), 1993. U.S. Geological Survey Professional Paper, in Regional aquifers in Kansas, Nebraska, and parts of Arkansas, Colorado, Missouri, New Mexico, Oklahoma, South Dakota, Texas, and Wyoming; geohydrologic framework, Report # P 1414-B, p. B1-B72. https://doi.org/10.3133/pp1414B.

Jorgensen, D. G., Helgesen, J.O., Signor, D.C., Leonard, R.B., Imes, J.L., and Christenson, S.C., 1996. Analysis of regional aquifers in the central Midwest of the United States in Kansas, Nebraska, and parts of Arkansas, Colorado, Missouri, New Mexico, Oklahoma, South Dakota, Texas, and Wyoming—Summary: U.S. Geological Survey Professional Paper 1414-A,67 p. https://doi.org/10.3133/pp1414A.

Juanes, R., Spiteri, E.J., Orr Jr, F.M., and Blunt, M.J., 2006. Impact of relative permeability hysteresis on geological CO_2 storage. Water Resources Research.

Kansas 2015, Kansas Seismic Action Plan, September 26, 2014, Amended January 21, 2015. Available at: https://www.kgs.ku.edu/PRS/Seismicity/2015/Seismic_Action_Plan.pdf.

Kestin, J., Khalifa, H., and Correia, R., 1981. Tables of the Dynamic and Kinematic Viscosity of Aqueous NaCl Solutions in the Temperature Range 20—150 ºC and the Pressure Range 0.1—35 MPa, Journal of Physical and Chemical Reference Data 10, 71(1981). https://doi.org/10.1063/1.555641.

Killough, J.E., 1976. Reservoir Simulation with History-dependent Saturation Functions, Trans. AIME 261, p 37-48, Society of Petroleum Engineers 5106.

Land, C.S., 1968. Calculation of Imbibition Relative Permeability for Two and Three-Phase Flow from Rock Properties, Soc. Petr. Eng. J., 1968; 8(2), 149-56. https://doi.org/10.2118/1942-PA.

Latta, B. F., 1973, Geology and Ground-water Resources of Barton and Stafford Counties, Kansas, Kansas Geological Survey, Bulletin 88, Lawrence, Kansas. https://www.kgs.ku.edu/General/Geology/Barton/Bull88.pdf.

Levandowski, W., Herrmann, R. B., Briggs, R., Boyd, O., and Gold, R., 2018. An updated stress map of the continental United States reveals heterogeneous intraplate stress. Nature Geoscience, 11(6), 433-437. https://doi.org/10.1038/s41561-018-0120-x.

MacFarlane, P.A., Townsend, M.A., Whittemore, D.O., Doveton, J., Staton, M., 1988. Hydrogeology and Water Chemistry of the Great Plains (Dakota, Kiowa, and Cheyenne) and Cedar Hills Aquifer in Central Kansas Open-file Report 88-39. https://www.kgs.ku.edu/Publications/OFR/1988/KGSOFR88-39.pdf.

Merriam, D. F., 1963, The geologic history of Kansas: Kansas Geological Survey Bulletin 162, 317. https://www.kgs.ku.edu/Publications/Bulletins/162/.

Mo, S., Zweigel, P., Lindeberg, E., and Akervoll, I., 2005. Effect of geologic parameters on CO_2 storage in deep saline aquifers. Society of Petroleum Engineers 93952. https://doi.org/10.2118/93952-MS.

National Academies of Sciences, Engineering, and Medicine, 2019. Negative Emissions Technologies and Reliable Sequestration: A Research Agenda, Washington, DC: The National Academies Press. https://doi.org/10.17226/25259.

Newell, K. D., Watney, W. L., Steeples, D. W., Knapp, R. W., and Cheng, S. W. L., 1989, Suitability of high-resolution seismic method to identifying petroleum reservoirs in Kansas—A geological perspective; in, Geophysics in Kansas, D. W. Steeples, ed.: Kansas Geological Survey, Bulletin 226, p. 9-30. https://www.kgs.ku.edu/Publications/Bulletins/226/Newell/2_newell.pdf.

Newell, K.D., Peterie, S., Killion, M., DeArmond, B., Ridley, C., Mandel, R., and Buchanan, R., 2020. Diminishing Depth to Water in Cambrian-Ordovician Arbuckle Group Disposal Wells in Kansas, Kansas Geological Survey, University of Kansas, Lawrence, Kansas 66047 2 Kansas Department of Health and Environment, Bureau of Environmental Remediation, Topeka, Kansas 66612 3 Kansas Department of Health and Environment, Bureau of Water/Geology, Topeka, Kansas 66612. https://doi.org/10.17161/mg.v1i.15525.

Peng, Q., Dong, Y., Qi, Y., Xiao, S., He, Y., and Ma, T., 2011. Effects of Nitrogen Fertilization on Soil Respiration in Temperate Grassland in Inner Mongolia, China. Environmental Earth Sciences, 62, 1163-1171. https://doi.org/10.1007/s12665-010-0605-4.

Peterie, S., 2023. Personal Communication, Research Geophysicist at Kansas Geological Survey.

Pruess, K., Xu, T., Apps, J., and Garcia, J., 2003. Numerical Modeling of Aquifer Disposal of CO_2, Society of Petroleum Engineers 884851.Rochelle, C.A., Czernichowski-Lauriol, I., and Milodowski, A.E., 2004. The impact of chemical reactions on CO_2 storage in geological formations: A brief review. Geological Society, London, Special Publications 233: 87-106.

Rocke, B.J., 2005, Type Log Showing Stratigraphic Horizons for Russell County, Kansas. Kansas Geological Survey, Open-file Report no. 2005-53. http://www.kgs.ku.edu/PRS/publication/2005/OFR05_53/index.html.

Russell City Planning Commission. 2016. Comprehensive Development Plan for the Russell Area, Kansas: 2016-2036. https://www.russellcity.org/documentcenter/view/303.

Rymer, M. and Ellsworth, W., 1990. The Coalinga, California, Earthquake of May 2, 1983. U.S. Geological Survey Professional Paper 1487. Retrieved from United States Government Printing Office website: http://pubs.usgs.gov/pp/1487/report.pdf.

Scheffler, A., 2012. Geochemical and Microbiological Characterization of the Arbuckle Saline Aquifer, a Potential CO_2 Storage Reservoir; Implications for Hydraulic Separation and Caprock Integrity. Graduate Degree Thesis of the University of Kansas.

Schwab, D., Bidgoli, T., and Taylor, M., 2017, Characterizing the Potential for Injection-Induced Fault Reactivation Through Subsurface Structural Mapping and Stress Field Analysis, Wellington Field, Sumner County, Kansas, Journal of Geophysical Research: Solid Earth 122(12), p. 10,132. https://doi.org/10.1002/2017JB014071.

Sloss, L.L., 1963, Sequences in the Cratonic Interior of North America: Geologic Society of America Bulletin, v. 74, p. 93-114. https://doi.org/10.1130/0016-7606(1963)74[93:SITCIO]2.0.CO;2.

Steeples, D.W., Brosius, L., 2024, Earthquakes, Kansas Geological Survey. https://kgs.ku.edu/earthquakes#:~:text=Earthquakes%20in%20Kansas,6.

USGS National Hydrography Dataset 2023, https://www.usgs.gov/national-hydrography/national-hydrography-dataset . The dataset is transitioning to become part of the USGS 3D Hydrography Program: https://www.usgs.gov/3dhp.

Watney, W. L., 1980, Cyclic sedimentation of the Lansing-Kansas City groups in northwestern Kansas and southwestern Nebraska: Kansas Geological Survey Bulletin, 220, 72. https://www.kgs.ku.edu/Publications/Bulletins/220/bull_220.pdf.

Watney, W. L., Franseen, E. K., Byrnes, A.P., and Nissen, S.E., 2008. Evaluating structural controls on the formation and properties of Carboniferous carbonate reservoirs in the northern Midcontinent, U.S.A., in J. Lukasik and J. A. Simo, eds., Controls on carbonate platform and reef development: SEPM Special Publication, 89, 21. https://doi.org/10.2110/pec.08.89.0125.

Whittemore, D.O, Macfarlane, P.A., and Wilson, B.B., 2014. Water Resources of the Dakota Aquifer in Kansas, Appendix. Bulletin 260, Kansas Geological Survey, Lawrence, Kansas. https://www.kgs.ku.edu/Publications/Bulletins/260/Bulletin_260_Dakota.pdf.

Zhang, D., Song, J., Mechanisms for Geological Carbon Sequestration, Procedia IUTAM 10 (0124) 319-327. https://doi.org/10.1016/j.piutam.2014.01.027.

Zhou, Q., Birkholzer, J.T., Tsang, C-F., and Rutqvist, J., 2008. A method of quick assessment of CO_2 storage capacity in closed and semi-closed saline formations. International Journal of Greenhouse Gas Control 2, 626-639. https://doi.org/10.1016/j.ijggc.2008.02.004.

Appendix A.I.1. Baseline Environmental Testing and Monitoring Data Review

APPENDIX A.I.1. BASELINE ENVIRONMENTAL TESTING AND MONITORING DATA REVIEW

RUSSELL CO_2 CAPTURE AND SEQUESTRATION

Table of Contents

List of Tables

List of Figures

A.I-1.1. Monitoring Overview

Drilling and installation of groundwater monitoring wells and vadose zone soil gas wells were conducted from September 12 to October 2, 2022. This was followed by quarterly sample events in October 2022, January 2023, April 2023, July 2023, October 2023, and January 2024. In addition to quarterly sampling, datalogger monitoring systems for groundwater and soil gas were installed in late 2022, underwent startup and optimization through February 2022, and initiated continuous measurements on February 28, 2023. The continuous measurements were processed by an automated datalogger that averaged values once per 12 hours.

The purpose of the baseline environmental testing and monitoring program (BETM) is to characterize geochemical conditions, spatial variability, and temporal (e.g., seasonal and more frequent) variability with the lowermost Underground Source of Drinking Water (USDW) and shallower environment. The following sections review data collected through early February 2023 (excluding January 2024 sampling data that are pending from the laboratory), sequencing from the lowermost USDW upwards. The results, detailed below, can be summarized as follows:

- General Observations/Comments
  - The Year 1 geochemical monitoring data collected from the Dakota Aquifer exhibited minimal temporal variation but did vary spatially, both concentration levels and primary constituents, across the project site and different monitoring stations.
  - Except for Monitoring Station 6 (SMW-6), the Year 1 geochemical monitoring data collected from the Water Table aquifer exhibited relatively little spatial or temporal variation.
  - The graphical and statistical methods of data analyses performed on these groundwater monitoring results will help geochemically characterize ("fingerprint") the groundwater quality data collected from each monitoring station and aquifer interval being monitored across the project site.
  - Furthermore, these manner of data analyses should improve the future ability to monitor for anomalous change detection potentially created from the subsurface migration of CO_2 into these monitored aquifer intervals.
- Dakota Formation groundwater (lowermost USDW)
  - Temperatures were steady over time and consistently approximately 15 ^{o}C across monitoring wells. Salinity was more variable between wells ranging from less than 0.5 parts per thousand to greater than 10 parts per thousand. The depths to groundwater at the majority of wells (DMW-2 was the exception) were demonstrably affected by groundwater sampling, sometimes resulting in multi-day periods of recharge.
  - The DMW-1 and DMW-4 groundwater are geochemically similar, with sodium and potassium as the dominant cations and chloride as dominant anion. The DMW-2 and SMW-3 groundwater have more even mixes of other cations and/or anions.

- Over time, the geochemistry of groundwater at any given well was relatively stable, indicating consistent conditions over time.

- Water Table aquifer
  - Temperatures were steady (approximately 15 ºC). Versus Dakota Formation groundwater, salinity was measured within a tighter range (2.34 to 4.35 parts per thousand as averages for the five wells). The depths to groundwater at all wells were demonstrably affected by groundwater sampling, sometimes resulting in multi-day periods of recharge.
  - The Water Table aquifer geochemistry was similar across monitoring wells. Sodium and potassium were the dominant cations and chloride was the dominant anion.
  - Over time, the geochemistry of groundwater was stable, with the exception of SMW-6. At that location, there was variability between sample events, including a switch from chloride as the dominant anion in October 2022, January 2023, and July 2023 to bicarbonate/carbonate as the dominant anion in April 2023.
- Soil gas CO_2
  - CO_2 concentrations were elevated above atmospheric levels at all stations and both depths (5 ft bgs and 10 ft bgs), indicating subsurface sources of CO_2.
  - Both 5 ft bgs and 10 ft bgs CO_2 concentrations exhibited increasing trends beginning approximately in April 2023. In addition to these general trends, the 5 ft bgs CO_2 concentrations varied on shorter time periods. The most extreme variation was at SVP-4, where multiple episodes of CO_2 concentration decreases to near atmospheric concentrations were followed by longer term elevated values.
  - Stable carbon isotopes in soil gas CO_2 were within an -11 to -21 ‰ range across measurement locations for all sample events.
- CO_2 effluxes
  - Mean CO_2 effluxes were similar in October 2022 and April 2023, with values in the 0.8 to 2.2 micromoles per square meter per second (μmol m^{-2} s^{-1}) range.
  - July 2023 mean CO_2 effluxes were relatively high across all stations, with values in the 5.9 to 11.3 μmol m^{-2} s^{-1} range.

A.I-1.2. Dakota Formation Groundwater

Four wells (DMW-1, DMW-2, SMW-3, and DMW-4) are screened within the Dakota Formation, which is the lowermost Underground Source of Drinking Water (USDW). Summary statistics for depth to water, salinity, and temperature through July 28, 2023 are provided in Table A.I-1.2-1. For each of the monitoring stations, the number of measurements was 698, corresponding to 349 days for the February 28, 2023 to February 12, 2024 timeframe. Time series for these dataloggers are provided in Figure A.I-1.2-1.Generally, temperatures at these wells were steady over the course of logging, with values near 14-15 ºC.

Table A.I-1.2-1. Summary Statistics for Conductivity / Depth / Temperature Loggers in Dakota Formation Groundwater Wells

		Dakota Formation Groundwater		
		Depth to Water	Salinity	Temperature
		ft-btoc	parts per thousand	°C
DMW-1	Number of Measurements	698	698	698
	Mean	181.12	11.19	15.19
	Median	180.71	10.38	15.19
	Standard Deviation	1.26	1.43	0.01
DMW-2	Number of Measurements	698	698	698
	Mean	176.12	0.50	14.82
	Median	176.10	0.49	14.82
	Standard Deviation	0.30	0.06	0.01
SMW-3	Number of Measurements	698	698	698
	Mean	64.78	0.42	13.77
	Median	64.86	0.42	13.77
	Standard Deviation	1.06	0.01	0.00
DMW-4	Number of Measurements	699	699	699
	Mean	171.02	3.65	14.96
	Median	170.98	3.75	14.97
	Standard Deviation	1.26	1.43	0.01

Notes:
ppm - parts per million
ft-btoc - feet below top of casing
ppt - parts per thousand
°C - degree Celsius
ft-bgs - feet below ground surface

Figure A.I-1.2-1. Time Series Plots for Conductivity / Depth / Temperature Loggers in Dakota Formation Groundwater Wells

DMW-1

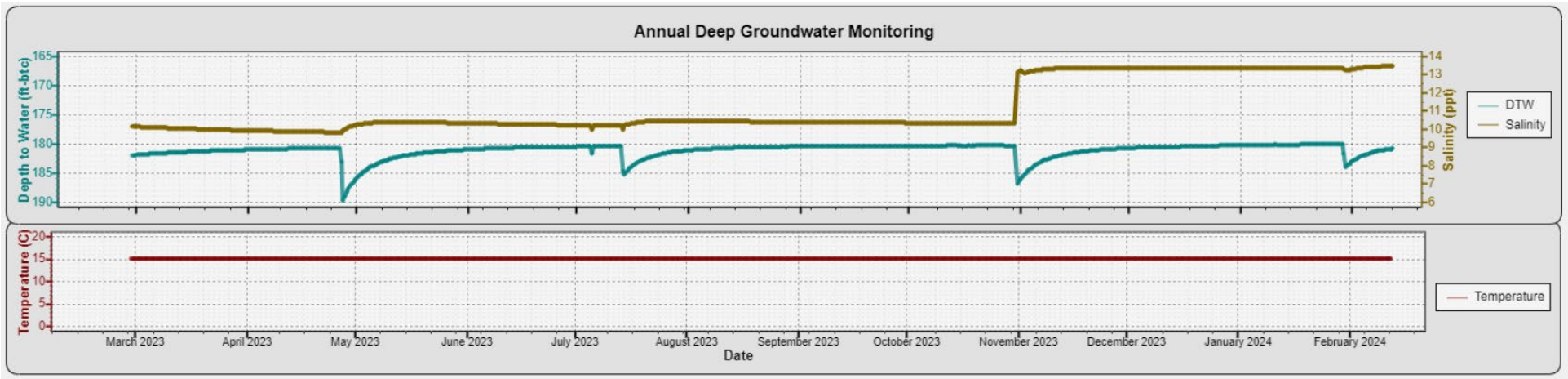

DMW-2

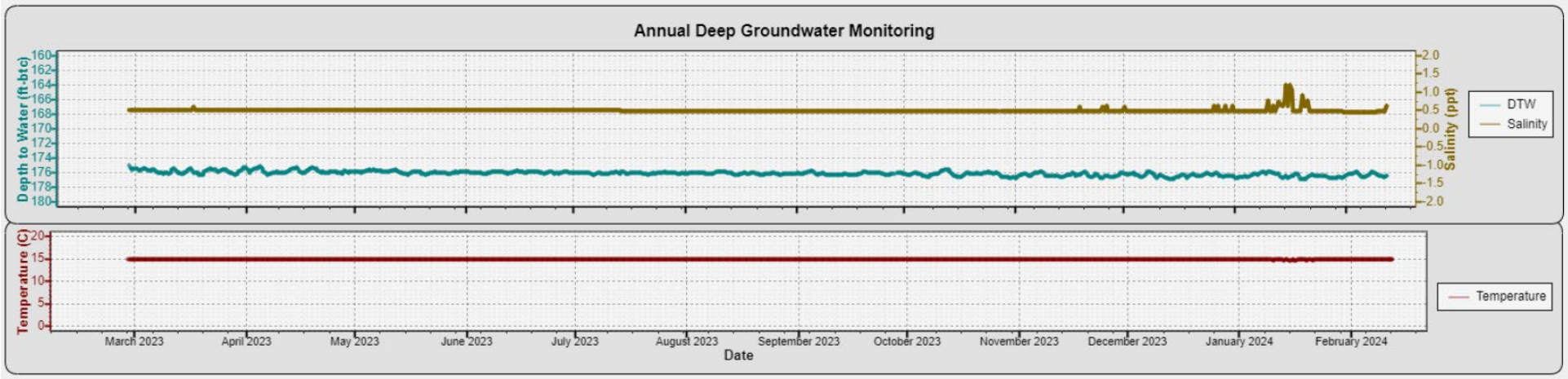

SMW-3

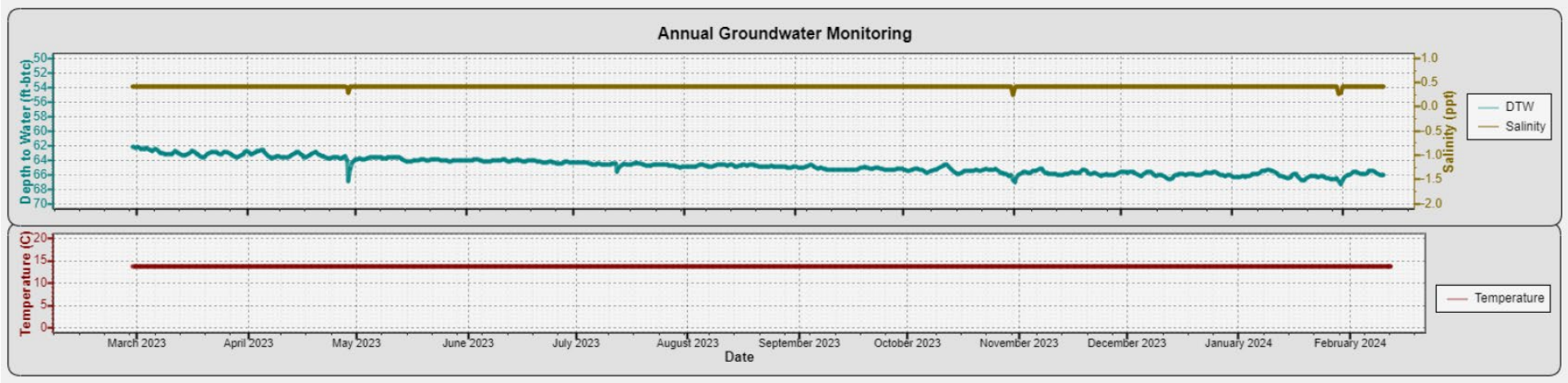
Annual Groundwater Monitoring
Depth to Water (ft-btc)
Salinity (ppt)
DTW
Salinity
Temperature (C)
Temperature
March 2023
April 2023
May 2023
June 2023
July 2023
August 2023
September 2023
October 2023
November 2023
December 2023
January 2024
February 2024
Date

DMW-4

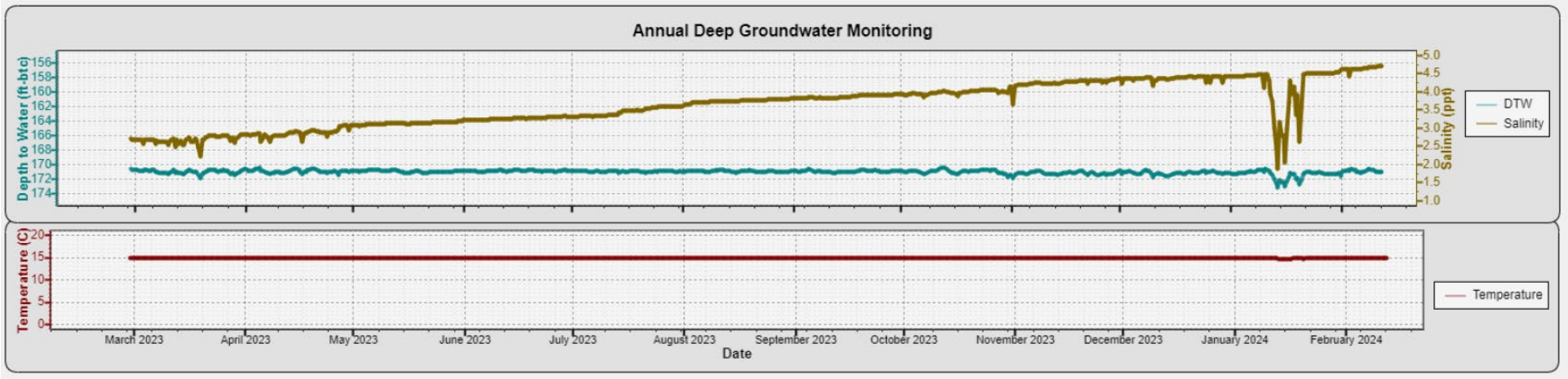
Annual Deep Groundwater Monitoring
Depth to Water (ft-btc)
Salinity (ppt)
DTW
Salinity
Temperature (C)
Temperature
March 2023
April 2023
May 2023
June 2023
July 2023
August 2023
September 2023
October 2023
November 2023
December 2023
January 2024
February 2024
Date

The mean depths to water were greater than 170 ft for all wells except SMW-3. This well has a lower ground surface elevation (1734.08 ft msl versus 1816.34 to 1832.83 ft msl) than the other wells, largely explaining the difference in depth to water. Converting to elevations, the water levels ranked from shallowest to deepest as SMW-3 (1,671.36 ft msl), DMW-4 (1,663.70 ft msl), DMW-1 (1643.69 ft msl), to DMW-2 (1642.29 ft msl). With SMW-3 in the center of the monitoring array and DMW-1 / DMW-4 at the edges, the data suggest a variable potentiometric surface for the Dakota Formation rather than a consistent broad flow direction.

Water depths showed greater temporal variation than groundwater temperatures. This was especially the case at wells DMW-1. There, sharp changes in water depths were likely associated with groundwater sampling. The sampling is conducted by low-flow methods, so the observed water depth changes are a potential indication of low aquifer transmissivities for the wells. Although the water depth at DMW-4 was not shown to have a significant change during groundwater sampling at the datalogger, field observations were that the well had a small water column that nearly dewatered. Thus, the aquifer transmissivity at this well is also inferred as low. In addition to the water depth changes associated with the groundwater sampling events, wells DMW-2 and SMW-3 showed a general decreasing trend over time.

Measured salinities varied between stations. Well DMW-1 had the highest mean value at 11.19 parts per thousand. The time series for salinity at this well appeared to respond to groundwater sampling as new water was pumped into the well. Well DMW-4 had the second-highest mean salinity at 3.65 parts per thousand. The salinity data fluctuates at DMW-4 to a greater extent than observed in the other deep monitoring wells following in mid-January 2024. The salinity variation at DMW-4 might be explained by some manner of interference between the probe sensors and data logger conductivity causing anomalous readings for a short period. The probe reading variations appear to have self-corrected itself after a short period. Nonetheless, a general increasing trend in salinity over time was observed at DMW-4. Wells DMW-2 and SMW-3 mean salinities were measured at or less than 0.50 parts per thousand, and the time series were generally steady over the course of logging.

For the deep groundwater (Dakota Formation/Aquifer) monitoring well sampling program, collected through January 2024, the summary statistics are provided in Table A.I-1.2-2, and the summary analytical results statistics are provided in Table A.I-1.2-3.

Table A.I-1.2-2. Summary of Deep Groundwater (Dakota FM) Monitoring Well Results

Analyte	Units	Min	Max	Geomean	Average	Non Detects	Detects	# of Samples
Bromide	mg/L	0.25	1.1	0.5	0.5	25	4	29
Chloride	mg/L	8.5	9,870	409	2,648	0	29	29
Fluoride	mg/L	0.1	2	0.5	0.7	8	21	29
Nitrate as N	mg/L	0.05	0.56	0.1	0.1	24	5	29
Sulfate	mg/L	79.8	1,660	293	534	0	29	29
Calcium	ug/L	12,500	123,000	44,217	59,086	0	29	29
Iron	ug/L	67	6,320	769	1,408	0	29	29
Magnesium	ug/L	3,950	147,000	22,264	48,533	0	29	29
Potassium	ug/L	7,280	58,000	15,917	20,904	0	29	29
Silicon	ug/L	5,320	23,600	7,205	7,592	0	29	29
Sodium	ug/L	93,100	4,960,000	636,833	1,705,693	0	29	29
Aluminum	ug/L	25	6,110	133	516	16	13	29
Antimony	ug/L	0.5	10	1.3	1.9	20	9	29
Arsenic	ug/L	0.5	5.7	2.0	2.4	14	15	29
Barium	ug/L	14	255	40.9	57.3	0	29	29
Cadmium	ug/L	0.25	1.25	0.4	0.5	29	0	29
Chromium	ug/L	0.5	11.2	1.3	2.2	20	9	29
Copper	ug/L	0.5	6.6	1.2	1.7	22	7	29
Lead	ug/L	0.5	10	1.0	1.5	27	2	29
Manganese	ug/L	3.1	197	49.4	81.9	0	29	29
Selenium	ug/L	0.5	2.5	0.8	1.1	28	1	29
Thallium	ug/L	0.5	10	0.8	1.3	29	0	29
Alkalinity, Total as CaCO3	mg/L	188	835	435	484	0	29	29
Alkalinity,Bicarbonate (CaCO3)	mg/L	246	835	453	502	0	25	25
Alkalinity,Carbonate (CaCO3)	mg/L	10	10	10.0	10.0	29	0	29
Total Dissolved Solids	mg/L	597	20,500	2,299	5,248	0	29	29

Table A.I-1.2-3. Deep Groundwater (Dakota FM) Monitoring Well Analytical Results

		FALL 2022 SAMPLING EVENT				WINTER 2023 SAMPLING EVENT					SPRING 2023 SAMPLING EVENT				
		SMW-3	DMW-1	DMW-2	DMW-4	SMW-3	DMW-1	DMW-2	DMW-4	Duplicate (DMW-1)	SMW-3	DMW-1	DMW-2	DMW-4	Duplicate (DMW-2)
Analyte	Units	Data Results (ND=0.5RL)	Data Results (ND=0.5RL)	Data Results (ND=0.5RL)	Data Results (ND=0.5RL)	Data Results (ND=0.5RL)	Data Results (ND=0.5RL)	Data Results (ND=0.5RL)	Data Results (ND=0.5RL)	Data Results (ND=0.5RL)	Data Results (ND=0.5RL)	Data Results (ND=0.5RL)	Data Results (ND=0.5RL)	Data Results (ND=0.5RL)	Data Results (ND=0.5RL)
Bromide	mg/L	0.5	0.5	0.5	0.5	0.5	0.5	0.5	0.5	0.5	0.5	0.5	0.5	0.5	0.5
Chloride	mg/L	10	5310	141	904	8.5	7430	131	1800	7050	9.2	6140	122	1490	126
Fluoride	mg/L	0.61	0.1	1.3	0.59	0.37	0.1	1	0.1	0.1	0.36	0.1	1.1	1	1.1
Nitrate as N	mg/L	0.05	0.05	0.05	0.05	0.05	0.05	0.05	0.05	0.05	0.48	0.05	0.05	0.05	0.05
Sulfate	mg/L	170	1190	138	225	181	1370	116	163	1330	184	1660	102	238	102
Calcium	ug/L	61,900	92,500	12,500	36,200	58,400	110,000	13,100	23,400	108,000	67,100	122,000	14,000	31,200	13,900
Iron	ug/L	385	1,140	404	6,320	520	974	132	311	956	4,500	1,120	142	1,410	133
Magnesium	ug/L	20,900	85,300	3,950	10,700	20,100	121,000	3,970	10,000	120,000	22,100	139,000	4,360	13,700	4,310
Potassium	ug/L	9,520	37,500	7,660	13,500	8,790	41,700	7,280	11,500	41,300	9,750	47,800	7,830	14,200	7,890
Silicon	ug/L	6,380	7,630	5,320	23,600	5,870	6,680	5,730	6,360	6,450	10,800	7,510	6,170	9,270	6,170
Sodium	ug/L	104,000	3,200,000	202,000	740,000	95,300	4,960,000	191,000	825,000	4,610,000	105,000	4,520,000	208,000	1,220,000	207,000
Aluminum	ug/L	111	910	716	6,110	102	75	92	82	75	2,240	125	25	1,300	25
Antimony	ug/L	0.5	2.4	1.4	0.5	0.5	1.5	3.9	0.5	1.5	0.5	2.5	3.8	0.5	4
Arsenic	ug/L	0.5	2.4	5.5	4.1	0.5	1.5	3.7	4	1.5	3.3	2.5	3.7	1.6	3.7
Barium	ug/L	25.2	97	15.4	51.1	20.9	107	15.3	35.5	107	36.2	107	15.2	45.5	15
Cadmium	ug/L	0.25	0.5	0.25	0.25	0.25	0.75	0.25	0.25	0.75	0.25	1.25	0.25	0.25	0.25
Chromium	ug/L	0.5	2.1	1.1	9.4	0.5	1.5	0.5	6.4	1.5	5.5	2.5	0.5	3.5	0.5
Copper	ug/L	0.5	2.8	0.5	6.6	0.5	1.5	1.3	0.5	1.5	3.6	2.5	0.5	3.7	0.5
Lead	ug/L	0.5	1	0.5	4	0.5	1.5	0.5	0.5	1.5	2.6	2.5	0.5	1	0.5
Manganese	ug/L	41.9	77.8	11.5	154	31.1	138	12.3	85.2	138	67.7	177	14.7	138	14.8
Selenium	ug/L	0.5	1	0.5	0.5	0.5	1.5	0.5	0.5	1.5	0.5	2.5	0.5	0.5	0.5
Thallium	ug/L	0.5	1	0.5	0.5	0.5	1.5	0.5	0.5	1.5	0.5	2.5	0.5	1	0.5
Alkalinity, Total as CaCO3	mg/L	303	596	188	386	302	774	246	476	780	302	819	282	528	280
Alkalinity,Bicarbonate (CaCO3)	mg/L	NA	NA	NA	NA	302	774	246	476	780	302	819	282	528	280
Alkalinity,Carbonate (CaCO3)	mg/L	10	10	10	10	10	10	10	10	10	10	10	10	10	10
Total Dissolved Solids	mg/L	628	3,900	619	2,310	612	14,400	610	3,360	15,600	651	11,900	634	4,210	648

		SUMMER 2023 SAMPLING EVENT					FALL 2023 SAMPLING EVENT					WINTER 2024 SAMPLING EVENT				
		SMW-3	DMW-1	DMW-2	DMW-4	Duplicate (DMW-1)	SMW-3	DMW-1	DMW-2	DMW-4	Duplicate (DMW-2)	SMW-3	DMW-1	DMW-2	DMW-4	Duplicate (DMW-1)
Analyte	Units	Data Results (ND=0.5RL)	Data Results (ND=0.5RL)	Data Results (ND=0.5RL)	Data Results (ND=0.5RL)	Data Results (ND=0.5RL)	Data Results (ND=0.5RL)	Data Results (ND=0.5RL)	Data Results (ND=0.5RL)	Data Results (ND=0.5RL)	Data Results (ND=0.5RL)	Data Results (ND=0.5RL)	Data Results (ND=0.5RL)	Data Results (ND=0.5RL)	Data Results (ND=0.5RL)	Data Results (ND=0.5RL)
Bromide	mg/L	0.25	1.1	0.25	0.25	1.1	0.25	0.89	0.25	0.51	0.25	0.5	0.5	0.5	0.5	0.5
Chloride	mg/L	9.1	7360	90.8	1530	6960	9.2	7020	74.1	1820	73	9.7	8640	67.1	2600	9870
Fluoride	mg/L	0.62	0.58	1.4	2	0.53	0.8	0.45	1.5	1.9	1.4	0.37	0.1	0.71	0.1	0.1
Nitrate as N	mg/L	0.56	0.05	0.2	0.05	0.05	0.55	0.05	0.05	0.05	0.05	0.55	0.05	0.05	0.05	0.05
Sulfate	mg/L	176	1290	89.3	158	1290	175	1320	88.2	199	87.8	190	1410	79.8	238	1530
Calcium	ug/L	61,000	112,000	14,000	30,500	116,000	64,700	117,000	16,300	32,700	16,800	64,500	123,000	22,800	39,000	119,000
Iron	ug/L	944	1,560	197	877	1,790	125	3,080	490	1,770	474	67	2,630	1,070	4,760	2,560
Magnesium	ug/L	21,200	131,000	4,080	12,300	134,000	22,100	135,000	4,990	18,300	5,140	21,900	147,000	6,450	22,600	142,000
Potassium	ug/L	8,910	40,700	7,590	12,600	42,000	10,100	58,000	8,840	21,600	8,860	9,320	42,800	8,880	17,100	42,700
Silicon	ug/L	6,500	7,480	5,860	7,300	7,350	6,090	8,560	6,240	11,000	6,410	5,670	7,040	6,720	7,190	6,830
Sodium	ug/L	93,100	4,650,000	195,000	887,000	4,710,000	105,000	4,420,000	179,000	1,390,000	181,000	98,700	4,600,000	169,000	1,790,000	4,810,000
Aluminum	ug/L	879	125	25	249	125	25	376	25	25	25	25	125	25	792	125
Antimony	ug/L	0.5	2.5	2.3	0.5	2.5	0.5	10	1.6	2.1	1.6	0.5	2.5	0.5	0.5	2.5
Arsenic	ug/L	0.5	2.5	2.5	1.1	2.5	0.5	2.5	3.2	5.7	2.9	0.5	2.5	1.8	1	2.5
Barium	ug/L	24.1	101	14	43.8	102	23.3	105	18.3	255	19	21.2	89.3	24.2	44.5	83.7
Cadmium	ug/L	0.25	1.25	0.25	0.25	1.25	0.25	1.25	0.25	0.25	0.25	0.25	1.25	0.25	0.5	1.25
Chromium	ug/L	1.7	11.2	0.5	1.7	2.5	0.5	2.5	0.5	0.5	0.5	0.5	2.5	0.5	1	2.5
Copper	ug/L	1.1	2.5	0.5	4.7	2.5	0.5	2.5	0.5	0.5	0.5	0.5	2.5	0.5	1	2.5
Lead	ug/L	0.5	2.5	0.5	0.5	2.5	0.5	10	0.5	0.5	0.5	0.5	2.5	0.5	1	2.5
Manganese	ug/L	19.8	163	18.2	113	164	7.7	151	22.1	31.6	22.3	3.1	171	32.2	197	158
Selenium	ug/L	0.5	2.5	0.5	0.5	2.5	0.5	2.5	0.5	1.9	0.5	0.5	2.5	0.5	1	2.5
Thallium	ug/L	0.5	2.5	0.5	0.5	2.5	0.5	10	0.5	0.5	0.5	0.5	2.5	0.5	1	2.5
Alkalinity, Total as CaCO3	mg/L	291	806	298	549	814	294	686	260	518	316	291	834	333	637	835
Alkalinity,Bicarbonate (CaCO3)	mg/L	291	806	298	549	814	294	686	260	518	316	291	834	333	637	835
Alkalinity,Carbonate (CaCO3)	mg/L	10	10	10	10	10	10	10	10	10	10	10	10	10	10	10
Total Dissolved Solids	mg/L	622	15,600	620	3,630	20,500	611	13,400	602	4,350	597	928	13,000	640	4,020	13,000

Notes:

The above data are summarized directly from laboratory reports and may not reflect any edits/flags added throught the data validation process.

NA - Not analyzed/reported

Groundwater geochemistry sampling results are summarized in Figure A.I-1.2-2 as a Piper diagram for the October 2023 sample event.

Figure A.I-1.2-2. Piper Diagram of Dakota Formation Groundwater Samples Collected in October 2023

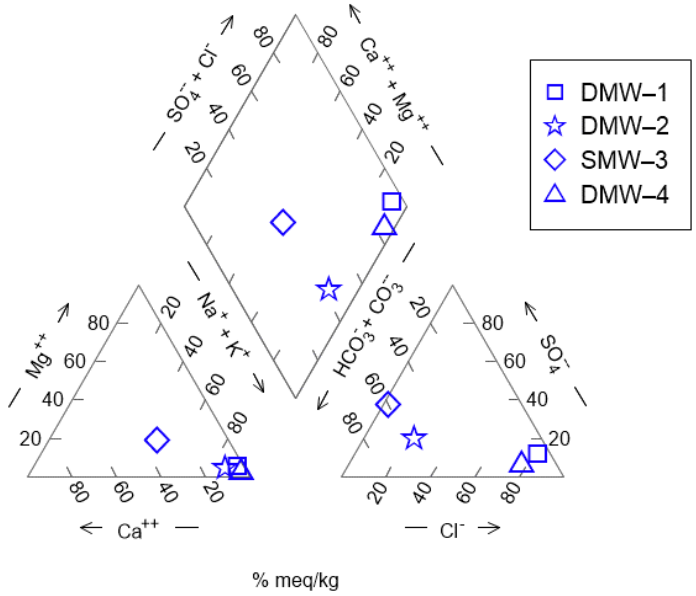

DMW-1 and DMW-4 clustered most closely together with high (>80%) sodium and potassium as the dominant cations, and high (>80%) chloride as the dominant anion. Well DMW-2 had a similar dominant cation composition (i.e., sodium and potassium), but the anions were a mix of bicarbonate/carbonate (near 60%), chloride (near 20%), and sulfate (near 20%). Well SMW-3 had a mix of both dominant cations (all three components 15% to 60%) and dominant anions (bicarbonate/carbonate near 60%, sulfate near 40%). Overall, the Piper diagram indicates spatial variability in groundwater geochemistry driven by DMW-2 and SMW-3.

Time series for groundwater geochemistry are presented in Figure A.I-1.2-3 with Stiff diagrams. Each of the data plots indicate stability in dominant cations and anions over the first five quarters of groundwater sampling. The results indicate spatial variability but minimal temporal variability.

Figure A.I-1.2-3. Stiff Diagrams of Dakota Formation Groundwater Samples

Note: Varied concentration scales to account for different dissolved solids contents

DMW-1

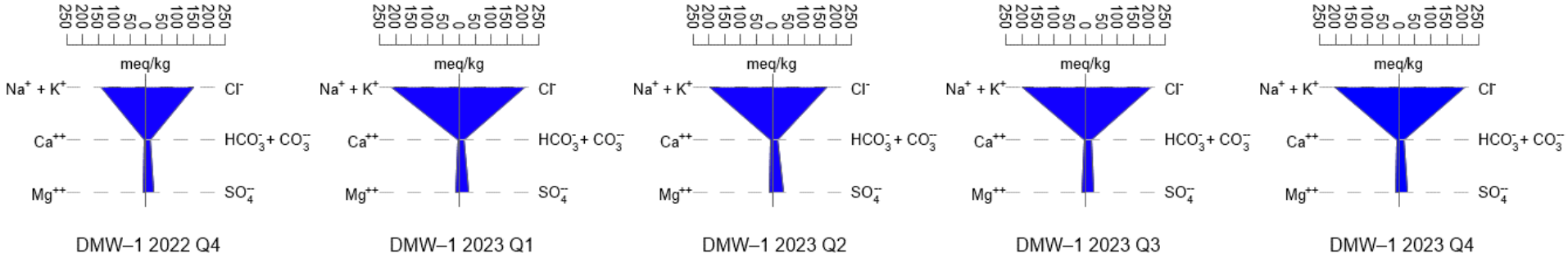

DMW-2

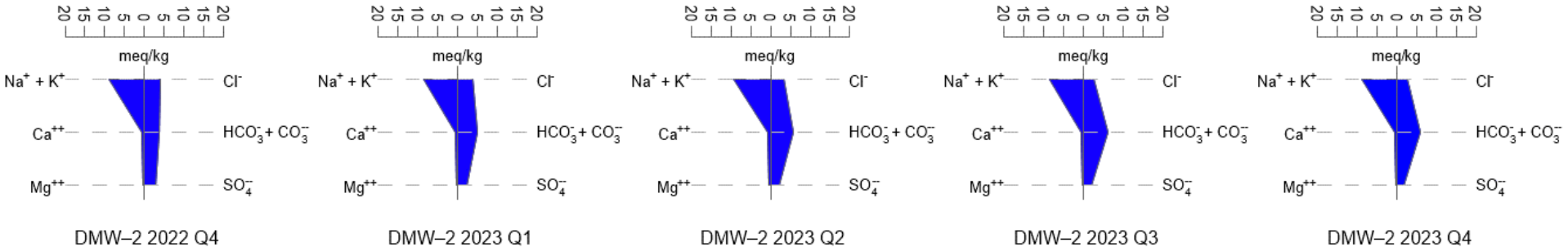

SMW-3

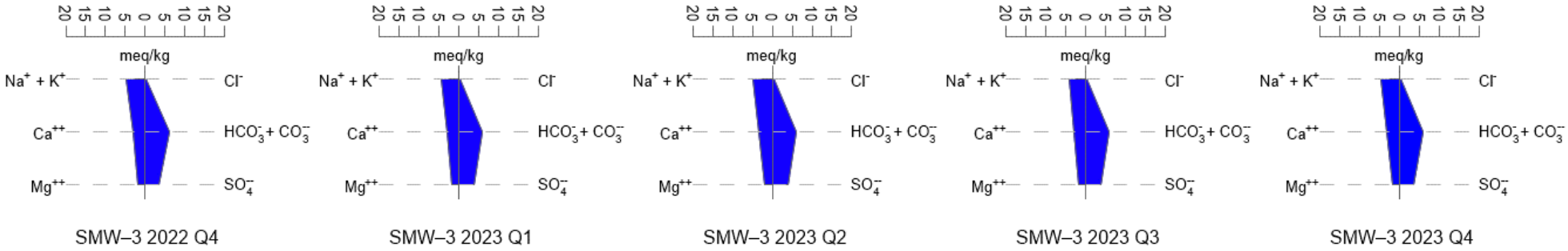

SMW–3 2022 Q4 | SMW–3 2023 Q1 | SMW–3 2023 Q2 | SMW–3 2023 Q3 | SMW–3 2023 Q4

DMW-4

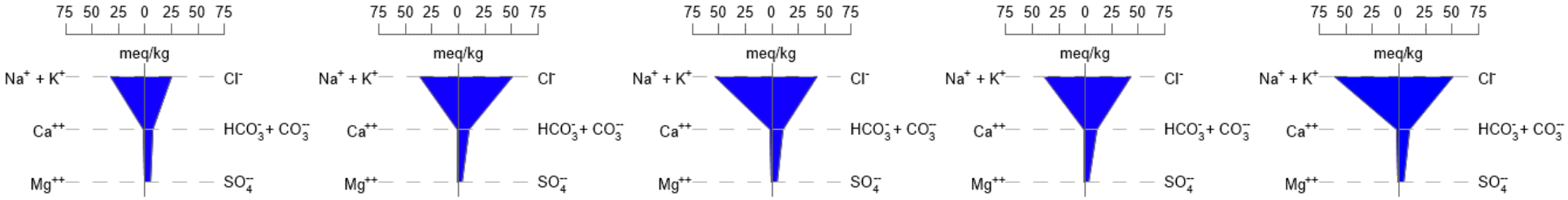

DMW–4 2022 Q4 | DMW–4 2023 Q1 | DMW–4 2023 Q2 | DMW–4 2023 Q3 | DMW–4 2023 Q4

A.I-1.3. Water Table Aquifer

Five wells (SMW-1, SMW-2, SMW-4, SMW-5, and SMW-6) are screened within the Water Table aquifer, which is the shallowest observed groundwater. Summary statistics for depth to water, salinity, and temperature through February 12, 2024 are provided in Table A.I-1.3-1.

Table A.I-1.3-1. Summary Statistics for Conductivity / Depth / Temperature Loggers in Water Table Aquifer Groundwater Wells

		Water Table Aquifer Groundwater		
		Depth to Water	Salinity	Temperature
		ft-btoc	parts per thousand	°C
SMW-1	Number of Measurements	662	662	662
	Mean	73.67	4.59	14.05
	Median	73.83	4.67	14.05
	Standard Deviation	3.90	0.23	0.02
SMW-2	Number of Measurements	699	699	699
	Mean	79.08	3.33	14.06
	Median	79.00	3.41	14.06
	Standard Deviation	1.24	0.49	0.01
SMW-4	Number of Measurements	411	411	411
	Mean	102.60	2.48	14.28
	Median	102.92	2.50	14.28
	Standard Deviation	0.91	0.16	0.01
SMW-5	Number of Measurements	699	699	699
	Mean	82.99	3.10	14.37
	Median	82.93	3.19	14.37
	Standard Deviation	2.26	0.44	0.04
SMW-6	Number of Measurements	657	657	657
	Mean	84.87	3.91	14.34
	Median	85.30	3.96	14.35
	Standard Deviation	1.69	0.28	0.01

Notes:
ppm - parts per million
ft-btoc - feet below top of casing
ppt - parts per thousand
°C - degree Celsius
ft-bgs - feet below ground surface

For three of the monitoring stations (SMW-2, SMW-5, and SMW-6), the number of measurements was greater than 650, corresponding to at least 325 days for the data logging timeframe. The SMW-4 downhole probe was observed to be higher than the water table (the well has a narrow water column), such that early measurements were deemed non-representative of groundwater conditions. This resulted in 411 representative measurements for this location. Time series for the dataloggers are provided in Figure A.I-1.3-1.

Figure A.I-1.3-1. Time Series Logs for Water Table Aquifer Groundwater Wells

SMW-1

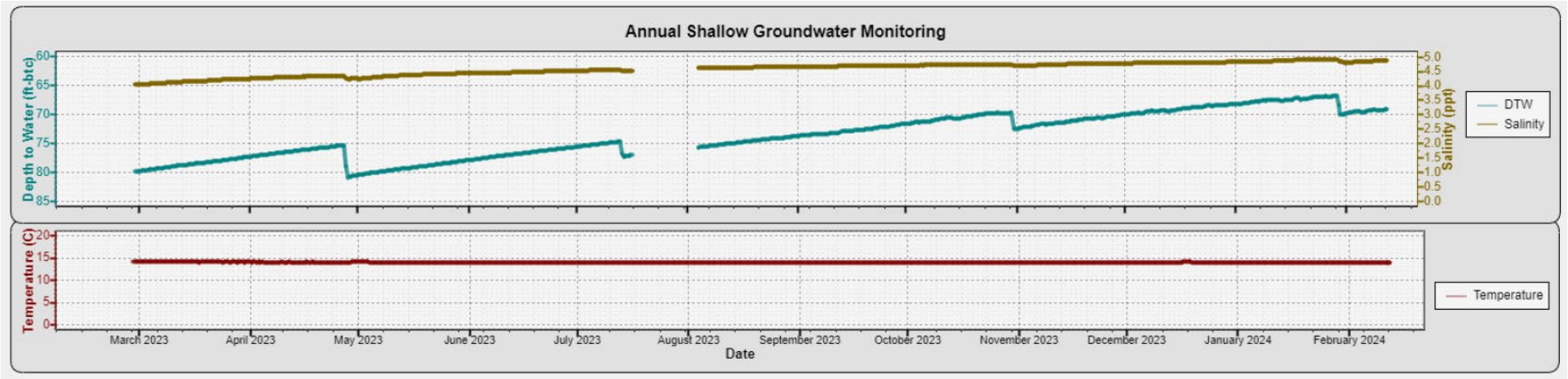

SMW-2

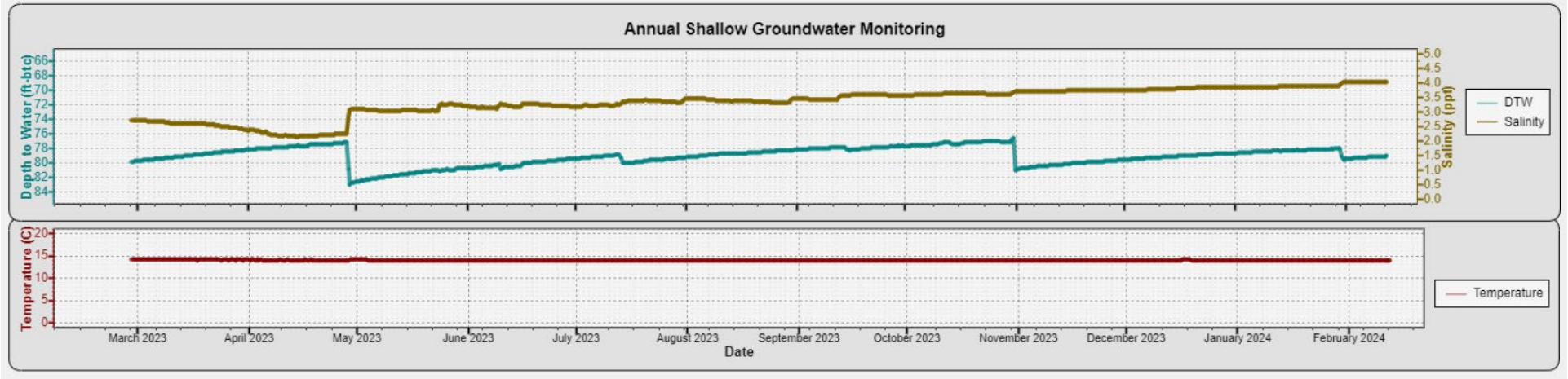

SMW-4

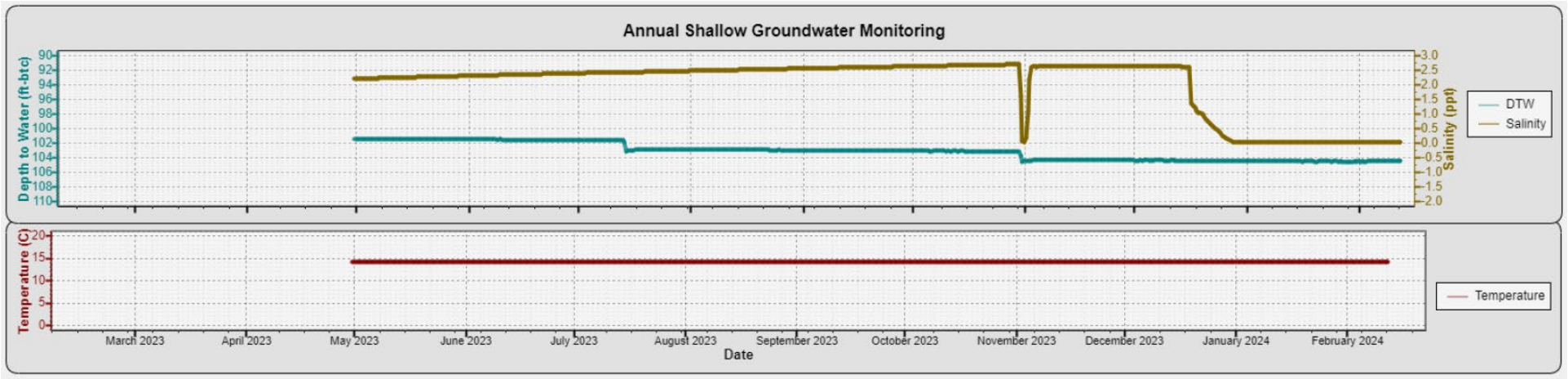
Annual Shallow Groundwater Monitoring
Depth to Water (ft-btc)
Salinity (ppt)
DTW
Salinity
Temperature (C)
Temperature
March 2023
April 2023
May 2023
June 2023
July 2023
August 2023
September 2023
October 2023
November 2023
December 2023
January 2024
February 2024
Date

SMW-5

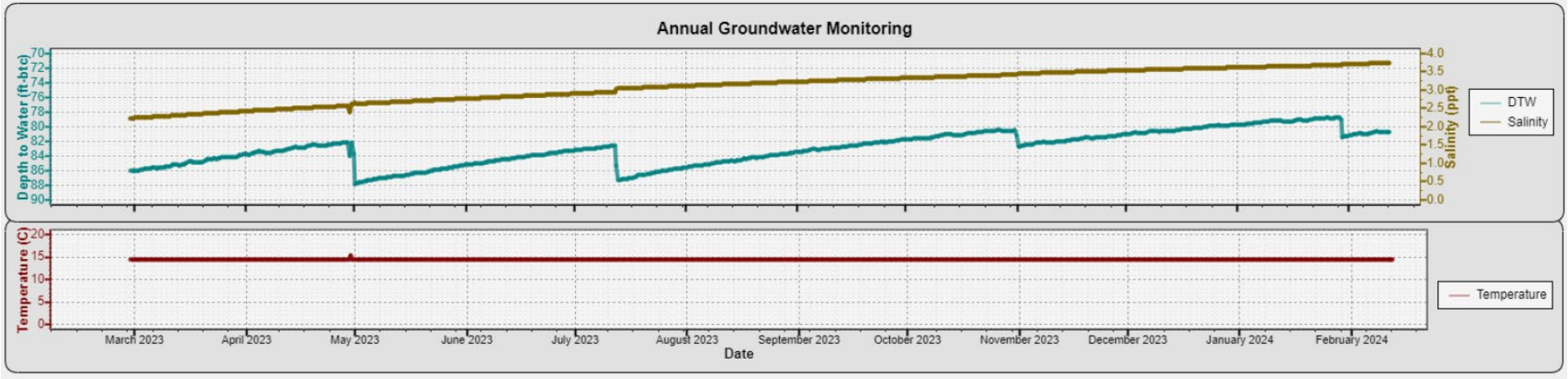
Annual Groundwater Monitoring
Depth to Water (ft-btc)
Salinity (ppt)
DTW
Salinity
Temperature (C)
Temperature
March 2023
April 2023
May 2023
June 2023
July 2023
August 2023
September 2023
October 2023
November 2023
December 2023
January 2024
February 2024
Date

SMW-6

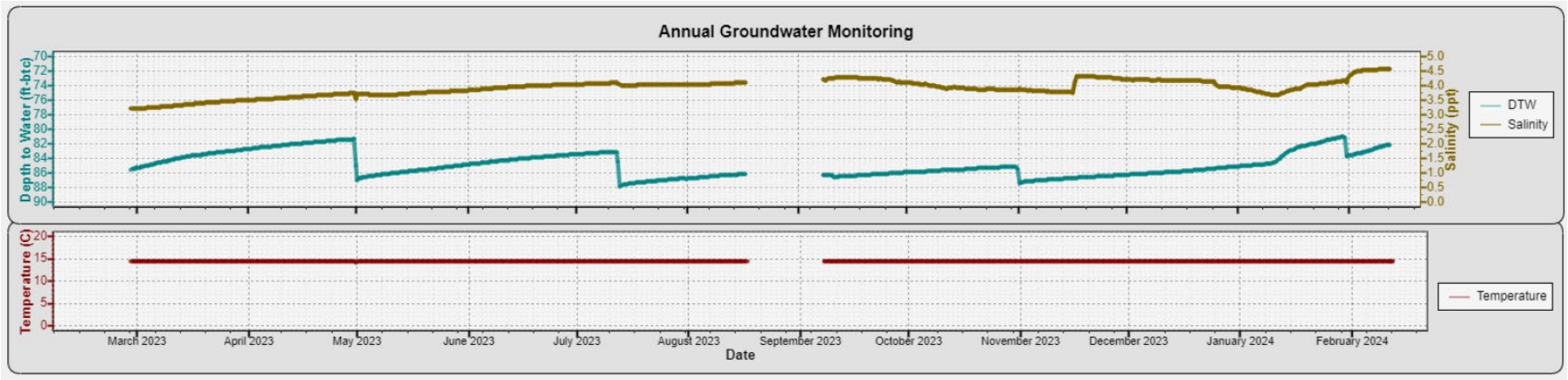
Annual Groundwater Monitoring
Depth to Water (ft-btc)
70
72
74
76
78
80
82
84
86
88
90
Salinity (ppt)
5.0
4.5
4.0
3.5
3.0
2.5
2.0
1.5
1.0
0.5
0.0
DTW
Salinity
Temperature (C)
20
15
10
5
0
Temperature
March 2023
April 2023
May 2023
June 2023
July 2023
August 2023
September 2023
October 2023
November 2023
December 2023
January 2024
February 2024
Date

Similar to the Dakota Formation groundwater, temperatures at these wells were steady over the course of logging, with temperatures in the 14.0 to 14.5ºC.

The mean depths to water ranged from 73.67 ft bgs to 102.60 ft bgs. Converting to elevations, the average depths to water rank from shallowest to deepest as SMW-1 (1751.28 ft msl), SMW-5 (1740.20 ft msl), SMW-6 (1739.83 ft msl), SMW-2 (1739.59 ft msl), to SMW-4 (1732.4 ft msl). This suggests a ridge of elevated water elevation along the SMW-1 to SMW-2 corridor, with lower elevations on either side (i.e., SMW-2 and SMW-4).

All five monitoring wells had probes that reported sharp changes in water depths that coincided with groundwater sampling events. The sampling is conducted by low-flow methods, so the observed water depth changes are a potential indication of low aquifer transmissivities for the wells.

Measured salinities were similar across stations ranging from a mean of 2.48 parts per thousand at SMW-4 to 4.59 parts per thousand at SMW-1. While some wells' salinity values showed responses to groundwater sampling, overall increasing trends over time could still be discerned at all wells except SMW-2. In addition, the salinity at SMW-4 did not rebound following a decrease in mid-December 2023.

For the shallow groundwater (water-table) monitoring well sampling program, collected through January 2024, the summary statistics are provided in Table A.I-1.3-2, and the summary analytical results statistics are provided in Table A.I-1.3-3.

Table A.I-1.3-2. Summary of Shallow Groundwater (Water-Table) Monitoring Well Results

Analyte	Units	Min	Max	Geomean	Average	Non Detects	Detects	# of Samples
Bromide	mg/L	0.5	1.1	0.6	0.6	24	12	36
Chloride	mg/L	9.2	2190	949	1203	0	36	36
Fluoride	mg/L	0.1	4.7	0.3	0.6	15	21	36
Nitrate as N	mg/L	0.05	4	0.1	0.3	27	9	36
Sulfate	mg/L	195	1880	802	936	0	36	36
Calcium	ug/L	23,000	190,000	79,175	94,292	0	36	36
Iron	ug/L	131	10,700	979	1,953	0	36	36
Magnesium	ug/L	8,480	86,400	31,938	41,189	0	36	36
Potassium	ug/L	11,000	30,100	17,324	18,125	0	36	36
Silicon	ug/L	4,450	51,800	8,174	9,205	0	36	36
Sodium	ug/L	351,000	1,810,000	1,016,928	1,115,778	0	36	36
Aluminum	ug/L	25	20,700	123	870	14	22	36
Antimony	ug/L	0.5	5.3	1.2	1.6	25	11	36
Arsenic	ug/L	1	13.2	3.3	4.5	8	28	36
Barium	ug/L	15.8	70.5	39.5	41.5	0	36	36
Cadmium	ug/L	0.25	1.25	0.4	0.4	35	1	36
Chromium	ug/L	0.5	23	1.8	3.4	15	21	36
Copper	ug/L	0.5	9.1	1.0	1.5	27	9	36
Lead	ug/L	0.5	2.8	0.8	1.0	35	1	36
Manganese	ug/L	7.9	127	48.5	59.4	0	36	36
Selenium	ug/L	0.5	2.5	0.8	0.9	33	3	36
Thallium	ug/L	0.5	2.5	0.8	0.9	36	0	36
Alkalinity, Total as CaCO3	mg/L	244	798	476	498	0	36	36
Alkalinity,Bicarbonate (CaCO3)	mg/L	361	798	519	535	0	30	30
Alkalinity,Carbonate (CaCO3)	mg/L	10	10	10.0	10.0	36	0	36
Total Dissolved Solids	mg/L	426	7,660	3,155	3,758	0	36	36

Table A.I-1.3-3. Shallow Groundwater (Water-Table) Monitoring Well Analytical Results

		FALL 2022 SAMPLING EVENT						WINTER 2023 SAMPLING EVENT						SPRING 2023 SAMPLING EVENT					
		SMW-1	SMW-2	SMW-4	SMW-5	SMW-6	Duplicate (SMW-4)	SMW-1	SMW-2	SMW-4	SMW-5	SMW-6	Duplicate (SMW-4)	SMW-1	SMW-2	SMW-4	SMW-5	SMW-6	Duplicate (SMW-4)
Analyte	Units	Data Results (ND=0.5RL)	Data Results (ND=0.5RL)	Data Results (ND=0.5RL)	Data Results (ND=0.5RL)	Data Results (ND=0.5RL)	Data Results (ND=0.5RL)	Data Results (ND=0.5RL)	Data Results (ND=0.5RL)	Data Results (ND=0.5RL)	Data Results (ND=0.5RL)	Data Results (ND=0.5RL)	Data Results (ND=0.5RL)	Data Results (ND=0.5RL)	Data Results (ND=0.5RL)	Data Results (ND=0.5RL)	Data Results (ND=0.5RL)	Data Results (ND=0.5RL)	Data Results (ND=0.5RL)
Bromide	mg/L	0.5	0.5	0.5	0.5	0.5	0.5	0.5	0.5	0.5	0.5	0.5	0.5	0.5	0.5	0.5	0.5	0.5	0.5
Chloride	mg/L	1060	317	421	328	470	414	1930	960	645	847	1780	591	1730	890	938	1200	9.2	787
Fluoride	mg/L	0.1	0.1	0.79	0.68	0.48	0.78	0.1	0.1	0.1	0.1	4.7	0.1	0.1	0.1	0.8	0.27	0.38	0.81
Nitrate as N	mg/L	0.05	0.05	0.05	0.05	0.05	0.05	0.21	0.05	0.05	0.05	0.05	0.05	1.2	0.05	0.05	0.05	0.05	0.05
Sulfate	mg/L	797	436	404	198	444	442	1290	1070	560	315	1530	541	1520	1290	759	465	195	637
Calcium	ug/L	109,000	32,100	27,800	91,200	50,400	23,000	148,000	55,600	39,200	46,200	73,900	38,800	190,000	77,700	56,800	58,100	146,000	53,500
Iron	ug/L	438	229	339	4,490	231	131	681	1,450	152	894	1,350	142	154	1,610	1,530	966	1,540	1,510
Magnesium	ug/L	39,200	11,000	8,920	14,300	17,100	8,480	59,500	22,600	12,400	16,100	30,800	12,100	82,200	38,000	15,900	25,100	53,300	15,900
Potassium	ug/L	18,200	11,300	11,300	12,900	13,300	11,000	22,000	13,700	11,600	12,800	16,900	11,400	26,200	17,800	13,200	14,900	18,400	13,600
Silicon	ug/L	7,480	6,220	5,510	51,800	8,640	4,450	7,620	6,910	5,690	12,600	8,310	5,630	7,810	8,550	7,080	11,500	15,200	6,770
Sodium	ug/L	810,000	473,000	447,000	351,000	562,000	414,000	1,450,000	819,000	609,000	613,000	888,000	596,000	1,430,000	1,220,000	855,000	963,000	1,310,000	836,000
Aluminum	ug/L	51.8	314	527	20700	371	316	95.5	25	53.1	3240	65.1	57.4	25	25	176	1900	75	94.4
Antimony	ug/L	3.5	2.9	4.8	3	4.3	5.3	1.6	0.5	0.5	2.5	1.1	0.5	1.8	0.5	0.5	0.5	1.5	0.5
Arsenic	ug/L	5.3	10.8	10.4	13.2	9.5	10.7	5.6	6	8.6	5.6	11.5	8.5	1.3	2.5	3.9	3.9	7.4	4
Barium	ug/L	62.7	26.6	16.5	44	41	15.8	70.5	53.4	26.5	40.6	59.8	26.9	58.4	52.6	31.8	48.5	54.5	30.8
Cadmium	ug/L	0.25	0.25	0.25	0.65	0.25	0.25	0.25	0.25	0.25	1.25	0.25	0.25	0.25	0.25	0.25	0.25	0.75	0.25
Chromium	ug/L	0.5	2	1.1	23	2.1	0.5	3.6	1.8	0.5	2.5	6.5	0.5	4.8	1.8	2.2	1.7	3.9	0.5
Copper	ug/L	0.5	1.2	0.5	9.1	0.5	0.5	0.5	0.5	0.5	2.5	2.7	0.5	0.5	0.5	0.5	1.7	3.6	0.5
Lead	ug/L	0.5	0.5	0.5	2.8	0.5	0.5	0.5	0.5	0.5	2.5	0.5	0.5	1	0.5	0.5	1	1.5	0.5
Manganese	ug/L	61.2	23.3	9.4	41.8	28.3	7.9	97.1	105	16.1	27.3	71.4	16	103	127	30.2	43.2	94.3	27.3
Selenium	ug/L	1.8	0.5	0.5	2.1	0.5	0.5	0.5	0.5	0.5	2.5	0.5	0.5	1	0.5	0.5	0.5	1.5	0.5
Thallium	ug/L	0.5	0.5	0.5	0.5	0.5	0.5	0.5	0.5	0.5	2.5	0.5	0.5	1	0.5	0.5	1	1.5	0.5
Alkalinity, Total as CaCO3	mg/L	338	346	244	351	372	244	425	594	398	361	596	395	452	693	483	417	681	485
Alkalinity,Bicarbonate (CaCO3)	mg/L	NA	NA	NA	NA	NA	NA	425	594	398	361	596	395	452	693	483	417	681	485
Alkalinity,Carbonate (CaCO3)	mg/L	10	10	10	10	10	10	10	10	10	10	10	10	10	10	10	10	10	10
Total Dissolved Solids	mg/L	2860	1480	960	1970	1660	1250	5100	3200	2340	3070	3280	2050	5200	4310	2510	453	426	3240

		SUMMER 2023 SAMPLING EVENT						FALL 2023 SAMPLING EVENT						WINTER 2024 SAMPLING EVENT					
		SMW-1	SMW-2	SMW-4	SMW-5	SMW-6	Duplicate (SMW-1)	SMW-1	SMW-2	SMW-4	SMW-5	SMW-6	Duplicate (SMW-1)	SMW-1	SMW-2	SMW-4	SMW-5	SMW-6	Duplicate (SMW-1)
Analyte	Units	Data Results (ND=0.5RL)	Data Results (ND=0.5RL)	Data Results (ND=0.5RL)	Data Results (ND=0.5RL)	Data Results (ND=0.5RL)	Data Results (ND=0.5RL)	Data Results (ND=0.5RL)	Data Results (ND=0.5RL)	Data Results (ND=0.5RL)	Data Results (ND=0.5RL)	Data Results (ND=0.5RL)	Data Results (ND=0.5RL)	Data Results (ND=0.5RL)	Data Results (ND=0.5RL)	Data Results (ND=0.5RL)	Data Results (ND=0.5RL)	Data Results (ND=0.5RL)	Data Results (ND=0.5RL)
Bromide	mg/L	1.1	0.82	0.55	0.71	0.99	1.1	1.1	0.89	0.6	0.8	1.1	1.1	0.5	0.5	0.5	0.5	0.5	0.5
Chloride	mg/L	1990	938	833	1360	1370	1760	1960	1040	957	1590	1630	2070	2190	1120	1300	1910	1790	2190
Fluoride	mg/L	0.5	0.87	1.5	0.88	0.65	0.48	0.46	1	1.7	0.96	0.66	0.58	0.1	0.1	0.1	0.1	0.1	0.1
Nitrate as N	mg/L	0.47	0.05	4	0.05	0.6	0.52	0.34	0.05	0.05	0.05	0.05	0.3	0.05	0.05	0.05	0.05	0.16	0.05
Sulfate	mg/L	1130	1380	687	525	1490	1150	1230	1610	686	597	1650	1220	1310	1690	789	663	1880	1100
Calcium	ug/L	162,000	73,100	46,200	63,200	149,000	173,000	183,000	83,800	45,000	69,500	132,000	181,000	175,000	89,800	39,800	72,800	171,000	168,000
Iron	ug/L	376	2,720	2,040	931	1,610	415	490	4,480	5,450	1,340	10,400	466	594	10,700	7,200	1,470	1,260	530
Magnesium	ug/L	76,900	41,000	15,400	30,100	63,700	80,600	85,100	46,100	16,400	34,500	71,200	84,200	86,400	50,800	15,300	37,100	82,600	82,500
Potassium	ug/L	23,100	17,000	12,200	15,900	21,300	24,000	30,100	23,300	16,700	22,000	27,400	28,700	24,100	19,300	13,000	17,500	23,600	22,800
Silicon	ug/L	7,350	8,420	6,560	9,650	11,200	7,850	7,730	7,890	6,570	8,650	9,520	7,590	6,860	8,040	6,380	7,970	8,870	6,510
Sodium	ug/L	1,560,000	1,400,000	811,000	950,000	1,480,000	1,620,000	1,610,000	1,410,000	871,000	1,260,000	1,710,000	1,510,000	1,610,000	1,630,000	1,300,000	1,400,000	1,810,000	1,580,000
Aluminum	ug/L	51.4	25	54.8	1440	25	58.7	263	125	25	406	25	125	50	50	112	233	50	75
Antimony	ug/L	2.1	0.5	0.5	0.5	0.5	2.1	2.5	2.5	1.5	0.5	0.5	2.5	1	1	0.5	1	1	1.5
Arsenic	ug/L	1.2	1.3	2.6	2.6	3.2	1.1	2.5	2.5	2	1.8	2.7	2.5	1	1	2.2	1	1	1.5
Barium	ug/L	46.2	41.1	30.7	47.1	50.4	47.2	44.2	42.9	30.7	49.1	44.9	45.9	33.2	31.6	34.4	42.9	34.8	35.6
Cadmium	ug/L	0.25	0.25	0.25	0.25	0.25	0.25	1.25	1.25	0.25	0.25	0.25	1.25	0.5	0.5	0.25	0.5	0.5	0.75
Chromium	ug/L	13.3	0.5	1.4	1.2	0.5	14.7	7.6	2.5	0.5	0.5	0.5	6	6.3	1	1	1	1	4.6
Copper	ug/L	0.5	0.5	0.5	1.2	4.9	0.5	2.5	2.5	0.5	1.6	0.5	2.5	1	1	0.5	1	3.3	1.5
Lead	ug/L	0.5	0.5	0.5	0.5	0.5	0.5	2.5	2.5	1.5	1	1.5	2.5	1	1	1	1	1	1.5
Manganese	ug/L	74	98.6	23	44.3	78.9	70.6	65.4	112	29.9	42.6	59.9	67.9	60.7	124	42.6	58.1	93.7	61.5
Selenium	ug/L	0.5	0.5	0.5	0.5	0.5	0.5	2.5	2.5	0.5	0.5	0.5	2.5	1	1	0.5	1	1	1.5
Thallium	ug/L	0.5	0.5	0.5	0.5	0.5	0.5	2.5	2.5	1.5	1	1.5	2.5	1	1	1	1	1	1.5
Alkalinity, Total as CaCO3	mg/L	444	720	551	421	693	446	390	762	516	442	748	376	452	798	681	455	727	446
Alkalinity,Bicarbonate (CaCO3)	mg/L	444	720	551	421	693	446	390	762	516	442	748	376	452	798	681	455	727	446
Alkalinity,Carbonate (CaCO3)	mg/L	10	10	10	10	10	10	10	10	10	10	10	10	10	10	10	10	10	10
Total Dissolved Solids	mg/L	5440	4540	3500	3450	5630	5920	5500	4490	3360	3660	6000	5480	6610	5820	4510	2620	7660	5750

Notes:
The above data are summarized directly from laboratory reports and may not reflect any edits/flags added throught the data validation process.
NA - Not analyzed/reported

Groundwater geochemistry sampling results are summarized in Figure A.I-1.3-2 a Piper diagram for the October 2023 sample event.

Figure A.I-1.3-2. Piper Diagram of Water Table Aquifer Groundwater Samples Collected in October 2023

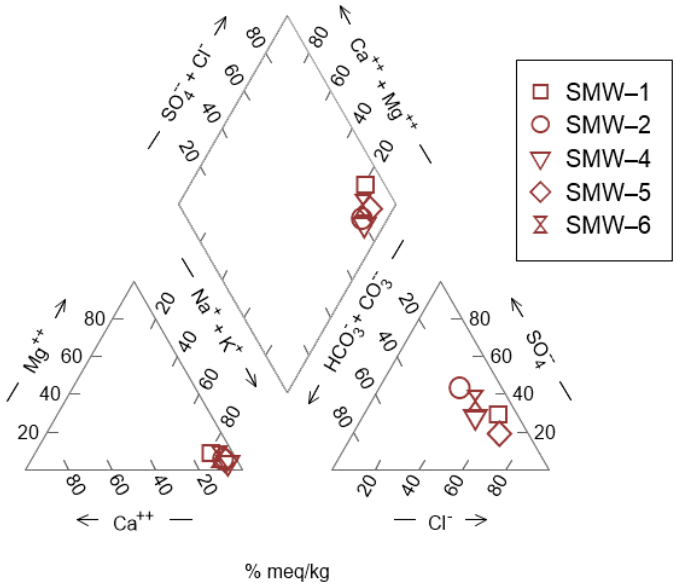

These Water Table aquifer wells clustered more tightly than the Dakota Formation wells. In each case, the dominant cation component was sodium and potassium at greater than 70%. The dominant anions were primarily chloride and sulfate (combined greater than 80%).

Time series for groundwater geochemistry are considered in Figure A.I-1.3-3 with Stiff diagrams. Most of the wells' diagrams indicate geochemical stability over time. The exception is SMW-6. At that well, the April 2023 data indicated a dominant cation of bicarbonate/carbonate, which contrasted with chloride and sulfate dominating other events. The April 2023 cation/anion balance was poor (approximately 70 milliequivalents per liter [meq/L] for cations versus approximately 16 meq/L for anions), although none of the major ions were identified as misreported by the data validation process. The growing dataset suggests that the April 2023 event for SMW-6 was anomalous, with undercounting of the sulfate and chloride concentrations by the lab.

Figure A.I-1.3-3. Stiff Diagrams of Water Table Aquifer Groundwater Samples

SMW-1

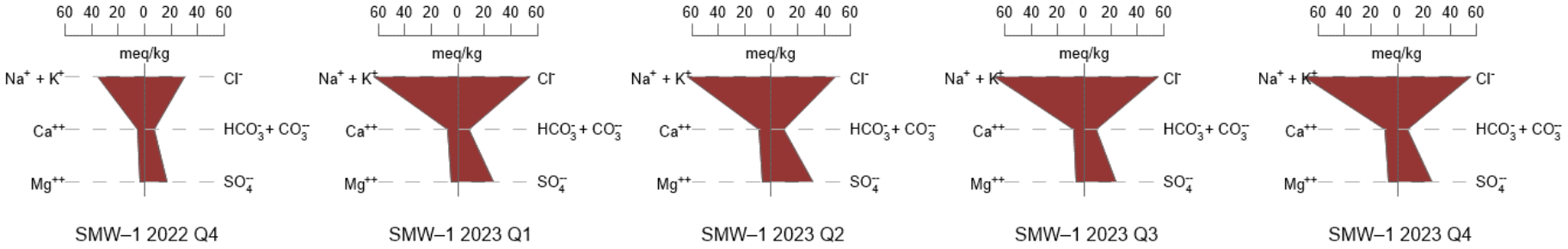

SMW-2

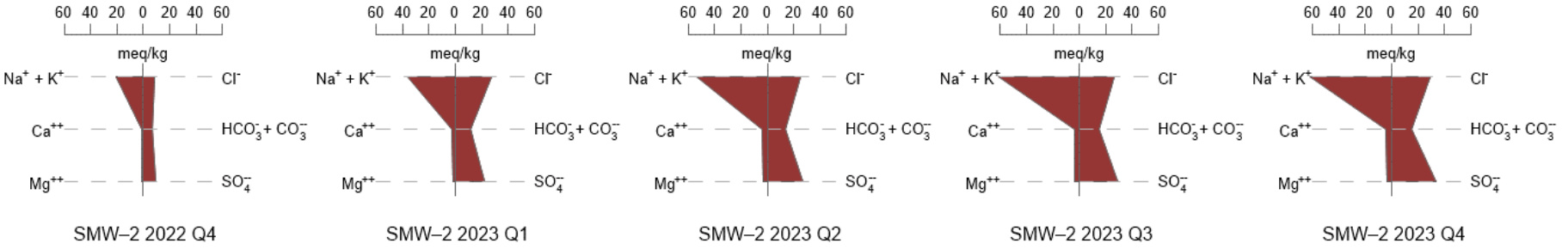

SMW-4

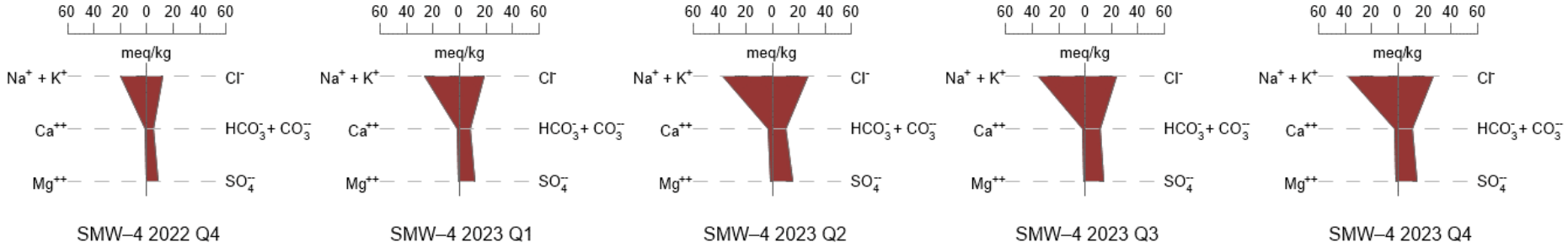

SMW–4 2022 Q4 | SMW–4 2023 Q1 | SMW–4 2023 Q2 | SMW–4 2023 Q3 | SMW–4 2023 Q4

SMW-5

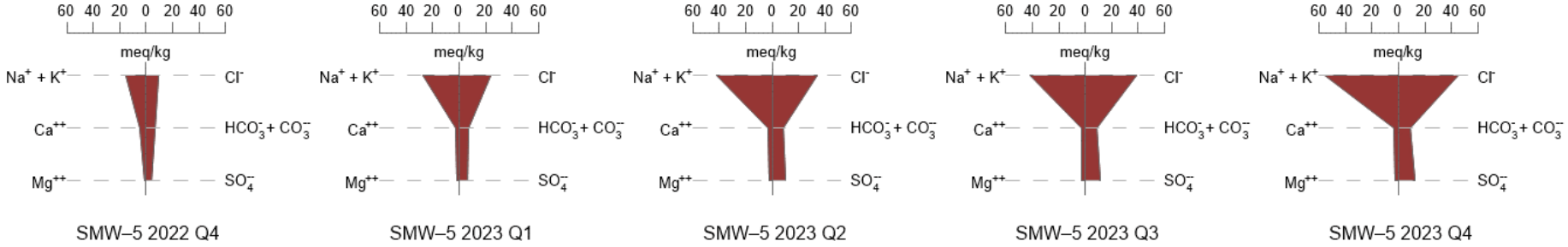

SMW–5 2022 Q4 | SMW–5 2023 Q1 | SMW–5 2023 Q2 | SMW–5 2023 Q3 | SMW–5 2023 Q4

SMW-6

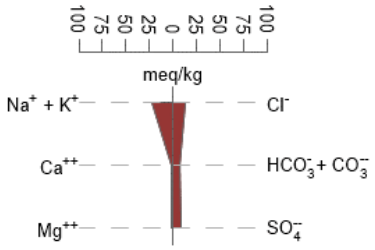

SMW–6 2022 Q4

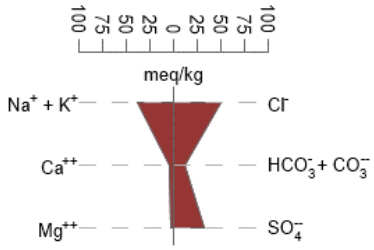

SMW–6 2023 Q1

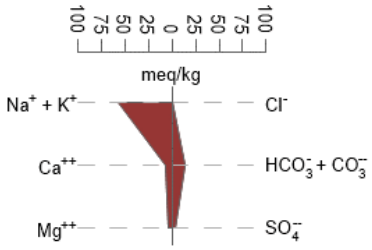

SMW–6 2023 Q2

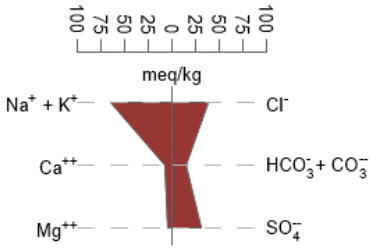

SMW–6 2023 Q3

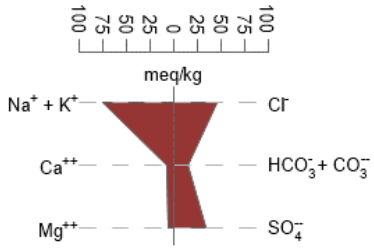

SMW–6 2023 Q4

A.I-1.4. Vadose Zone CO_2

Descriptive statistics for the CO_2 concentrations measurements are presented in Table A.I-1.4-1.

Table A.I-1.4-1. Summary Statistics for Vadose Zone Soil Gas Data Loggers.

		CO_2 Concentration at 5 ft bgs	CO_2 Concentration at 10 ft bgs
		ppm	ppm
MS-1	Number of Measurements	571	698
	Mean	4,937	5,410
	Median	4,281	4,625
	Standard Deviation	2,583	2,578
MS-2	Number of Measurements	699	699
	Mean	8,834	13,600
	Median	5,630	12,868
	Standard Deviation	6,868	4,021
MS-3	Number of Measurements	699	652
	Mean	7,096	14,656
	Median	5,306	13,529
	Standard Deviation	4,242	2,599
MS-4	Number of Measurements	667	699
	Mean	5,433	12,404
	Median	3,976	12,506
	Standard Deviation	3,860	2,578
MS-5	Number of Measurements	499	699
	Mean	13,439	22,521
	Median	11,982	22,807
	Standard Deviation	6,674	4,051
MS-6	Number of Measurements	550	658
	Mean	4,695	6,899
	Median	3,551	6,036
	Standard Deviation	3,058	3,126

Notes:
ppm - parts per million
ft bgs - feet below ground surface

The number of measurements for the majority of the probes was greater than 650, corresponding to at least 325 days of data logging. Four of the probes (MS-1 at 5 ft bgs, , MS-5 at 5 ft bgs, and MS-6 at 5 ft bgs) were affected by moisture on the sensor windows, decreasing the number of measurements. Once the moisture problem was identified, desiccant was added to the casing within each sensor well as a mitigation measure. CO_2 time series for 5 ft bgs and 10 ft bgs probes reported by the dataloggers are presented in Figure A.I-1.4-1.

Figure A.I-1.4-1. Time Series for Vadose Zone Soil Gas CO_2 Sensors

MS-1

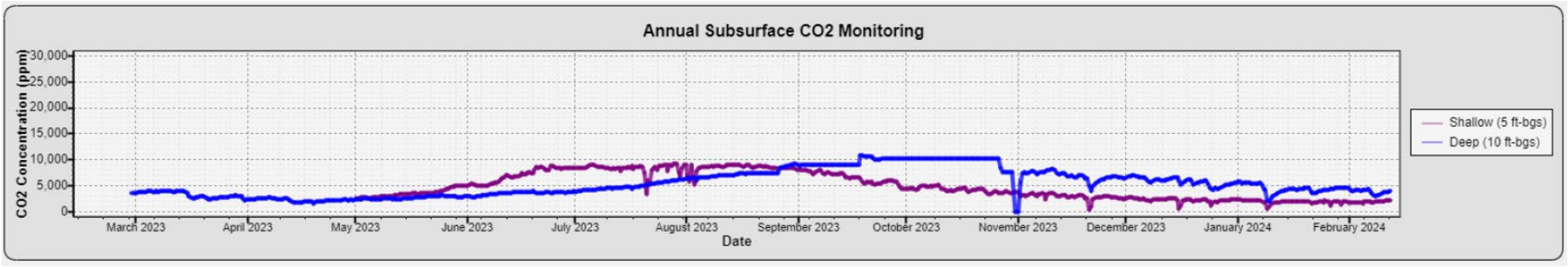

MS-2

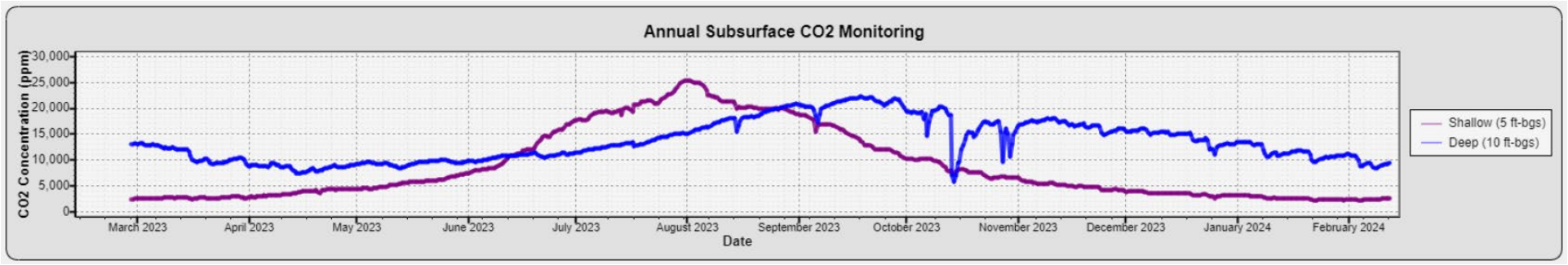

MS-3

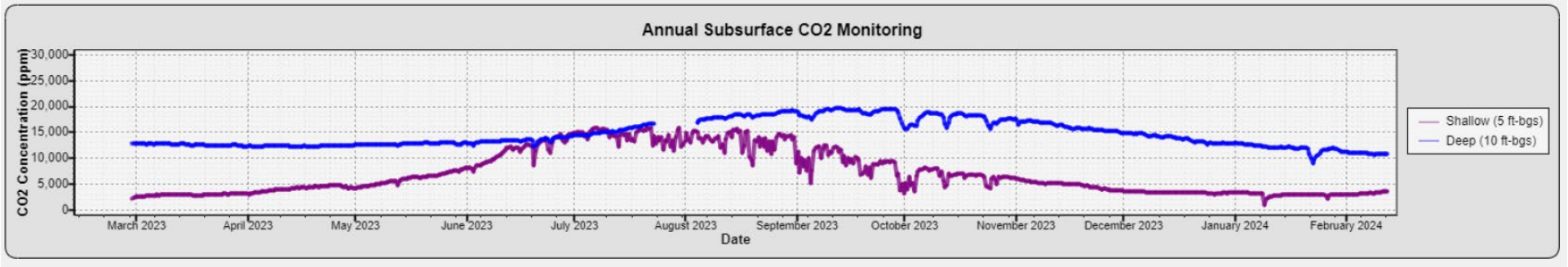
Annual Subsurface CO2 Monitoring
CO2 Concentration (ppm)
30,000
25,000
20,000
15,000
10,000
5,000
0
March 2023
April 2023
May 2023
June 2023
July 2023
August 2023
September 2023
October 2023
November 2023
December 2023
January 2024
February 2024
Date
Shallow (5 ft-bgs)
Deep (10 ft-bgs)

MS-4

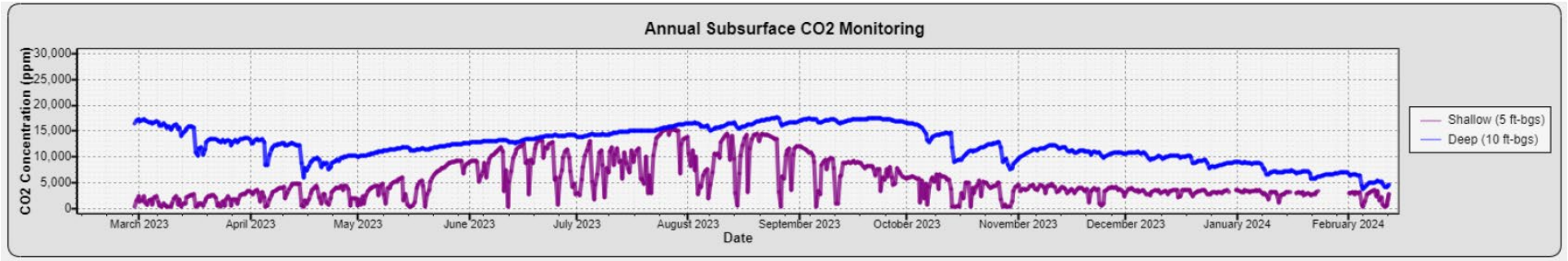
Annual Subsurface CO2 Monitoring
CO2 Concentration (ppm)
30,000
25,000
20,000
15,000
10,000
5,000
0
March 2023
April 2023
May 2023
June 2023
July 2023
August 2023
September 2023
October 2023
November 2023
December 2023
January 2024
February 2024
Date
Shallow (5 ft-bgs)
Deep (10 ft-bgs)

MS-5

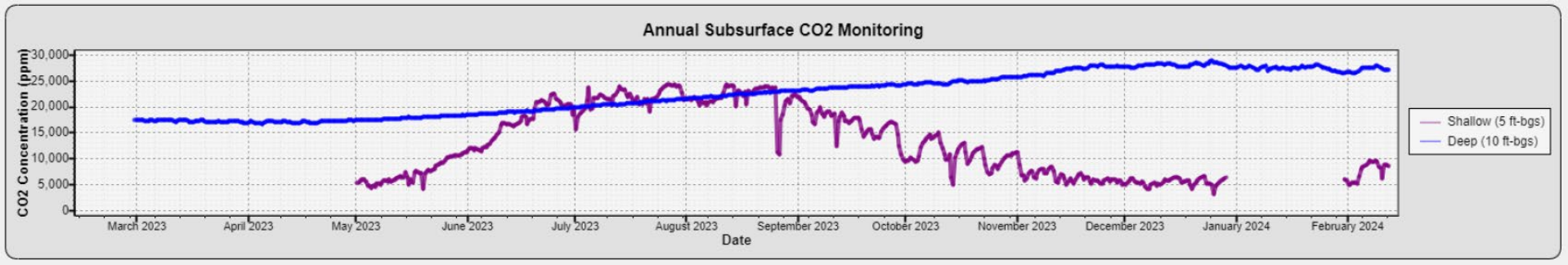
Annual Subsurface CO2 Monitoring
CO2 Concentration (ppm)
30,000
25,000
20,000
15,000
10,000
5,000
0
March 2023
April 2023
May 2023
June 2023
July 2023
August 2023
September 2023
October 2023
November 2023
December 2023
January 2024
February 2024
Date
Shallow (5 ft-bgs)
Deep (10 ft-bgs)

MS-6

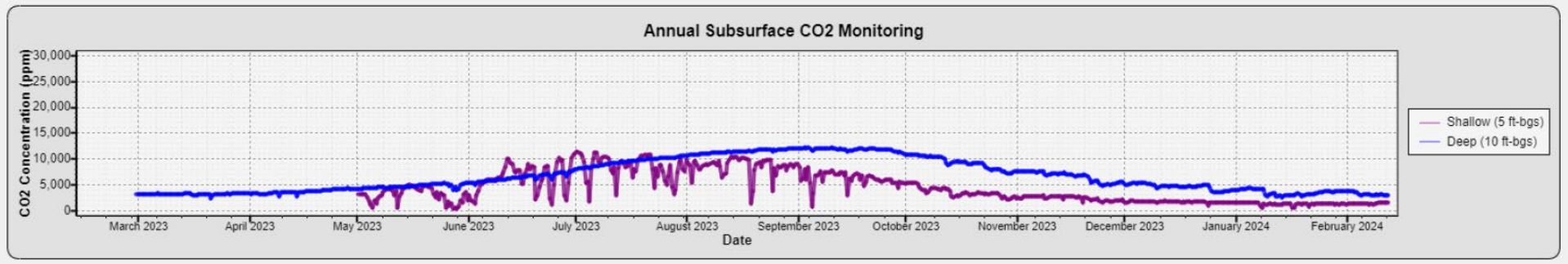
Annual Subsurface CO2 Monitoring
CO2 Concentration (ppm)
30,000
25,000
20,000
15,000
10,000
5,000
0
March 2023
April 2023
May 2023
June 2023
July 2023
August 2023
September 2023
October 2023
November 2023
December 2023
January 2024
February 2024
Date
Shallow (5 ft-bgs)
Deep (10 ft-bgs)

Mean CO_2 concentrations were greater than 1,000 parts per million (ppm) at all stations and depths. The atmospheric CO_2 concentration is currently approximately 412 ppm, so the elevated vadose zone CO_2 concentrations indicate sources below ground surface. Stations MS-2 through MS-5 had mean CO_2 concentrations greater than 10,000 ppm for at least one of the probes, further supporting an inference of subsurface CO_2 sources. Overall, as evidenced both by standard deviation values in the summary statistics table, and in the time series charts, the variability of 5 ft bgs CO_2 concentrations was greater than 10 ft bgs CO_2 concentrations. The most significant short term variation was observed at MS-4, where the 5 ft bgs CO_2 concentrations showed episodic decreases to near atmospheric concentrations, followed by rebound to the longer term elevated values. Generally, the maximum values in CO_2 concentrations at 5 ft bgs occurred in the summer, followed by a delay for maximum CO_2 concentrations to be observed at 10 ft bgs.

Soil gas sampling was conducted so that the stable isotopes of carbon in CO_2 could be measured in October 2022, January 2023, and October 2023. The deep samples for SVP-1, SVP-4, and SVP-5 had insufficient CO_2 for reporting the first two events due to tight soils that caused atmospheric air to enter the sample train. This problem was corrected, and additional sampling events were conducted for stable isotopes in July 2023 and October 2023. The results are plotted in Figure A.I-1.4-2.

All $\delta^{13}C$ in CO_2 values fell within the -21 to -11 ‰ range. At SVP-1, SVP-5 and SVP-6, all 5 ft bgs $\delta^{13}C$ values were higher than those at 10 ft bgs. At SVP-4, the situation was reversed, and at the remaining two locations, the ranking changed depending on the sample event. Temporal variability was observed at all locations, with SVP-3 being the most stable when considering both depths (all values within 3 ‰).

Figure A.I-1.4-2. Sampling Results for Soil Gas Stable Carbon Isotopes in CO_2

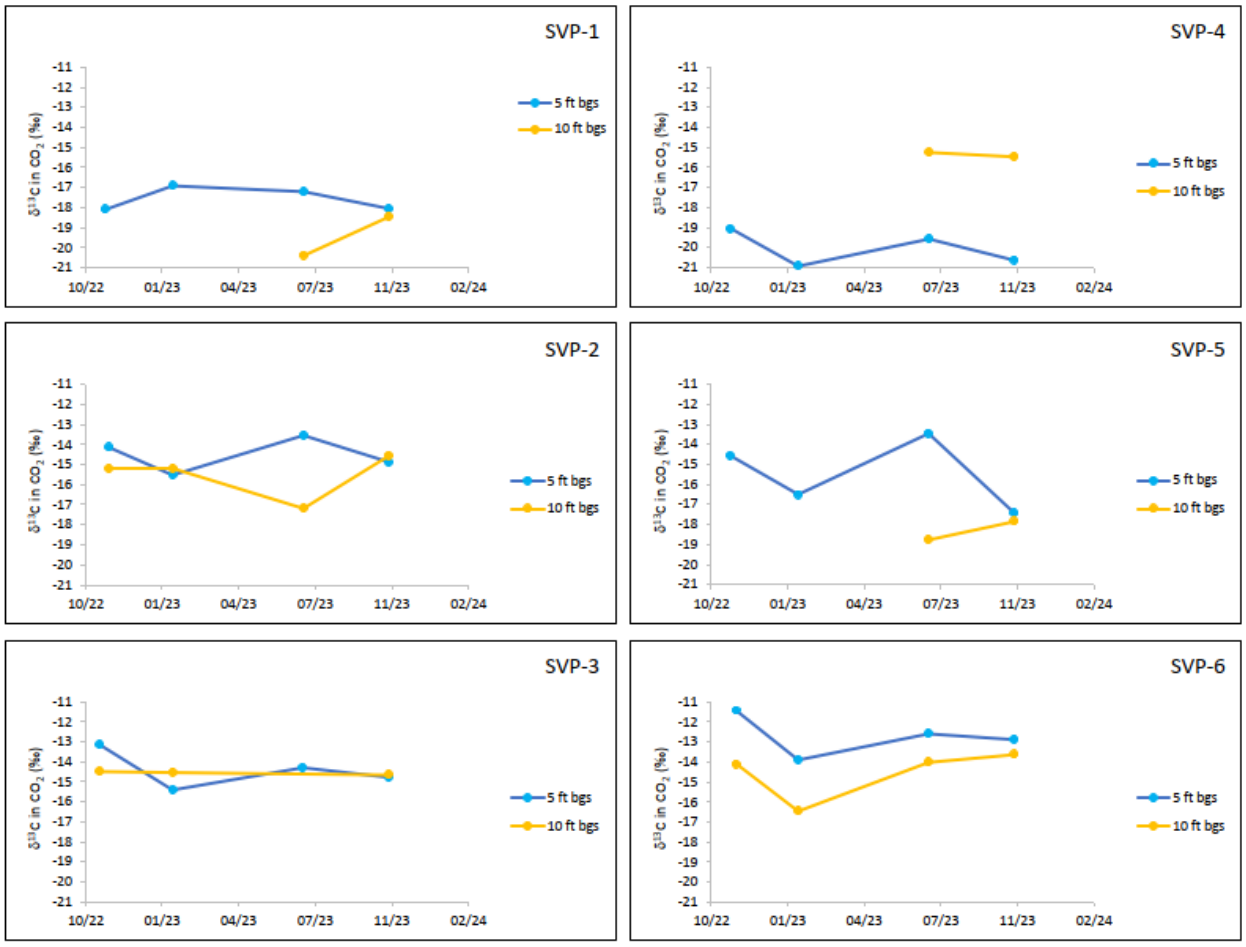

A.I-1.5. CO_2 Effluxes

CO_2 effluxes were measured at ground surface at 16 soil collars for each station in October 2022, April 2023, July 2023, October 2023, and January 2024. A January 2023 event was attempted, but the soil collars were covered in ice and snow and not viable for data collection. Mean CO_2 effluxes for each station, with error bars representing one standard error of the mean, are presented in Figure A.I-1.5-1. The lowest fluxes were measured in January 2024, with mean values ranging from 0.2 to 0.3 2.2 µmol m^{-2} s^{-1}. Mean CO_2 effluxes for the October 2022 January 2023, and October 2023 events were moderate, ranging from 0.5 to 2.2 µmol m^{-2} s^{-1}. Mean CO_2 effluxes for July 2023 were relatively high at all stations, ranging from 5.9 to 11.3 µmol m^{-2} s^{-1}. These results are indicative of seasonal variability, with the highest values measured in the summer, the lowest values in the winter, and intermediate values in spring and fall.

Figure A.I-1.5-1. Field Measurement Results for CO_2 Effluxes

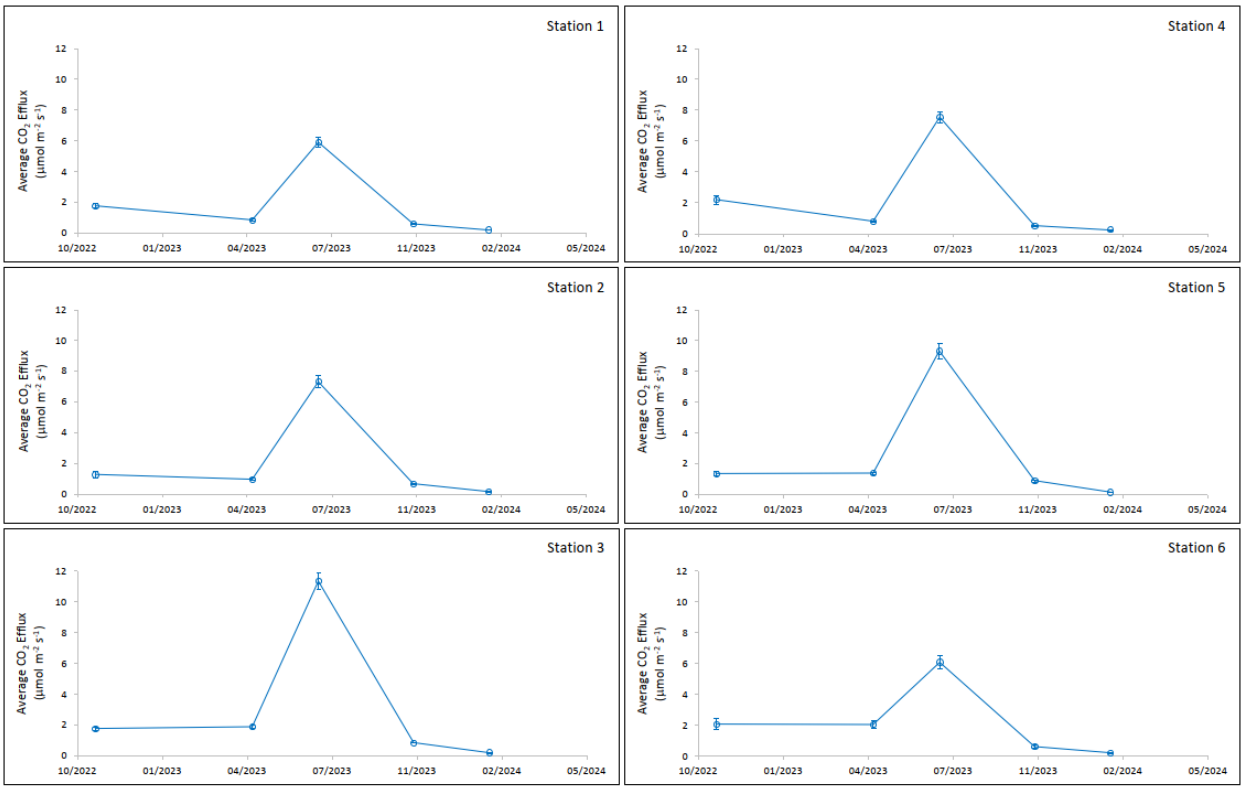

Appendix A.I.2. History Match for CSS #1 Nov 2022 Step Rate Test

APPENDIX A.I.2. HISTORY MATCH FOR CSS #1 NOV 2022 STEP RATE TEST

RUSSELL CO_2 CAPTURE AND SEQUESTRATION

Table of Contents

List of Tables

List of Figures

List of Acronyms and Abbreviations

Kv/Kh = Ratio of the vertical permeability divided by the horizontal permeability	SRT = step rate test SWNM = single well numerical model

A.I.2.1. Summary

A Single Well Numerical Model (SWNM) was built to support initial history matching of the full field computational model using field data from the November 2022 step rate test (SRT) of CSS #1. Three history matching trials found a set of average values for horizontal permeability and the ratio of vertical permeability to horizontal permeability (Kv/Kh ratio) that result in a close match for flowing bottom pressures between the field data and the SWNM results. Values obtained by history matching were then incorporated into the full field computational model used in development of the Class VI permit application package.

A.I.2.2. Construction of the Single Well Numerical Model

A brief description is provided for the SWNM along with presentation of the SRT field data.

A.I.2.2.1. Well Configuration and Field Data

CSS #1 was defined in the simulator based on the simplified mechanical diagram shown in Figure A.I.2.2-1, with the down-hole pressure gauge located at a depth of 3,560 ft and the perforated interval at depths between 3,580 – 3,600 ft. The raw field data obtained from the SRT was processed and prepared in a compatible format to be used by the numerical simulator. Figure A.I.2.2-2 shows the field data for flowing bottom hole pressure and injection rate.

Figure A.I.2.2-1. CSS #1 Well Configuration for SWNM

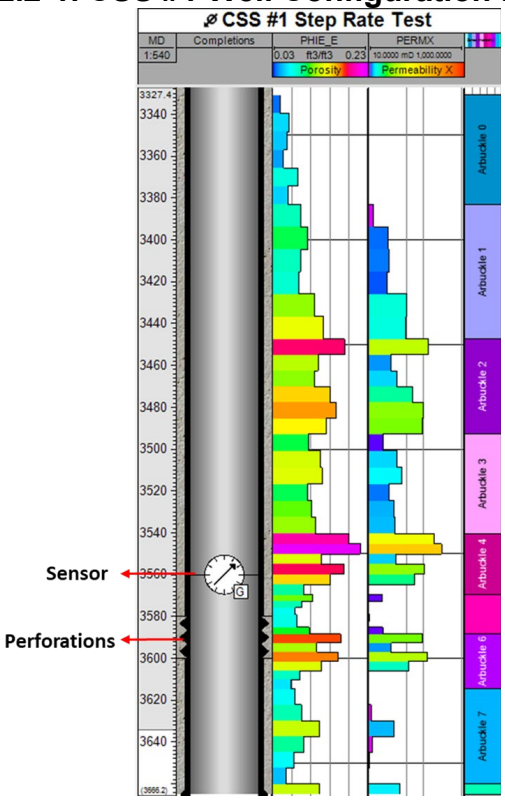

Figure A.I.2.2-2. SRT Field Data from CSS #1 November 2022

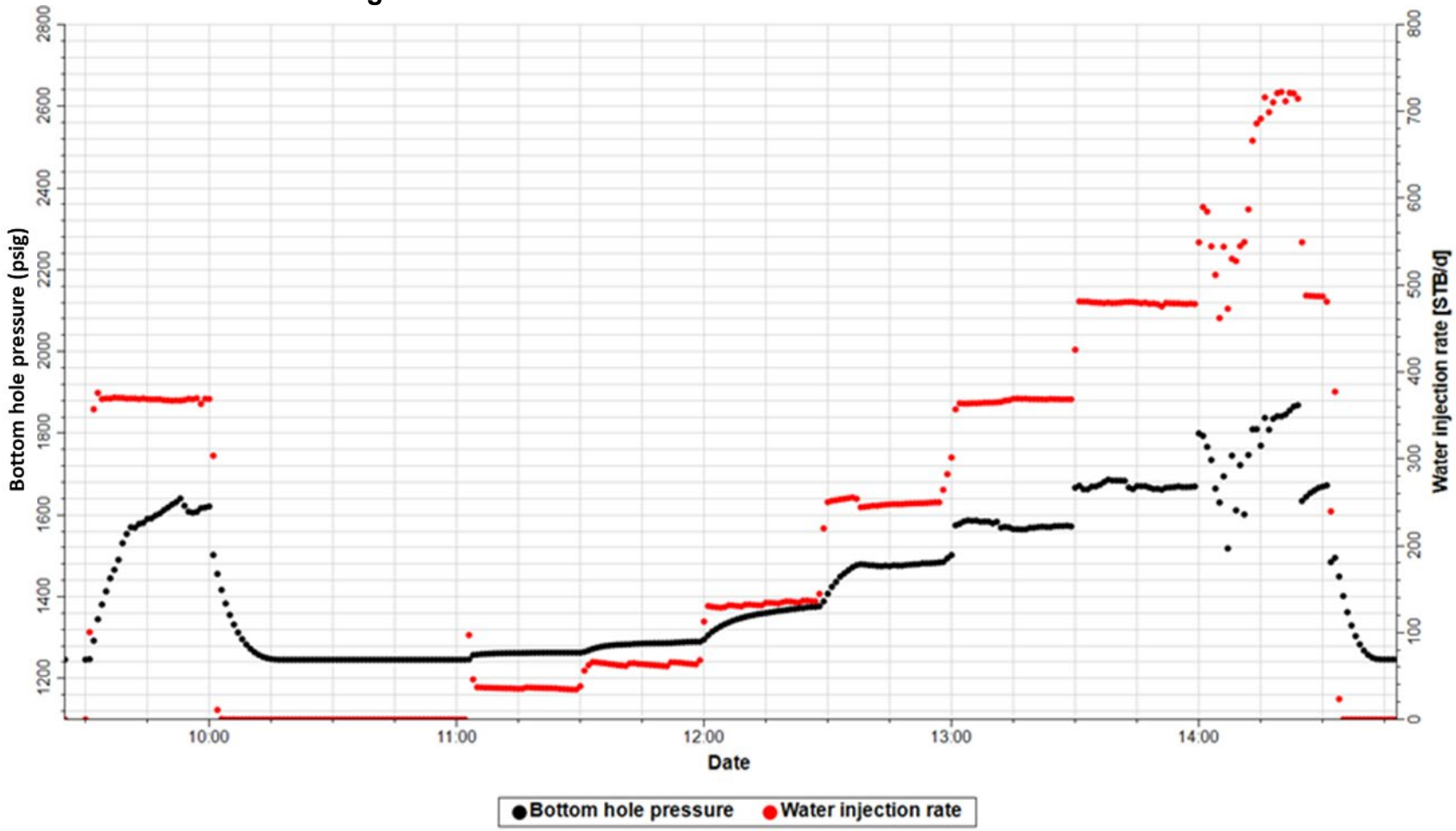

A.I.2.2.2. Simulation Grid

The SWNM consists of a Cartesian sector model with a radial extent of approximately 300 meters (984 ft). The SWNM grid was extracted from the Full Field model. The horizontal cell dimensions are 100x100 ft with vertical resolution of 6 ft. Additionally, a local refinement was carried out in an area of 150x150 feet in the vicinity of the well CSS #1. The horizontal dimensions of the cells in the local grid refinement are approximately 10x10 feet.
Figure A.I.2.2-3 shows the SWNM grid. Petrophysical properties in the SWNM correspond to those defined in the full field model.

Figure A.I.2.2-3. SWNM Grid

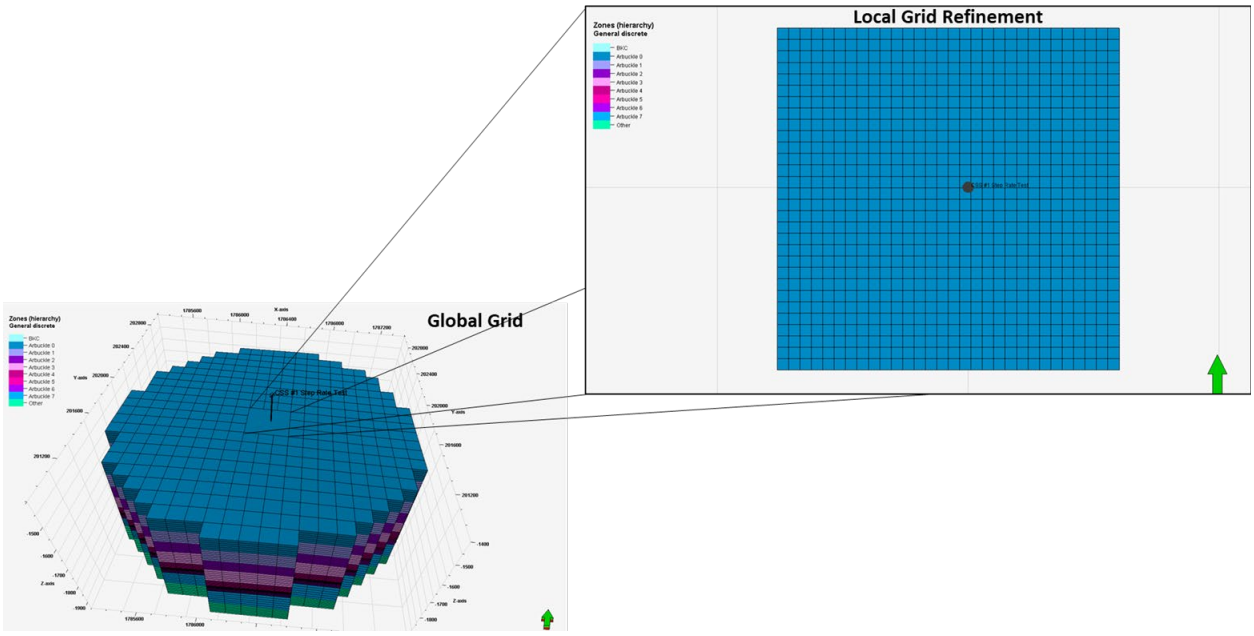

A.I.2.2.3. Boundary Conditions

The analytical aquifer model proposed by Carter and Tracy was used to define boundary conditions, similar to the method used to define boundary conditions for the full-field model. The cells that connect the aquifer with the single well numerical model of the CSS #1 well are shown in Figure A.I.2.2-4.

Figure A.I.2.2-4. Carter & Tracy Aquifer Boundary

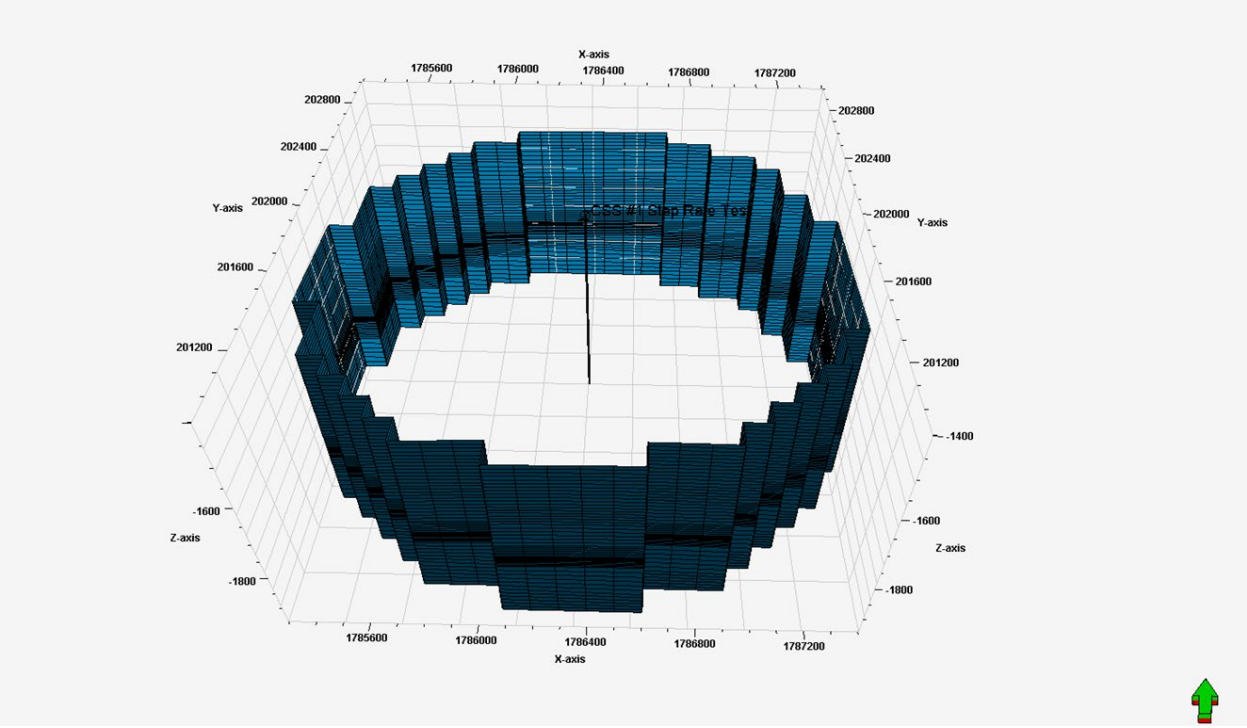

A.I.2.2.4. Initial Conditions

The initialization process for the SWNM consists of reproducing the initial reservoir pressure measured at the depth of the bottom hole gauge. The dynamic equilibrium of the single well model was monitored for a simulation time of >5 hours to guarantee dynamic stability between the single well numerical model and the Carter and Tracy analytical aquifer, thus ruling out possible impacts during history matching of the SRT data. Figure A.I.2.2-5 show the variation of the initial pressure with depth (left panel) and the dynamic equilibrium between the single well model and the analytical aquifer without fluid injection (right panel).

Figure A.I.2.2-5. SWNM Initial Conditions

Left: Variation of Initial Pressure with Depth; Right: Stable Dynamic Equilibrium Over Time

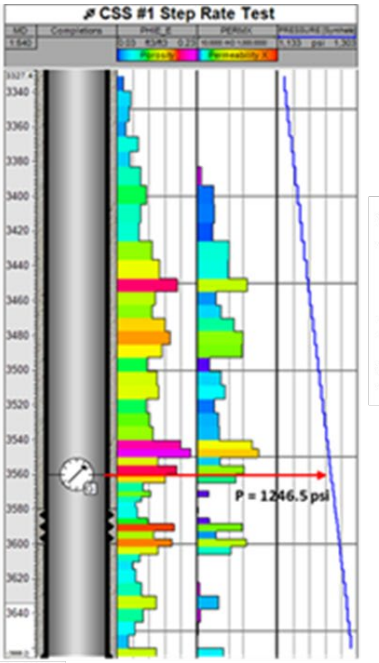

Single well model initial pressure match

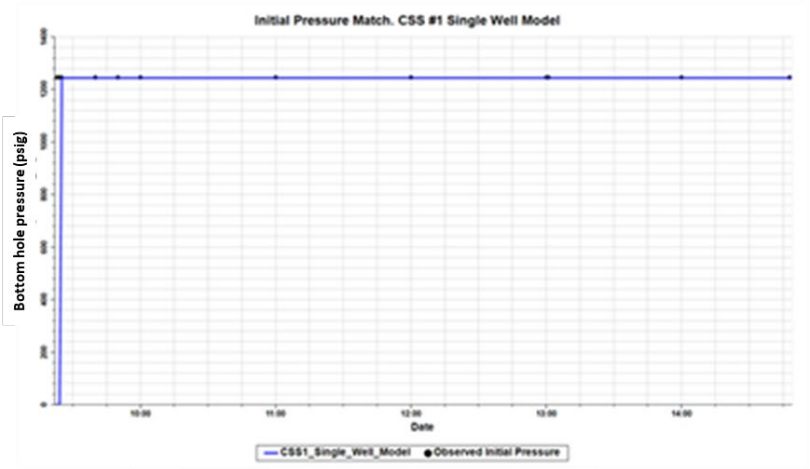

Stable dynamic equilibrium over time

A.I.2.3. Results

The history match consisted of performing a sensitivity analysis over the uncertainty variables (horizontal permeability and Kv/Kh ratio) in the SWNM to force a match between the bottom pressures reported in the SRT and the bottom pressures reported by the SWNM. Values for horizontal permeability and Kv/Kh ratio were manually adjusted by examination of graphical deviations between the field data and the SWNM values for bottom pressure over time. The injection rate used in the SWNM was the same as the injection rate reported in the SRT.

Table A.I.2.3-1 and Figure A.I.2.3-1 provides a summary of the three history match trials performed. Results from Trial 3 were incorporated into the Base Case computational model.

Table A.I.2.3-1. Summary of History Matching Trials

Case	Permeability multiplier factor	
	Horizontal Permeability	Kv/Kh
Trial 1	1	0.01
Trial 2	0.5	0.01
Trial 3	0.38	2.632

A.I.2.3.1. Trial 1

This trial utilizes the original petrophysical properties of the full field model. Figure A.I.2.3-2 shows the results from the SWNM predict a lower bottom pressure compared to the field data, which suggests the original permeability in the model is too low.

A.I.2.3.2. Trial 2

This trial considers a horizontal permeability equal to 0.5 times the original value in the full field model and a Kv/Kh ratio of 0.01. Figure A.I.2.3-3 shows the SWNM provides a good approximation of the bottom pressures reported in the field data, however a slight deviation occurs during pressure fall-off at the end of the test.

A.I.2.3.3. Trial 3

This trial considers a horizontal permeability equal to 0.38 times the original value in the full field model and a Kv/Kh ratio of 2.632. Results of Trial 3 show that the single well model reproduces excellently the bottom hole pressures (injection pressure) reported in the Step-Rate Test, managing to improve the representativeness of the simulated pressure data at the end of the test as seen in Figure A.I.2.3-4.

Figure A.I.2.3-1. Summary of History Match Trials

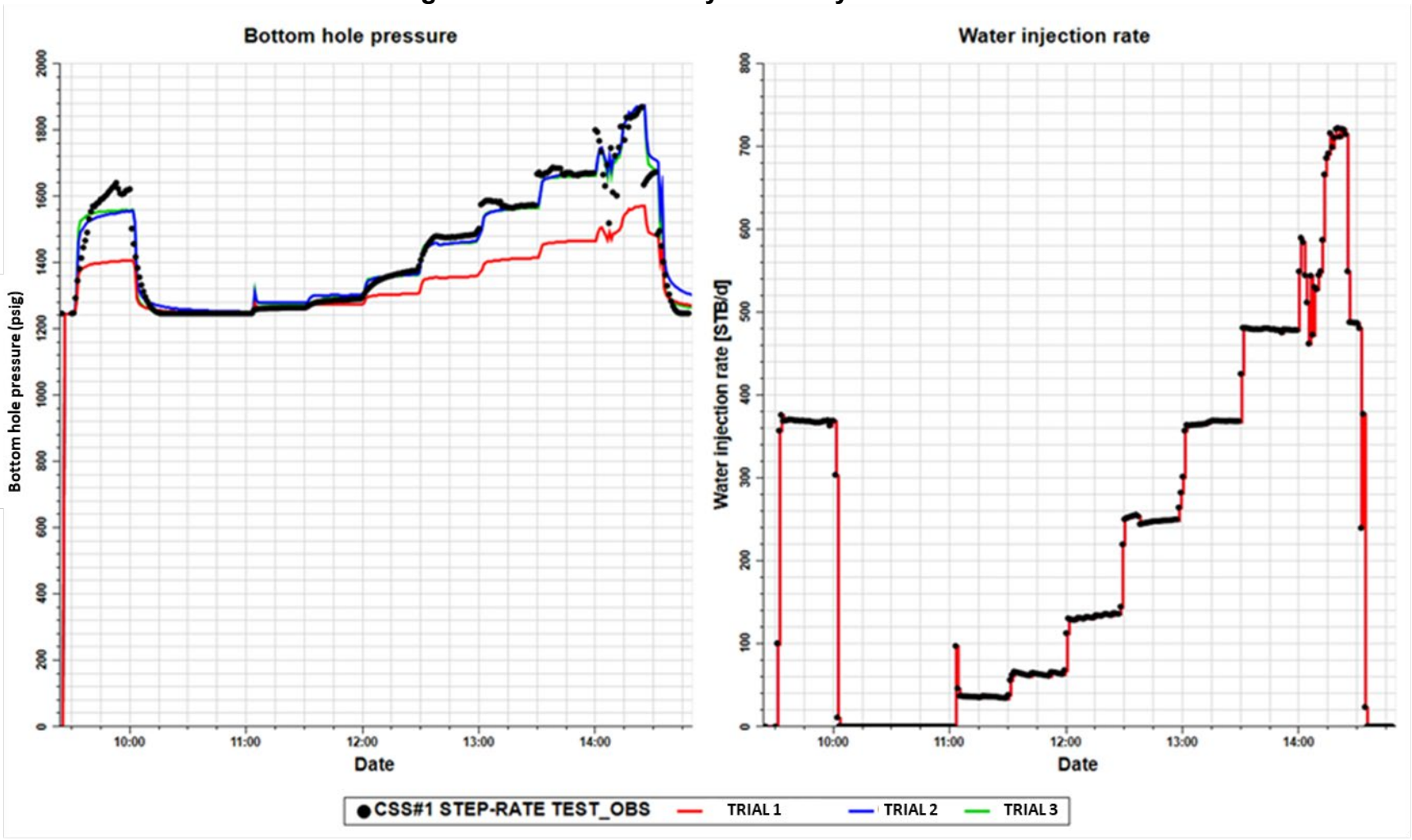

Figure A.I.2.3-2. History Match – Trial 1

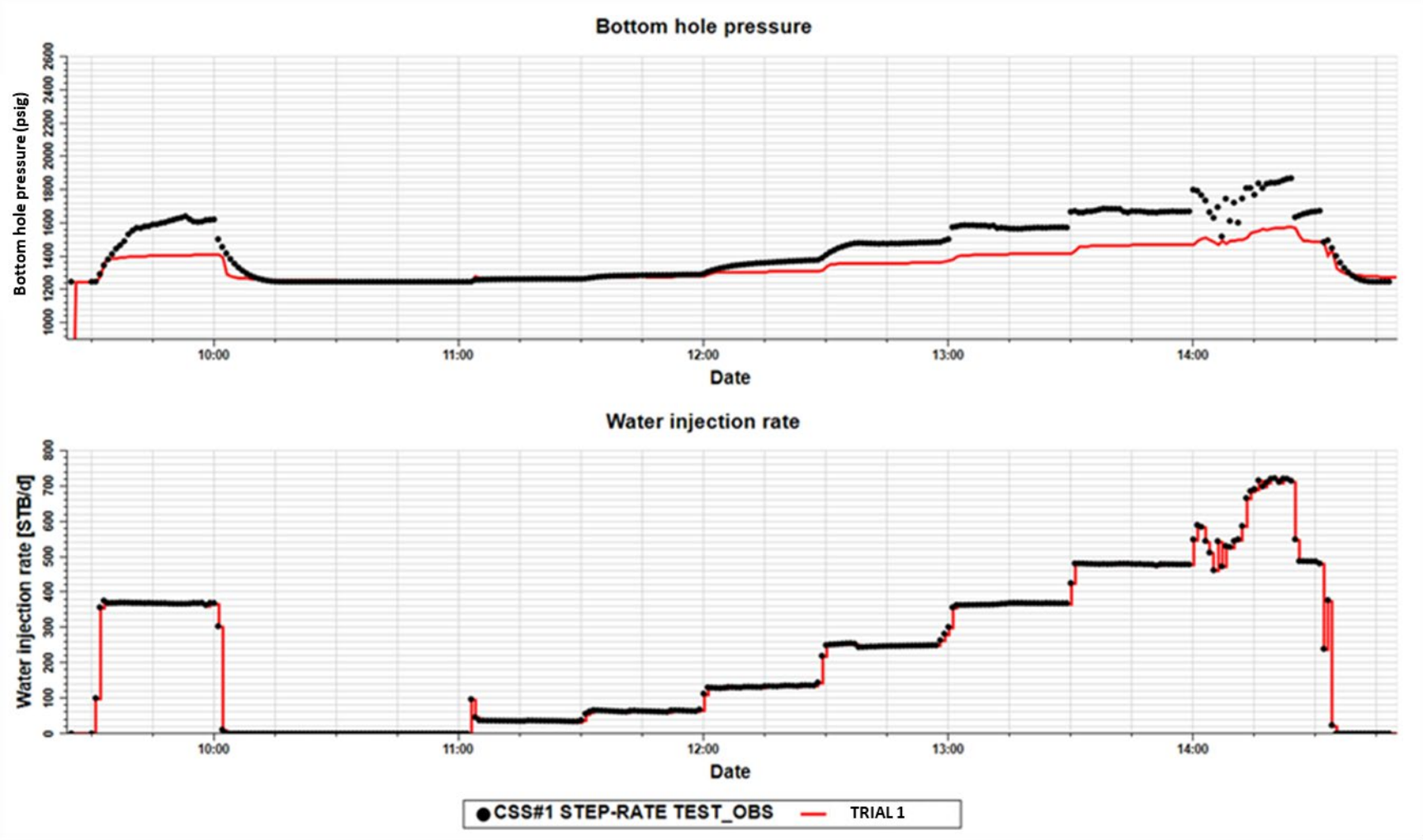

Figure A.I.2.3-3. History Match – Trial 2

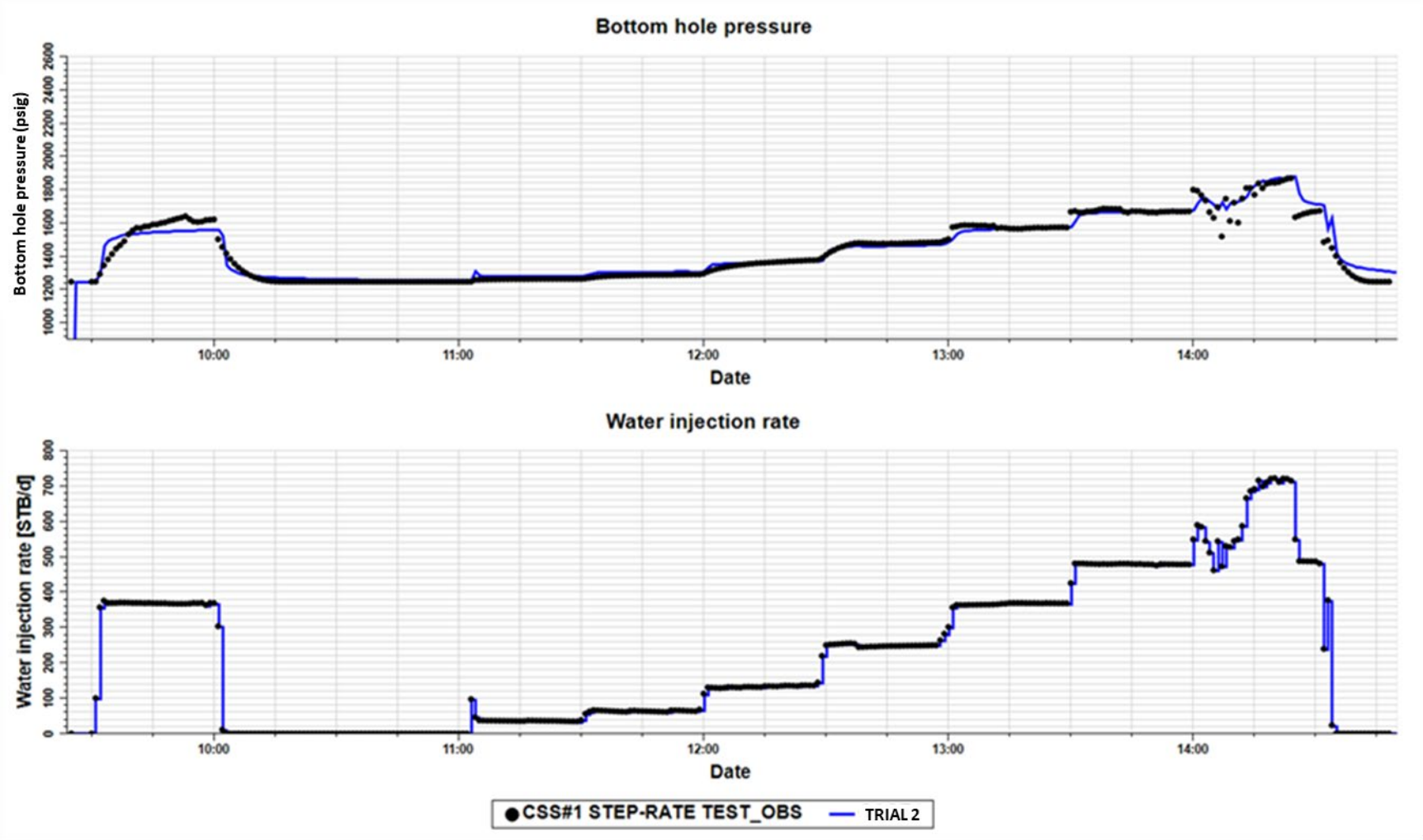

Figure A.I.2.3-4. History Match – Trial 3